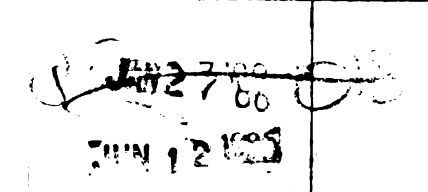


RETURNING MATERIALS:
Place in book drop to remove this checkout from your record. FINES will be charged if book is returned after the date stamped below.



RADAR TARGET DISCRIMINATION USING K-PULSES FROM A "FAST" PRONY'S METHOD

Ву

Lance Lynwood Webb

A DISSERTATION

Submitted to
Michigan State University
in partial fulfillment of the requirements
for the degree of

DOCTOR OF PHILOSOPHY

Department of Electrical Engineering and Systems Science

Copyright | Lance Lynw

1954

Copyright by
Lance Lynwood Webb
1984

An a technique is Expansion Metion) for the pulse convoluterum into a decendent para algorithm is moise sensiti

Origi Primary Objec radar target

K-Pulse form.

"quiet" radar, for this purpo

ABSTRACT

RADAR TARGET DISCRIMINATION USING K-PULSES FROM A "FAST" PRONY'S METHOD

Bv

Lance Lynwood Webb

An aspect-angle independent and range independent processing technique is disclosed which is based upon the SEM (Singularity Expansion Method) model solution of the EFIE (E-field integral equation) for transient electromagnetic scattering. The derived kill-pulse convolution forms conveniently decompose the radar target return into aspect-angle <u>independent</u> parameters and aspect-angle <u>dependent</u> parameters. A near real-time "fast" Prony's method algorithm is performed on empirical data to exploit the inherent noise sensitivity of the ordinary Prony's method to obtain a second K-Pulse form.

Original contributions of this dissertation in addition to the primary objective of developing a range and aspect-angle independent radar target discrimination technique potentially compatible with "quiet" radar, are four original analytical tools developed solely for this purpose:

1.

2.

3.

4.

The radar t

racar data

- "Fast Prony's method algorithm" for real-time invariant parameter calculation of 4-dimensional radar data.
- "Prony K-Pulse" for calculating SEM coupling coefficients from retarded scattered E-field sampled data.
- "Polar mode A-scope" display file processing replacing part of the conventional radar targetindependent matched filter.
- 4. "Mode ratio discrimination detectors" for automatic radar target trigger and identification channels.

The radar target discrimination technique is evaluated on experimental radar data obtained from NSWC.

To my parents

Maurine and Lynwood Webb

academic advisor for research and A special note of in-depth critic The aut

The auti

his committee,

Lastly,

NSmC, Dahlgrer {
furnished meas

ACKNOWLEDGMENTS

The author wishes to express strong appreciation to his academic advisor, Dr. Kun-Mu Chen, for providing interesting topics for research and a very exciting and worthwhile dissertation goal. A special note of thanks is due to Dr. Dennis P. Nyquist for his in-depth critiques and analyses before this final form.

The author wishes to express his thanks to other members of his committee, Dr. Byron Drachman and Dr. S. Sayegh for their helpful comments.

Lastly, the author wishes to thank Dr. Bruce Hollmann of NSWC, Dahlgren, VA for collaboration on several papers for which he furnished measurement data also used herein.

LIST OF TABLES

LIST OF FIGURES

Chapter

1. INTRODUC

2. TRANSIES

2.1 E1d Ta² 2.2 Sir 2.3 As: Sci 2.4 E0, Rei 2.5 Pri

3. PROCESS WAVEFOR

3.1 Re
3.2 Sa
3.3 Pr
3.4 E/
3.5 ":
3.6 Me
Ex
3.7 Sc
3.8 Ot
3.9 E/
F1

4. PRONY

4.1 7. 4.2 7. 4.3 p.

TABLE OF CONTENTS

																	Page
LIST 0	F TAB	LES	• ,		•	•	•	•			•	•	•	•	•	•	vi
LIST O	F FIG	URES	•	•	•		•	•	•	•	•	•	•	•	•	•	vii
Chapte	r																
1.	INTR	ODUCT	ION	•	•	•	•	•	•	•	•	•	•	•	•	•	1
2.	TRAN	SIENT	ELE	CTRO	MAG	NET	ICS	FOF	R RA	NDAF	R TA	ARGE	ETS	•	•	•	8
	2.1			Fie	eld.	Inte	egra	al E	Equa	tic	on 1	for	Rac	dar			0
	2.2	Sing												tior	1	•	8 11
	2.4	Scat	tere	ed E- et Se	Fie	ld	•	•			•	•	•		>+ i/		17
	2.4		ptic			ν ι ι				•		:C L1	·	•			21
	2.5	Proc	essi	ng b	y D	igit	ta 1	Clu	itte	er M	1 ap	•	•	•	•	•	26
3.		ESSIN FORMS		CHN I	QUE	S F(OR I	EXTR	RACT	ING	S NA	\TUF	RAL •	MO[DE •	•	30
	3.1	Rece	ntic	n of		Dada	. n	Ta wo	ıat	C_ C	امنت	d					30
	3.2	Samp											•	•	•	•	32
	3.3	Proc	essi	ng a	Sc	atte	erec	1 E-	·Fie	eld'	Rec	ept	ior)	•	•	33
	3.4	Exci	tati	on c	f a	Sir	ng 1 e	e Na	tur	a 1	Mod	le h	lave	efor	m		35
	3.5 3.6	"Pol Meas	ar M	lode	A-S	cope	e" [Disp	lay	'S	.1.	·	la 1			•	43
	3.0	Extr	acti	on T	ech	nial	16 IIGUK	.e ()	_	, .			ia ve	. 01	-111	50
	3.7	Scal mete	ing	of t	he	Inva	aria •	ant	Rac	la r	Tar	get	. Pa	ra-	•	•	53
	3.8	Obse Wave			of	the	Abs	senc	e c	of a	Na	tur	al	Mod	ie	_	74
	3.9		nsio	n of			ode	to	Un	kno	own	Na t	ura	1	•	•	80
4.	PRON'	Y'S M					(-Pl	JLSE			•	•	•	•	•	•	82
•	4.1	The	Oria	inal	Pr	onv'	'c N	Meth	hod			_			_		82
	4.2	The Pron	"Pro	ny K	-Pu	3 <i>,</i> 1 se'	'			•	•	•	•	•	•	•	88
	4.3	Pron	v's	Meth	od	and	the	- K-	Pu1	Se	Der	ri va	tic	n	_		89

5. THE "FAS

5.1 Per Dis 5.2 Par 5.3 Par 5.4 Par 5.5 Cor 5.6 Spe

6. RADAR TA

6.1 Rei Dis 6.2 Dis 6.3 Pa

0.5 Pa 6.6 Pa 6.7 E-

7. CONCLUS

\$3010YES

A. Laplace Series

B. Laplace Sampler

C. Couplet

0. Compute Parts a

SECRETE

Chapte	er			Page
	4.4 Skip Sampling in Prony's Method 4.5 Zeros in the Data Matrix and "Class 2 Pro	ony	•	96
	Series"		•	107
	Series"		•	111
	4.7 Complex Root Degrees of Freedom	•	•	112
5.	THE "FAST" PRONY'S METHOD	•	•	117
	5.1 Performance Enhancements for Radar Targe	et		
	Discrimination		•	117
	5.2 Part 1The K-Pulse		•	119
	5.3 Part 2Roots for Excitation			130
	5.4 Part 3Amplitudes and Coupling Coefficie	ents		135
	5.5 Computational Comparisons for Part 1		•	138
	5.6 Special Cases for SEM Computations	•	•	143
	3.0 Special cases for Still compacations	•	•	143
6.	RADAR TARGET DISCRIMINATION TECHNIQUE	•	•	156
	6.1 Requirements for Automatic Radar Target			156
	Discrimination	•	•	156
	6.2 Discrimination Algorithm for Radar Target6.3 Part ATarget Library Prony K-Pulse Con-		•	157
	volution		•	160
	6.4 Part B "Fast Prony Convolution Algorithm	ı" .		163
	6.5 Part CDual "Polar Mode A-Scope" Display		_	164
	6.6 Part DTarget Trigger and Identification	1 .		165
	6.7 Empirical Illustration		•	168
7.	CONCLUSIONS		•	175
APPEND	DICES	•	•	178
Α.	LaPlace Transforms and Z-Transforms for Prony			
	Series	•	•	179
В.	LaPlace Transform Convolution Theorem for the			
	Sampler	•	•	199
С.	Couplets and the K-Pulse Singularity Theorem .	. •	•	208
D.	Computer Code for "Fast Prony's Method Algorit	:hm"		
.	Parts and other Programs		•	224
DEEEDE	ENCES			241

Table

4-1 Prony's M

4-2 Late-Time

5-1 K-Pulse T

5-2 Computati

5-3 Calculat

6-1 Radar Tar

6-2 Mode Rati Surrary

LIST OF TABLES

Table		Page
4-1	Prony's Method Tests	115
4-2	Late-Time Model Test of Prony's Methods	116
5-1	K-Pulse Termination Flags	129
5-2	Computation Comparison for Part 1	141
5-3	Calculations for the "Fast" Prony K-Pulse	142
6 - 1	Radar Target Discriminant	159
6-2	Mode Ratio Discrimination Detector Performance	167
	Summary	10/

Figure

- I-1 Typi
- 1-2 Top Wave
- 2-1 A Pe Tran
- 2-2 Illu Reta
- 2-3 Ante
- 2-4 Equi
- 2-5 Tran
- 2-6 Rada
- 2-7 Meas 12" at a
- 2-8 Clut
- 3-1 Clut
- 3-2 TEM Pada
- 3-3 2nd
- 3-4 2rd
- 3-5 2nd
- 3-8 2nd
- 3-7 Sahe Figu

LIST OF FIGURES

Figure	,	1	Page
1-1	Typical Radar Environment and Target RCS		2
1-2	Top Views of Aspect-Angle Dependencies of Object Waveforms of Speech and Radar	•	3
2-1	A Perfectly Conducting Target Illuminated by a Transient Incident E-field	•	9
2-2	Illustration of Assured Late-time Response of Retarded Scattered E-field	•	16
2-3	Antenna Plots of the Magnitude of Four of the Farfield Modes of a Thin Cylinder	•	20
2-4	Equipment Set-Up for Transient EM Reception		22
2-5	Transmitter Pulse Observed in Transmission Line .	•	23
2-6	Radar Receiving TEM Horn Antenna	•	25
2-7	Measured Pulse Response of a Cylindrical Target of 12" Length 12" Above a Ground Plane Illuminated at an Aspect Angle of 45 Degrees	•	27
2-8	Clutter-reduced 12" Skew Wire Radar Target	•	28
3-1	Clutter-reduced 18" Spherical (imaged) Radar Target Return		44
3-2	TEM Horn Receiving Antenna Used for Spherical Radar Targets		45
3-3	2nd Cosine Mode Convolution	•	47
3-4	2nd Sine Mode Convolution	•	47
3-5	2nd Mode Envelope Radar A-Scope	•	49
3-6	2nd Mode Rotation Radar A-Scope	•	49
3-7	Spherical Radar Target Response by Deconvolving Figure 3-2 from Figure 3-1	•	52

3-10 3rd Mo

3-11 4th Mc

3-11 46/17

3-12 Clutte Respon

3-13 lst Mo Cylind

3-14 1st Mo Cylin

3-15 1st M Cylin

3-16 3rd M

3-17 3rd M Cylir

3-18 3rd 1 Cylin

3-19 5th Cyli

3-20 5th Cyli

3-21 5th Cyl-

3-22 7th Cyl

3-23 7th Cy1

3-24 7th Cy1

Figure		Page
3-8	1st Mode Waveform Excitation of a 19" Diameter Sphere	54
3-9	2nd Mode Waveform Excitation of a 19" Diameter Sphere	55
3-10	3rd Mode Waveform Excitation of a 19" Diameter Sphere	56
3-11	4th Mode Waveform Excitation of a 19" Diameter Sphere	57
3-12	Clutter-Reduced 18.6" Radar Target Antenna Terminal Response	59
3-13	1st Mode Waveform Excitation of Correctly-Sized Thin Cylinder Baseline Radar Target	61
3-14	1st Mode Waveform Excitation of 10% Undersized Thin Cylinder Radar Target	63
3-15	1st Mode Waveform Excitation of 10% Oversized Thin Cylinder Radar Target	64
3-16	3rd Mode Waveform Excitation of Correctly-Sized Thin Cylinder Baseline Radar Target	66
3-17	3rd Mode Waveform Excitation of 10% Undersized Thin Cylinder Radar Target	68
3-18	3rd Mode Waveform Excitation of 10% Oversized Thin Cylinder Radar Target	69
3-19	5th Mode Waveform Excitation of Correctly-Sized Thin Cylinder Baseline Radar Target	- 70
3-20	5th Mode Waveform Excitation of 10% Undersized Thin Cylinder Radar Target	71
3-21	5th Mode Waveform Excitation of 10% Oversized Thin Cylinder Radar Target	72
3-22	7th Mode Waveform Excitation of Correctly-Sized Thin Cylinder Baseline Radar Target	73
3-23	7th Mode Waveform Excitation of 10% Undersized Thin Cylinder Radar Target	75
3-24	7th Mode Waveform Excitation of 10% Oversized Thin Cylinder Radar Target	76

3-26 4th Mod Cylinde

3-27 10th Mc Cylinde

4-1 Undeter

4-2 Major S Display

4-3 Clutter (18"), Convolu

4-4 First M Skip Sa

4-5 Convolu Figure the Rac

4-6 Convol. Figure Target

4-7 Third 'Sample:

4-8 Convol. Figure Radar

4-9 Convol Figure Target

4-10 Synthe Incide

5-1 Major

5-2 Flow c Algori

Figure		Page
3-25	2nd Mode Waveform Excitation of Baseline Thin Cylinder Radar Target at Normal Incidence	78
3-26	4th Mode Waveform Excitation of Baseline Thin Cylinder Radar Target at Normal Incidence	79
3-27	10th Mode Waveform Excitation of Baseline Thin Cylinder Radar Target at Normal Incidence	81
4-1	Undetermined Coefficients of Prony's "Essai "	87
4-2	Major Steps in the Generation of Radar A-Scope Displays	93
4-3	Clutter-Reduced Radar Response of a Thin Cylinder (18"), the Prony K-Pulse from Skip Samples, the Convolution, and Its Envelope in Decibels	94
4-4	First Mode Waveform Excitation Synthesized from Skip Samples of a Thin Cylinder Radar Target	98
4-5	Convolution of the First Mode Excitation Vector of Figure 4-4 with a New Set of Skip Data Points in the Radar Target Response File	100
4-6	Convolution of the First Mode Excitation Vectors of Figure 4-4 with all of the Data Points in the Radar Target Response File	102
4-7	Third Mode Waveform Excitation Synthesized from Skip Samples of a Thin Cylinder Radar Target	103
4-8	Convolution of the Third Mode Excitation Vectors of Figure 4-7 with a New Set of Skip Data Points in the Radar Target Response File	105
4 -9	Convolution of the Third Mode Excitation Vectors of Figure 4-7 with all of the Data Points in the Radar Target Response File	106
4-10	Synthetic "Class 2 Prony Series" at 1 Milliradian Incidence	114
5-1	Major Parts of Prony's Method Summarized	118
5-2	Flow Chart for K-Pulse Part of "Fast Prony's Method Algorithm"	131

Figure

5-3 "F

"F 5-4

"F F: 5-5

5-6 Pr

5-7 Pr

5-8 No

5-9 No

5-10 Tw

5-11 Tw

5-12 Tm

6-1 Pa

6-2 ":

6-3 DU

6-4 Du Mo

6-5 Di Mi

7-1 FC

A-1 A;

A-2 Ct

A-3 A;

A-4 C(

9-1

Re Ti

Figure		Page
5-3	"Fast Prony's Method Algorithm" Block Diagram	. 134
5-4	"Fast Prony's Method Algorithm" Substituted in Figure 4-6	. 139
5-5	"Fast Prony's Method Algorithm" Substituted in Figure 4-9	. 140
5-6	Prony K-Pulse Worksheet #1	. 145
5-7	Prony K-Pulse Worksheet #2	. 146
5-8	Non-Late-Time Prony K-Pulse Worksheet #1	. 148
5-9	Non-Late-Time Prony K-Pulse Worksheet #2	. 150
5-10	Two Mode Prony K-Pulse Worksheet #1	. 151
5-11	Two Mode Prony K-Pulse Worksheet #2	. 152
5-12	Two Mode Prony K-Pulse Worksheet #3	. 153
6-1	Radar Target Discrimination Algorithm Summary	. 158
6-2	"Unknown Target" Sampled Data Files	. 169
6-3	Dual "Polar Mode A-Scope" Displays for 1st Target	. 103
0-3	Mode	. 171
6-4	Dual "Polar Mode A-Scope" Displays for 2nd Target Mode	. 172
6-5	Dual "Polar Mode A-Scope" Displays for 3rd Target Mode	. 174
7-1	Forecasted Radar Target Discrimination Capability	. 176
A-1	Approximating Function from Sampled Data	. 182
A-2	Change of Variable from z-plane to s-plane	. 188
A-3	Approximating Function for Fixed m	. 191
A-4	Contour Integration for V(z,m)	. 198
B-1	Region of Absolute Convergence for a Product in	
D-I	Time Domain	205

C-2 Single

C-3 Two Ter

Figure									Page
B-2	Counterclockwise Contour Closure	•	•	•	•	•	•	•	206
B-3	Clockwise Contour Closure	•	•	•	•	•	•	•	206
C-1	Single Term "Prony Series," v(t)	•	•	•	•	•	•	•	213
C-2	Single Term "Prony series," w(t)	•	•	•	•	•	•	•	214
C-3	Two Term "Prony Series," s(t) .	•		•				•	217

which is radar set the trans target in scattered to the race terminals of the tay the radar based sole The radar target asp

Figure 1-2

mtating s

is to rade

ratural mo

believed to

foundation

In

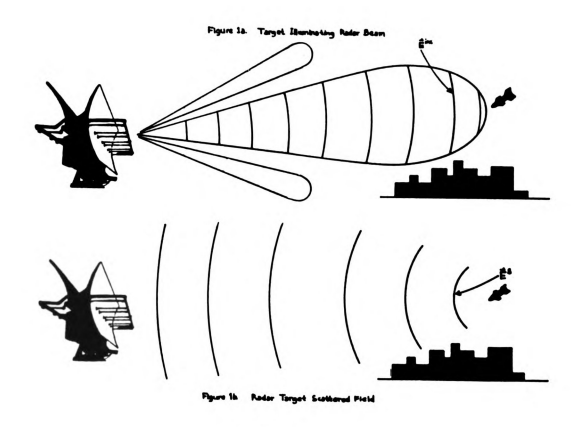
CHAPTER 1

INTRODUCTION

A radar target discrimination technique will be developed which is machine implementable. Figure 1-1 illustrates a typical radar set with a radar target cross-section plot. In the top sketch the transmitted waveform is propagated from the antenna to the radar target in the presence of ground clutter. In the middle sketch the scattered electric field from the target and clutter is propagated to the radar receiving antenna. The received signal at the antenna terminals is very highly dependent upon the location and orientation of the target relative to the radar site. This is illustrated by the radar target cross-section plot. A positive target identification based solely on the target radar skin return is not an easy problem. The radar target discrimination solution disclosed here will be radar target aspect-angle independent and target range independent. Figure 1-2 illustrated an analogy with human brain processing of a rotating speaker. The crucial characteristic of the target required is to radiate a reasonable portion of its energy in one or more natural mode waveforms. All conducting vehicles with sharp edges are believed to adequately satisfy this requirement.

In Chapter 2 we will develop the transient electromagnetic foundation of the technique. We start with the electric field integral





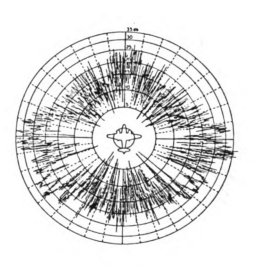


Figure 1-1. Typical Radar Environment and Target RCS.



Figure

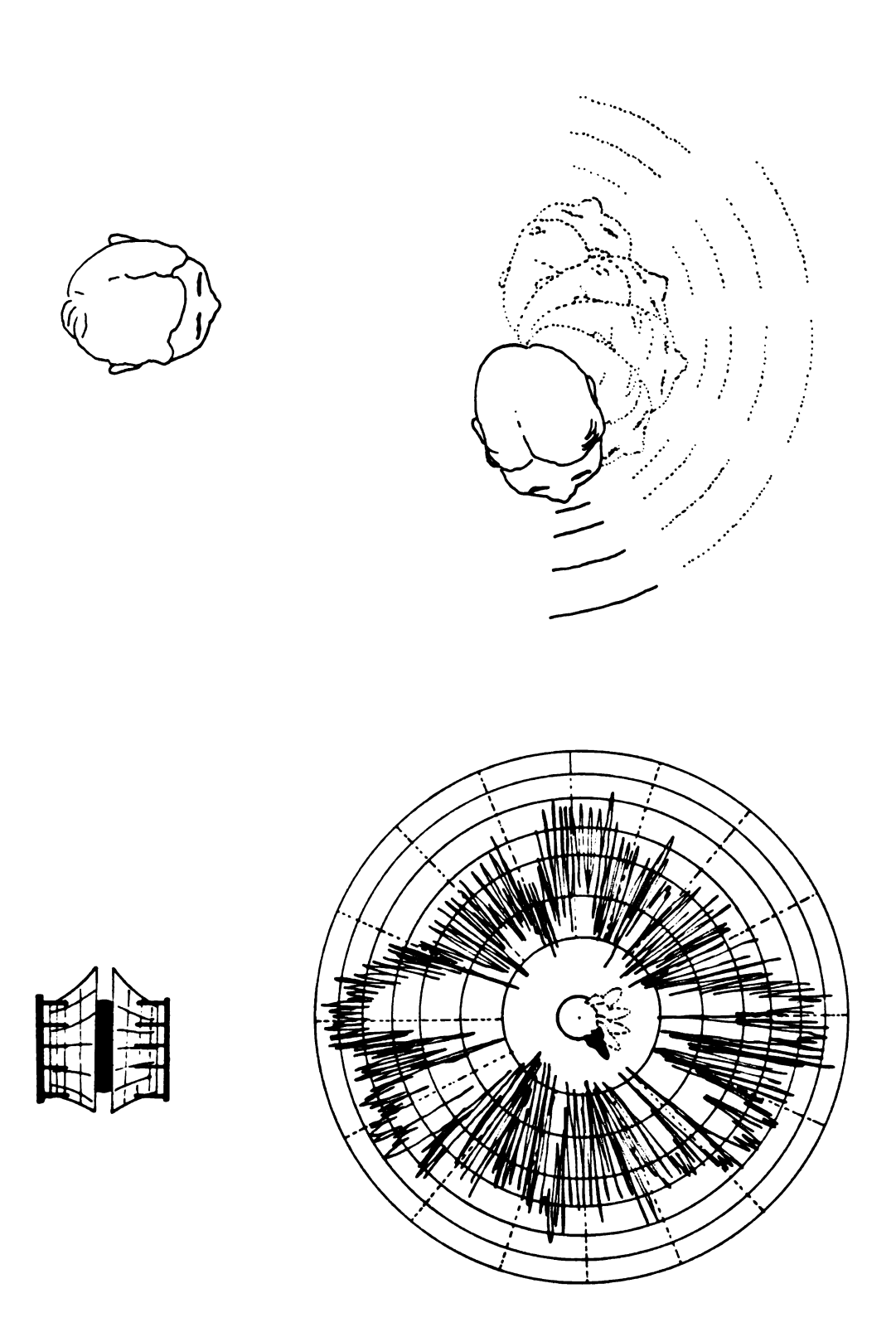


Figure 1-2. Top Views of Aspect-Angle Dependencies of Object Waveforms of Speech and Radar.

equation (propelled Method (Samodel solution) assect—and then present shift in the country of th

extracting collection primary conference is important display. It radar targe replace par filter and tracking.

is not pla

In

noise." The tions, uncar

Presents di

of that pre

In (^{when} the rad equation (EFIE) which is extremely difficult to solve for any self-propelled radar target. We introduce the Singularity Expansion Method (SEM) as a model solution to the EFIE. We show that this model solution has, even for a simple scatterer, all the extreme aspect-angle dependencies observed in the empirical radar data. We then present the equipment set-up for obtaining radar data and then the ground clutter map processing. Note that we cannot have Doppler shift in this stationary set-up. For clarity Doppler exploitation is not placed in the formulation.

In Chapter 3 we introduce the processing techniques for extracting a single natural mode waveform from a large but finite collection of natural mode waveforms. We then introduce one of the primary contributions of this dissertation, rectangular and polar representations of natural mode waveforms. The polar representation is important enough that we shall call it a radar "polar mode A-scope" display. The data from this display will be used in the automatic radar target discrimination algorithm. The data of these displays replace part of the conventional radar target-independent matched filter and detector techniques traditionally used for detection and tracking. In this chapter we use empirical radar data which always presents difficulties to the discrimination process much in excess of that presented by synthetic data artificially corrupted by "white noise." The observed defects are primarily due to equipment distortions, uncancelled clutter, thermal noise, and quantitization errors.

In Chapter 4 we introduce our primary technique to be used when the radar target possesses a complexity which is obviously

beyond the Ca Prony's meth of the SEM m duce E. Kenn contemplated formulation o first part of our "Prony's discriminatio original Pror notation der which for laconditioned. introduce a on empirica brown, 2 wet popular th the import concept a ™agnetic the super; Prony's ne

discrimination of constitution of constitution of me

beyond the capabilities of analytical calculation. Our technique, Prony's method, can be used to experimentally obtain the parameters of the SEM model of the radar target's EFIE. We will also introduce E. Kennaugh's K-Pulse concept. His transmit formulation is not contemplated to ever be used. However it is shown that a receive formulation of the K-Pulse can be generated as an extension of the first part of Prony's method. This K-Pulse, properly specified as our "Prony's K-Pulse," is a crucial building block in our radar target discrimination technique. In this chapter we will introduce the original Prony's method, and then perform the now standard matrix notation derivation. This lends to standard matrix computer routines which for large numbers of sampled data values are increasingly "ill conditioned." To minimize the size of the matrix to be used, we introduce a skip sampling technique and illustrate its performance on empirical radar target data. We then introduce the extended Prony's method or least-squares formulation which is probably more popular than the regular Prony's method. At this point we introduce the important concept of "complex root degrees of freedom." This concept appears to be quite useful for our 4-dimensional electromagnetic problem. A dramatic example is presented which illustrates the superiority of the regular Prony's method over the extended Prony's method in certain cases which will be used in our radar target discrimination technique. Further, the regular Prony's method does not constitute an irreversible process as do all least-squares processing techniques. This is an important consideration for the design of modern "quiet" radars.

In C+

an original c is desired fo plex root deg hardware reso speed by appr mear real-tir and its subse

The s for the firs: Promy's meth

processing.

solution. B be a useful

In C

ination algo use of the scope" dispi sersitivity !

a second ti-

plays make p Suitable for

In c ittlementat: In Chapter 5 we present the "fast" Prony's method, which is an original contribution of this dissertation. The "fast" algorithm is desired for two reasons. The first is to fully exploit the "complex root degrees of freedom" concept to the maximum with minimal hardware resources. The second is to increase the computational speed by approximately an order of magnitude in order to permit near real-time calculation of a dual "polar mode A-scope" display and its subsequent processing for automatic target discrimination processing.

The structure of the unsymmetric Toeplitz matrix is explored for the first time and there is an additional by-product of the "fast Prony's method algorithm": it produces two solutions instead of one solution. Both are usable, but a comparison of the two appears to be a useful analytical tool.

In Chapter 6 we present the automatic radar target discrimination algorithm. Several of the crucial original concepts are the use of the "2nd K-Pulsed convolution" and the dual "polar mode Ascope" displays, where for the first time we exploit the well known sensitivity of Prony's method to noise by performing a Prony's method a second time. Further, the format of the "polar mode A-scope" displays make possible the original "mode discrimination ratio detectors" suitable for automatic processing in a monopulse-like fashion.

In Chapter 7 we shall make some forecasts on the technique's implementation and uses and the impact of Doppler shift.

Appentransforms, z for notation
Appenthe analytica varying opera
Appen
K-Pulse Singuingte easily de

Appen

useful.

٠

.

Appendix A is a complete section for review of Laplace transforms, z-transforms, modified z-transforms, and consultation for notation used throughout this dissertation.

Appendix B is the Convolution Theorem for the Sampler. It is the analytical tool necessary for the handling of the linear, <u>time</u>-varying operation of the sampler.

Appendix C is an introduction to time domain couplets and the K-Pulse Singularity Theorem. These are simple but powerful tools not easily derivable in the continuous time domain.

Appendix D is the collection of computer programs found useful.

boundary valu

In the

be the foundat

which we will

have already o

Let us

in Figure 2-1

concepts. The

transient, in a

target surfact

density, c(F,

generate a sc:

dent and scat

dition, that

conductor mus

equation (2-1

CHAPTER II

TRANSIENT ELECTROMAGNETICS FOR RADAR TARGETS

2.1 Electric Field Integral Equation for Radar Targets

In this section we shall develop the transient electric field boundary value problem for a perfectly conducting object. This will be the foundation for the electromagnetic response of our radar target which we will assume is highly conducting at radar frequencies. We have already described the physical formulation in Figure 1-1.

Let us examine a simple 3-dimensional radar target shape as in Figure 2-1 in order to define our electromagnetic quantities and concepts. The perfectly conducting radar target is illuminated by a transient, incident plane wave, $\vec{E}^{inc}(\vec{r},t)$, which excites, on the target surface, the induced current density $\vec{K}(\vec{r},t)$, and charge density, $\sigma(\vec{r},t)$. These induced current and charge densities, in turn, generate a scattered wave, $\vec{E}^{s}(\vec{r},t)$. It is the summation of the incident and scattered wave which must satisfy the familiar boundary condition, that the tangential electric field at the surface of a perfect conductor must be zero for all time. This relation is expressed by equation (2-1).

$$\hat{t} \cdot (\vec{E}^{inc}(\vec{r},t) + \vec{E}^{s}(\vec{r},t)) = 0 \quad \text{for all } \vec{r} \in A$$
 (2-1)

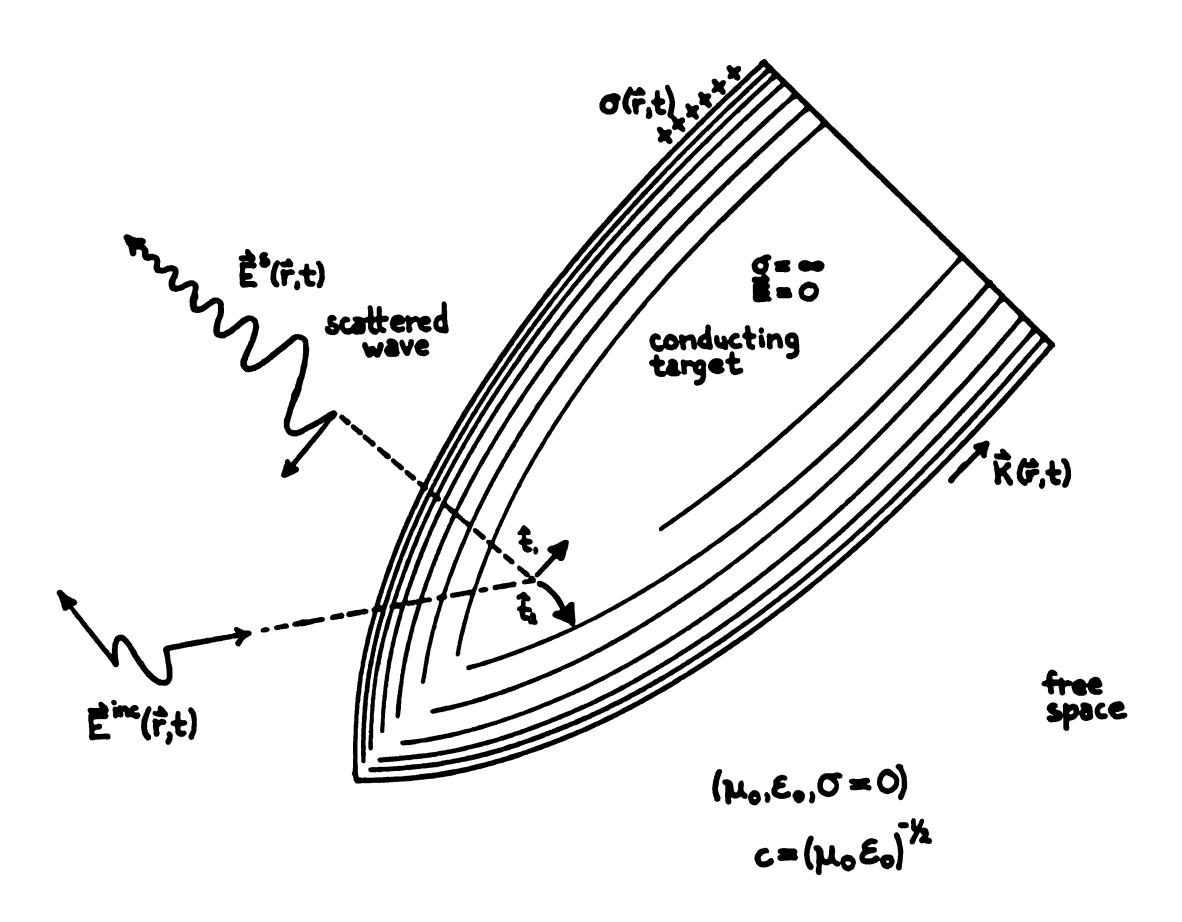


Figure 2-1. A Perfectly Conducting Target Illuminated by a Transient Incident E-field.

In equation radar target

ř.

We w

the retarded

(2-2).

 $\vec{E}^{S}(\vec{r},t)$

These retard

Ā(r,

We will ultim

when it is c

7.7

Next we shall

(2-5) to obt

Es

In equation (2-1), A denotes the set of all external points of the radar target and \hat{t} is any unit tangent vector to the targer surface at \vec{r} .

We wish to express the scattered field, $\vec{E}^S(\vec{r},t)$, in terms of the retarded scalar and vector potential (ref 2-1) given by equation (2-2).

$$\vec{E}^{S}(\vec{r},t) = -\nabla \Phi(\vec{r},t) - \frac{\partial}{\partial t} \vec{A}(\vec{r},t)$$
 (2-2)

These retarded potentials are given by equations (2-3) and (2-4).

$$\Phi(\vec{r},t) = \int_{A} \frac{\sigma(\vec{r},t-R/c)}{\epsilon_{\bullet}^{4}\pi R} dA', \quad R = |\vec{r}'-\vec{r}| \qquad (2-3)$$

$$\vec{A}(\vec{r},t) = \int_{\Delta} \frac{\mu \vec{k}(\vec{r},t-R/c)}{4\pi R} dA', \quad R = |\vec{r}'-\vec{r}| \qquad (2-4)$$

We will ultimately use conservation of charge given by equation (2-5) when it is convenient to eliminate $\sigma(\vec{r},t)$.

$$\nabla \cdot \vec{K}(\vec{r},t) = -\frac{\partial}{\partial t} \sigma(\vec{r},t)$$
 (2-5)

Next we shall take the Laplace transforms of equations (2-1) through (2-5) to obtain equations (2-6) through (2-10)

$$\hat{t} \cdot (\hat{E}^{inc}(\vec{r},s) + \hat{E}^{s}(\vec{r},s)) = 0 \quad \text{for } \vec{r} \in A$$
 (2-6)

$$\vec{E}^{S}(\vec{r},s) = -\nabla \Phi(r,s) - s\vec{A}(\vec{r},s) \qquad (2-7)$$

In equati

ř.

the retar

(2-2).

Ē^S(r̄,

These ret

•

We will use when it is

-

Next we shall (2-5) to o

î

ξs

In equation (2-1), A denotes the set of all external points of the radar target and \hat{t} is any unit tangent vector to the targer surface at \vec{r} .

We wish to express the scattered field, $\vec{E}^S(\vec{r},t)$, in terms of the retarded scalar and vector potential (ref 2-1) given by equation (2-2).

$$\vec{E}^{S}(\vec{r},t) = -\nabla \Phi(\vec{r},t) - \frac{\partial}{\partial t} \vec{A}(\vec{r},t)$$
 (2-2)

These retarded potentials are given by equations (2-3) and (2-4).

$$\Phi(\vec{r},t) = \int_{A} \frac{\sigma(\vec{r},t-R/c)}{\varepsilon 4\pi R} dA', \quad R = |\vec{r}'-\vec{r}| \qquad (2-3)$$

$$\vec{A}(\vec{r},t) = \int_{\Delta} \frac{\vec{k}(\vec{r},t-R/c)}{4\pi R} dA', \quad R = |\vec{r}'-\vec{r}| \qquad (2-4)$$

We will ultimately use conservation of charge given by equation (2-5) when it is convenient to eliminate $\sigma(\vec{r},t)$.

$$\nabla \cdot \vec{K}(\vec{r},t) = -\frac{\partial}{\partial t} \sigma(\vec{r},t)$$
 (2-5)

Next we shall take the Laplace transforms of equations (2-1) through (2-5) to obtain equations (2-6) through (2-10)

$$\hat{t} \cdot (\hat{t}^{inc}(\hat{r},s) + \hat{t}^{s}(\hat{r},s)) = 0 \quad \text{for } \hat{r} \in A$$
 (2-6)

$$\vec{E}^{S}(\vec{r},s) = -\nabla \Phi(r,s) - s\vec{A}(\vec{r},s) \qquad (2-7)$$

7

Substituti (2-6), we

> ^ †

Equation (EFIE (Elec

 $\int_{A} (7!7)$

where

2.2 Singuestration (Si

The for the phy

$$\Phi(\vec{r},s) = \int_{A} \frac{\sigma(\vec{r},s) \exp(-sR/c)}{\epsilon_0 4\pi R} dA'$$
 (2-8)

$$\vec{A}(\vec{r},s) = \int_{A} \frac{\mu_0 \vec{K}(\vec{r},s) \exp(-sR/c)}{4\pi R} dA'$$
 (2-9)

$$\nabla \cdot \vec{K}(\vec{r},s) = -s\sigma(\vec{r},s)$$
 (2-10)

Substituting equation (2-10) into (2-8) and equation (2-9) into (2-6), we obtain equation (2-11).

$$\hat{\mathbf{t}} \cdot (\hat{\mathbf{E}}^{inc}(\hat{\mathbf{r}},s) + \nabla \int_{A} \frac{\nabla^{\bullet} \cdot \hat{\mathbf{K}}(\hat{\mathbf{r}},s) \exp(-sR/c)}{s \varepsilon_{0} 4\pi R} dA'$$

$$- s \mu_{0} \int_{A} \frac{\hat{\mathbf{K}}(\hat{\mathbf{r}},s) \exp(-sR/c)}{4\pi R} dA') = 0 \qquad (2-11)$$

Equation (2-11) rewritten as in equation (2-12) is often called the EFIE (Electric Field Integral Equation).

$$\int_{A} (\nabla^{!} \vec{k} (\vec{r}, s) (\hat{t} \cdot \nabla) - \gamma^{2} \hat{t} \cdot \vec{k} (\vec{r}, s)) \frac{\exp(-sR/c)}{4\pi R} dA' = -\epsilon_{0} s \hat{t} \cdot \vec{E}^{inc} (\vec{r}, s)$$
for all $\vec{r} \in A$ (2-12)

where $\gamma = s/c$

2.2 Singularity Expansion Method (SEM) Notation

The EFIE, equation (2-12) is not particularly easy to solve for the physical radar targets. The method of attack used in this

dissertation nated for motivation the appear

S(t) :

cosinusoi

As is well

L(exp

The right ity in th

יש ווו ציו

(2-12) in

is a prob time vari

could be

excitatic

yet separ

(rather t

For simpl

(2-15).

dissertation is called the Singularity Expansion Method (SEM), originated for electromagnetics by C. E. Baum (ref. 2-2). The physical motivation for SEM is the observation that radar returns signals have the appearance of being a sum of damped cosinusoids. A single damped cosinusoid will be represented as in equation (2-13).

$$S(t) = \frac{1}{2}A(\exp(s_1t) + \exp(s_1^*t))$$
 with $Re(s_1) < 0$ (2-13)

As is well known, the Laplace transforms of a complex exponential is given by equation (2-14)

$$L(exp(s_1t) = (s-s_1)^{-1}, Re(s) > s_1$$
 (2-14)

The right-hand side of equation (2-14) displays a simple pole singularity in the s-plane from which the SEM obtains part of its nomenclature.

There are two issues to be kept in mind about using equation (2-12) in the physical radar problem that SEM must address. One, it is a problem which must be simultaneously solved in 3 space and one-time variables. Two, the simplest physical radar excitations which could be observed are not impulses in space and time, but plane wave excitations. Hence the aspect-angle dependencies need to be present, yet separable, if the solution actually models the radar target.

Without loss of generality, we will assume only simple poles (rather than multiplicities of finite degree as developed in ref. 2-2). For simple poles the SEM solution to the EFIE is given by equation (2-15).

$$\vec{K}_{p}(\vec{r},s) = \sum_{\alpha} \eta_{\alpha}(\P,s) \stackrel{\rightarrow}{\nu_{\alpha}} (\vec{r}) \hat{f}_{p}(s) (s-s_{\alpha})^{-1} + \vec{W}^{\kappa}(\P,\vec{r},s)$$
 (2-15)

where α is the index for all of the target natural frequencies

 s_{α} is a natural frequency of the radar target

 $(s-s_{\alpha})^{-1}$ is the s-plane pole at s_{α}

- $\hat{f}_{p}(s)$ is the pulse shape of the incident radar plane wave
- $\eta_\alpha(\P,s)$ an entire function is the coupling coefficient from the incident plane wave to the natural mode of current density
- p denotes one of the possible incident polarizations
- ¶ is the aspect-angle dependent vector
- $\vec{W}^{\kappa}(\vec{r},\vec{r},s)$ is the entire function which may be required for convergence

It should be observed that equation (2-15) appears similar to a partial fraction expansion of a (meromorphic) function with a finite number of pole singularities. The less usual term, the entire function of the far right, \overrightarrow{W}^{K} , is due to the infinite summation index, α . The Mittag-Leffler theorem (ref. 2-9) warns us that this may (or may not) be required. An entire function is analytic everywhere in the finite s-plane, but may have poles at infinity. For our radar target natural modes with Re(s) < 0, we could expect the existence of a representation of the entire function with its poles at infinity on the left-hand side of the s-plane. In general, the entire function

will not be obdefined).

For an

entire function this entire for interested in

 $\vec{k}_{p}(\vec{r},s) =$

rewrite equat

In equidependencies coefficient w

target's uniq It is

domain since

containing s time domain.

wave is purel

^{one} convoluti

coupling coef

tion called a

yields the "l

expresed by e

 $\vec{k}(\hat{r},t) =$

will not be observable in what we shall call the "late-time" (to be defined).

For any finite summation on α , we shall formally drop the entire function. For the infinite summation we shall suppress writing this entire function, \vec{W}^{K} , recalling its presence only when we are interested in "early-time" results. With this in mind, we shall now rewrite equation (2-15) and use equation (2-16) from now on.

$$\vec{k}_{p}(\vec{r},s) = \sum_{\alpha} \eta_{\alpha}(\P,s) \vec{v}_{\alpha}^{\kappa}(\vec{r}) \hat{f}_{p}(s) (s-s_{\alpha})^{-1}$$
 (2-16)

In equation (2-16) it should be noted that all aspect angle dependencies for an individual natural mode occur only in the coupling coefficient which is a factor in the complex amplitude of the radar target's unique natural mode of current density and natural frequency.

It is not quite so simple to write equation (2-16) in the time domain since in each term of the series there are 3 distinct factors containing s dependencies. These factors become convolutions in the time domain. For clarity, we will assume that the incident plane wave is purely impulsive, making f(s) = 1 and we are left with only one convolution which when performed is called an SEM "class 2" coupling coefficient for the current density. There is a simplification called an SEM "class 1" coupling coefficient which accurately yields the "late time" value of the natural mode current density as expresed by equation (2-17).

$$\vec{K}(\vec{r},t) = u_{-1}(t-t') \sum_{\alpha} \eta_{\alpha}(\P,s_{\alpha}) \vec{v}_{\alpha}^{\kappa}(\vec{r}) \exp(s_{\alpha}t)$$
 (2-17)

The numique, it si ling coefficient is the time 1 coefficient if as well as the causality to thin cylinder be somewhere assured that in general, I have propagated somewhere propagated somewhere assured that in general, I have propagated somewhere assured that in general, I have propagated somewhere propagated somewhere assured that in general, I have propagated somewhere propagated somewhere propagated somewhere assured that in general, I have propagated somewhere assured that in general, I have propagated somewhere propagated somewhere assured that in general is the propagated somewhere assured that it is the propagated somewhere assured the propagated somewhere as the propagated some

t" = max 8,:

for some sha

equation (2-

conservative
shape is not
From causali
the far side
require, in

incident imposed ficient

scattered E.

The new constant t' is a new parameter which need not be unique, it simply states when (in time) we may use a simplified coupling coefficient. We will be interested in a still later time t" which is the time lag for which we may use the simplified "class 1" coupling coefficient for the calculation of the retarded scattered E-field as well as the current density. In the general case we will invoke causality to derive a parameter we will use later. Let us consider a thin cylinder radar target as in Figure 2-2. Let our observation point be somewhere on the negative z-axis (e.g., z = 0-). In order to be assured that the simplified coupling coefficient may be used, we must, in general, have a delay long enough for the incident plane wave to have propagated clear of our target as viewed in retarded time at our observation point. This assured value of time, t", is given by equation (2-18) for an impulsive plane wave on a very thin cylinder.

$$t'' = \max_{\theta, \phi} \{L/c + L/c \cos \theta\} = \max_{\theta, \phi} \{2-\text{way transit time}\}$$
 (2-18)

For some shapes (e.g., a perfect sphere), this is known to be too conservative (ref. 2-2). But his a priori knowledge of its complete shape is not a permissible part of a radar discrimination problem. From causality we would not know for sure if there existed a defect on the far side of the sphere. Propagation at the speed of light will require, in general, a two-way transit time of the object by the incident impulsive plane wave in order to use the simplified coupling coefficient for the damped cosinusoid responses in the retarded scattered E-field.

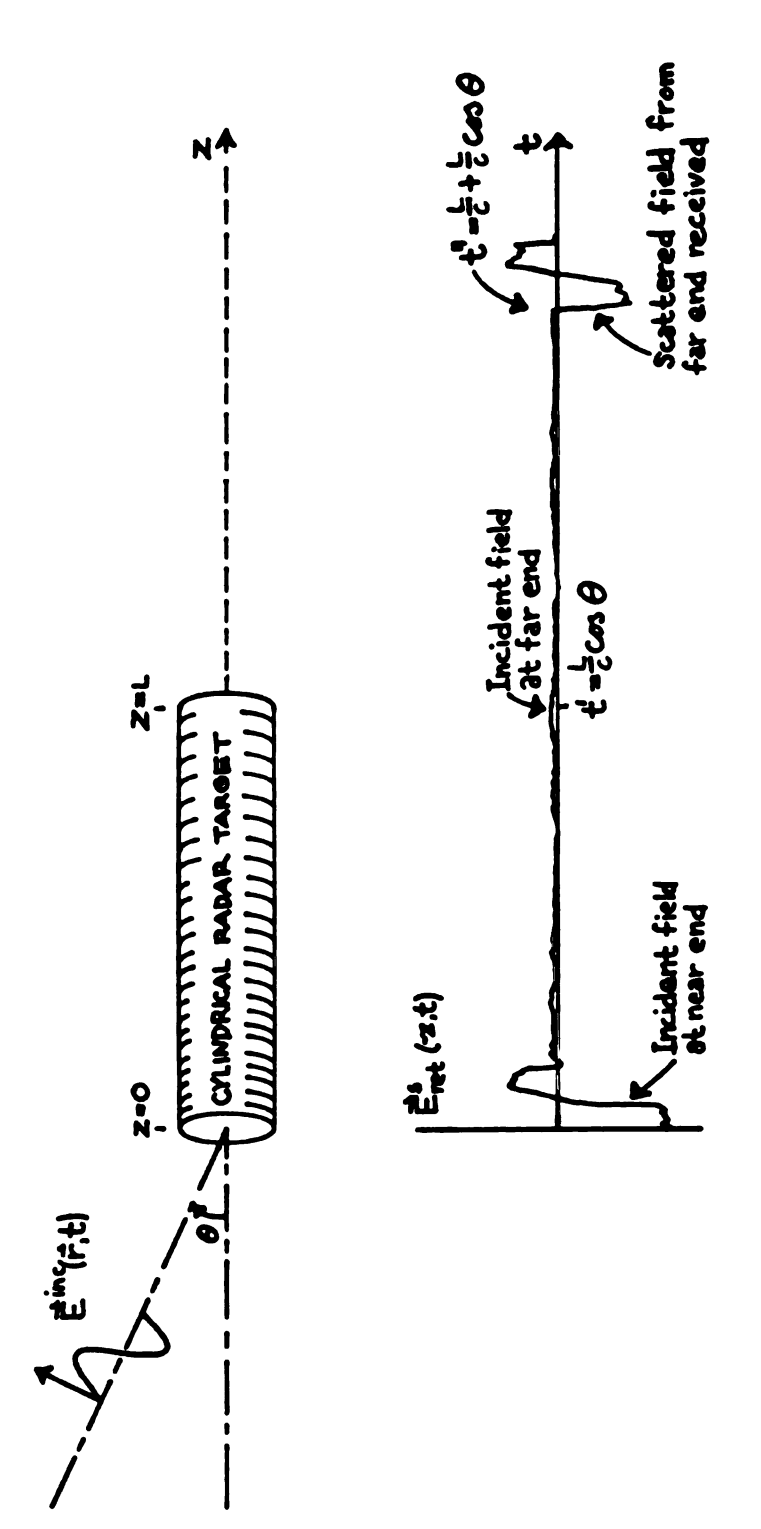


Figure 2-2. Illustration of Assured Late-time Response of Retarded Scattered E-field.

Keepi

coefficients or t > t", we the "late-time SEM time-doma radar discrime tional technological technolo

2.3 Aspect Radar Tange

We

tice of the

target curr
may calcula
substitutio
for one or
culate the

the z-axis

from equa:

Keeping in mind that both the "class 1" and "class 2" coupling coefficients will give identical time domain results in the "late-time" or t > t", we need several more observations. First it is only in the "late-time" region that the aspect-angle dependent factors in the SEM time-domain expansion are constant. Our aspect-angle independent radar discrimination technique will exploit this effect. Our computational technique, however, will be convolutional and will resemble a "class 2" type calculation. We will now look at the difference between a "class 2" and "class 1" representation. In the time domain the difference is obviously a time limited function for each individual mode. This is because of causality prior to the incident plane wave and identity of the two representations in the "late-time." Therefore, the aspect-angle dependence of the individual modes, potentially lasts on the basis of causality for a duration of t", the two-way transit time of the radar target by an incident plane wave.

2.3 Aspect-Angle Dependency of Radar Target Scattered E-Field

We have used the EFIE to conceptually calculate the radar target current density. After solving for the current density, we may calculate the scattered E-field, $\vec{E}^S(\vec{r},t)$, anywhere in space by substitution into equation (2-7). In fact, only the far-field E-field for one or two polarizations are all that are desired. We will calculate the E_θ far-field pattern for a wire-like target aligned with the z-axis. The numerical value of the scattered field is calculated from equation (2-7) to give equation (2-19).

from equation associated of observance far-field p

in equation

(2-9) requi

E^S ret

We will no

- **317**CH

Ê

Now using (2-22).

È, (÷

*here

$$\vec{v} \cdot \hat{\vec{E}}^{S}(\vec{r},s) = -s \vec{\theta} \cdot \hat{\vec{A}}(\vec{r},s) - \vec{\theta} \cdot \nabla \Phi(\vec{r},s)$$

$$\approx + s \sin \hat{\vec{A}}_{Z}(\vec{r},s) - \frac{1}{r} \frac{\partial}{\partial \theta} \Phi(\vec{r},s) \qquad (2-19)$$

From equation (2-19) we note the additional inverse distance associated with the scalar potential will, in general, eliminate its observance in the far-field pattern. Before we define the normalized far-field pattern, note that the presence of exp(-sR/c) in equation (2-9) requires our introduction of the retarded scattered field as in equation (2-20).

$$\hat{E}_{ret}^{s}(r,s) = \exp(s|r|/c) \hat{E}^{s}(r,s)$$
 (2-20)

We will not define the far field ${\rm E}_{\theta}$ total scattered radiation field as given by equation (2-21).

$$\hat{E}_{\theta}(\theta,\phi,s) = \lim_{|\vec{r}| \to \infty} |\vec{r}| \hat{E}_{ret}^{s}(\vec{r},s) \cdot \hat{\theta}$$
 (2-21)

Now using only the first term in equation (2-19), we obtain equation (2-22).

$$\hat{E}_{\epsilon}(\theta,\phi,s) = \lim_{|\vec{r}| \to \infty} |\vec{r}| s \sin\theta \hat{A}_{z}(\vec{r},s) \exp(s |\vec{r}|/c)$$

$$= \vec{\theta} \cdot s \sin\theta \frac{\mu_{0}}{4\pi} \int_{A} \vec{K}(\vec{r},s') \exp(-s\Delta R/c) dA' \qquad (2-22)$$

where
$$\Delta R = \lim_{|\vec{r}| \to \infty} \{|\vec{r}' - \vec{r}| - |\vec{r}|\}$$

Now the SEM sci that each mode scattered far i pole as in Equ.

 $E_{\xi}^{\alpha}(\theta, \tau) =$

= 5,5

its maximum va the coupling c r' (on the sur coupling coeff

for a far fiel

ξ²₆,(ξ,:) :

normalized pat

for f

As an example thin wire sca

tinctly diffe

time dependen

Now the SEM solution for $\vec{K}(\vec{r},s)$ was given by equation (2-15). Noting that each mode has its own pole singularity, we can obtain the scattered far field of a single mode by the Cauchy residue about that pole as in Equation (2-23).

$$E_{\theta}^{\alpha}(\theta, \phi) = \text{Residue } \hat{E}_{\theta}(\theta, \phi, s)$$
 ?-23)

$$= s_{\alpha}^{\alpha} \sin \theta \frac{\mu_{0}}{4\pi^{0}} \int_{A} \eta_{\alpha}(\P, s_{\alpha}) \vec{\nabla}_{\alpha}^{\kappa}(\vec{r}') \hat{f}(s_{\alpha}) \exp(-s_{\alpha} \Delta R/c) dA' \qquad (2-24)$$

For a far field pattern, we normalize equation (2-24), typically by its maximum value. Note carefully that the pulse shape, f(s), and the coupling coefficient are not functions of the integration variable r' (on the surface, A). Assuming only that the pulse shape and coupling coefficient are nonzero, they will not be part of the normalized pattern $E_{\Theta n}^{\alpha}(\theta,\phi)$ given by equation (2-25).

$$E_{\theta n}^{\alpha}(\theta, \phi) = \frac{E_{\theta}^{\alpha}(\theta, \phi)}{\max_{\theta} E_{\theta}^{\alpha}(\theta, \phi)} = \frac{\sin \theta}{\sin \theta} \int_{A}^{\infty} \tilde{\nabla}_{\alpha}^{\kappa}(\tilde{r}) \exp(-s_{\alpha} \Delta R/c) dA'$$

for
$$\hat{f}(s_{\alpha})\neq 0$$
, $\eta_{\alpha}(\P,s_{\alpha})\neq 0$ (2-25)

As an example, (ref. 2-3, pp. 1609), the patterns of four modes of a thin wire scatterer are illustrated in Figure 2-3.

It should be observed that the individual patterns are distinctly different as a function of aspect-angle after the nonharmonic time dependence has been surpressed. For actual reception of a radar

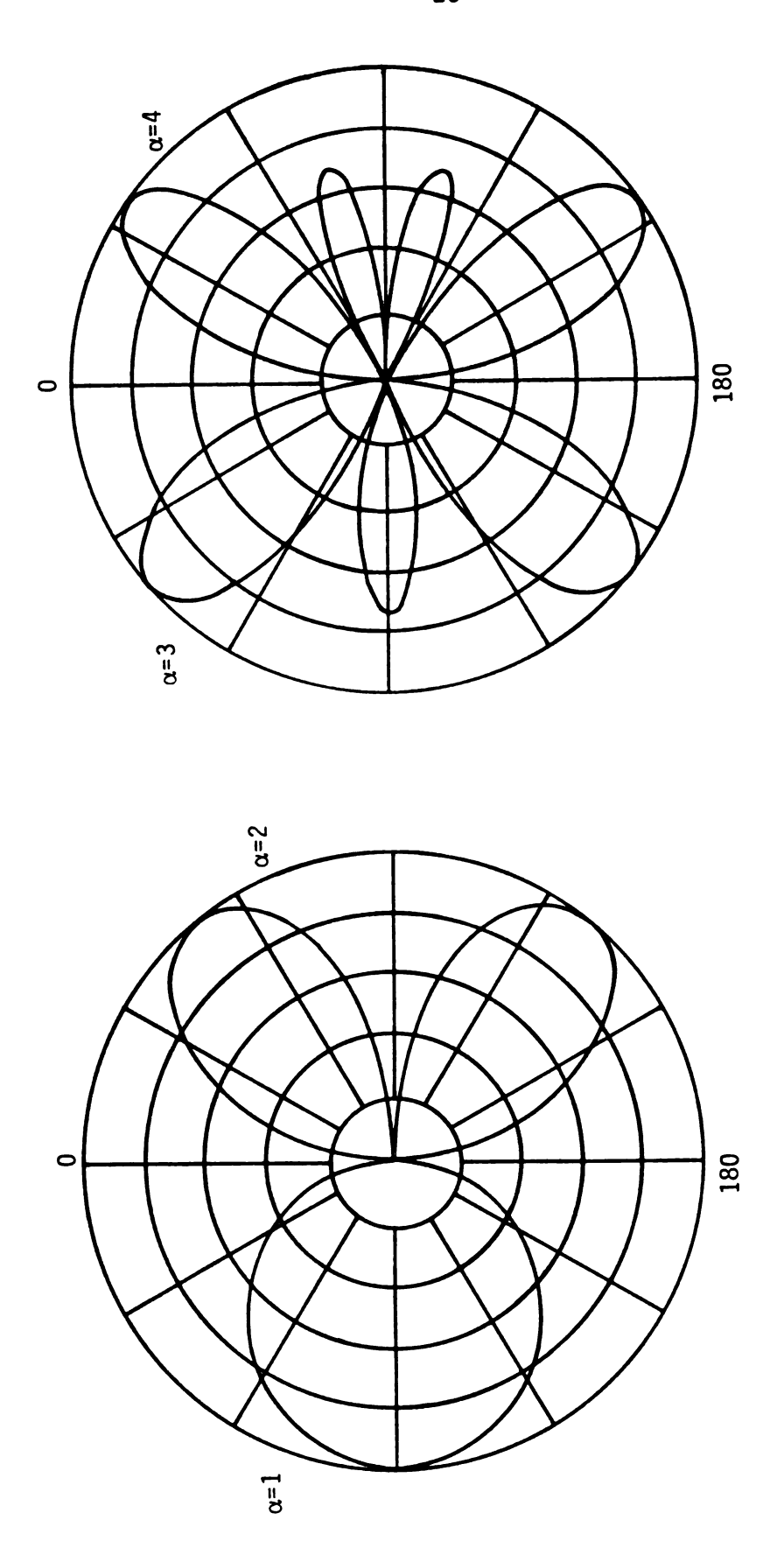


Figure 2-3. Antenna Plots of the Magnitude of Four of the Far-field Modes of a Thin Cylinder.

target return dependence must based on its e

2.4 Equipment Electromagneti

The trefrom an electric ties due to the plane wave or ment is optimeradar pulse smit is not in goor target. He enhanced the consetup for the data in this consetured the consetup for the data in this consetured the consetup for the data in this consetured the co

The triggre 2-5, wr.

3 ns fall tirextending app.

Hollmann at th

equipment self

for processing

plane wave on

target return the nonharmonic time dependence and the aspect angle dependence must be decoded simultaneously to identify a radar target based on its electromagnetic invariant parameters.

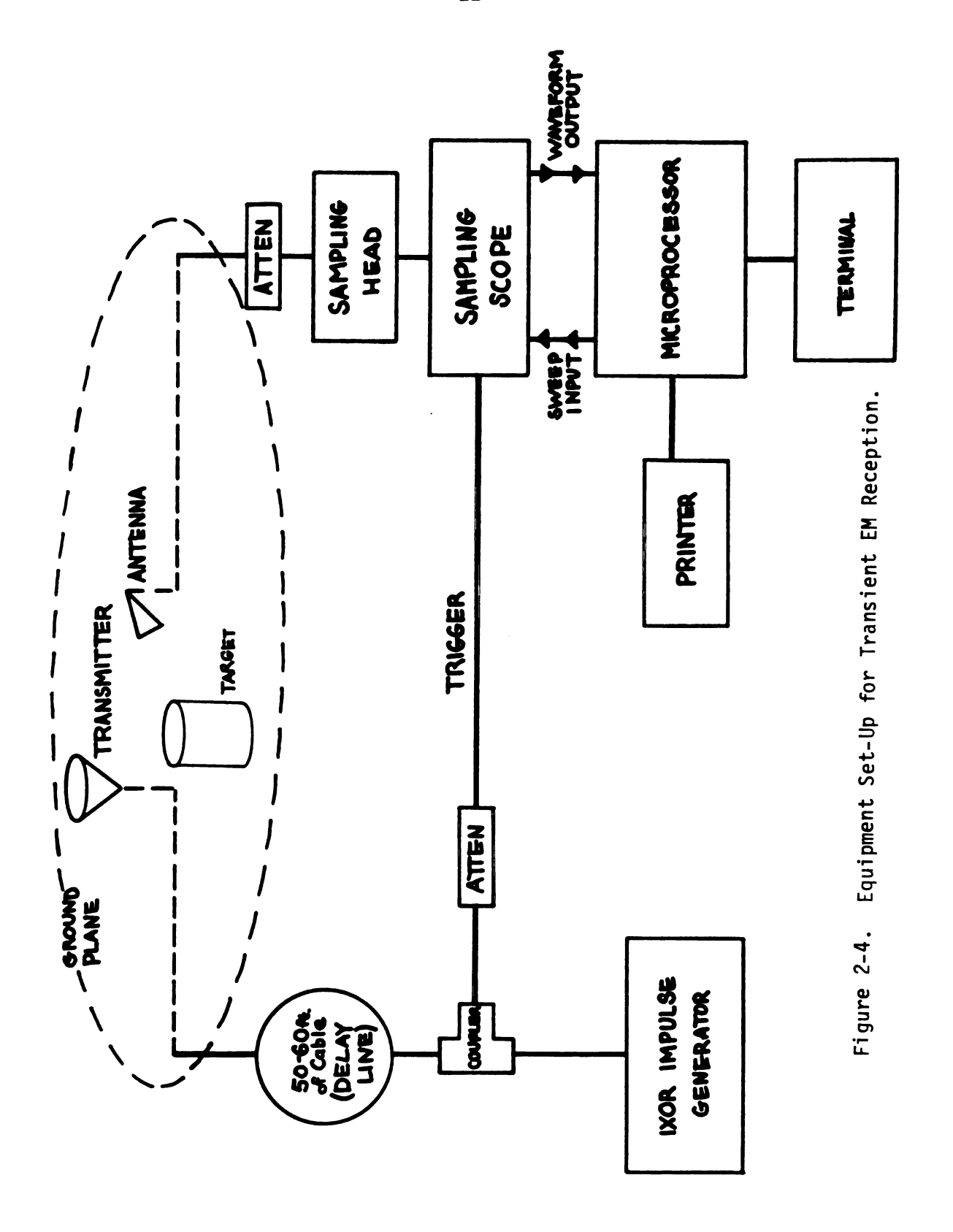
2.4 Equipment Set-Up for Transient Electromagnetic Reception

The theory of SEM has shown (Ref. 2-3) that the radar return from an electromagnetic scatterer can be decomposed into singularities due to the scatterer and those originating with the radar pulsed plane wave or transmitted signal. A radar receiver in a benign environment is optimized to enhance the signal-to-noise ratio of the returned radar pulse shape. It may also have provisions to reject clutter, but it is not in general optimized for the return of a specific scatterer or target. Hence we require a different reception technique to enhanced the discrimination process. Figure 2-4 shows the equipment set-up for transient electromagnetic reception used for the initial data in this dissertation. The data were collected by Dr. Bruce Hollmann at the Naval Weapons Center at Dahlgren (ref. 2-5).

The transmitted pulse originates from an impulse generator, Figure 2-5, with approximately .2 ns rise time, .7 ns duration, and .3 ns fall time. The transmit antenna is an imaged conical antenna extending approximately 10 feet over an aluminum ground plane. These equipment selections are made to avoid adding singularities to the pulse shape, f(s), of the incident plane wave on the radar target. For processing simplicity it is desirable to approximate an impulsive plane wave on the radar target.

TRANSMITTER

۳ کا



1.2

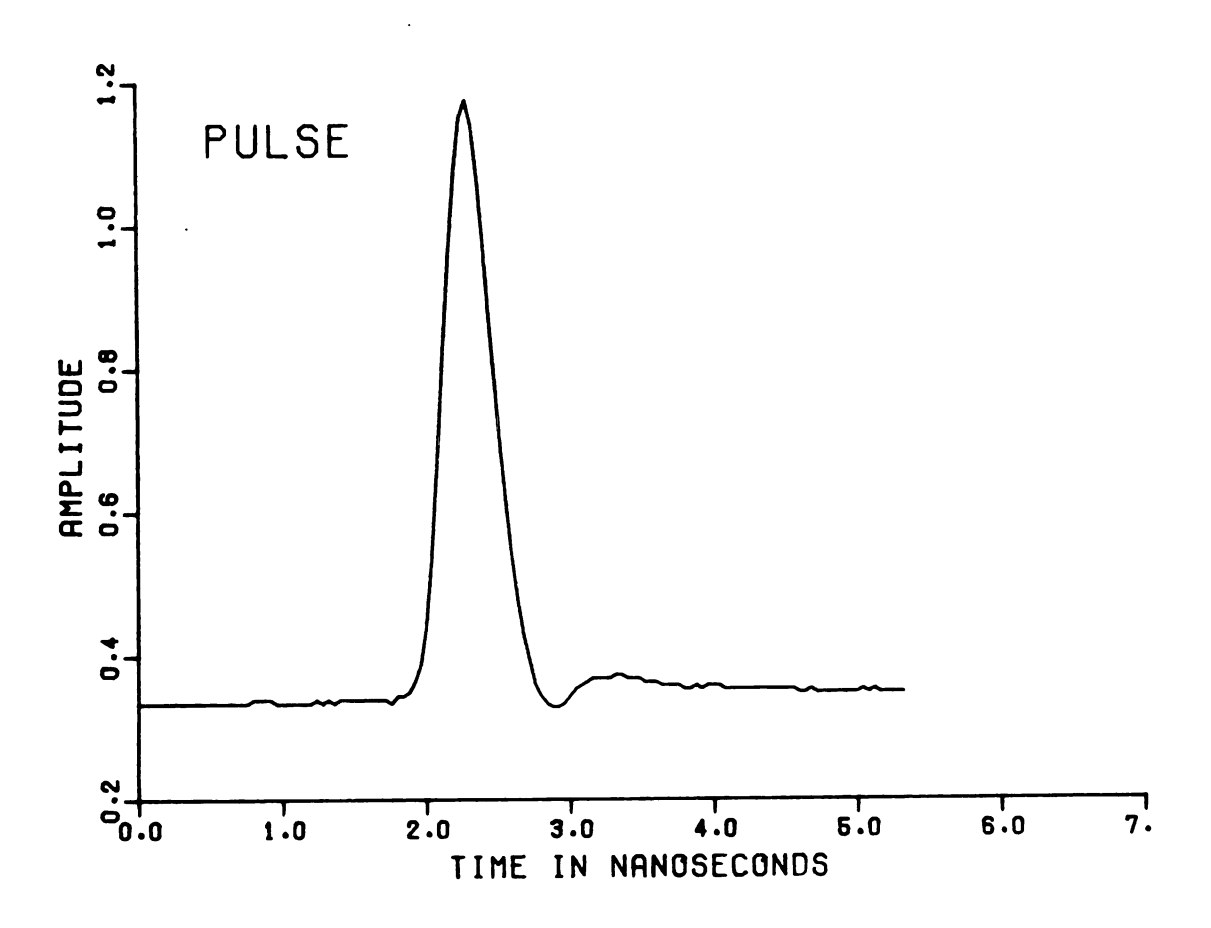


Figure 2-5. Transmitter Pulse Observed in Transmission Line

plare. gain, ar

on the r

sampling response

the anal

at 256 pr

are quant

only sign

uniform q

introduce

 $E^{r}n_{q}^{2}$

So the qua

conversion Th

and receive

lateral tr

 $^{
m erator}$ $_{
m dire}$

time respon

The receiving antenna is a TEM horn also imaged on the ground plane. This choice is made as a trade-off among usable bandwidth, high gain, and minimum blockage and distortion of the incident plane wave on the radar target.

The radar receiver in this equipment set-up is a microwave sampling oscilloscope. The sampling heads of the oscilloscope have a response into the 12.5 GHz range. A microcomputer actually samples the analog output waveforms of the sampling oscilloscope.

The microprocessor stores sampled data values of radar return at 256 precise discrete time values. At each of these 256 discrete times, 100 radar return sampled data values are averaged. All values are quantized to 8 bits. The quantized 100 sample averaging is the only signal-to-noise enhancement performed by the equipment. For uniform quantitization, the rms value of the quantitization noise introduced is (ref. 2-6) given by equation (2-26).

$$E\{n_q^2\} = \frac{\Delta^2}{12} = \frac{2^{-2} \text{ bits}}{12} = (-6 \text{ bits} - 10.8)_{in dB}$$
 (2-26)

So the quantitization rms noise is at least -58.8 dB for an 8 bit A/D conversion.

The spatial orientation of the transmit antenna, radar target, and receive antenna is important. For the bistatic radar data used in this dissertation, they are configured approximately as an equilateral triangle. Figure 2-5 shows the output of the impulse generator directly into the sampling oscilloscope. Figure 2-6 is the time response waveform for the TEM horn directly viewing the transmit

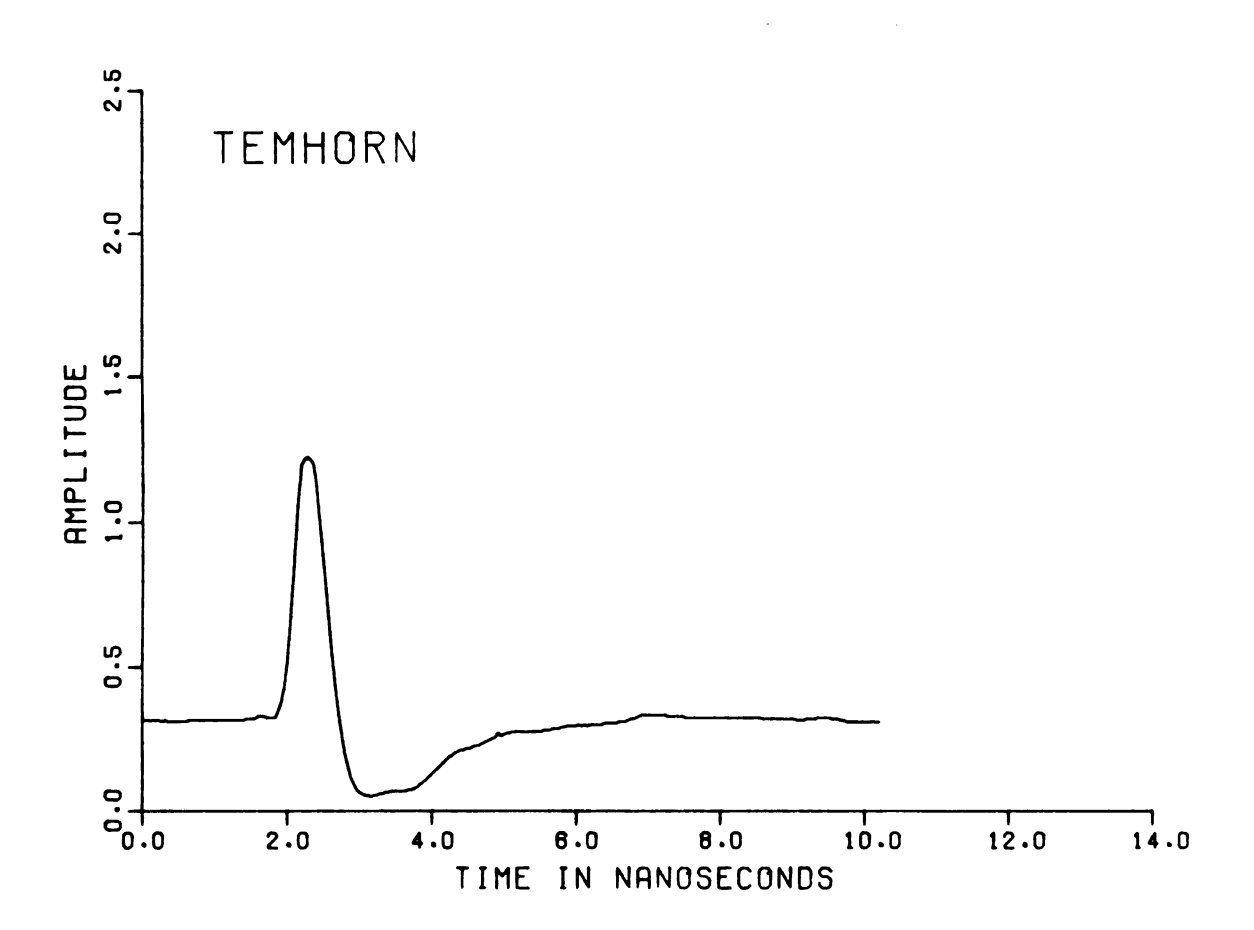


Figure 2-6. Radar receiving TEM horn antenna.

antenna.

form in 1

waveform

2.5 Proc

amounts (

moise.]

repeatab?

ground re

quently (

storage (

called a

Red data

clutter;

is physic

plus noi:

the direc

is not of

directly

thermal ,

Note tha

can cause

an expand

file. I

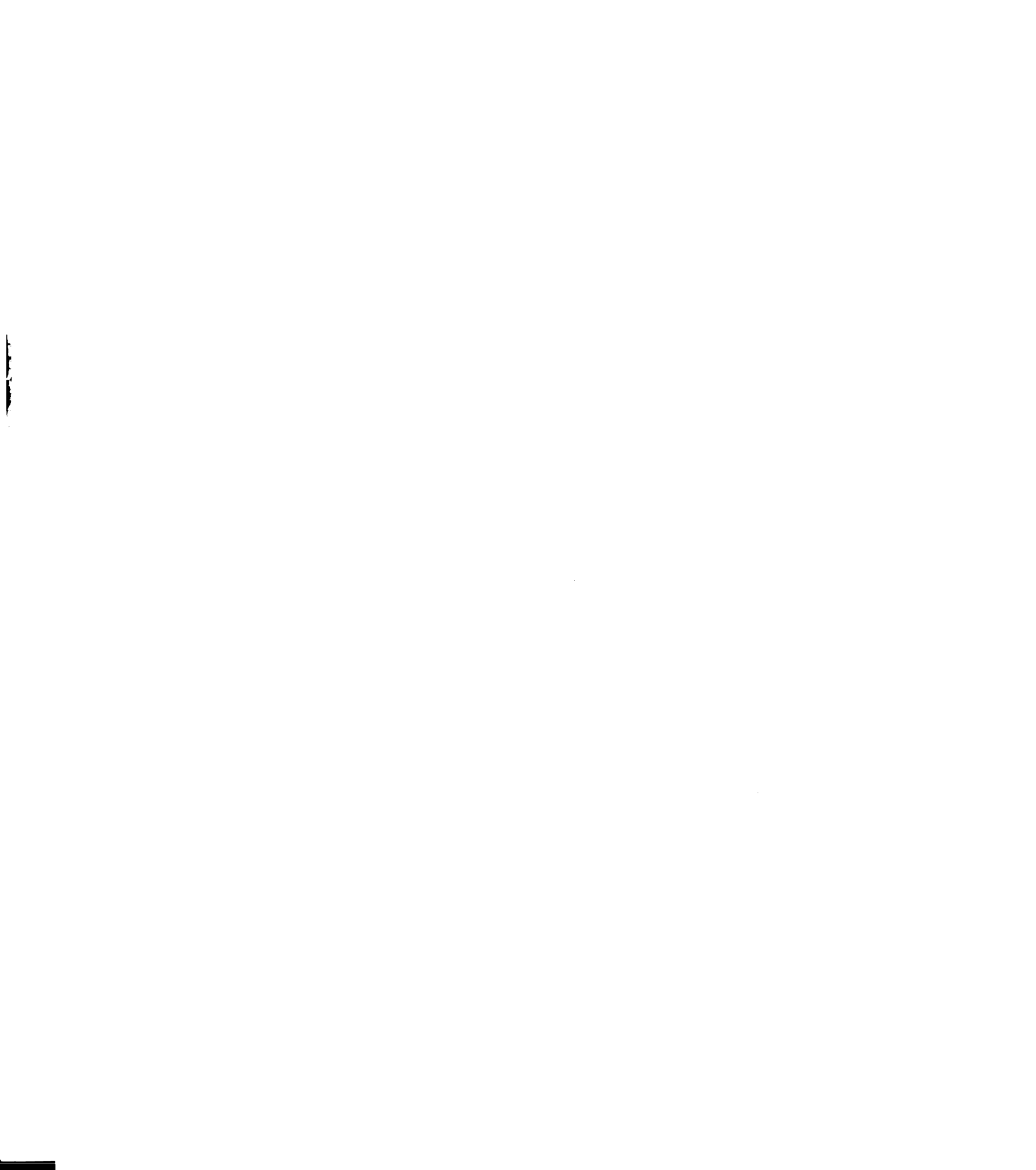
antenna. It may be seen that even with the care provided, the waveform in the receiving antenna transmission line is distorted from the waveform in the pulse generator transmission line.

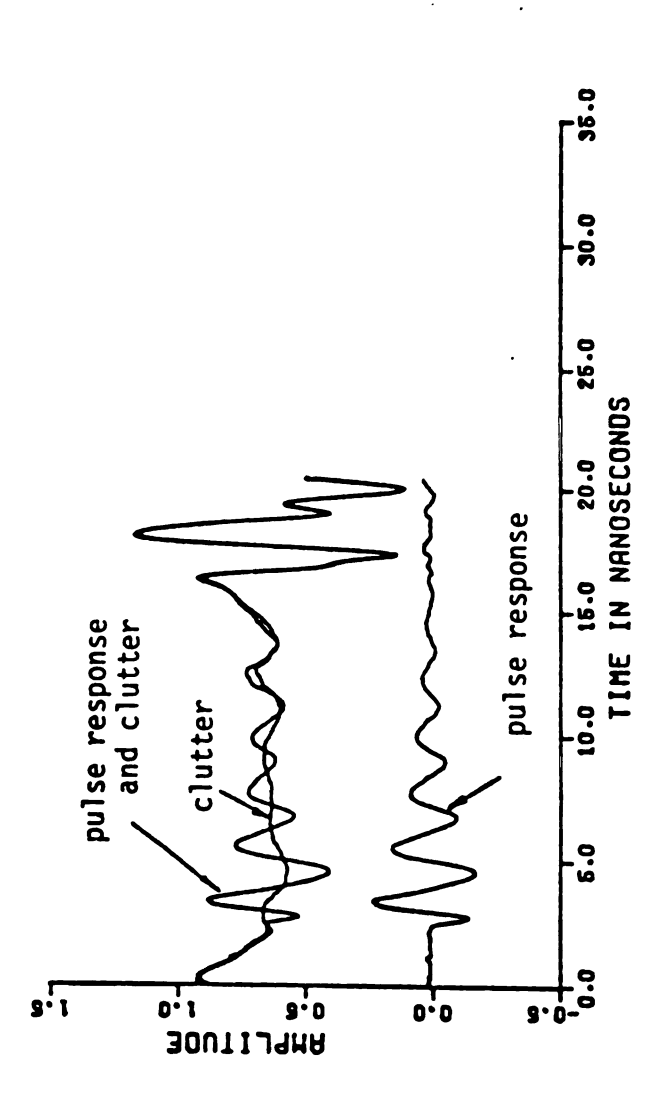
2.5 Processing by Digital Clutter Map

Any radar equipment set-up can be expected to have large amounts of radar clutter (Ref. 2-7, pp. 9) in addition to thermal noise. In the short-time period, the clutter is deterministic and repeatable. An early method of clutter rejection is to store the background returns for a radar without a target present and then subsequently perform a comparison with radar target might be present. The storage of the background radar return without a target is often called a "ground clutter map" (ref. 2-8, p. 403).

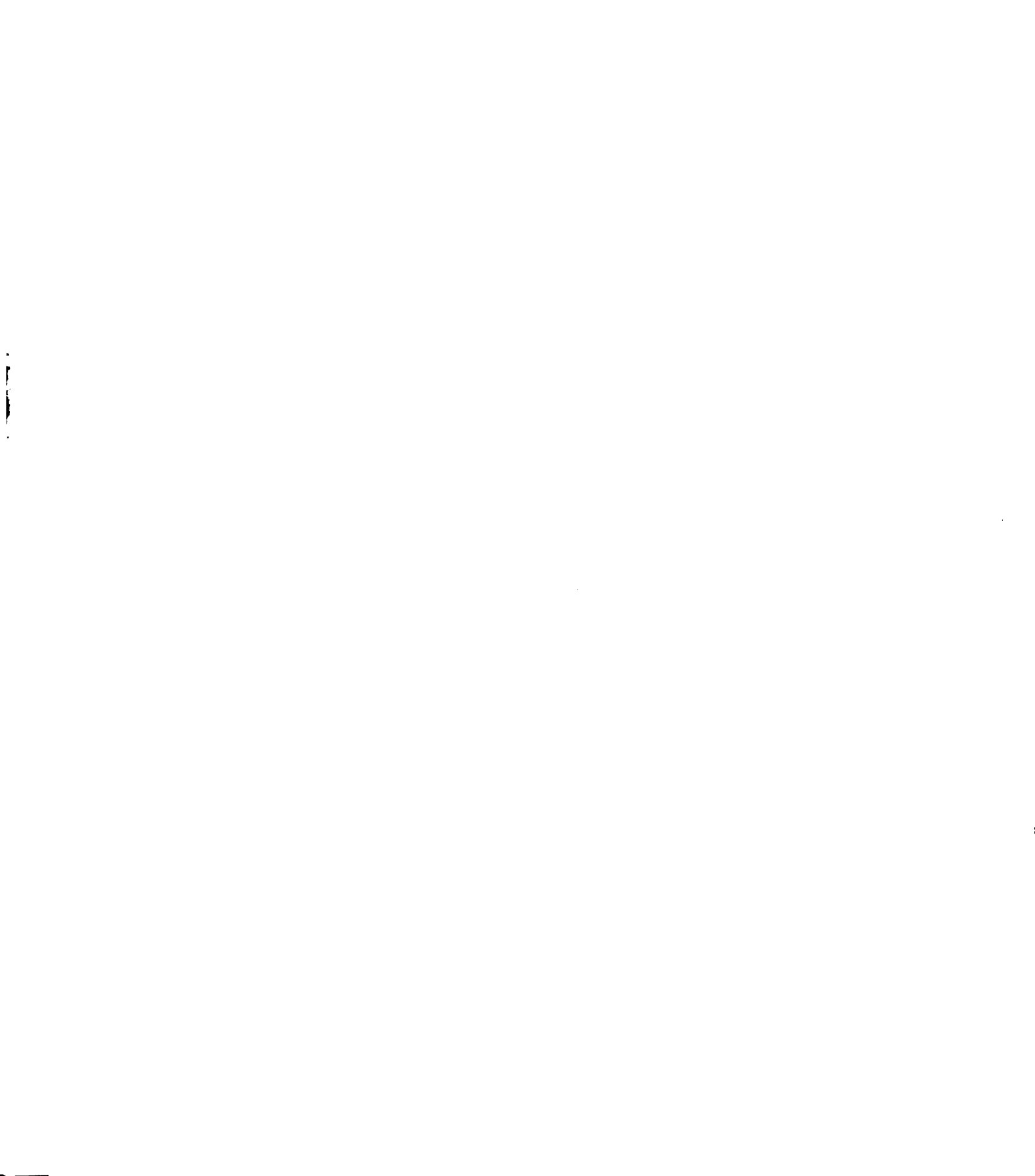
Pigure 2-7 contains three traces each of which is 256 sampled data points. One of the top two traces is labeled target plus clutter and noise. The other trade is labeled clutter. The target is physically absent during the measurement of this file of clutter plus noise. This clutter trace constitutes our ground clutter map in the direction of the target to be measured. The 8 bit quantitization is not obvious from these two traces. The processing performed is to directly substract the clutter map from the target plus clutter and thermal noise file. The bottom trace is the processed difference.

Note that any drift in DC level or gain drift of the analog amplifiers can cause distortion. Figure 2-8 is the same processed file, but with an expanded scale. Now the quantitization and drift is visible in the file. It can also be calculated that the maximum number of bits used





Measured Pulse Response of a Cylindrical Target of 12" Length 12" Above a Ground Plane Illuminated at an Aspect Angle of 45 Degrees. Figure 2-7.



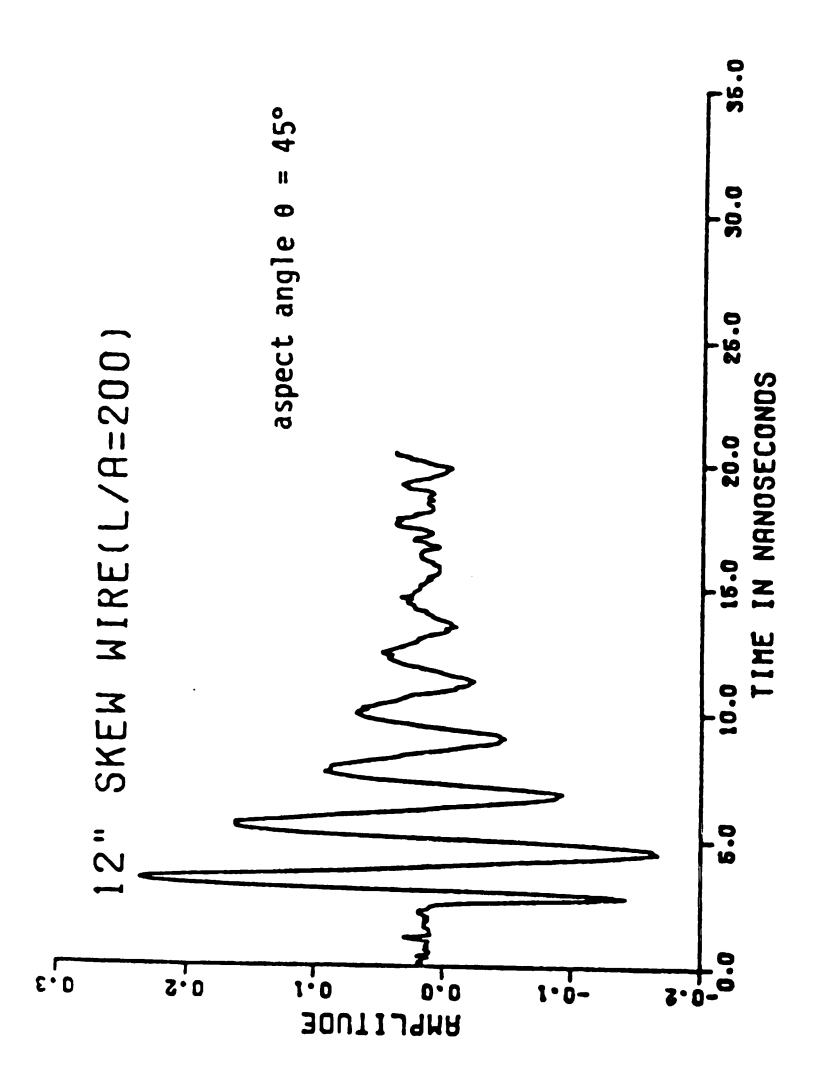


Figure 2-8. Clutter-reduced 12" Skew Wire Radar Target.

by the process end is only 3

-46.8 dB to -2

The quisamples adjace

or order of o

to completely

by the processed radar target return is a peak of 6 bits, but near the end is only 3 bits. Hence the quantitization noise varies from -46.8 dB to -28.8 dB.

The quantitization is further exaggerated by differencing of samples adjacent in time. The rationale for the time differencing is to completely eliminate DC bias in the data and to reduce the degree or order of other distortions which may be present.

In th

will receive

far-field ret

antenna termi the antenna t

scattered fie

ing antenna's

polarization

pair of pola

this chapter

component. We s

tered retard

 $tar_{g}(t)$

The TÂR (e, equation (2-

CHAPTER III

PROCESSING TECHNIQUES FOR EXTRACTING NATURAL MODE WAVEFORMS

3.1 Reception of a Radar Target E-Field

In the previous chapter we developed expressions for the far-field retarded scattered E-field. The radar receiving antenna will receive a portion of this scattered E-field and deliver it at the antenna terminals to a transmission line. The response observed at the antenna terminals depends upon the polarization match of the scattered field and the radar receiving antenna as well as the receiving antenna's response for a particular direction. We can account for polarization effects if we always calculate or measure an orthogonal pair of polarizations for the scattered E-field and the antenna. In this chapter we shall perform these calculations only for a θ -polarized component. The orthogonal component procedes identically.

We shall denote the θ -polarized far-field radar target scattered retarded E-field by equation (3-1).

$$tar_{\theta}(t) = L^{-1}(\hat{TAR}_{\theta}(\theta, \phi, s))$$
 (3-1)

The \hat{TAR}_{θ} (0, ϕ ,s) is the frequency domain expression we obtained in equation (2-21) for this particular radar target scatterer.

In a splane wave implane wave implane wave implants a TEM_horn, b

 $tem_{\theta}(t) =$

This time TEM

antenna termi from directio antenna bores impulsive res

the frequency (3-1).

which is incidently through the aby performing

It s

will simultar

and noise res

giver, by equa

 $v(t) = \int_{-\infty}^{\infty}$

= [·

In a similar notation, we shall represent the θ -polarized plane wave impulse response of our particular radar receiving antenna, a TEM $_{\theta}$ horn, by tem $_{\theta}(t)$, in equation (3-2)

$$tem_{\theta}(t) = L^{-1}(\widehat{TEM}_{\theta}(\theta', \phi', s))$$
 (3-2)

This time $\hat{TEM}_{\theta}(\theta',\phi',s)$ is the frequency domain expression for the antenna terminal response to a unit θ -polarized impulsive plane wave from direction (θ',ϕ') . We shall hereafter assume that the radar antenna boresight is oriented toward the radar target. That the impulsive response of a planar aperture antenna can be obtained from the frequency domain antenna response is well developed in reference (3-1).

It should be observed that the transmitted plane wave pulse which is incident on the radar target should also be received at least through the antenna sidelobes by the radar receiving antenna. However, by performing the ground clutter map processing of Section 2-5, we will simultaneously eliminate the sidelobe leakage of the originating transmitted plane wave pulse, $\vec{E}^{inc}(\vec{r},s)$, from the target plus clutter and noise response of the radar receiving antenna. We will denote the clutter-suppressed radar target antenna terminal response by v(t) as given by equation (3-3).

$$v(t) = \int_{-\infty}^{+\infty} tem_{\theta}(\tau) tar_{\theta}(t-\tau) d\tau$$

$$= L^{-1} \{T\widehat{E}M_{\theta}(\theta', \phi', s) T\widehat{A}R_{\theta}(\theta, \phi, s)\}$$
(3-3)

frequ.

As we can observe from equation (3-3), the antenna transmission line will contain natural mode waveforms from the radar target, the reception antenna, and less obviously from the plane wave incident upon the radar target. In our notation the possible natural modes of the incident plane wave pulse were not separated from $\hat{TAR}_{\rho}(\theta,\phi,s)$.

3.2 Sampling the Radar Antenna Response

So far we have characterized both the scattered E-field of the radar target scatterer and the receiving antenna response as linear, time-invariant processes with Laplace transforms. This allows us the option of computing the composite response either by a time domain convolution or a transform domain product.

There is one process we shall use that is not "linear, time-invariant." It is our sampling process or A/D conversion. The operation of sampling is characterized as a multiplication or modulation (ref. 3-5, pp. 30). As a mathematical computation there is nothing new. Only the roles of the time domain and the frequency domain have been switched. This time domain product becomes a convolution in the frequency domain. For uniform sampling, we might characterize the system as linear, frequency-invariant or linear periodically time-varying.

Although taken alone the sampler may be mathematically simple, we must use it in combination with linear time-invariant processing and electromagnetic scatterers. This makes both the time domain and frequency domain representations more complex conceptually but

general ing cond

reviewi

(3-4) i multipl

÷-

.

Equation termina

ant

3.3 Pr E-field

scatter

obtain real na mode ph at the data va

The for Figure

occurs

tinuous

generally more convenient computationally. For the purpose of gaining conceptual fluency, Appendix B is recommended reading after reviewing the notation of Appendix A.

There are two equations we will use extensively. Equation (3-4) is simply the definition of the sampler of period T which will multiply the antenna terminal response.

$$\delta_{\mathsf{T}}(\mathsf{t}) = \sum_{\mathsf{n}=-\infty}^{+\infty} \delta(\mathsf{t}-\mathsf{n}\mathsf{T}) \tag{3-4}$$

Equation (3-5) is the output of this sampler placed at the antenna terminals for our radar target scatterer.

$$ant_{T}(t) = \delta_{T}(t)(tem_{\theta}(t) * tar_{\theta}(t))$$
 (3-5)

3.3 Processing a Scattered E-field Reception

Our next objective is by means of simple processing of the scattered field observed at the terminals of the reception antenna to obtain a single, j-th mode waveform. This could be either a purely real natural mode waveform representation of one of the complex natural mode phasor waveforms of an equivalent representation. Our processing at the antenna terminals will be a weighted summation of N sampled-data values of the retarded far-field reception antenna response. The form of this process for a conventional radar is illustrated in Figure 3-1. In our experimental set-up of Figure 2-4, the sampling occurs in the sampling head of the sampling oscilloscope. Any continuous representations of the retarded far-field antenna response

are st We may

ز

of the function

In equa

ing fu

process

presen

٧^j

The exc (3-6) a

e^j(

In a sin

equatio:

are stretched and/or filtered versions of these sampled data values. We may represent this process by equation (3-6).

$$v^{j}(t) = p(t) * \sum_{k=0}^{N-1} a_{k}^{j} \delta(t-kT) * ant_{T}(t)$$
 (3-6)

In equation (3-6), the function p(t) represents the final smoothing of the output waveform after or during the processing. The impulse function $\delta(t-kT)$ is, of course, synchronized with the sampler on the antenna terminals. For convenience, we will always choose the smoothing function, p(t), of finite duration in time.

When the retarded scattered E-field from the radar target is present at the antenna terminals, we may represent the j-th mode processed antenna response, $v^{j}(t)$, as in equation (3-7).

$$v^{j}(t) = \int_{0-}^{NT+} e^{j}(\tau) \operatorname{ant}_{T}(t-\tau) d\tau$$
 (3-7)

The excitation function, $e^{j}(t)$, is easily identified from equation (3-6) and is given by equation (3-8).

$$e^{j}(t) = e_{d}^{j}(t) * p(t) = p(t) * \sum_{k=0}^{N-1} a_{k}^{j} \delta(t-kT)$$
 (3-8)

In a similar manner we will define the pulse shape independent sampled mode response $v_d^j(t)$ by equation (3-9) and its transform by equation (3-10).

٧,

Ŷ

termine in circle Typical and column do analog zation. The us

this p

and (3

زر

3.4 E

under w

$$v_d^{j}(t) = \sum_{k=0}^{N-1} a_k^{j} \delta(t-kT) * ant(t)$$
 (3-9)

$$\hat{V}_{d}^{j}(s) = \sum_{k=0}^{N-1} a_{k}^{j} \exp(-sTk) \hat{ANT}_{T}(s)$$
 (3-10)

Before we make any simplifications in the sampled antenna terminal response, we need to make a generalization which is necessary in circumstances when more than one file or data set are used together. Typical cases which require synchronization of data are deconvolution and comparison of more than one data file. For the real radar problem we do not know the synchronization of the sampler relative to the analog retarded antenna terminal response. To specify this synchronization, we shall use the modified z-transform notation of Appendix A. The use of m as an argument in parenthesis shall denote the use of this parameter. Equations (3-9) and (3-10) become equations (3-11) and (3-12).

$$v^{j}(t,m) = \sum_{k=0}^{N-1} a_{k}^{j} \varepsilon(t-kT) * ant_{T}(t,m)$$
 (3-11)

$$V^{j}(z,m) = \sum_{k=0}^{N-1} a_{k}^{j} z^{-k} ANT(z,m)$$
 (3-12)

3.4 Excitation of a Single Natural Mode Waveform

The objective of this section is to determine the conditions under which the output convolution of equation (3-13) can be a single natural mode waveform using N coefficients $\{a_k^j\}_{k=0}^{N-1}$.

 $v_{d}^{j}(t,r)$

At this poresponse to using m =

 $\operatorname{ant}_{\mathsf{T}}($

ν<u>;</u>(t,

Now tar_g(like targ

ÂP_E

Using SEI

TAR

The Laply actually change of SEM mode

Appendix

$$v_{d}^{j}(t,m) = \int_{0_{-}}^{NT_{k-1}^{+}} (\sum_{k=0}^{N-1} a_{k}^{j} \delta(\tau - kT)) ant_{T}(t - \tau, m) d\tau$$
 (3-13)

At this point we will simplify the sampled scattered antenna terminal response by assuming that the receiving antenna is nondistorting and using m = 1 as given by equation (3-14) and (3-15).

$$ant_{T}(t,m=1) = \delta_{T}(t) tar_{A}(t)$$
 (3-14)

$$v_{d}^{j}(t,m=1) = \left(\sum_{k=0}^{N-1} a_{k}^{j} \delta(t-kT)\right) * \left(\delta_{T}(t) tar_{\theta}(t)\right)$$
(3-15)

Now $\tan_{\theta}(t)$ is more succintly known by equation (2-22) for a wirelike target.

$$\widehat{TAR}_{\theta}(\theta,\phi,s) = s \sin\theta \frac{\mu}{4\pi} \overrightarrow{\theta} \cdot \int_{A} \overrightarrow{K}(\overrightarrow{r}',s) \exp(-s\Delta R/c) dA' \qquad (2-22)$$

Using SEM the model form of the solution is given by equation (3-16).

$$\widehat{TAR}_{\theta}(\theta,\phi,s) = \sum_{\alpha} (s-s_{\alpha})^{-1} \widehat{C}(\theta,\phi,s)$$
 (3-16)

The Laplace transform of the sampled antenna terminal response is actually the z-transform of the antenna terminal response after the change of variable from s to z. Due to the simple pole form of the SEM model solution, the evaluation is performed term-wise as in Appendix A to yield equation (3-17).

Ť,

We will domain

in the

Ŷį

ciated (2-18)

Note t

the si

tine"

tar_é(t

ľ

We sha Also,

tne ra

contai

We the

equati(

$$\widehat{TAR}_{\theta}(\theta,\phi,z) = \sum_{\alpha} (1-z_{\alpha}/z)^{-1} \widehat{C}(\theta,\phi,z)$$
 (3-17)

We will now rewrite the simplified equation (3-13) in the frequency domain to illustrate what excitation of the single j-th mode implies in the frequency domain as given by equation (3-18).

$$\hat{V}_{d}^{j}(s) = \sum_{k=0}^{N-1} a_{k}^{j} \exp(-sTk) \sum_{\alpha} (1 - \exp((s_{\alpha} - s)T))^{-1} \hat{C}(\theta, \phi, s) (3-18)$$

Note that we have suppressed the entire function which may be associated with the infinite index set, α . From equations (2-27) and (2-18) we know that in the time domain, $\tan_{\theta}(t)$, can be calculated from the simplified current density coupling coefficient in the "last-time" of the retarded far-field scattered E-field. We note that $\tan_{\theta}(t)$ is composed of terms of the form given by equation (3-19).

$$L^{-1}\{(s-s_{\alpha})^{-1}\hat{C}_{\theta}(\theta,\phi,s)\} = u_{-1}(t-t'')C_{\alpha}(\theta,\varepsilon)\exp(s_{\alpha}t)$$
 (3-19)

We shall use this new representation in $tar_{\theta}(t)$ in the "late-time". Also, we have used this opportunity to change from the SEM vector containing the aspect angle dependency of the incident plane wave on the radar target with the more conventional spherical angles (θ, ϕ) . We then obtain equation (3-20) for the "late-time" representation of equation (3-18) now in the time domain.

equa

cate

appr

coup

abso is t

retu

set

Reca

tine disa

tor.

Сопус

autpu

$$v_{d}^{j}(t) = \sum_{k=0}^{N-1} a_{k}^{j} \delta(t-kT) * \sum_{\alpha} u_{-1}(t-t'') \exp(s_{\alpha}t) C_{\alpha}(\theta,\phi) \delta_{T}(t)$$
for t-nT > t'', n an integer (3-20)

We will not be able to achieve our desired objective with equation (3-20) as it stands. The change we shall make is to truncate the infinite summation on the index set α . This is a reasonable approximation in the late-time for all targets which yield "class 1" coupling coefficients in the retarded scattered far-field which are absolutely convergent. In this case we obtain equation (3-21) which is the fundamental equation for signal processing of the radar target return. We will denote this finite summation by denoting the index set by m instead of α .

$$v_{d}^{j}(t) = \sum_{k=0}^{N-1} a_{k}^{j} \delta(t-kT) * \sum_{m=1}^{N} u_{-1}(t-t'') \exp(s_{m}t) C_{m}(\theta,\phi) \delta_{T}(t)$$

$$t - nT > t''$$
(3-21)

Recall that our star notation denotes the convolution operator in the time domain. For t in the "late-time" the step function $u_{-1}(t-t")$ disappears and this allows a simple evaluation of the integral operator. In order to formalize in a matrix form we shall calculate the convolution of the processing with the coefficients of the sampler output to obtain equation (3-22).

The s

We no

M

of a

to de

נ

We wi

by eq

٧

Let u

Wayef

We not

۷.

starts

receive

$$(t-kT)*exp(smt) = \int \delta(\tau-kT)exp(sm(t-\tau))d\tau$$

$$= exp(smt)Mmk (3-22)$$

The scalar constants M_{mk} are given by equation (3-23).

$$M_{mk} = \exp(-s_m T k), m = 1, ..., N; k = 0, ..., N-1$$
 (3-23)

We note, in passing, that these scalar constants are functions only of a single natural frequency and the sampling time kT. Next we wish to define a natural mode waveform $C_m(\theta,\phi,t)$ by equation (3-24).

$$C_{m}(\theta,\phi,t) = C_{m}(\theta,\phi)\exp(s_{m}t) \quad m = 1, \dots, N$$
 (3-24)

We will now rewrite equation (3-21) in terms of the quantities defined by equations (3-22) through (3-24) to give equation (3-25).

$$v_{d}^{j}(t) = u_{-1}(t-t'')\sum_{k=0}^{N-1} a_{k}^{j}\sum_{m=1}^{N} C_{m}(\theta,\phi,t) M_{mk} \delta_{T}(t), t=nT > t''$$
 (3-25)

Let us now suppose that we desire the processed (pulse-independent) radar target return to be samples of a single "late-time" natural mode waveform of the form given by equation (3-26).

$$v_d^j(t) = C_j(\theta, \phi, t)\delta_T(t) t=nT > t'' + NT, n an integer$$
 (3-26)

We note that in equation (3-27) we have exactly N unspecified constants to be used. If use exactly N sampled data values of the received waveform, we can potentially solve for the unknowns $\{a_k^j\}_{k=0}^N$.

In or

1:000

C

nê Tê

nd ex

Upon

will .

٧

So in

conce

wh. ch

In order to facilitate a matrix formulation, we need to compress our notation a little further as given by equations

$$v_n^j = v^j(nT), \qquad n = 0, 1, ..., N-1$$
 (3-27)

$$C_{nm} = C_{m}(,,nT), n = 0, 1, ..., N-1; m = 1, ..., N (3-28)$$

We may now write N sampled data values of v_n^j as a column vector v_n^j nd express equation (3-25) as the matrix equation (3-29).

Upon observing the structure of equation (3-29), we observe that we will obtain equation (3-30) if equation (3-31) is satisfied.

$$v_n^j = C_{nj}, n = 0,1,...,N-1; j = 1,...,N/2$$
 (3-30)

$$\begin{bmatrix} 0 \\ 0 \\ \vdots \\ 1 \\ \vdots \\ 0 \end{bmatrix} = \begin{bmatrix} M_{mk} \\ a_k \end{bmatrix}$$
 (one in j-th row) (3-31)

So in order to excite the desired natural mode wave form, we need concern ourselves with the matrix of frequency/sampling constants \mathbf{M}_{mk} which are independent of aspect angle.

(3of

for

evi

:

tion evid

of f

exci

tice

Sa--

of r

He w

Coef

quen

וְדֵוֹנ

Perf(

Hopefully, the reader will recognize the form of equation (3-31) and note that the $\{a_k^j\}_{k=0}^{N-1}$ may be obtained as the j-th column of the inverse matrix of M_{mk} . Writing out all N natural mode wave form excitation vectors in matrix form, the relationship is more evident in equation (3-32).

$$\begin{bmatrix} M_{mk} \end{bmatrix} \begin{bmatrix} a_0^1 & \dots & a_0^N \\ \vdots & & \vdots \\ a_{N-1}^1 & \dots & a_{N-1}^N \end{bmatrix} = \begin{bmatrix} 1 & 0 & \dots & 0 \\ 0 & 1 & \dots & 0 \\ \vdots & & & \vdots \\ 0 & 0 & \dots & 1 \end{bmatrix}$$
(3-32)

Hence if we can obtain all of the natural mode waveform excitation vectors, we have, in fact, the inverse matrix of M_{mk} which is evident from equation (3-32). We may now conclude that if the matrix of frequency/sampling constants is invertible, then we can obtain excitation coefficients for each of the finite number, N, of natural mode waveforms. In fact, we are able to separate them in the "latetime". It should be observed that whether or not the frequency/ sampling constants matrix is invertible is determined by the collection of natural frequencies and sampling time and is independent of the aspect-angle of the target or the amplitude of the received waveform. We will later observe that we may be able to obtain the excitation coefficients for natural mode waveforms even when the matrix of frequency/sampling constants is not invertible. The procedure is similar to the K-Pulse Singularity Theorem of Appendix C and is performed automatically in the "fast" Prony's method of Chapter 5.

excita

call i

of th

ke n

rere

cies

are

A simila

equati

For the case when $[M_{mk}]$ is invertible, the j-th mode excitation coefficient vector is given by equation (3-33). We shall call the vector on the far right of equation (3-33) with the 1 in the j-th row as the selection vector. It simply selects on the columns of the inverse matrix of frequency/sampling constants.

$$\begin{bmatrix} a_k^j \end{bmatrix} = \begin{bmatrix} M_{mk} \end{bmatrix}^{-1} \begin{bmatrix} 0 \\ 0 \\ \vdots \\ 1 \\ 0 \end{bmatrix}$$
 (one in j-th row)

Now suppose we desire to extract a real natural mode waveform. We may, for example, select the 1st cosine natural mode excitation by remembering the order in which we placed conjugate natural frequencies in the matrix of frequency/sampling constants. In our case they are index staggered by N/2, so we obtain equation (3-34).

$$\begin{bmatrix} a_{k}^{jc} \end{bmatrix} = \begin{bmatrix} M_{mk} \end{bmatrix}^{-1} \begin{bmatrix} \frac{1}{2} \\ 0 \\ \vdots \\ \frac{1}{2} \\ 0 \\ \vdots \end{bmatrix} = \frac{1}{2} \begin{bmatrix} a_{k}^{j} \end{bmatrix} + \frac{1}{2} \begin{bmatrix} a_{k}^{j+N/2} \end{bmatrix} = \text{Re} \begin{bmatrix} a_{k}^{j} \end{bmatrix} \quad (3-34)$$

$$j=1$$

A similar relation holds for the 1st sine natural mode excitation. Similarly, we may obtain the 1st sine natural mode excitation by equation (3-35).

. E

Super for t

3.5

A-sc proc

> at b that

tran

rada

trig

erive extre

tempt tange

of our

radar

the TEX

data is

$$\begin{bmatrix} a_k^{1s} \end{bmatrix} = \begin{bmatrix} M_{mk} \end{bmatrix}^{-1} \begin{bmatrix} 1/2 \\ 0 \\ \vdots \\ -1/2 \\ 0 \\ \vdots \end{bmatrix} = \underbrace{\begin{bmatrix} a_k^{1} \end{bmatrix}}_{2} \begin{bmatrix} a_k^{1} \end{bmatrix} - \underbrace{\begin{bmatrix} a_k^{1+N/2} \end{bmatrix}}_{2} \begin{bmatrix} a_k^{1+N/2} \end{bmatrix}$$
(3-35)

Superscripts s and c shall denote these real excitation coefficients for the $e^{\mathbf{j}}(t)$ of equation (3-8).

3.5 "Polar Mode A-Scope" Displays

One of the fundamental radar displays is called a radar A-scope. This is a retarded transmitter triggered display of the processed received target response as a function of time, generally at baseband (carrier removed). The significance of the display is that for a target much stronger than clutter, the envelope of the transmitter pulse is often viewable although it is altered by the radar system response and the radar target. The time delay of the triggered radar return behind a replica of the transmitter pulse envelope gives the radar range estimate. If it were not for the extreme aspect-angle dependence of the radar return, one would be tempted to use the amplitude of the radar return as an estimate of target size. Figure 3-1 is a radar A-scope display of the response of our experimental radar system, Figure 2-4, to a hemispherical radar target imaged on a conducting ground plane. For completeness, the TEM horn antenna associated with this particular radar target data is given by Figure 3-2.

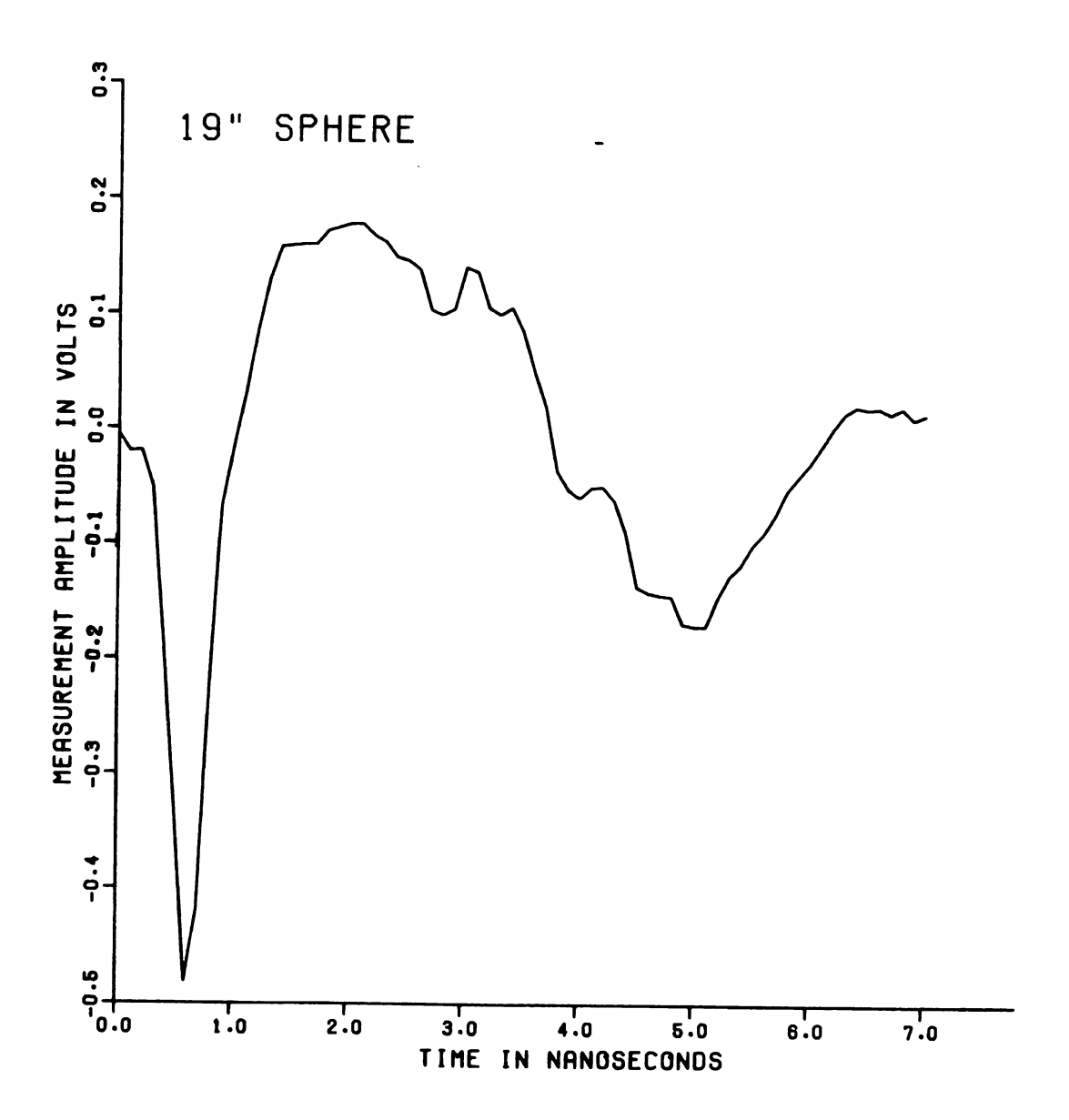


Figure 3-1. Clutter-reduced 18" Spherical (imaged)
Radar Target Return.

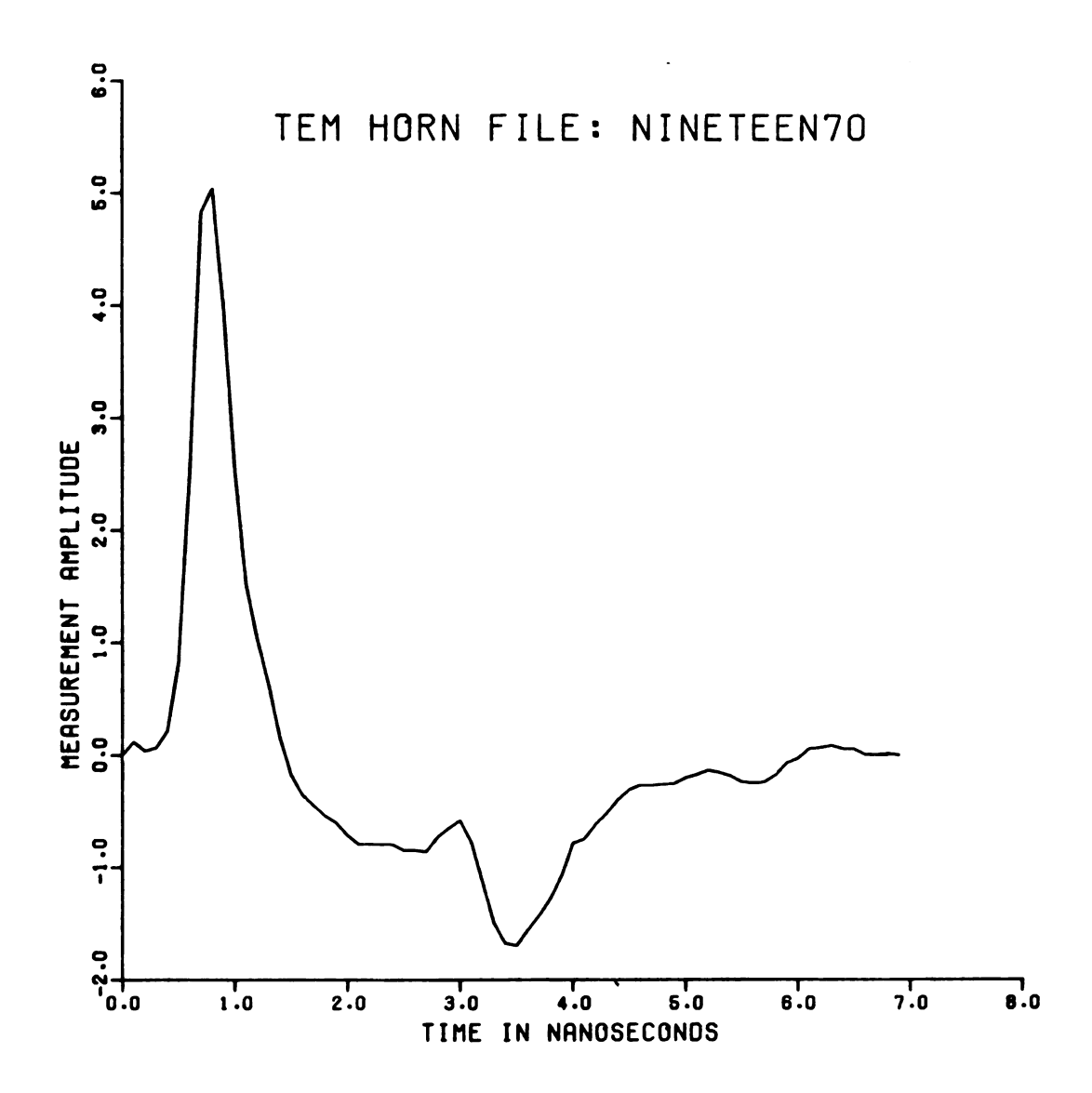


Figure 3-2. TEM Horn Receiving Antenna used for Spherical Radar Targets.

crimina displa

plays v

ph edi

our ta

5

firs rati

For 1

sect

æn:

(j=2 is a

this

with

٤

8

We are now ready to develop the special radar A-scope displays which are destined to play a crucial role in the final discrimination technique of this dissertation. In order to describe the display, we shall in this section <u>only</u> use a synthetic data file for our target response at the antenna terminals. The data is created by equation (3-36) which we shall call a "prony series".

$$S(t) = \sum_{m=1}^{N} c_m \exp(s_m t), \quad t = nT > 0, \text{ n an integer}$$
 (3-36)

For the natural frequencies in equation (3-36), we shall choose the first 10 complex conjugate pairs of a 6" wire with a length-to-radius ratio (L/a) of 400. Hence N is 20 and our excitation technique of section 3.4 yields an excitation coefficient vector $\begin{bmatrix} a_k^j \end{bmatrix}$ of 20 elements. Convolving by equation (3-37) the 2nd cosine mode excitation (j=2) with the synthetic "prony series" we obtain Figure 3-3. There is another real natural mode waveform which looks quite similar to this. Convolving by equation (3-38), the 2nd sine mode excitation with the synthetic "prony series" we obtain Figure 3-4.

$$A_{j}(t) = \int_{0-}^{NT+} e^{jc}(\tau) S(t-\tau) d\tau$$
 (3-37)

$$B_{j}(t) = \int_{0-}^{NT+} e^{js}(\tau) S(t-\tau) d\tau$$
 (3-38)

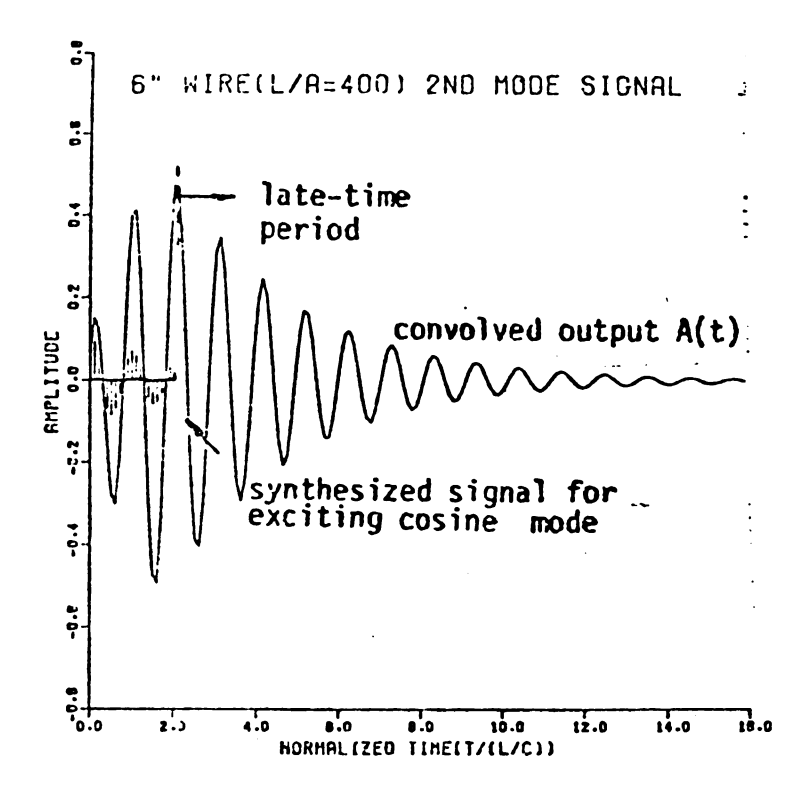


Figure 3-3. 2nd Cosine Mode Convolution.

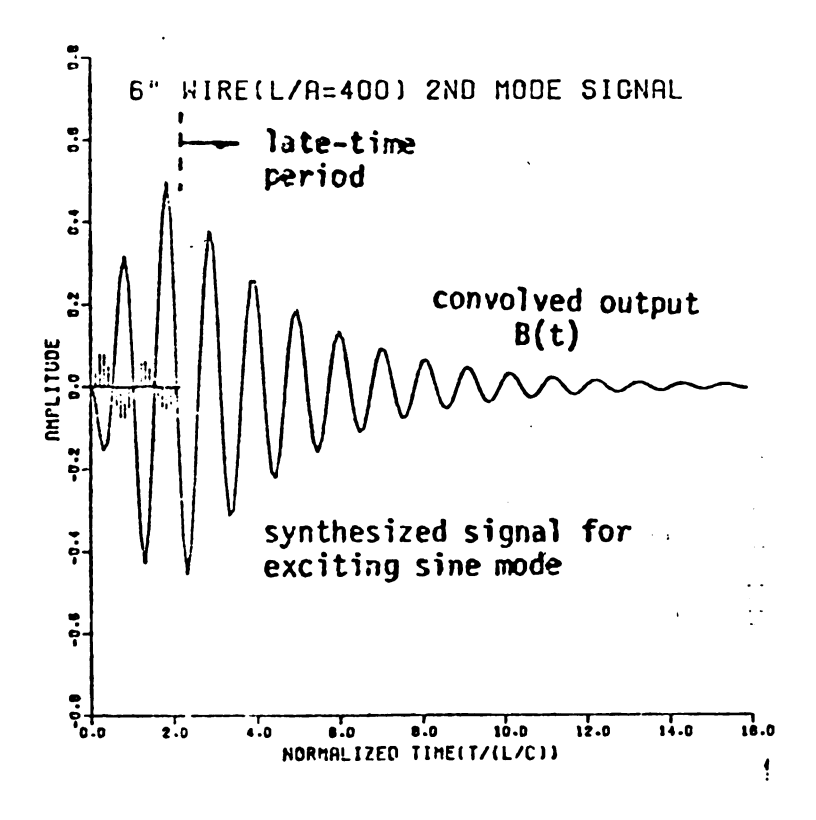


Figure 3-4. 2nd Sine Mode Convolution.

as th

time.

\$3°°¢

inde Also

are

The

à r

the

giv

Wher

Figu with

2nd n

envel: sa.-p1₆

(a]] n plex 10

It is important to note that each of these convolutions appear as the expected damped cosinusoids starting at t=2.04 normalized time. It takes that length of normalized time to accumulate 20 samples of the "Prony series" in order to satisfy the conditions of independent data samples under which equation (3-32) was derived. Also visible as pulses on the left-hand side of Figures 3-3 and 3-4 are the j-th mode excitation coefficient vectors for the 2nd mode. The two convolved waveforms $A_j(t)$ and $B_j(t)$ are what we shall call a rectangular j-th mode radar A-scope plot.

We shall now perform a seemingly simple transformation of these two rectangular mode radar A-scope plots into a polar form as given by equations (3-39), (3-40), and (3-41).

$$C(t) = AIt) - jB(t)$$
 (3-39)

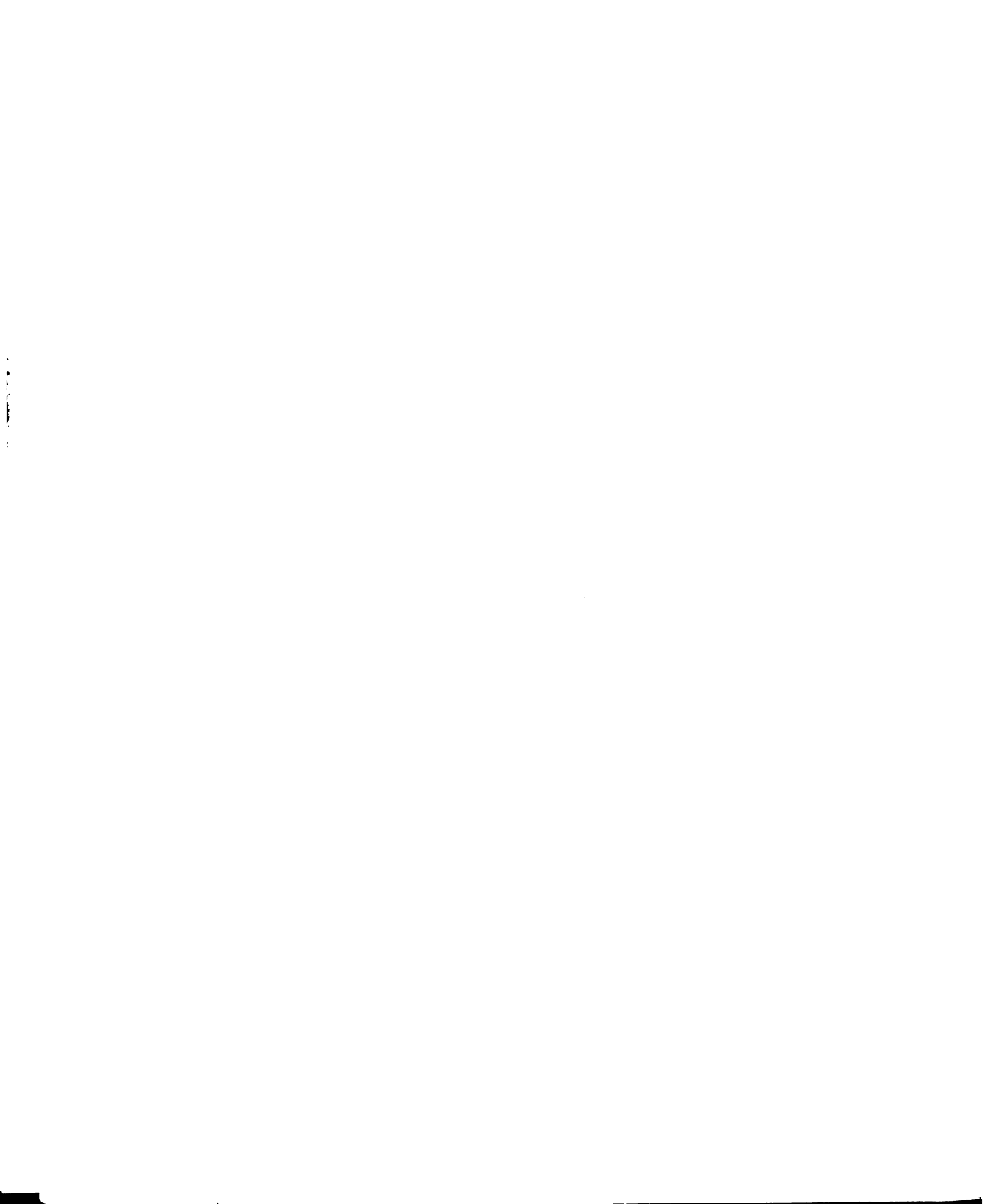
$$env(t) = Re(clog(c(t)))$$
 (3-40)

$$rot(t) = Im(clog(C(t)), conts. phase$$
 (3-41)

where clog() is the complex logarithm with phase made continuous.

Figure 3-7 shows the envelope, env(t) as a function of normalized time with a straight line of slope equal to the damping coefficient of the 2nd natural frequency of the synthetic "Prony series". Note that the envelope does not meet with the straight line until the 20 nonzero samples have been accumulated.

The last equation of the transformation yields what we shall call "rotations" which is an analytically continued phase of the complex logarithm. Only the continuation operation is not easily



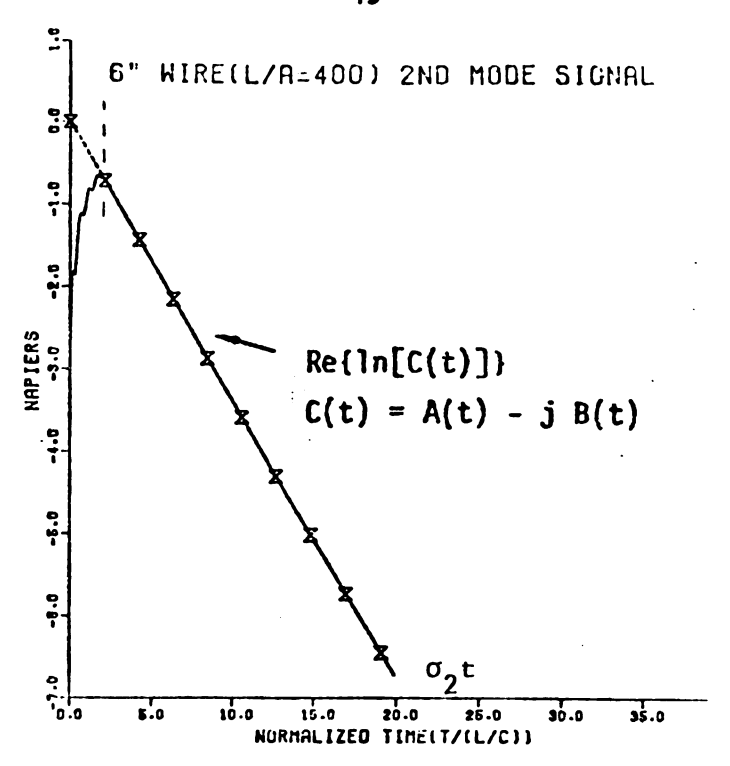


Figure 3-5. 2nd Mode Envelope Radar A-Scope.

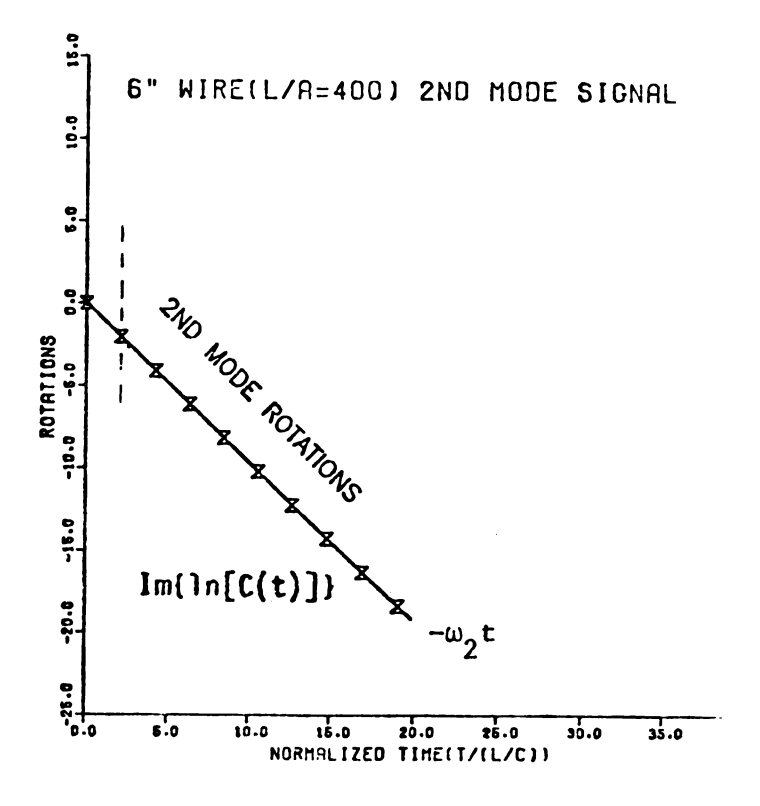


Figure 3-6. 2nd Mode Rotation Radar A-Scope.

inpi not

ceps

rod

pha tri

dis

ur.

to

jņ

the the

the

be con

3.6 515 ect

oota: from

from

dampe

Sa.7516

implementable in either analog or digital hardware. However, we do not need the exotic phase unwrapping algorithms necessary for cepstral analysis (ref. 3-6). This is because we only have a single mode remaining rather than a large sum of complex exponentials whose phase is to be continuous. To continue the phase we make only a trivial logical comparison of the previous sample throughout this dissertation. It should be noted that only the starting point is not unique for "rotations."

The radar A-scope plots of rotations yields some interesting information not observable in the previous three plots. There appears to be <u>no</u> early time transient in this plot. Starting with sample one, the "rotations" plot align with the straight line whose slope equals the minus imaginary part of the second natural frequency of the synthetic "Prony series."

The display of equations (3-40) and (3-41) shall hereafter be called the "polar mode A-scope" display. We shall expand upon this concept in Chapter 6.

3.6 Measurement Performance of Single Mode Waveform Extraction Technique

We shall now attempt to extract a single natural mode waveform from the radar target scatterer of Figure 3-1. Our objective is to obtain the j-th mode real natural mode waveforms $A_j(t)$ and $B_j(t)$ which from our synthetic data of Figures 3-3 and 3-4 we now can resemble damped cosinusoids for normalized time for which only nonzero data samples are used in equations (3-37) and (3-38). These results are

for

thr rec

res

tio

All

the hor

con

Fig:

beca

Tàt

rec.

The white

give

atys

Sepe

for a "Prony series" which we cannot expect unless the following three conditions are met on the incident plane wave plus shape, the receiving antenna response, and the "late-time" target far-field response:

- (1) $f(t) = \delta(t)$ from equation (2-15)
- (2) tem (t) = δ (t) from equation (3-14)
- (3) $t_{ret} > t''$ (2-way transit time) from equation (2-18)

All three of these conditions are troublesome. The "late-time" condition would be easy if the first two were satisfied. Figure 2-5 shows the originating pulse shape and Figure 3-2 shows the receiving TEM horn antenna response.

We will perform a slightly defective correction to meet these conditions. A digital deconvolution of the receiving antenna response, Figure 3-2, will be performed on the clutter-reduced radar target response, Figure 3-1. Deconvolution is difficult on measurement data because one cannot obtain the sampling synchronization (which is automatic with synthetic files with subsequent additive noise) which is required by equation (3-13). The deconvolution technique we will use is the discrete time Least-squares Wiener filtering of reference 3-7. The results of our deconvolution are shown in Figure 3-7 for a prewhitening parameter of 5%. A good error analysis of deconvolution is given in reference 3-8 of the "Deconvolution" collection of the Geophysics reprint series.

This technique for extracting the natural mode waveforms depends upon a priori knowledge of the natural frequencies. Used in

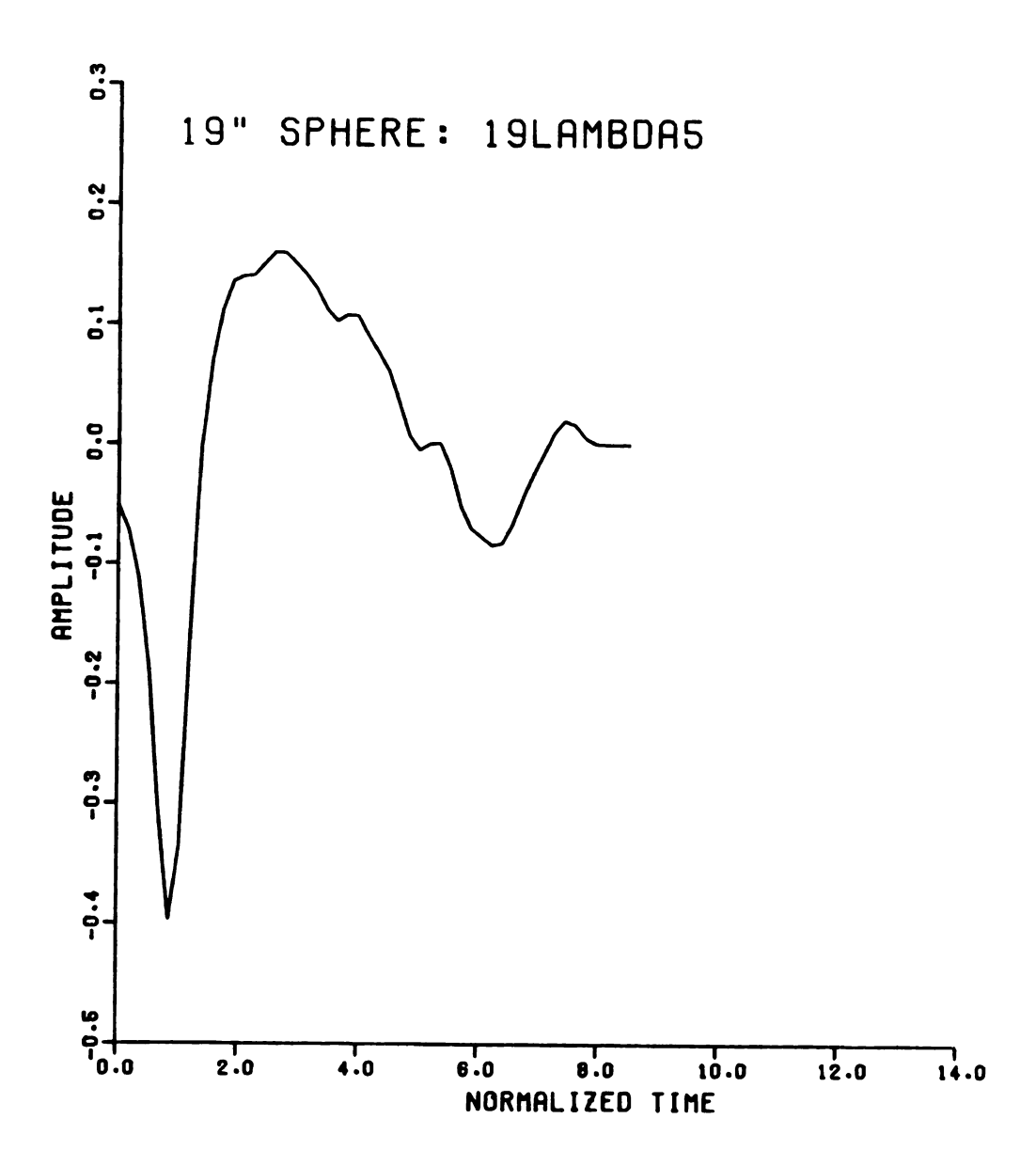


Figure 3-7. Spherical Radar Target Response by
Deconvolving Figure 3-2 from Figure 3-1.

the inva para

the

pain

deco

hani

A₁(

spo

WBV

as

see

the

lin

in

nat

nat

rad

Way

209

for

dat

3.7 Rã 3 the synthesis of these excitation waveforms are 19 natural frequency pairs from reference 3-9. Figure 3-8 shows the results for the deconvolved 19" spherical radar target of Figure 3-7. On the lefthand side in sub-figures (a) and (b) we have the desired waveforms $A_1(t)$ and $B_1(t)$ and also just below on the same plots, the corresponding excitation vector, $\begin{bmatrix} e_k^{1c} \end{bmatrix}$ and $\begin{bmatrix} e_k^{1s} \end{bmatrix}$, for each of the desired waveforms. On the right hand side we have the plots we have defined as the "polar mode radar A-scope." In these two plots we can clearly see that in the time period (of nonzero samples in the convolution), the output data displayed is clearly parallel to the correct damping line $\sigma_1 t$ in the envelope display and the correct rotation line $\omega_1 t$ in the rotation display. This is positive confirmation of a pure natural mode waveform in this time period. The results for the 2nd natural mode waveforms are in Figure 3-9. Again the "polar mode radar A-scope" plots give a confirmation of the desired natural mode waveform in the output convolutions. Figures 3-10 and 3-11 give positive confirmations for the 3rd and 4th mode natural mode waveforms. As this was one of our earliest targets, more desirable longer data sequence was not taken.

3.7 Scaling of the Invariant Radar Target Parameters

In the previous two sections we have presented displays of the invariant parameters of a radar target for the cases when the invariant parameters were known a priori and we excited these known parameters. We must also be interested in what happens when a

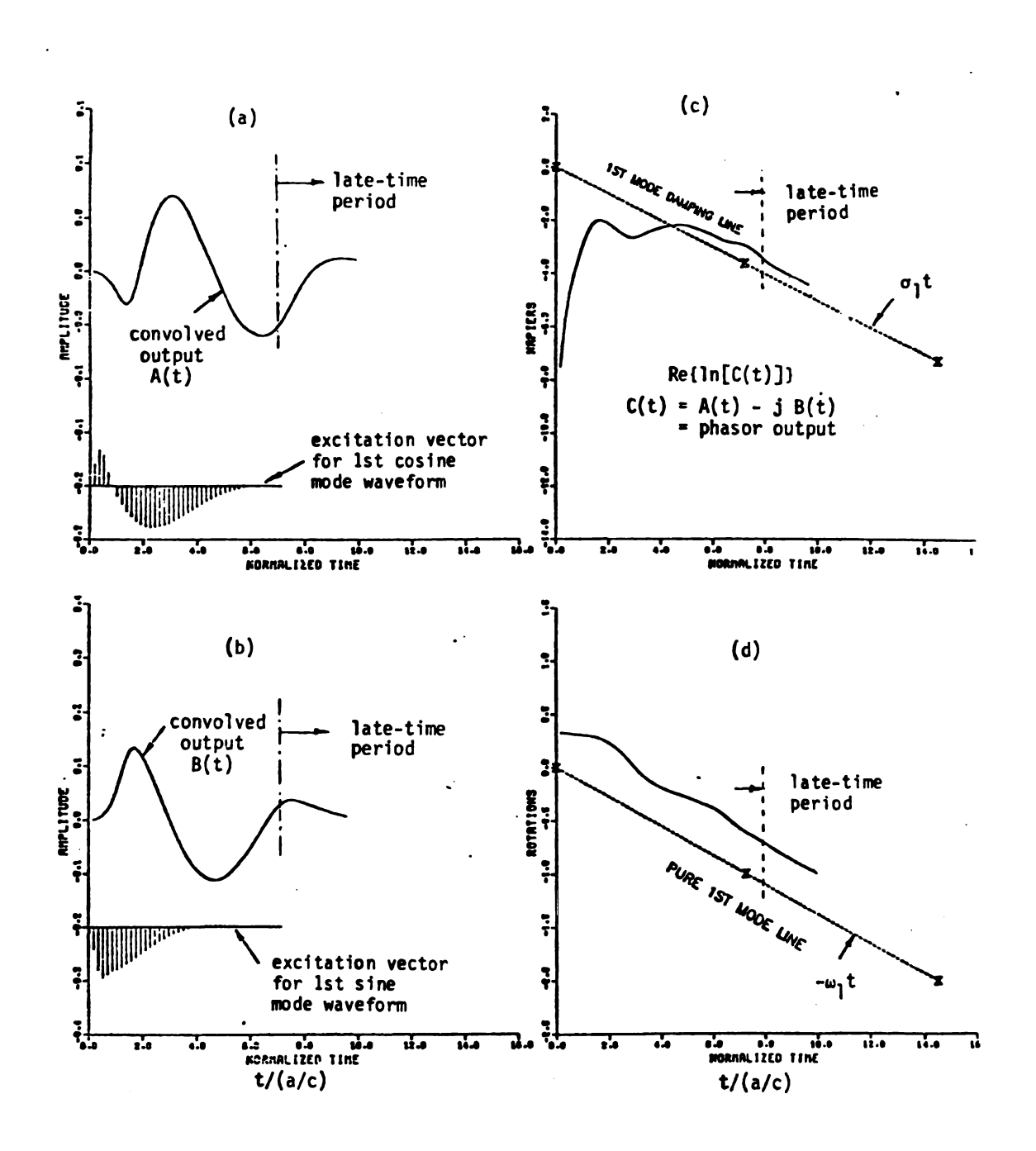


Figure 3-8. 1st Mode Waveform Excitation of a 19" Diameter Sphere.

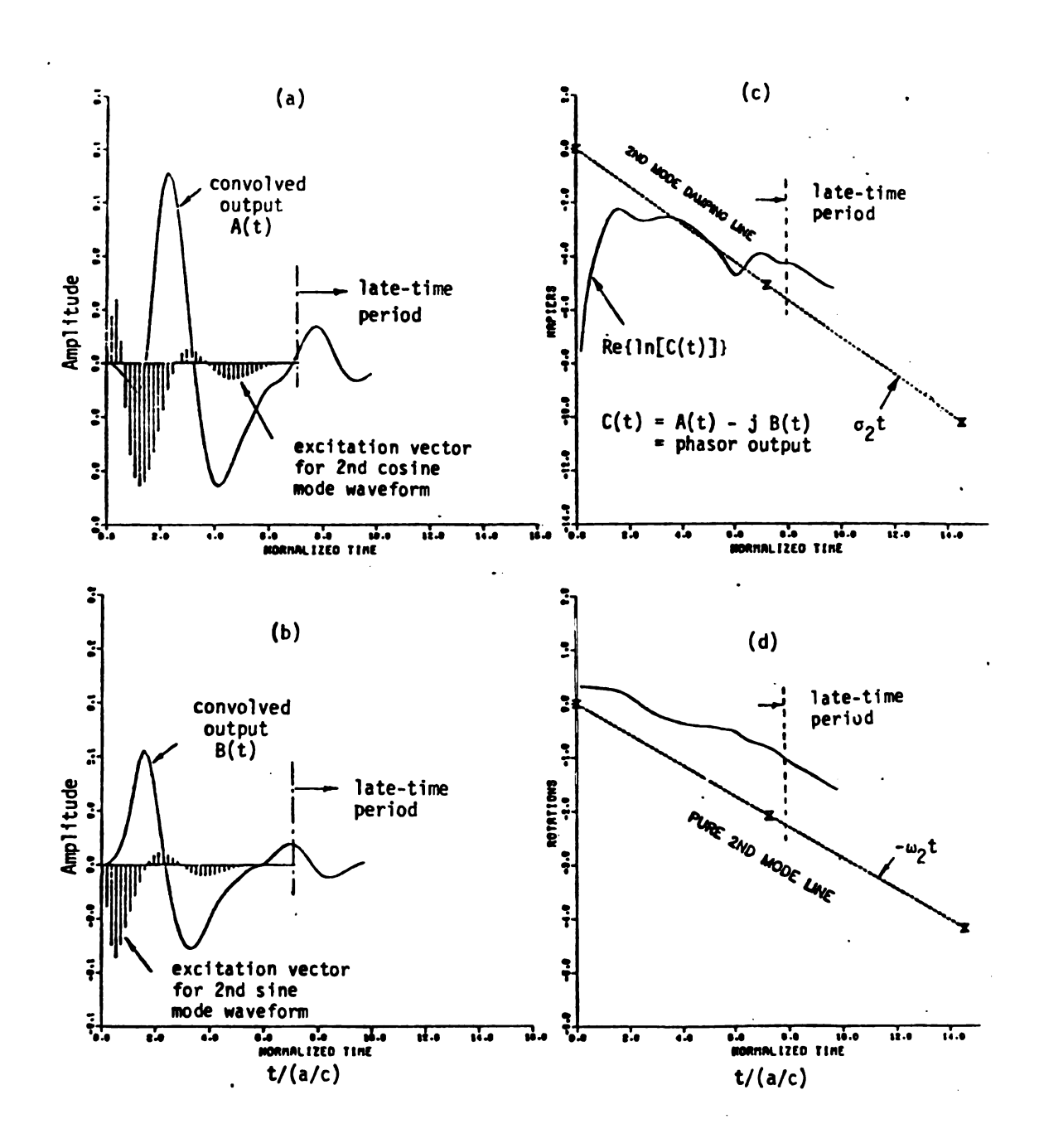


Figure 3-9. 2nd Mode Waveform Excitation of a 19" Diameter Sphere.

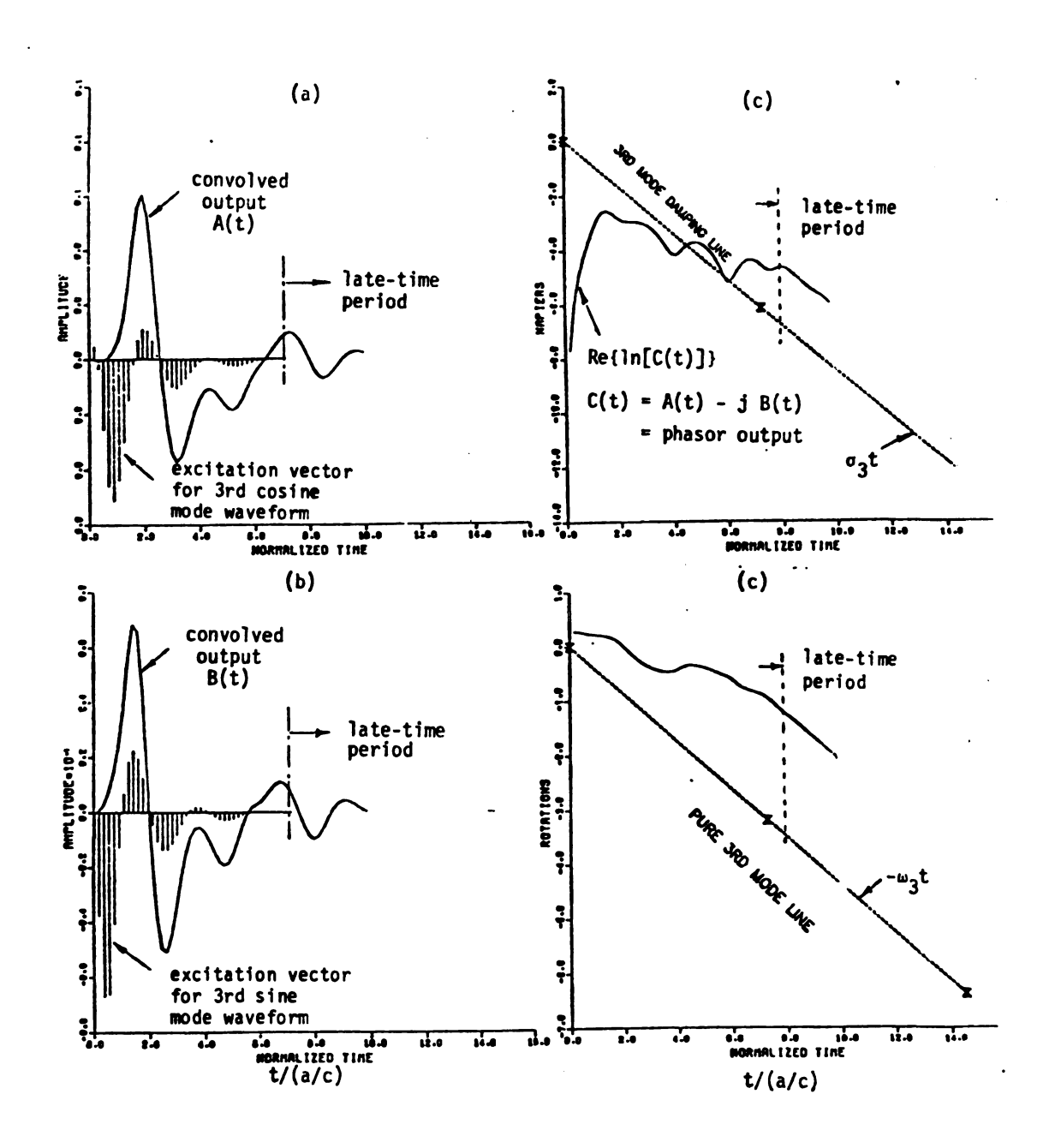


Figure 3-10. 3rd Mode Waveform Excitation of a 19" Diameter Sphere.

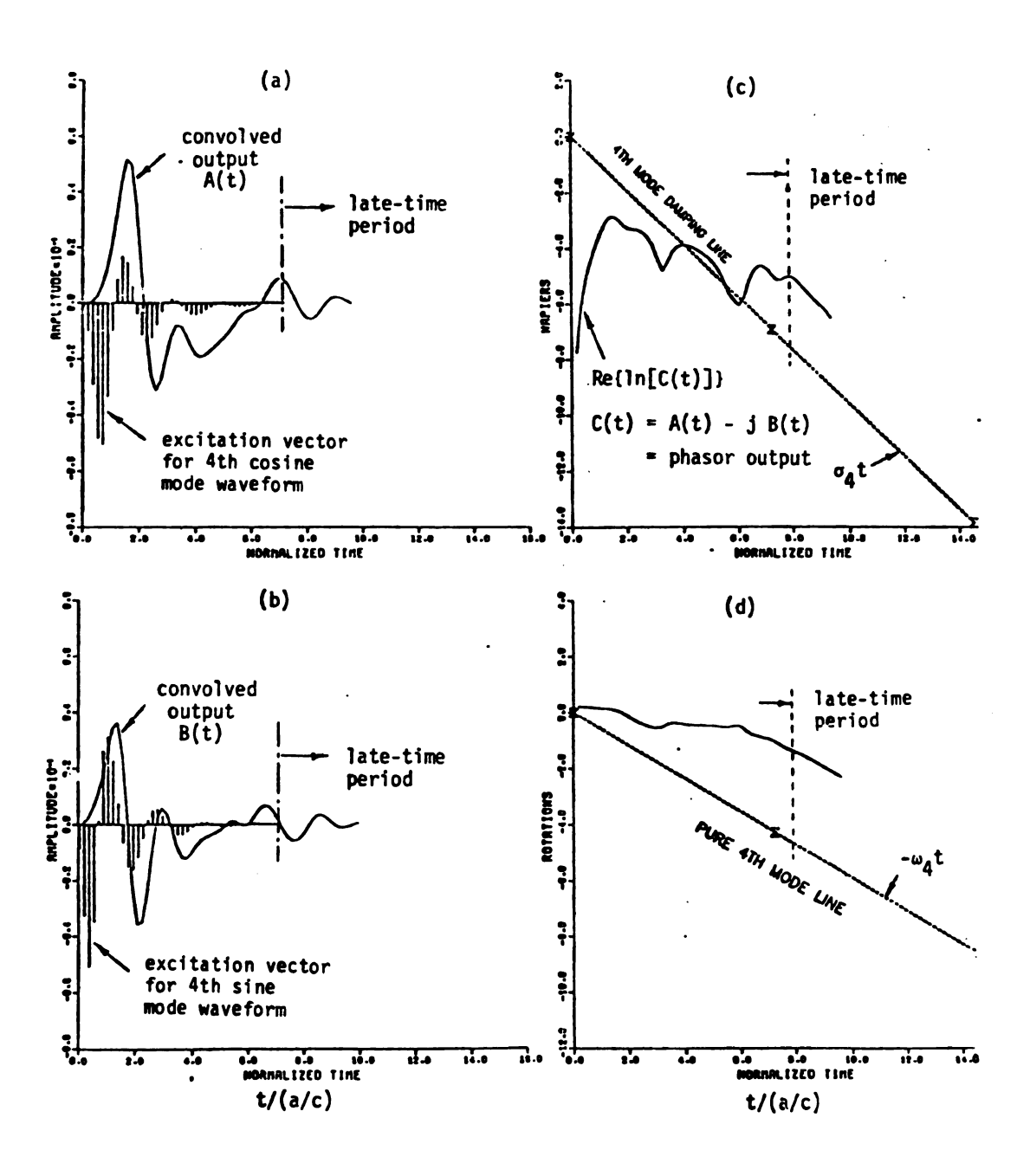


Figure 3-11. 4th Mode Waveform Excitation of a 19" Diameter Sphere.

natural mode waveform is present, but it is not the one of the target modes that we are looking for. Our derivation so far gives us no clues in this case. The only thing we know for certain is that when we are exciting the j-th mode waveform, the (j+1)-th waveform will not be passed. The "late-time" suppression of the (N-1) modes not excited depends on many items. For our implementation this is known to be approximately 210 dB. Only on the sensitive envelope plot of the "polar mode A-scope" is the extent of this suppression viewable. Again, it must be emphasized that if the undesired mode waveform is not exactly one of the natural frequencies used in the matrix of frequency/sampling constants, equation (3-34) we have not yet developed a method of calculating its suppression.

In this section we will examine the effect of small departures of the natural frequencies from the values used in the frequency/ sampling constants matrix. For our baseline we will use an 18" wire (inclusive of the image) for a radar target scatterer. The particular wire is actually making good electrical contact to our conducting ground plane at normal incidence. The natural frequencies of the wire are less damped than that for the sphere. This means that the natural mode waveforms of the wire target are relatively strong in the "late-time" making deconvolution of the receiving TEM horn antenna of dubious value. Figure 3-12 shows our clutter-reduced radar target antenna terminal response. The length-to-radius of this wire target (L/a) is 400. We may readily calculate by method of moments 10 pairs of natural frequencies which we shall use in the frequency/ sampling constants matrix of equation (3-34). As a note to be

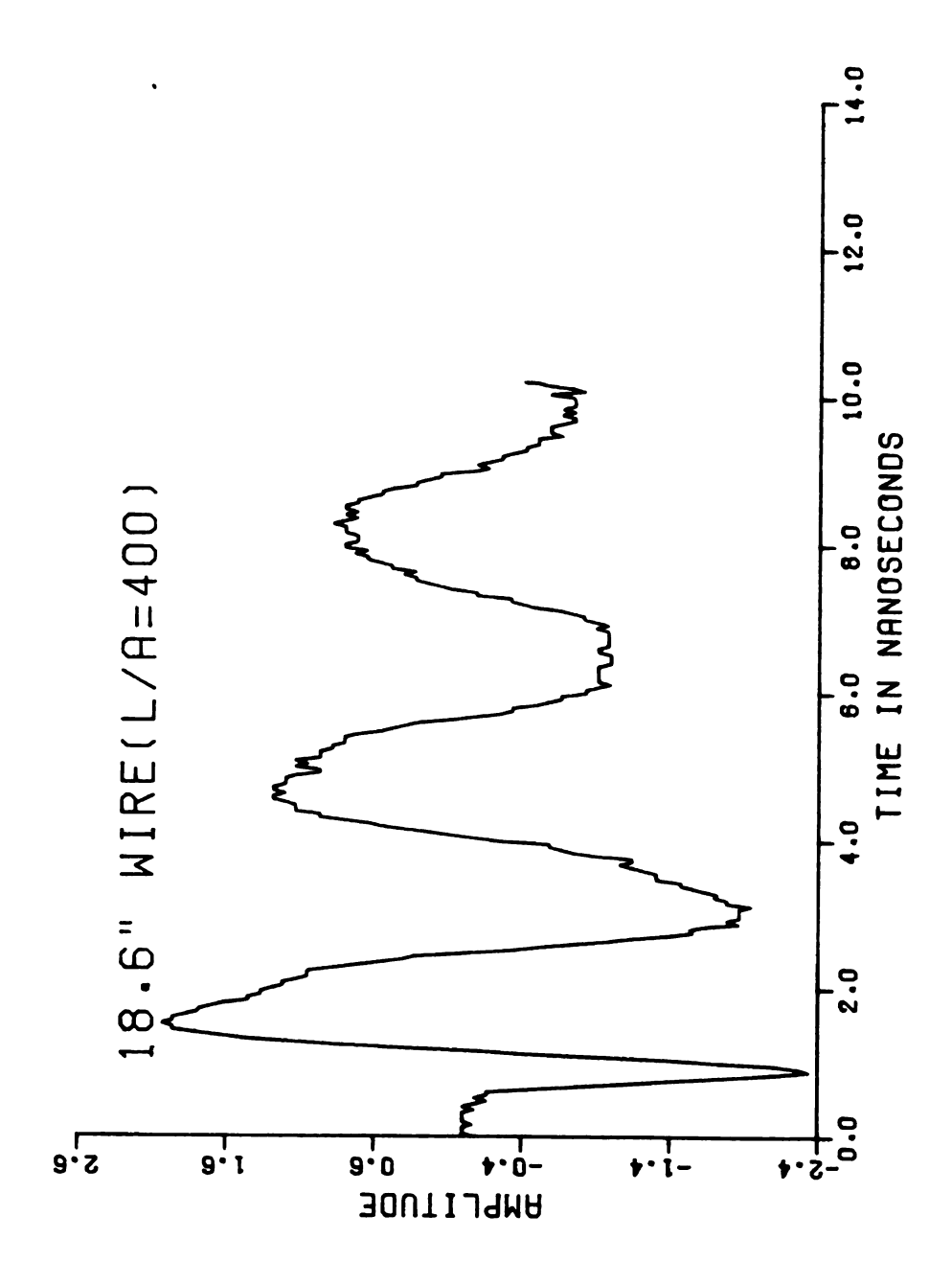


Figure 3-12. Clutter-Reduced 18.6" Radar Target Antenna Terminal Response.

justified in the latter chapters, we choose the sampler period to be such that the total length of the excitation vector is greater than t", the maximal 2-way transit time of the target, of equation (2-18).

Figure 3-13 shows the radar A-scope plots for the 1st natural mode waveform excitation of the correctly-sized (and no Doppler) target. The rectangular plots on the left-hand side illustrate the expected damped cosinusoids starting at the retarded time for which nonzero data for the full length of the excitation vector occurred. The polar plots on the right-hand side give a very sensitive indicator of the purity of the 1st natural mode waveforms. The double triangle pointers on the dashed damping mode linear, separated by exactly one excitation vector time length. From the envelope plot in the upper right hand corner, we can identify nearly pure natural mode waveform occurring starting at approximately 0.5 normalized time units past the end of the excitation vector. There are about 0.5 normalized time units of zeros at the beginning of this file. Next to be observed is the rotations plot on the lower right-hand corner. In this case, we can detect a constant slope which is close to the exact rotation line which is dashed. The measured rotation line is slightly more negative. From a comparison with data to follow, we could estimate the wire to be about 2% shorter than the length we are using for our frequency/sampling constants matrix. A 2% error in reading the ruler is not unreasonable. This constitutes our baseline A-scope plots for the 1st mode excitation of a correctly-sized cylindrical radar target.

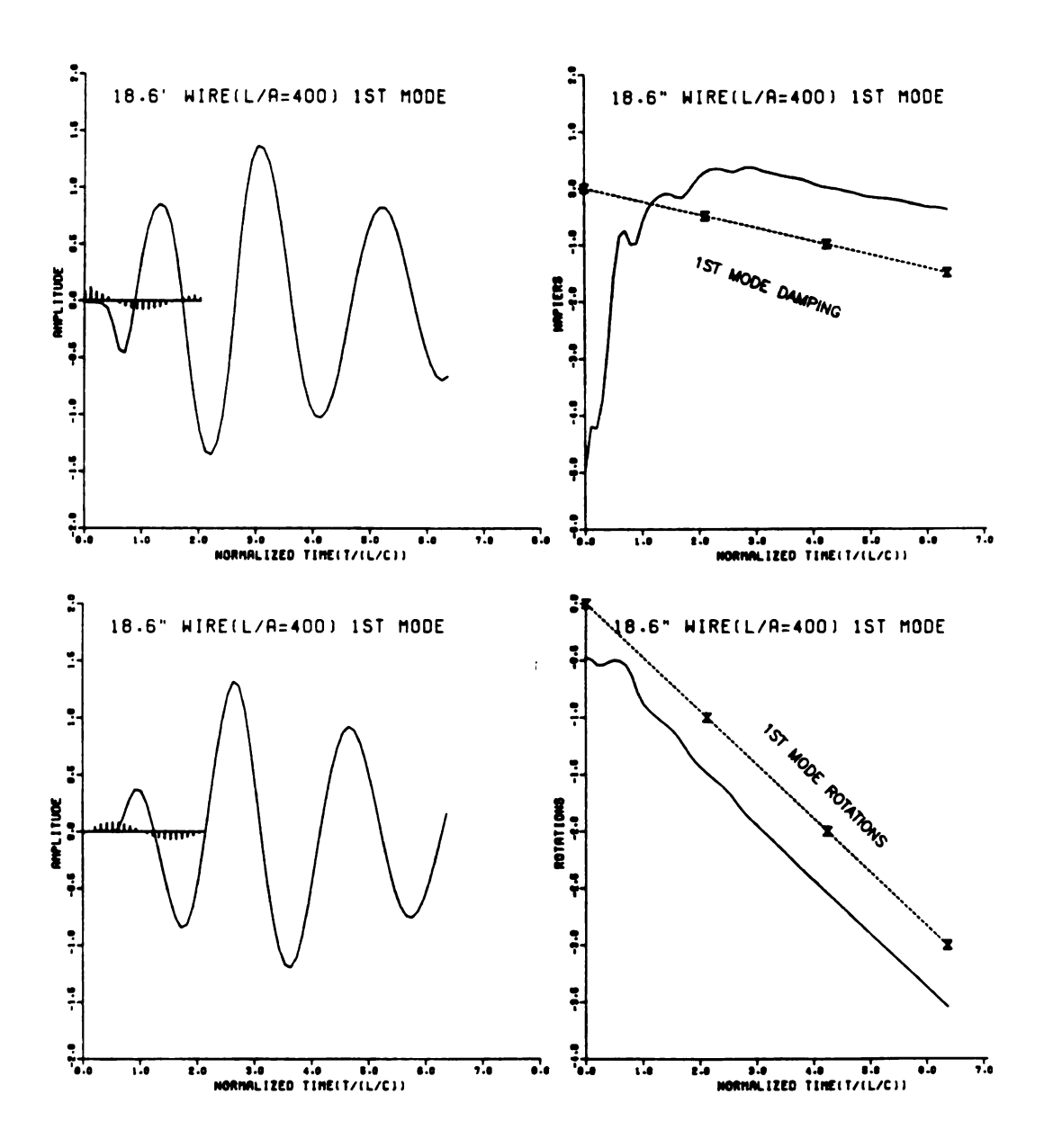


Figure 3-13. 1st Mode Waveform Excitation of Correctly-Sized Thin Cylinder Baseline Radar Target.

Next we shall scale the clutter-reduced radar target antenna terminal response by 10% physical undersize, but retain the excitation vectors for the correctly sized radar target we have just viewed. The undersized (and oversized) radar target antenna terminal response files we will be using are created from the original correctly sized sampled data files. The first step is rescaling the time coordinate of the samples. Next cubic splines (references 3-4 and 3-10) are used to obtain sample data points in synchronism with the excitation vector samples.

Figure 3-14 displays the 1st mode excitation for the original sized target processed on the 10% undersized clutter-reduced radar target antenna terminal response. The rectangular radar A-scope displays are different by heuristic examination by eye, but not by a quantifiable amount. The polar mode radar A-scope gives a more quantifiable identification of a dominant natural mode waveform. It should be noted that the rotation plot of Figure 3-14 has a constant "late-time" slope. However, this constant slope differs from the expected slope for the correctly-sized radar target by a slight, but definitely greater, negative slope. The envelope plot has more ripples than that for the baseline, Figure 3-13, for the 1st mode.

Let us now examine Figure 3-15 which is for a 10% oversizing of the original baseline response of Figure 3-13. The rectangular plots of the radar A-scope are again similar but difficult to interpret. They are difficult to interpret because one cannot use either the amplitude of the mode waveform or the time delay of the mode

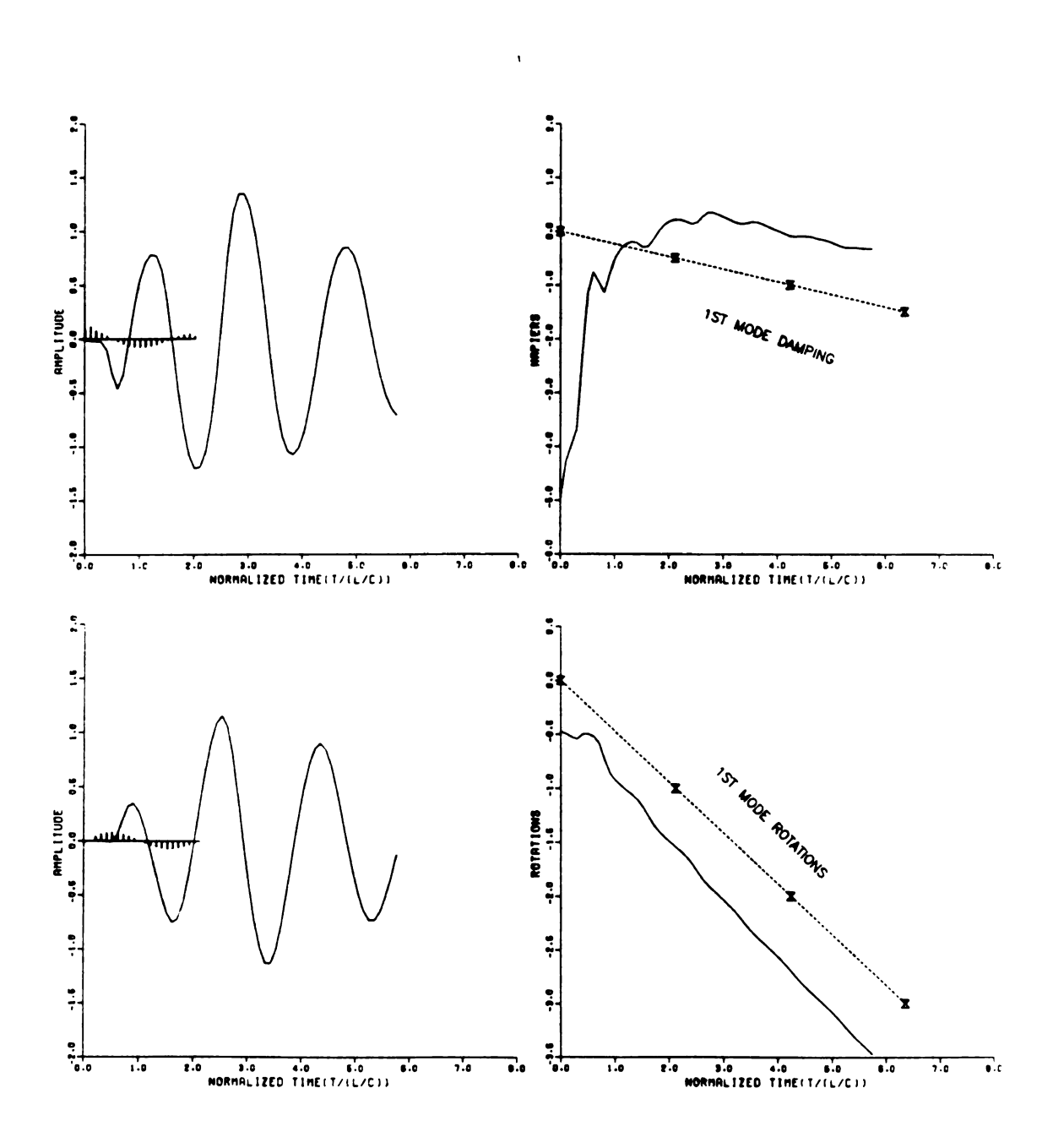


Figure 3-14. 1st Mode Waveform Excitation of 10% Undersized Thin Cylinder Radar Target.

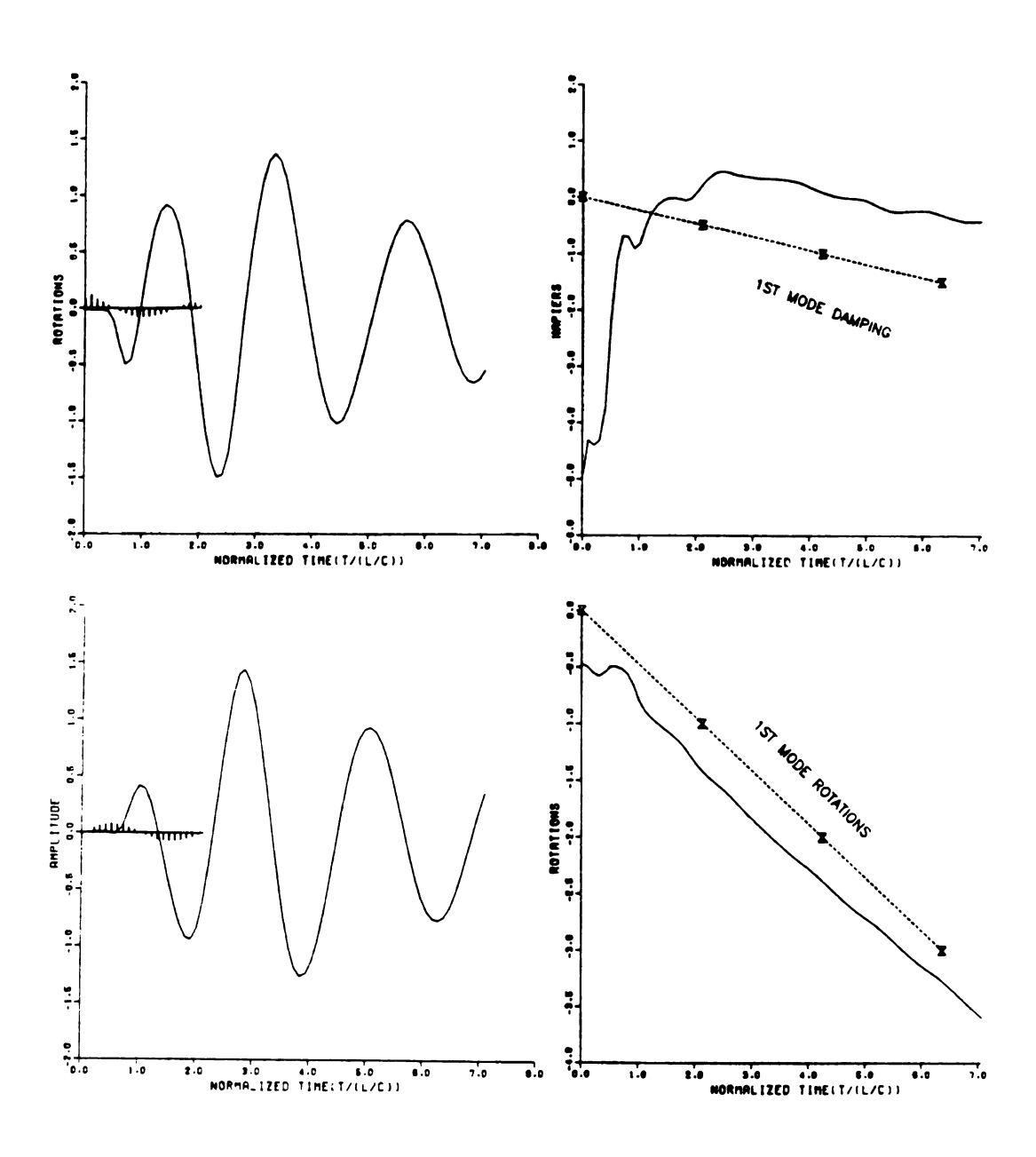


Figure 3-15. 1st Mode Waveform Excitation of 10% Oversized Thin Cylinder Radar Target.

waveform for target discrimination. One cannot use the amplitude because both range dependence and aspect-angle dependence of the target destroy its use as an aspect angle independent radar target discrimination techinque. One cannot use time delay for discrimination for two reasons: one is its obvious range dependence and the second is that even if a radar range estimate is available from other processing algorithms, its resolution will not, in general, be precise enough to calibrate individual modes. The rotations plot is not quite as clear as before. The slope does not appear to be as constant as the two preceding cases, but there is a slight trend to be less negative than either of the two preceding rotation plots. The envelope plot for the 10% oversized radar target is more lumpy than the plot for the correctly-sized radar target antenna terminal response.

We shall temporarily skip the second mode processing. The reason for this is that for the normal incidence on the thin cylinder, no even natural mode waveforms would be excited. This follows from symmetry arguments.

Figure 3-16 is the 3rd mode waveform excitation processing on the correctly-sized 18.6" (L/a = 400) radar target antenna terminal response. The rectangular radar A-scope plots clearly indicate the presence of a waveform of at least approximately correct frequency. The rotation plot clearly indicates a constant slope, but more negative than the exact rotation line. This would positively correlate with our 1st mode estimate of a 2% undersizing of the original data

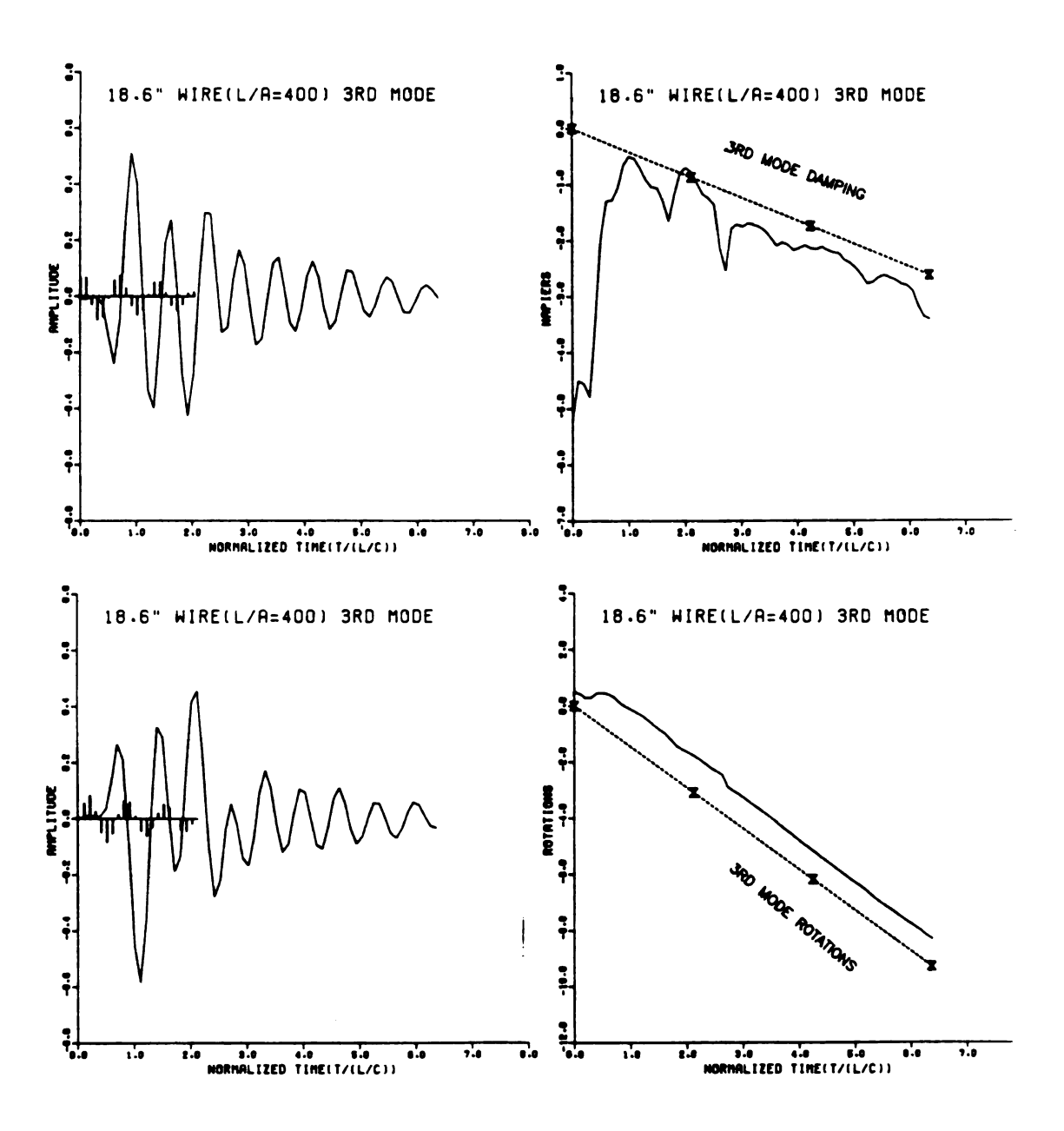


Figure 3-16. 3rd Mode Waveform Excitation of Correctly-Sized Thin Cylinder Baseline Radar Target.

file either by a ruler measurement or by method of moments natural frequency calculation. Another good confirmation with the 1st mode is in the envelope plot. The 3rd mode envelope plot has a "latetime" relatively constant slope that also starts approximately 0.5 normalized time units behind the end of the excitation vector. This is the same as for the 1st mode envelope.

For the 10% undersized radar target antenna terminal response processed for the correctly-sized 3rd mode waveform, we obtain Figure 3-17. The rectangular 3rd mode plots are not indicating the same waveform purity as before. The polar mode radar A-scope plots show observable departures from the expected constant "late-time" behavior. For the 10% oversized radar target antenna terminal response processed for the correctly-sized 3rd mode waveform on Figure 3-18, the rectangular plots differ by a difficult to quantify amount. In the polar mode radar A-scope plots the difference from the 3rd mode baseline is most obvious.

Figure 3-19 constitutes our baseline for fith mode waveform processing with the correctly-sized radar target. Only the rotation plot can give a waveform confirmation for this extremely weak mode waveform. Figure 3-20 gives the 10% undersized plots. In this case, the fifth mode waveform cannot realistically be observed and a distinction can be made from Figure 3-19. A similar situation holds for the 10% oversized plots of Figure 3-21.

Figure 3-22 constitutes our baseline for the 7th mode waveform processing with the correctly-sized radar target. Only the rotation plot can give a waveform confirmation for this extremely weak mode

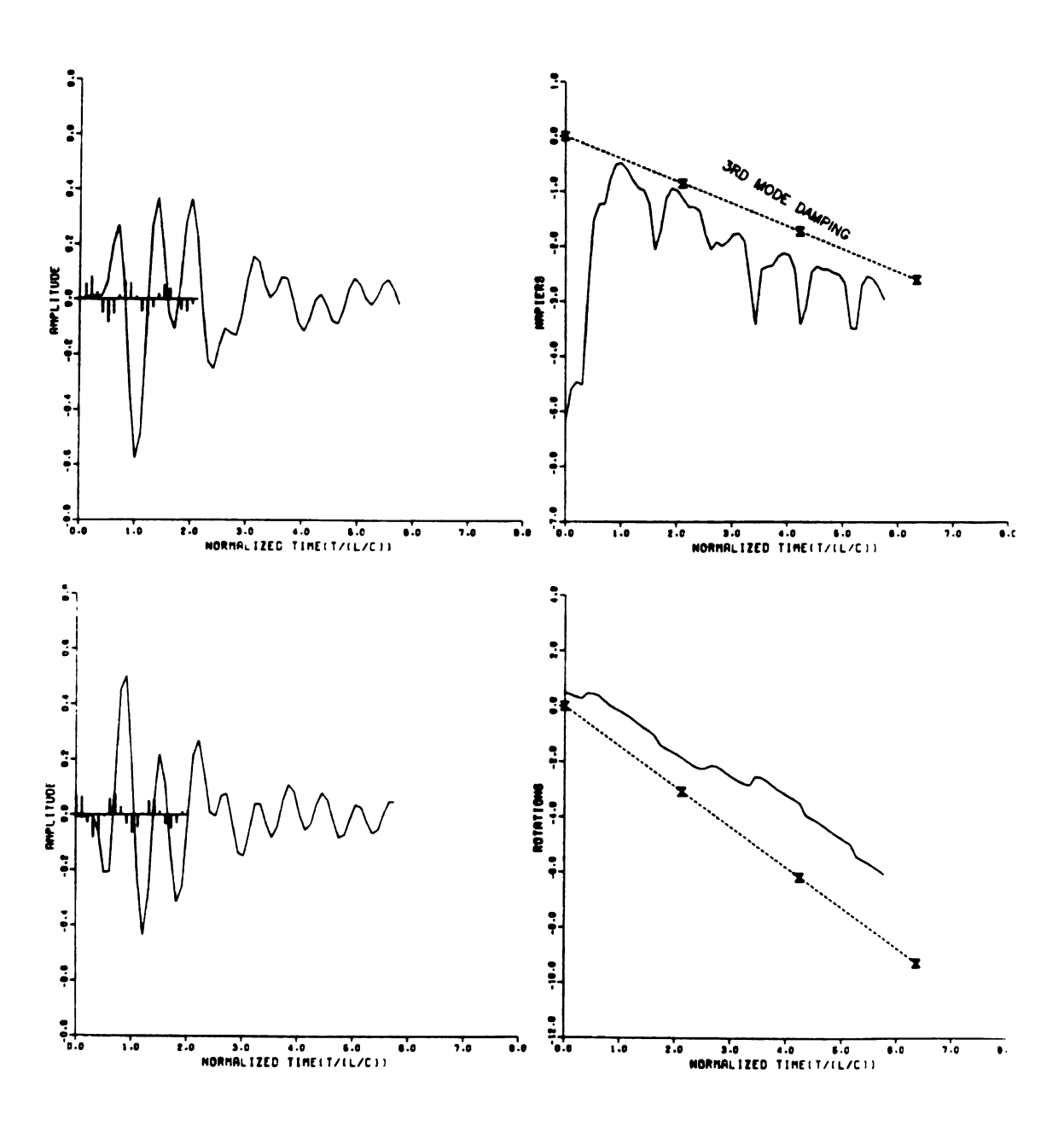


Figure 3-17. 3rd Mode Waveform Excitation of 10% Undersized Thin Cylinder Radar Target.



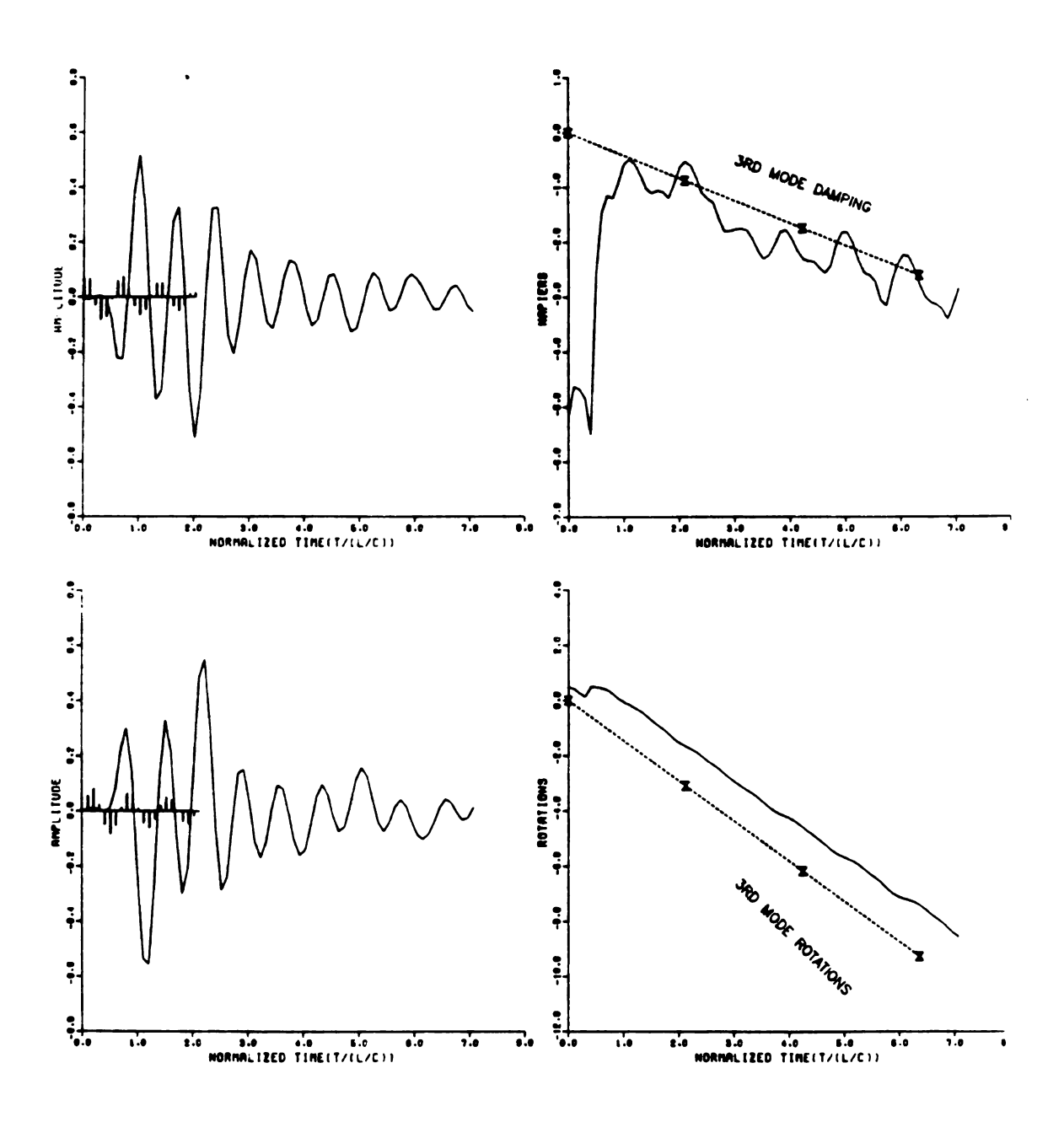


Figure 3-18. 3rd Mode Waveform Excitation of 10% Oversized Thin Cyliner Radar Target.

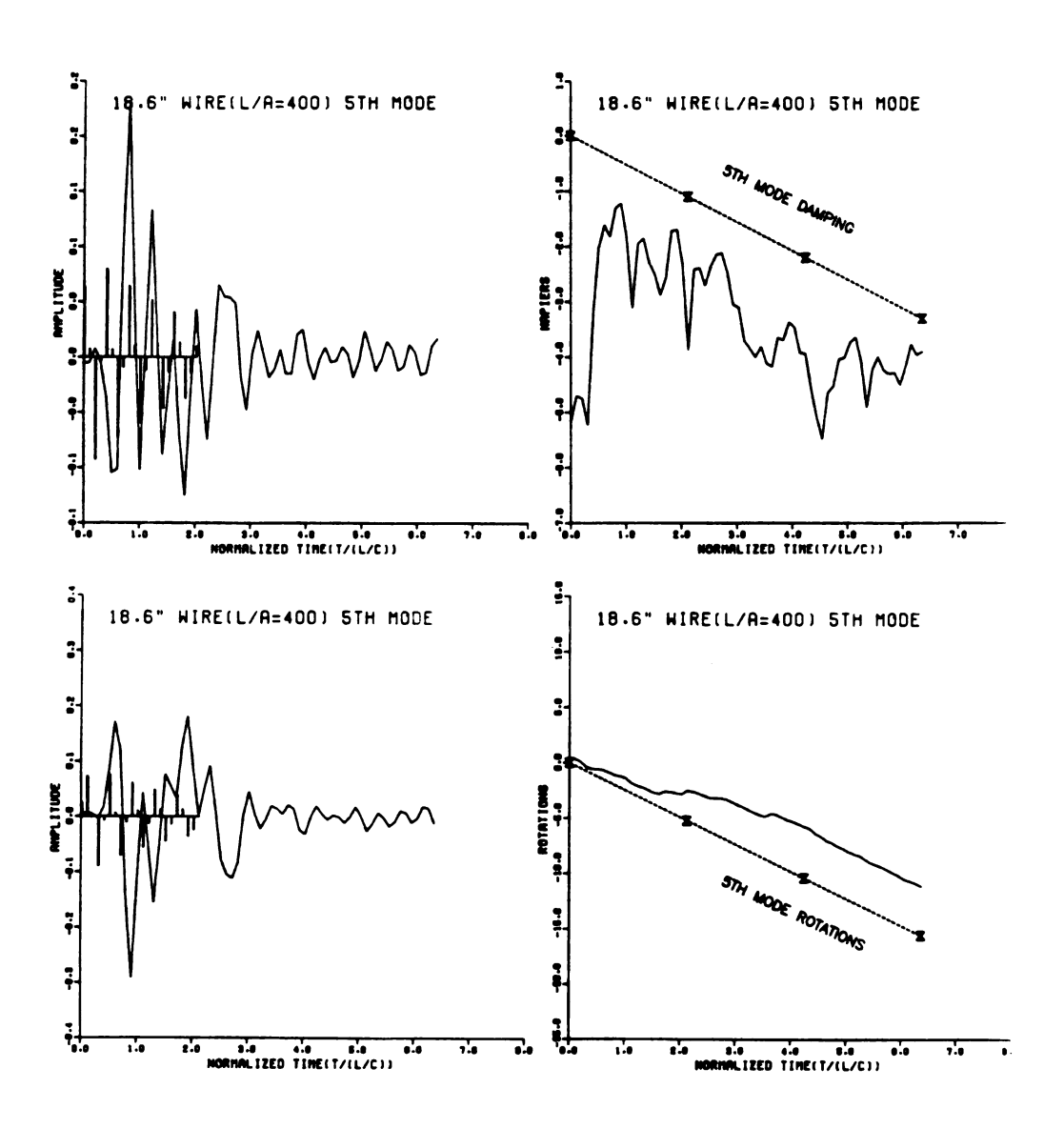


Figure 3-19. 5th Mode Waveform Excitation of Correctly-Sized Thin Cylinder Baseline Radar Target.

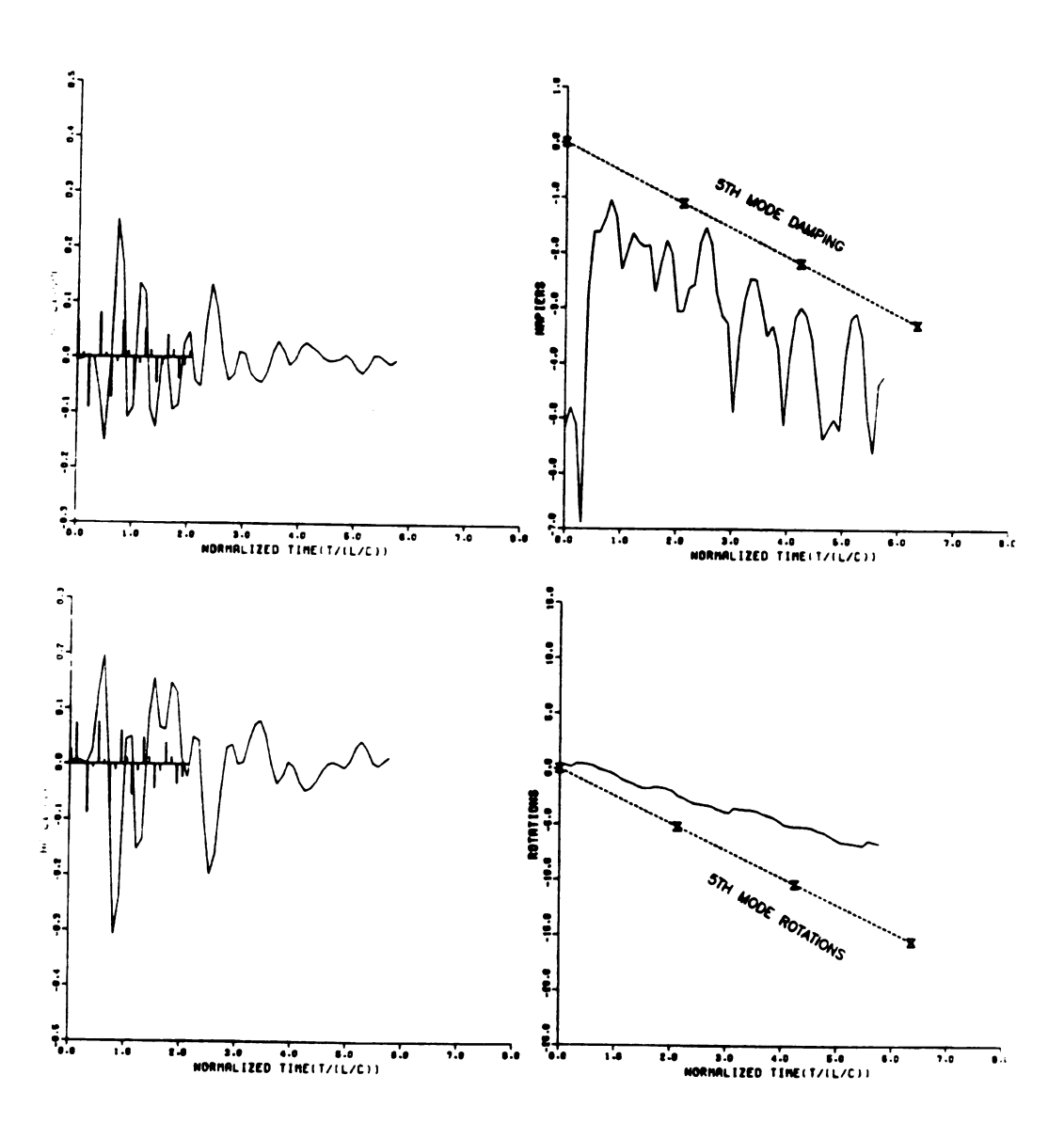


Figure 3-20. 5th Mode Waveform Excitation of 10% Undersized Thin Cylinder Radar Target.

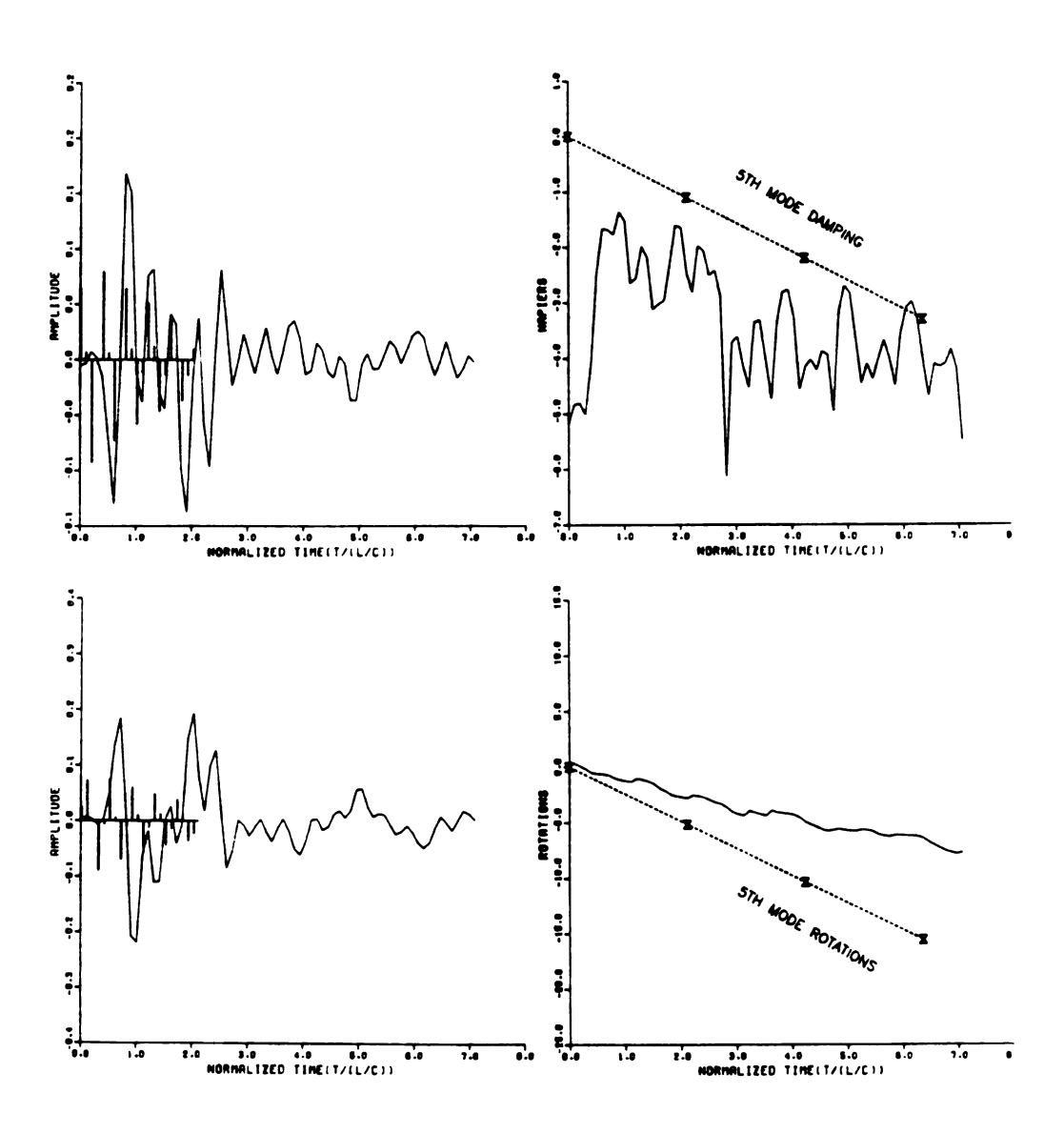


Figure 3-21. 5th Mode Waveform Excitation of 10% Oversized Thin Cylinder Radar Target.

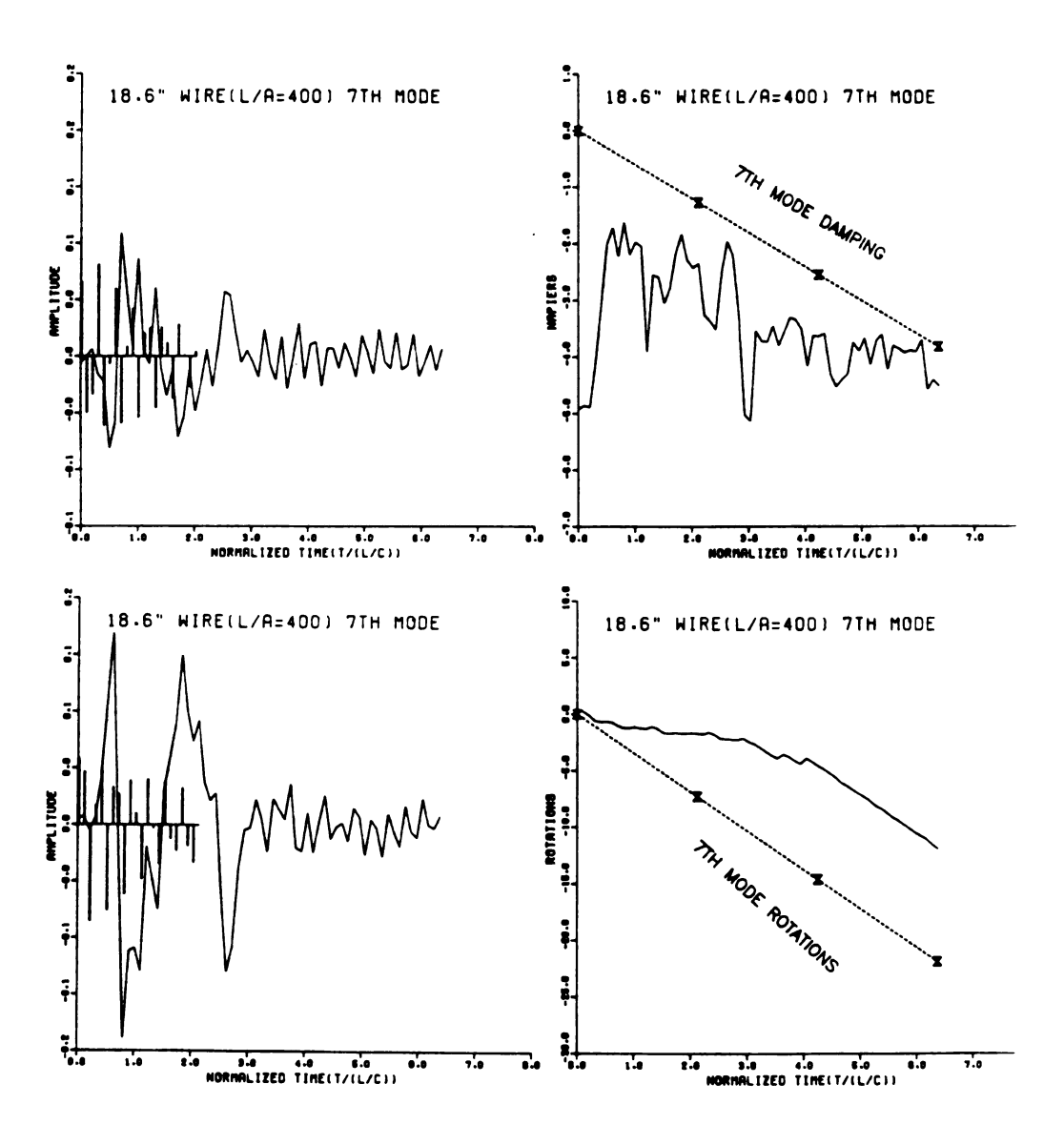


Figure 3-22. 7th Mode Waveform Excitation of Correctly-Sized Thin Cylinder Baseline Radar Target.

waveform. Figure 3-23 gives the 10% undersized plots. In this case, the seventh mode rotation plot completely breaks down. A negative confirmation is easy. Figure 3-24 gives the 10% oversized plots for the seventh mode excitation. In this case the rotation plot (note different scale) breaks down in another manner for this mode. A negative confirmation of this mode is easy.

3.8 Observation of the Absence of a Natural Mode Waveform

From the preceding two sections we developed techniques to recognize or detect specific natural mode waveform. For the standard radar problem always contending with thermal noise, propagation scintillation, target glint, false targets, receive nonlinearities, etc., our initial technique is at most half a useful procedure for a radar. If these were not critical issues, we could use synthetic radar target files exclusively and ignore the difficulties of empirical radar target data which we will deal with exclusively. Complementary to the detection of specific natural mode waveforms is the detection of "false alarms". In fact, the signal-to-noise ratio of a radar system is sometimes characterized in terms of its probability of detection versus its "false alarm" (reference 3-10).

In this section we shall observe the absence of a radar target natural mode waveform in three cases. The data we shall use are our baseline correctly-sized radar target antenna terminal response of the previous section. Note that it is not deconvolved for either the antenna response or for the incident plane wave pluse shape. We will be observing target mode excitations for which no radar target natural

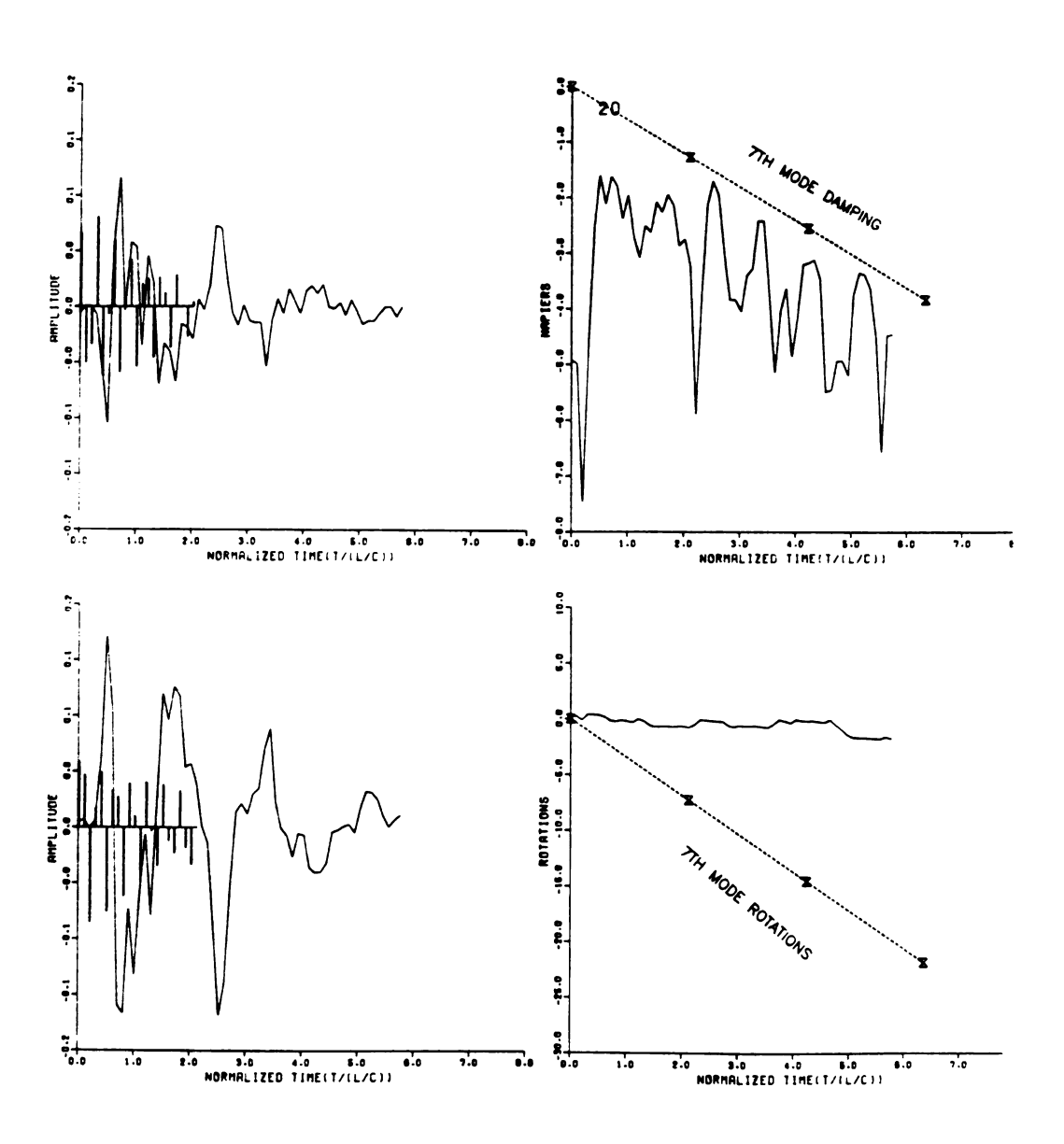


Figure 3-23. 7th Mode Waveform Excitation of 10% Undersized Thin Cylinder Radar Target.

				Ŧ
			4	

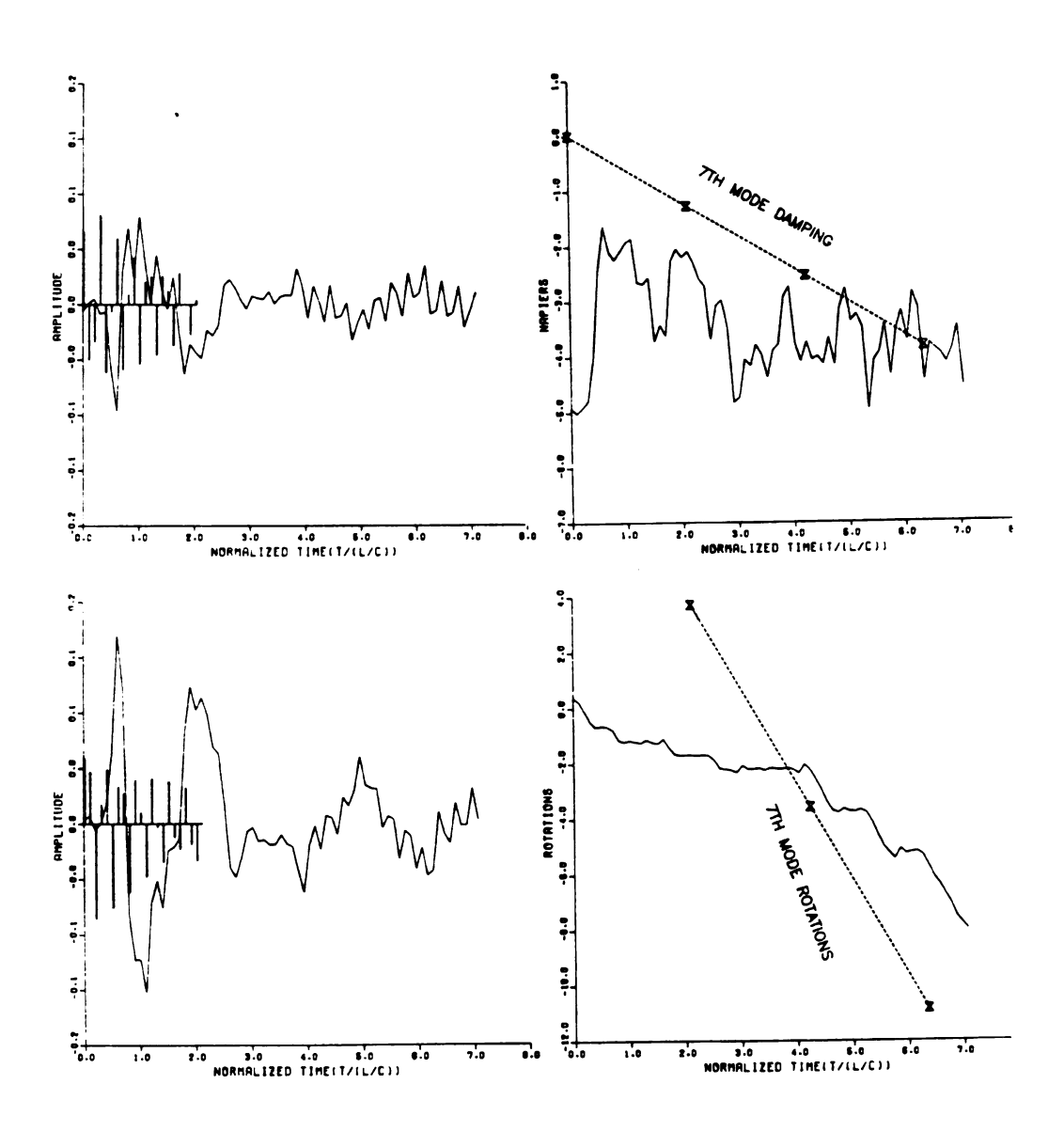


Figure 3-24. 7th Mode Waveform Excitation of 10% Oversized Thin Cylinder Radar Target.

mode waveforms are present. We may do this because there are physical configurations for which the coupling coefficients of certain current density natural mode must be zero. For the thin cylinder illuminated by a normally incident plane wave, there can be no even natural modes excited. This is due to the perfect symmetry of this particular radar target with respect to the incident E-field.

In Figure 3-25 we observe the second mode waveform processing of our baseline correctly-sized radar target antenna terminal response. From the rectangular plots we observe a strong transient located during the first nonzero samples of the excitation vector, but followed by no corresponding natural mode waveform response in the expected "late-time" portion observed in the odd mode waveforms. The envelope plot shows a pulse-like envelope of time length equal to the excitation vector time length. (Remember that our envelope plot are on a compressed logarithmic scale.) We will observe this pulse-like shape in the envelope plot again in the next chapter and we will call its aspect-angle independent excitation vector a K-Pulse for a specific radar target.

In Figure 3-26 we observe the fourth mode waveform processing of our baseline correctly-sized radar target antenna terminal response. There should be no waveform originating from the radar target at this frequency. The rotation plot does, however, indicate a waveform with a rotation slope slightly lower to that of the correct fourth natural mode waveform. The envelope plot appears as a pair of staggered pulse shapes and is not explainable as a target mode waveform. The rectangular plots indicate perhaps the existence of two distinct ringing

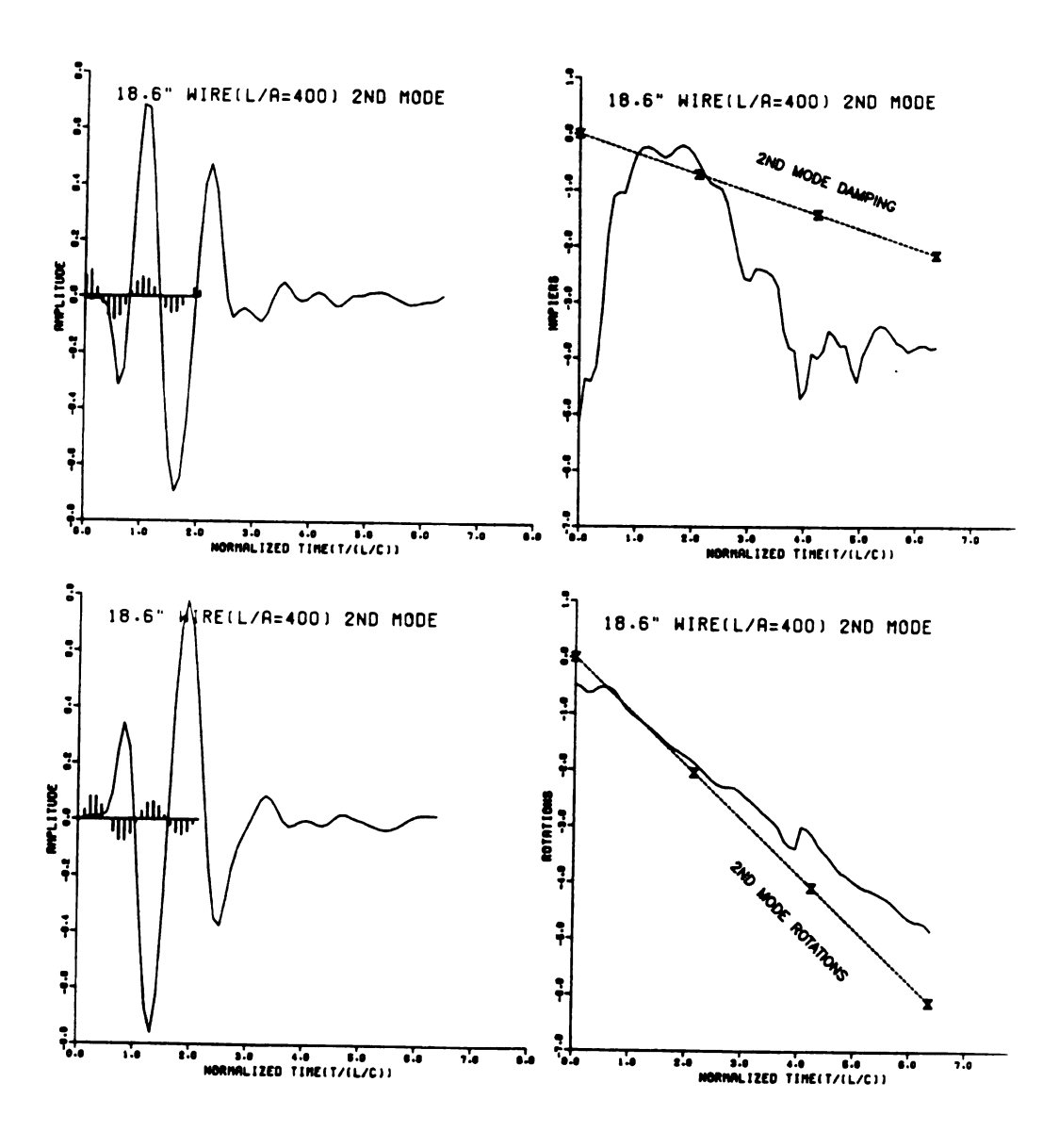


Figure 3-25. 2nd Mode Waveform Excitation of Baseline Thin Cylinder Radar Target at Normal Incidence.

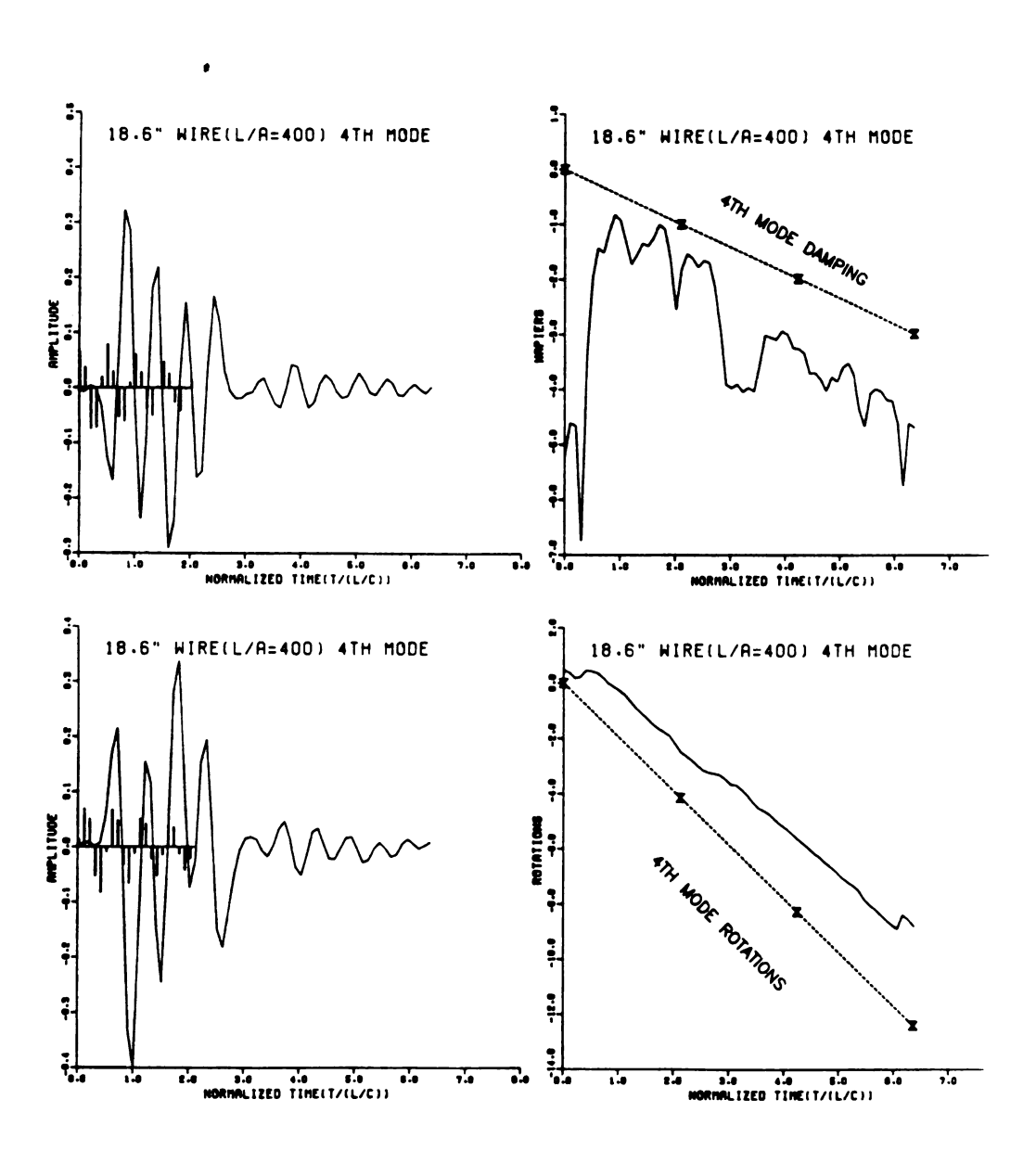


Figure 3-26. 4th Mode Waveform Excitation of Baseline Thin Cylinder Radar Target at Normal Incidence.

waveforms, one in the early-time and one of small amplitude starting at 3½ normalized time units. It is believed this is a mode originating within the radar system set-up, rather than from thermal noise. This is suggested by the coherence displayed by the rotation plot.

In Figure 3-27 we observe the tenth mode waveform processing of our baseline correctly-sized radar target antenna terminal response. There does not appear to be any coherent signal energy at this natural frequency since the rotation plot fails to match the expected slope. These plots are what we should expect to be generated from thermal noise within the radar system.

3.9 Extension of the Model to Unknown Natural Frequencies

So far everything we have done is based upon a priori exact knowledge of the invariant radar target parameters—the natural frequencies. There are no flyable airborne radar targets for which the natural frequencies are known in an analytically closed form. We have also seen that the radar system itself may contribute some natural frequencies to the radar return. Further we should not expect to observe all of the system natural frequencies on a specific radar target return. However, if we can obtain these radar target invariant parameters by another route, we will use them in exactly the same manner we would use equation (2-22).

In the next chapter we shall initiate a reliable procedure for obtaining these natural frequencies from measurement data. So we must add another goal in our quest for an aspect-angle independent radar target discrimination technique.

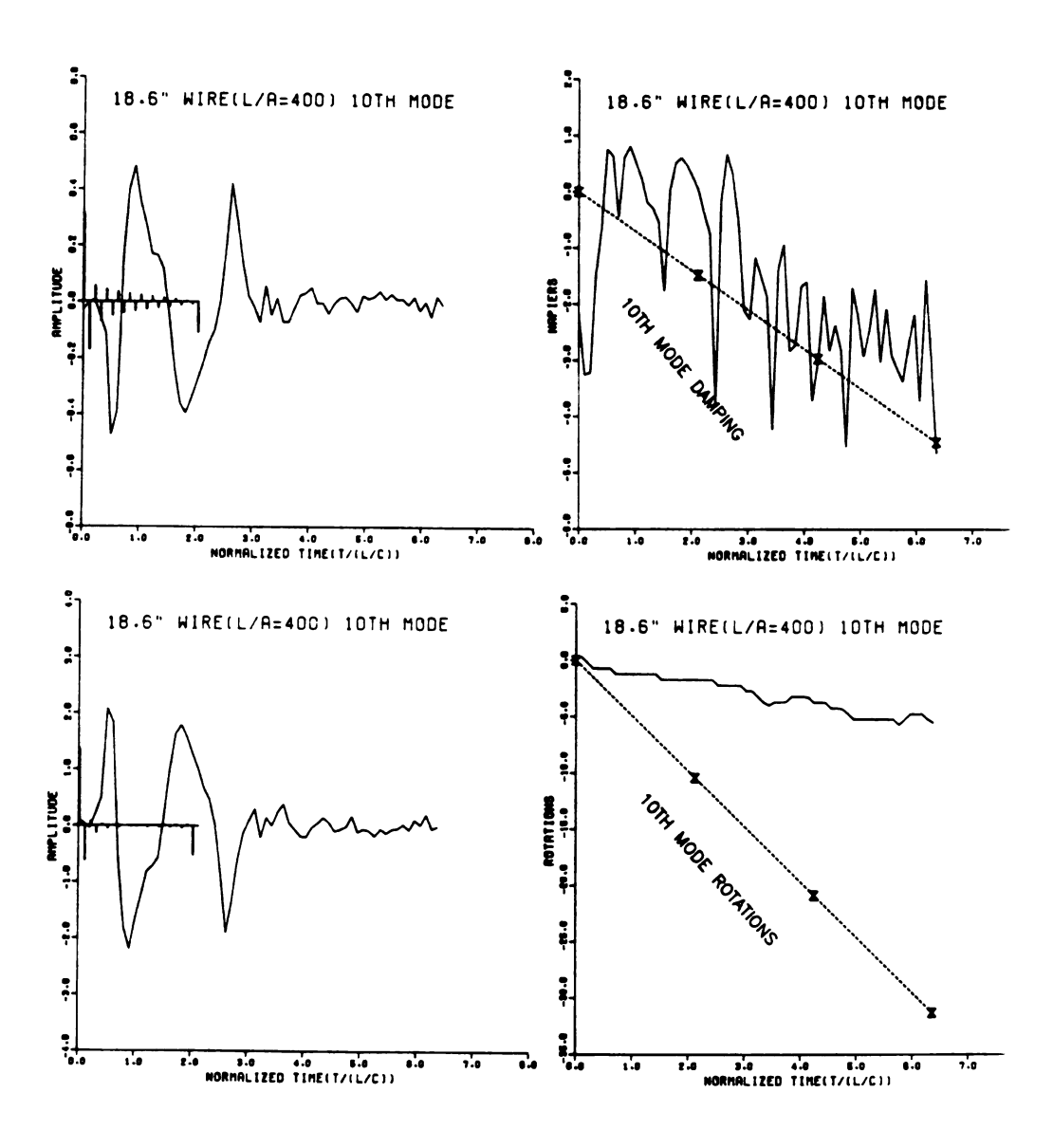


Figure 3-27. 10th Mode Waveform Excitation of Baseline Thin Cylinder Radar Target at Normal Incidence.

CHAPTER 4

PRONY'S METHOD AND THE K-PULSE

4.1 The Original Prony's Method

Almost 200 years ago (1795) a measurement-based technique using a finite series of complex exponentials was developed by R. Prony (ref. 4-1). Although the original technique was developed for evaluating the temperature dependence of vapor pressures over liquids, we shall find it of use to use in the radar target discrimination problem. We have already used in equation (3-36) what we have called a "Prony series". With a few exceptions, Prony's method will perfectly match a Prony series to equally spaced continguous sampled data points of a continuous function. For example, for 2N sampled data points, Prony's method will solve for the unknown constants of an N term Prony series.

In addition there is a least-squares formulation of the complex exponential matching technique called the "extended Prony's method" (ref. 4-2). Similar to the "extended Prony's method" are many recent techniques such as linear prediction, maximum likelihood, and maximum entropy method which also have a least-squares formulation (ref. 4-3, 4-4). These latter techniques are often expressed in terms of an analysis spectrum or of a synthesis filter. However in 1795, Gauss had not yet disclosed the famous least-squares technique. Hence Prony's method is the only one of the above techniques not

influenced by the least-squares technique. Least-squares techniques are not reversible to the original data. A "reversible operation" like Prony's method is a desirable building block feature for a modern "quiet" radar design.

We shall start the derivation of Prony's method with a definition of a Prony series of N complex exponentials in continuous time by equation (4-1).

$$v(t) = \sum_{k=1}^{N} C_k \exp(s_k t) , t \ge 0$$
 (4-1)

The invertible sampled data version of equation (4-1) is given by equation (4-2).

$$v(t,m) = \sum_{k=1}^{N} c_k \exp(s_k(nT+mT-T))$$
 (4-2)

where t = nT + mT-T

n an integer

$$0 < m \leq 1$$

We have used the notation of the modified z-transform described in Appendix A. We will not revert to a more common sampled data notation of the ordinary z-transform notation, equation (4-3), by picking a specific synchronization, m = 1.

$$v(t,m=1) = \sum_{k=1}^{N} C_k \exp(s_k^T n) = \sum_{k=1}^{N} C_k \{\exp(s_k^T)\}^n,$$
 (4-3)

In order to prepare for matrix notation, we will compress the notation of equation (4-3) into equation (4-4).

$$v_n = \sum_{k=1}^{N} C_k \{ \exp(s_k T) \}^n = \sum_{k=1}^{N} C_k z_k^n, \quad n=0,1,...,2N-1$$
 (4-4)

Let us consider an arbitrary sequence of 2N equally spaced sample data values $\{v_n\}_{n=0}^{2N-1}$. We should observe that in equation (4-4), there are exactly 2N unknowns on the right hand side to match the 2N sampled data values on the left hand side. Prony's method is a procedure to determine the unknown constants of the series of complex exponentials.

Prony's method consists of a procedure we shall divide into three parts. The first part always appears to be the least motivated on physical grounds. Remember that we are going to determine the 2N constants of the n term "Prony series" of equation (4-4) by 2N sampled data values of the empirical data. The simultaneous determination of the 2N constants of the N term "Prony series" is not a linear problem such as the 2N term Fourier series based upon the same 2N sampled data values.

Conceptually, suppose the natural frequencies have been determined. Then the complex amplitudes for each term of the "Prony series" could be determined from any N sampled data values of equation (4-4). We will, for example, take the first N sample values and put them into matrix notation of equation (4-5). Hence the crucial step is to obtain the natural frequencies. This will occur in two steps. If we possessed a differential equation, we would take the Laplace transform and obtain a polynomial in frequency. The roots of the

$$\begin{bmatrix} 1 & 1 & 1 & 1 & \\ exp(s_1^T) & exp(s_2^T) & exp(s_N^T) & \vdots & \\ exp(s_1^T(N-1))exp(s_2^T(N-1)) \dots exp(s_N^T(N-1)) \end{bmatrix} \begin{bmatrix} c_1 \\ c_2 \\ \vdots \\ c_N \end{bmatrix} = \begin{bmatrix} v_0 \\ v_1 \\ \vdots \\ v_{N-1} \end{bmatrix}$$
(4-5)

homogeneous polynomial would be our natural frequencies. Equation (4-6) gives the Laplace transform of the "Prony series" and equation (4-7) is the modified z-transform for m = 1.

$$\hat{v}(s) = \sum_{k=1}^{N} c_k (s-s_k)^{-1}, Re(s) > \max_{k} (Re(s_k))$$
 (4-6)

$$V(z,m=1) = \sum_{k=1}^{N} C_k (1-z_k/z)^{-1}, |z| > \max_{k}(|z_k|)$$
 (4-7)

Instrinsic to Prony's method is the exclusive use of sampled data values. So we do not observe continuous waveforms characterized by differential equations, but we do have a characterization of difference equations. From 2N sampled data values we could form a polynomial of degree 2N-1. But this is too large, since we wish to match it to the N term "Prony series". We shall be looking for some function a(nT) such that when convolved with v(nT) will yield an output with no natural mode waveform, o(t) in equation (4-8), remaining. Alternatively, o(z) in equation o(4-9), is an entire function.

$$o(t) = a(t)*v(t)$$
, $t=nT$, n is an integer (4-8)

$$O(z) = A(z)V(z) \tag{4-9}$$

But equation (4-8) can be expressed as equation (4-10), and equation (4-11) must hold.

$$o(nT) = \oint A(z)V(z)z^{n-1}\frac{dz}{2\pi j}, n > 0$$
 (4-10)

$$o(nT) = \begin{cases} unknown, & n=0,1,...,N-1 \\ 0, & n=N,N+1,...2N-1 \\ 0, & n \ge 2N & \text{if } V(z) \text{ has only N poles} \end{cases}$$
 (4-11)

The significant feature which A(z) possesses is that it possesses zeros exactly where V(z) possesses poles. For A(z) to possess N zeros, it must be of degree N, with in general N+1 terms. This means that a(nT) will be of finite length, (N+1)T. Figure 4-1 shows the page in Prony's "Essai . . ." where N equations in N+1 unknowns were originally set up. We show this for a number of reasons: (1) it is different from modern matrix presentations, (2) he could solve it by hand, (3) our "fast" Prony's method in the next chapter will resemble it more than the modern matrix presentations.

In Prony's notation $[z_i]_{i=1}^{2N-1}$ represent the sampled data values. Equation (4-12) is a matrix representation of the Prony system of N equations in N + 1 unknowns $[A_i]_{i=0}^{N}$

$$\begin{bmatrix} z_{0} & z_{1} & \cdots & z_{N-1} & z_{N} \\ z_{1} & z_{2} & \cdots & z_{N} & z_{N+1} \\ \vdots & \vdots & & \vdots & \vdots \\ z_{N-2} & z_{N-1} & \cdots & z_{2N-3} & z_{2N-2} \\ z_{N-1} & z_{N} & \cdots & z_{2N-2} & z_{2N-1} \end{bmatrix} \begin{bmatrix} A_{0} \\ A_{1} \\ A_{N-1} \\ A_{N} \end{bmatrix} = \begin{bmatrix} 0 \\ 0 \\ \vdots \\ 0 \\ 0 \end{bmatrix}$$

$$(4-12)$$

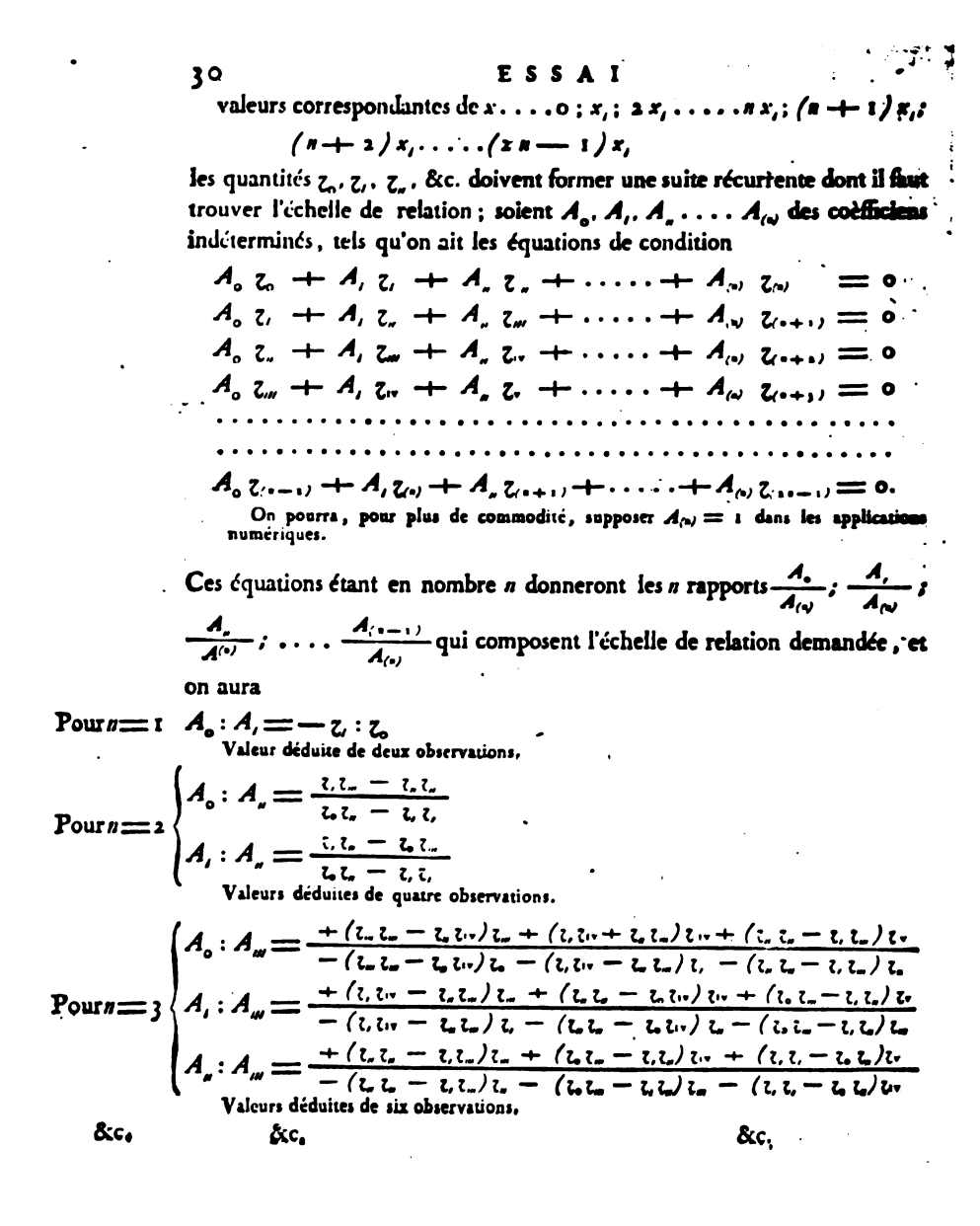


Figure 4-1. Undetermined coefficients of Prony's "Essai. . . . "

Hopefully there are enough matrix entries that the data matrix can be identified as a Hankel matrix. In a Hankel matrix all entries along a diagonal from lower left to upper right possess an identical value. This is the case here even though equation (4-12) is not a square matrix.

By solving equation (4-12) we will obtain a polynomial, in terms of A(z), which we can root. From these N roots, we can obtain the N natural frequencies of the "Prony series". Then we can solve equation (4-5) for the complex amplitudes. Then we will possess the values of all 2N constants of the "Prony series" of equation (4-1).

We shall close this introductory section and discontinue the Prony notation. In the next section, we shall define the "Prony K-Pulse". After defining the "Prony K-Pulse", we shall solve the three parts of Prony's method using the now more common matrix notation and techniques.

4.2 The "Prony K-Pulse"

The original "kill-pulse" or K-Pulse concept (ref. 1-2) is a time-limited excitation waveform, k(t), (like our a(t) in equation (4-8)) which when convolved with the radar target scatterer yields no natural mode waveform in the scattered E-field. Alternatively, we can specify that $\hat{K}(s)$ be an entire function.

It appears that the original K-Pulse concept is solely a transmitting formulation. Hence the K-Pulse, $\hat{K}(s)$, could be the plane wave "pulse shape", $\hat{f}(s)$ in equation (2-15), of our basic SEM model solution of the EFIE.

We shall decline to advocate the transmit formulation of the K-Pulse if we are confined to use either analog radar transmitters or analog transmitting antenna. We will find extensive use for the K-Pulse in our receiving formulation of our radar problem solution. We shall use it as fluently as one might use a multi-dimensional impulse function for a specific radar target.

There are two useful facts we will close this section on. First, the entire function, $\overrightarrow{W}^{\kappa}(\P,\overrightarrow{r},s)$, must be in the time domain of duration less than the maximal one-way transit time of the radar target itself. This is based upon the hypothesis that there exists a retarded time for which the "class 1" current density coupling coefficients are valid. Its contribution in the far-field scattered E-field may last as long as a maximal 2-way transit time of the incident plane wave over the radar target. Second the K-Pulse can be as short as a maximal 2-way transit time of the plane wave over the radar target. This is not to say that shorter K-Pulses are not possible for some aspect-angles and some targets, but we are stating the general, aspect-angle independent case.

The "Prony K-Pulse" is defined as one of the kill vectors, a(nT), of equation (4-8) or equation (4-9) whose time length is not less than t" of equation (2-18).

4.3 Prony's Method and the K-Pulse Derivation

We have already defined a "Prony series" by equation (4-1). We shall now recast part 1 of Prony's method by recasting equation (4-12) in terms of our standard sampled data values $[v_i]_{i=0}^{2N-1}$ by (4-13).

$$\begin{bmatrix} v_{N} & v_{N-1} & \cdots & v_{0} \\ v_{N+1} & v_{N} & \cdots & v_{1} \\ \vdots & \vdots & & \vdots \\ v_{2N-1} & v_{2N-2} & \cdots & v_{N-1} \end{bmatrix} \begin{bmatrix} a_{0}' \\ a_{1}' \\ \vdots \\ a_{N}' \end{bmatrix} = \begin{bmatrix} 0 \\ 0 \\ \vdots \\ \vdots \\ 0 \end{bmatrix}$$

$$(4-13)$$

The modern method of solving this equation is to note that the vector $[a_i^*]$, can be divided by a_0^* without alteration of the solution and then moving the left hand column to the right hand side to obtain equation (4-14) which possesses the same a_0^* normalized solution. Note that in equation (4-13) we performed a trivial reflection of the sampled data matrix which we will exploit in the next chapter.

$$\begin{bmatrix} v_{N-1} & v_{N-2} & \cdots & v_0 \\ v_N & v_{N-1} & \cdots & v_1 \\ \vdots & \vdots & & \vdots \\ v_{2N-2} & v_{2N-3} & \cdots & v_{N-1} \end{bmatrix} \begin{bmatrix} a_1 \\ a_2 \\ \vdots \\ a_N \end{bmatrix} = - \begin{bmatrix} v_N \\ v_{N-1} \\ \vdots \\ v_{2N-1} \end{bmatrix}$$
(4-14)

This equation may be solved for the unknown vector $[a_i]$ by either standard matrix arithmetic or by the fast "Covariance method" (ref. 4-5). Our "Prony K-Pulse" is now given by equation (4-15).

$$\{\kappa_{i}\}_{i=0}^{N} = \{1, a_{1}, a_{2}, \dots, a_{N}\}\$$
 (4-15)

Part 2 of Prony's method is to find the N roots $\{z_i\}_{i=1}^N$ of the Prony polynomial P(z). We shall define the Prony polynomial from the solution set $\{a_i\}_{i=0}^N$ ($a_0 = 1$) by means of equation (4-15).

$$P(z) = \sum_{i=0}^{N} a_i z^i = \prod_{k=1}^{N} (z-z_k), a_0 = 1$$
 (4-16)

As one would expect from equation (4-4), we may obtain the natural frequencies by taking the complex logarithm of the calculated roots. These roots are obtainable by standard computer library routines. For polynomials of very large degree, this is a difficult problem of active interest. Equation (4-17) gives us the nonunique natural frequencies. We shall normally take the branch with the smallest numerical value.

$$s_k = T^{-1} \operatorname{clog}(z_k), k = 1, 2, \dots, N$$
 (4-17)

Part 3 of Prony's method is to solve for the complex amplitudes of the "Prony series" now that the natural frequencies are known.

This is readily solved by use of equation (4-18).

$$\begin{bmatrix} 1 & 1 & \cdots & 1 \\ z_1 & z_2 & \cdots & z_N \\ \vdots & \vdots & & \vdots \\ z_1^{N-1} & z_2^{N-1} & \cdots & z_N^{N-1} \end{bmatrix} \begin{bmatrix} c_1 \\ c_2 \\ \vdots \\ c_N \end{bmatrix} = \begin{bmatrix} v_0 \\ v_1 \\ \vdots \\ v_{N-1} \end{bmatrix}$$
(4-18)

Equation (4-18) is solved for the unknown amplitudes, $C_{\rm m}$, either by standard matrix arithmetic or by methods more suitable to Vandermonde matrices (ref. 4-6, 4-7, 4-8).

At this point all of the 2N constants of the Prony series of equation (4-1) are now known. Our technique of radar target identification will use these parameters and further processing of equation (4-15), the Prony K-Pulse.

Figure 4-2 summarizes the major steps we will perform to obtain our plots of the radar A-scope displays. Note that the first step is the generation of a "Prony K-Pulse". This by itself will be found to be inadequate for radar target discrimination. We form individual mode excitations by deleting one root from the Prony polynomial. Alternatively this may be done in the time domain by couplet convolution and deconvolution as in Appendix C. Using couplets as in equation (4-19), then the j-mode excitation vector would be numerically evaluated by deleting the j-th couplet from this convolution, leaving only N-1 convolutions as in equation (4-20).

$$[k_n]_{n=0}^{N} = (1,-z_1)*(1,-z_2)*...*(1,-z_j)*...*(1,-z_N)$$
 (4-19)

$$[e_n^j]_{n=0}^{N-1} = (1,-z_1)*(1,-z_2)*...*(1,-z_N)$$
 (4-20)

Figure 4-3 is a diplay of the original clutter-reduced radar target antenna terminal response file on the upper left with the computed K-Pulse on the upper right. The output K-Pulse convolution with the sampled data file is given on the lower left corner. Note

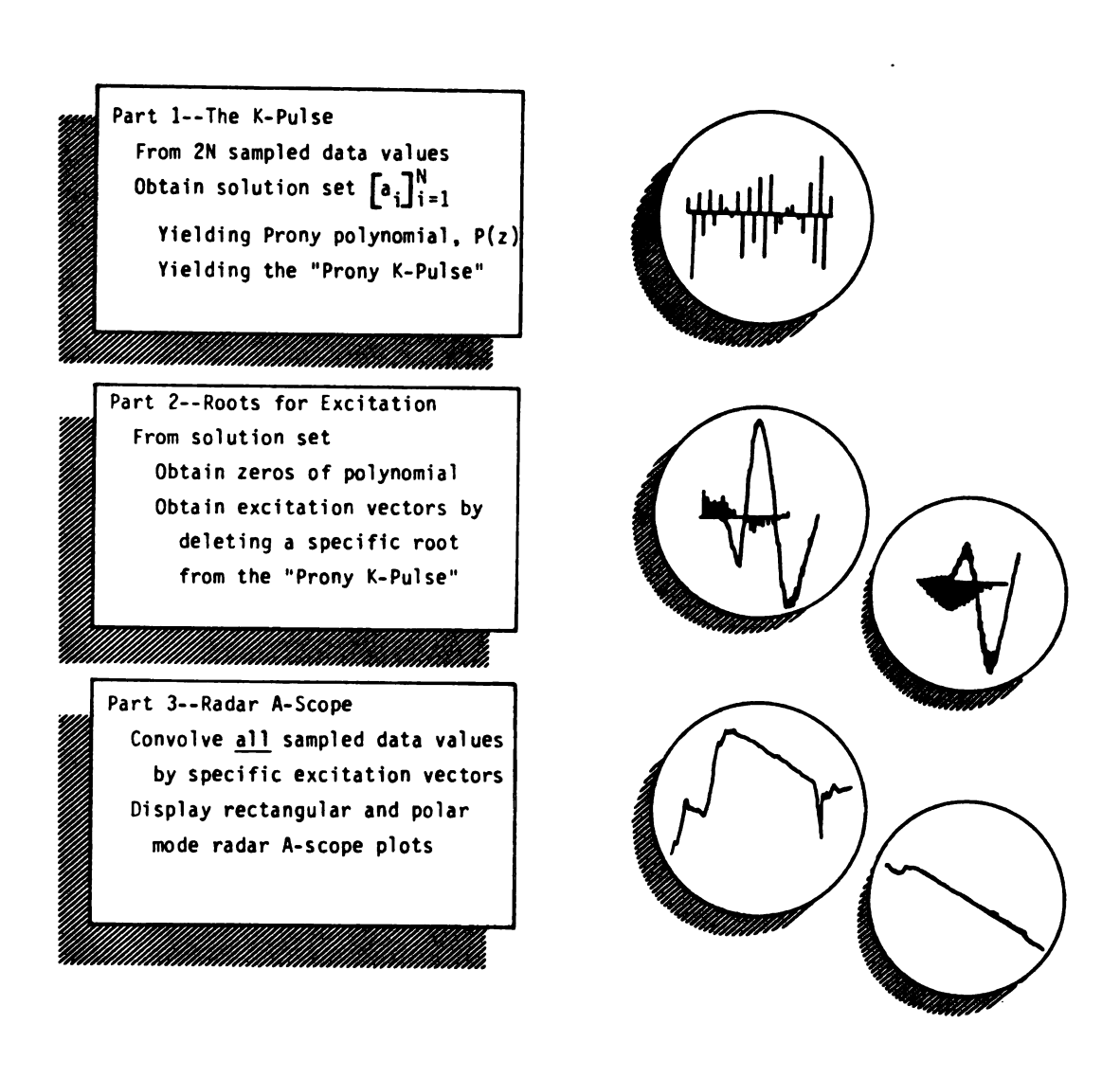
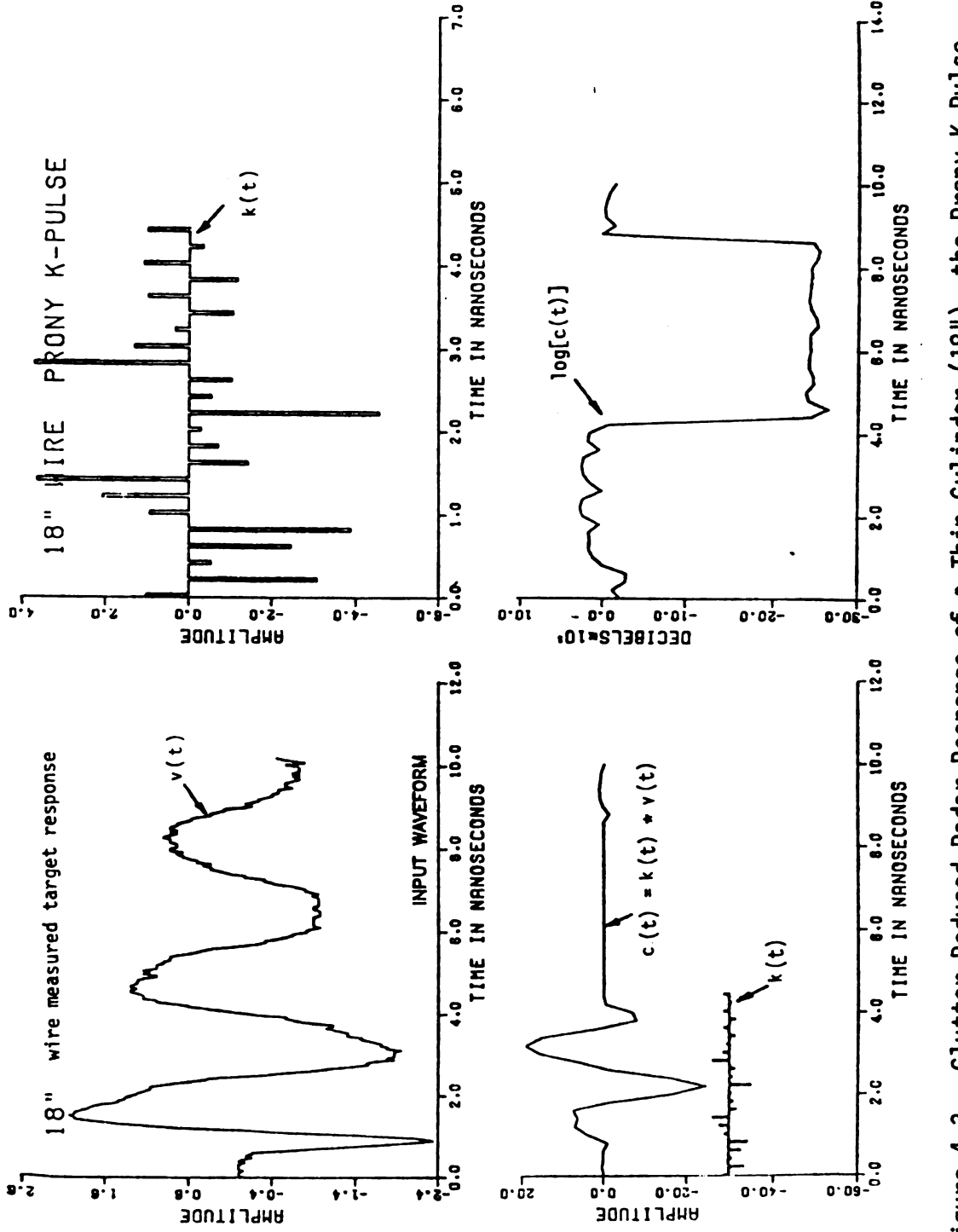


Figure 4-2. Major Steps in the Generation of Radar A-Scope Displays.



Clutter-Reduced Radar Response of a Thin Cylinder (18"), the Prony K-Pulse from Skip Samples, the Convolution, and Its Envelope in Decibels. Figure 4-3.

that the "late-time" response (remember that the "Prony K-Pulse" is defined so that "Class 1" assumptions should be satisfied for the retarded scattered E-field of this target) is approximately zero. However, using the compressed logarithmic scale for the envelope radar A-scope plot on the lower right corner, we see that the envelope is suppressed about 250 decibels for a two-way transit time and then is suppressed by only about 15 decibels. If we possessed all the radar target natural frequencies within our K-Pulse, noise permitting we would continue the 250 dB suppression with increasing retarded time. We will increase our radar target discrimination tools by next examining single mode excitation vectors and their convolutions with our radar target file.

There is an important concept that does not arise much in the literature that we need to understand. In the absence of data noise and numerical "ill conditioning," if the N-th order matrix equation (4-14) of 2N sampled data points is nonsingular, but the (N+1)-th order matrix equation (4-14) of 2(N+1) nonzero sampled data points is singular, we say that we have "identified a Prony series" which has only a finite number of terms, namely N. We should expect all subsequent time values, t > 2NT, of data from a continuous physical process to be perfectly predicted by this "Prony series."

Finally, we shall provide the motivation for the skip sampling of the next section. If we use standard matrix arithmetic as was done on all empirical data in this chapter, the standard matrix equation solvers may generate errors in the solution set. Certain, even small, errors can be catastrophic to Prony's method. A particular

error observed which destroys our target discrimination technique is the splitting of a root. If the root corresponds to a target natural frequency of large amplitude, we are defeated. The solution used in this chapter is to reduce the order of the matrix and hence the degree of the Prony polynomial. Since the "Prony K-Pulse" has a minimum time length, to use the sampled data values, we must methodically skip some data. We call this skip sampling.

4.4 Skip Sampling in Prony's Method

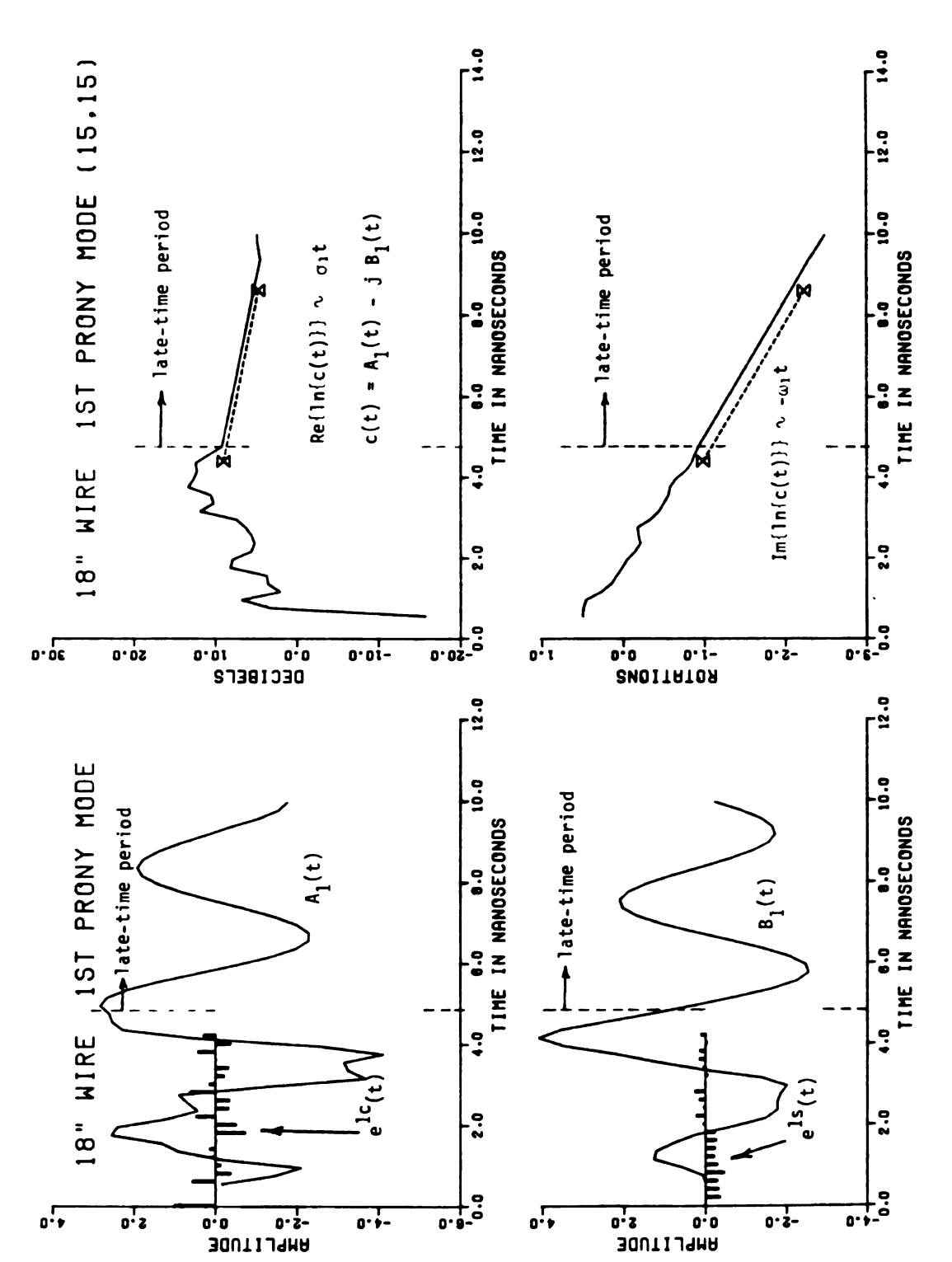
A frame of sampled data used in the standard Prony's method consists of 2N sampled data points. For the special case of 2N+1 sampled data points, Prony differenced the original data to obtain a new sequence of 2N sampled data values. In either case, there are now N simultaneous equations such as Figure 4-1. Now in our matrix formulation, either equation (4-14) or (4-18) might become "singular." If equation (4-14) becomes singular, this is a highly desirable event for Prony's method. In the next chapter we shall use this criterion for terminating the length of the Prony K-Pulse. In the absence of thermal noise or quantization errors, this implies that an N-1 term Or less "Prony series" will do as well as the N term "Prony series." When the transposed Vandermonde matrix, equation (4-18) goes singular, this is a totally different situation. This often observed event is almost solely due to "ill-conditioning" of the matrix system. "Illconditioning" of matrices typically increase with matrix size, all else remaining equal. For this reason alone, it is often in our best interest to keep the size of our matrices as small as possible. Hence in order to satisfy our "Prony K-Pulse" definition, and minimize the effects of "ill-conditioning," we may choose to thin or skip some of our sampled data when we construct equations (4-14) and (4-18).

There are many reasons why the target "Prony series" may underspecify the empirical sampled data. Three good reasons are:

- 1. Thermal noise
- 2. "Class 1" coupling coefficient observation may not be valid for all of the sampled data. Note that our definition of the "Prony K-Pulse" assures us that at least N sampled data points are in the "class 1" observation for an impulsive plane wave incident upon the radar target
- 3. Incident plane wave pulse shape possesses a duration comparable to the equivalent length of important, but highly damped, natural mode waveforms

In the next chapter we shall find out that the "fast" Prony's method can at least obtain the correct natural frequencies for an N-term "Prony series" if at least N sample data points satisfy the "class 1" coupling coefficient E-field observation criterion t > t" of equation (2-18).

Figure 4-4 shows the radar A-scope displays for the 1st mode excitation; this time obtained by removing a first mode zero from the "Prony K-Pulse." The top left plot illustrates the cosine excitation vector for a target natural mode and the resulting output convolution of this excitation vector with the clutter-reduced radar target antenna terminal response. The lower left plot shows the same for the 1st sine mode excitation vector. The polar mode radar A-scope displays are shown



First Mode Waveform Excitation Synthesized from Skip Samples of a Thin Cylinder Radar Target. Figure 4-4.

on the right hand side. The upper right plot is the envelope display in decibels. The rotation plot of the first mode is displayed in the lower right of this same figure. We have employed a skip sampling in obtaining this figure. We have selected from the response file the 1st, 5th, 9th, 13th, etc., sample. We will be using every fourth sample and can select the synchronization. In Figure 4-4 the excitation vectors were selected by starting the data at the 5th sample. The same synchronization was used in the output convolutions.

Now to determine if these radar A-scopes are part of a useful radar target discrimination tool, we need to determine if acceptable results can be obtained for different thermal noise and different amplitudes and phases of the natural move waveforms of the radar target. An ideal check of this technique is to use a different synchronization of the same skip sampling. Since our clutter-reduced radar target antenna terminal response file has not been smoothed subsequent to the receiver thermal noise, the noise samples are uncorrelated. Further, if the output convolution is properly time-tagged, the results are directly comparable with the cycle 15 synchronization.

Figure 4.5 shows the results of changing the synchronization.

This skip sampled file (cycle 14) contains <u>none</u> of the clutterreduced radar target antenna response sampled data points which were
used in the computation of the excitation vector we are using in the
radar A-scope displays. For the first mode the performance is similar,
but definitely not perfect in the time period from 4.96 to 9.36 ns.

In the polar mode A-scope plots, it can be seen that the rotations

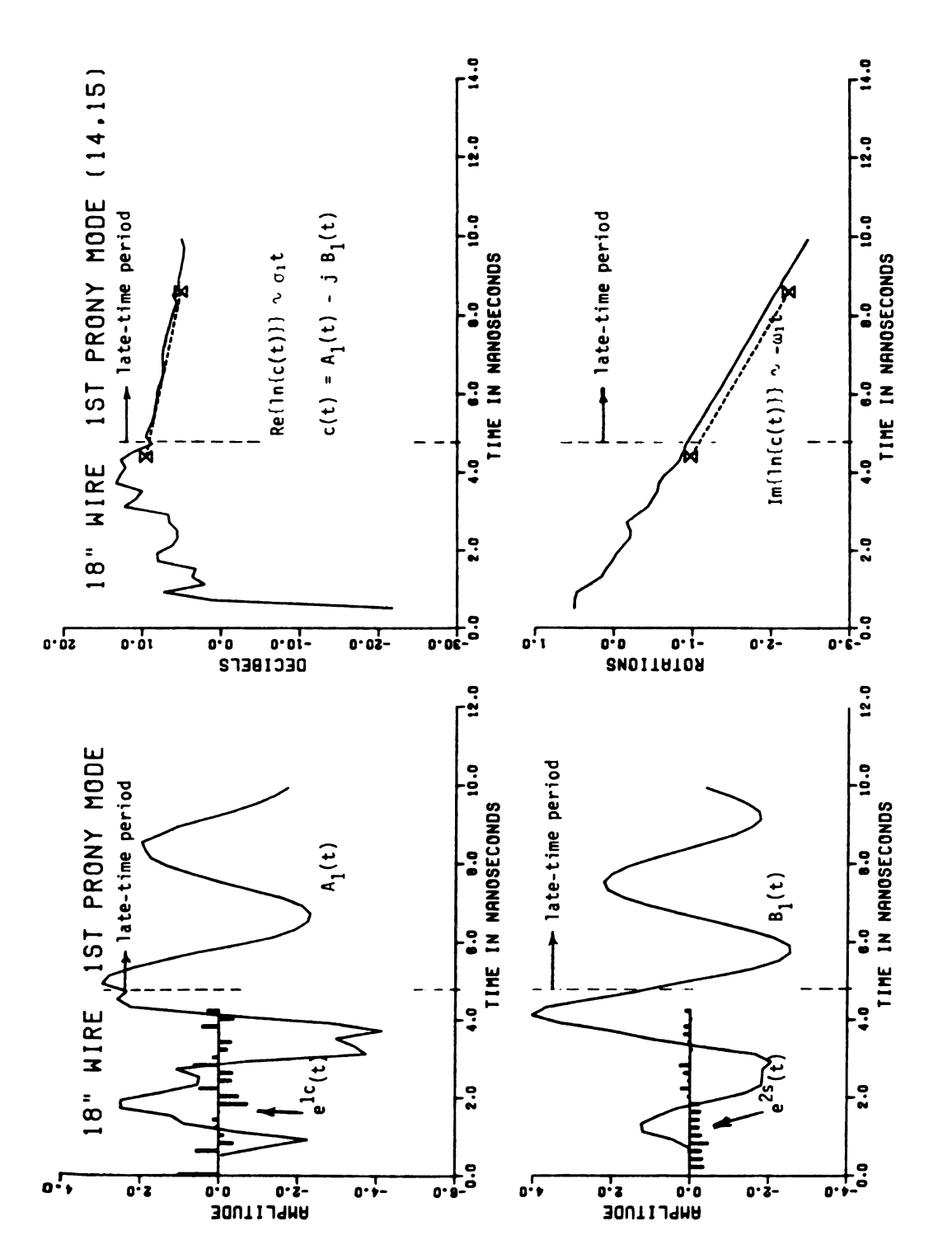
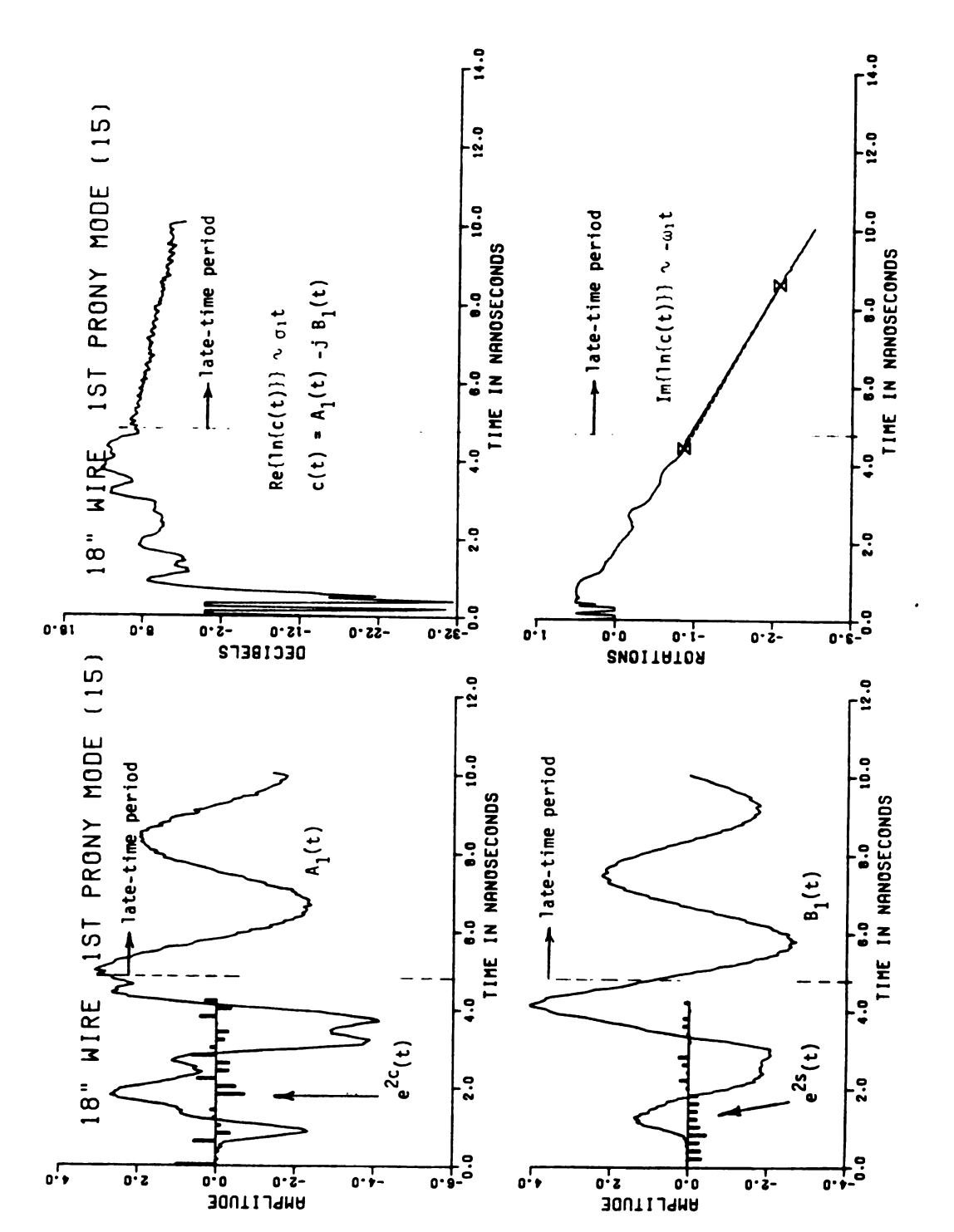


Figure 4-5.--Convolution of the First Mode Excitation Vector of Figure 4-4 with a New Set of Skip Data Points in the Radar Target Response File.

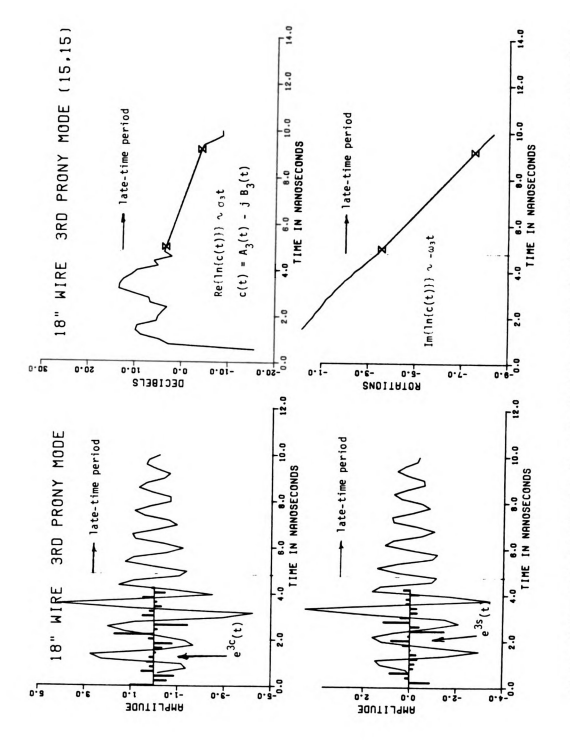
are virtually identical, but there is a very small ripple in the envelope A-scope plot. The only visible defect in the rectangular A-scope plots on the left hand side of the figure are due to the skip sample granularity.

The next test is of great interest. All of the data in the radar target antenna response file is convolved with the first mode excitation vector. This is done by actually exploiting the form of the modified z-transform (Appendix A) notation, v(t,m). Convolutions are performed for the four fixed values of m. Then, the outputs are properly demultiplexed. Of the total number of points used, 256, only 44 or 17% were used in the computation of the excitation vector. Only 9% of the displays output convolution points are expected to be a perfect synthesis of the natural mode waveform. Another 48% of the points potentially satisfy "class 1" conditions for the waveform. The plot result of Figure 4-6 shows impressive performance. The rectangular A-scope plots show thermal noise and quantitization noise similar to the original data file. The polar mode A-scope identifies a rotation rate which is virtually constant from 4 to 9.4 ns. Although the envelope A-scope plot shows about a decibel of ripple in the same time interval, the mean value appears to have a constant slope.

Similar calculations were performed for the 3rd Prony mode of the 18.6" wire (L/a = 400). The 3rd mode waveform is the second largest amplitude for this wire because of the normal incidence of the transmitted plane wave to the thin cylinder target. Figure 4-7 are the A-scope displays for the 3rd mode excitation vector. The starting point for the convolution is the same as for Figure 4.4. The



Convolution of the First Mode Excitation Vectors of Figure 4-4 with all of the Data Points in the Radar Target Response File. Figure 4-6.

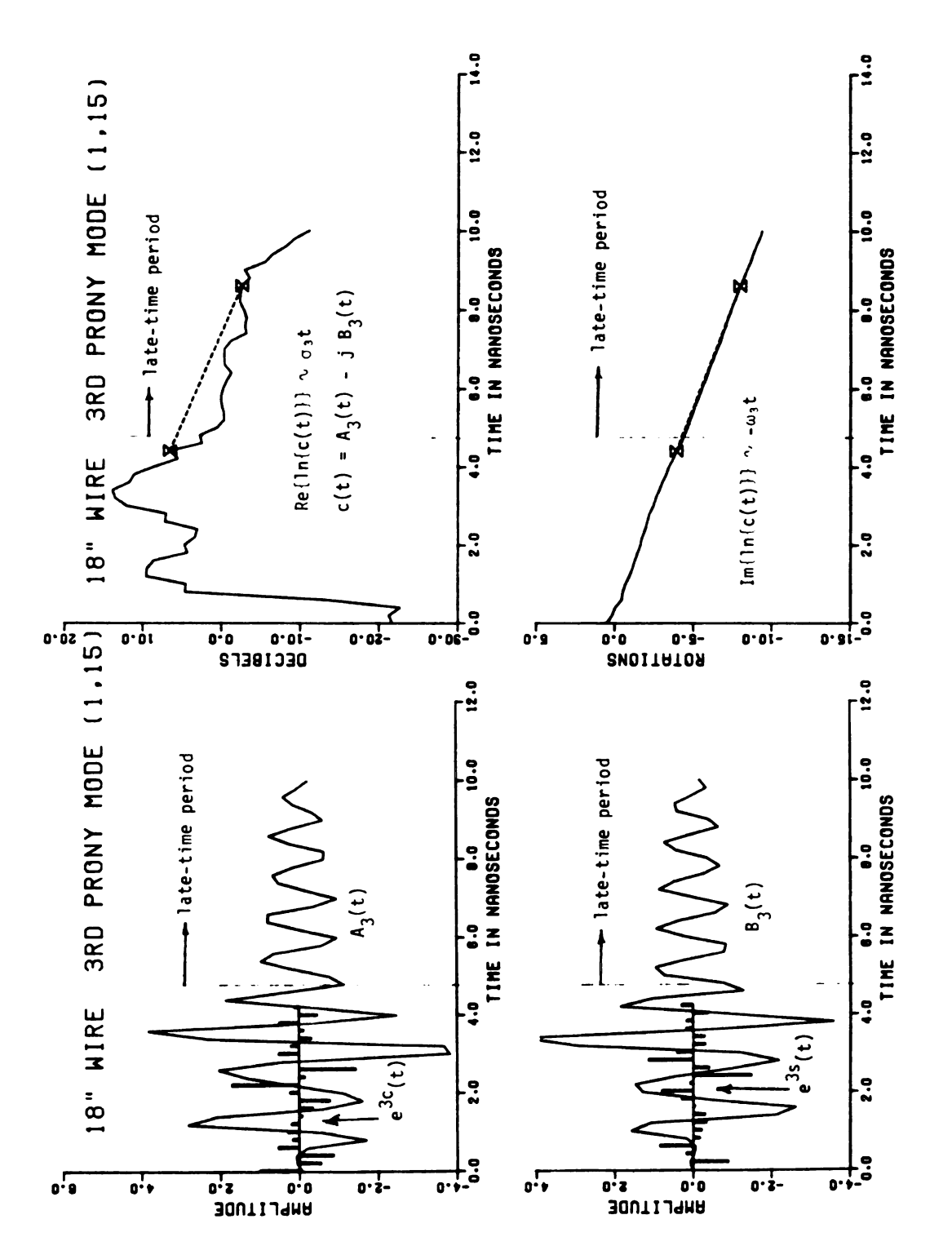


Third Mode Waveform Excitation Synthesized from Skip Samples of a Thin Cylinder Radar Target. Figure 4-7.

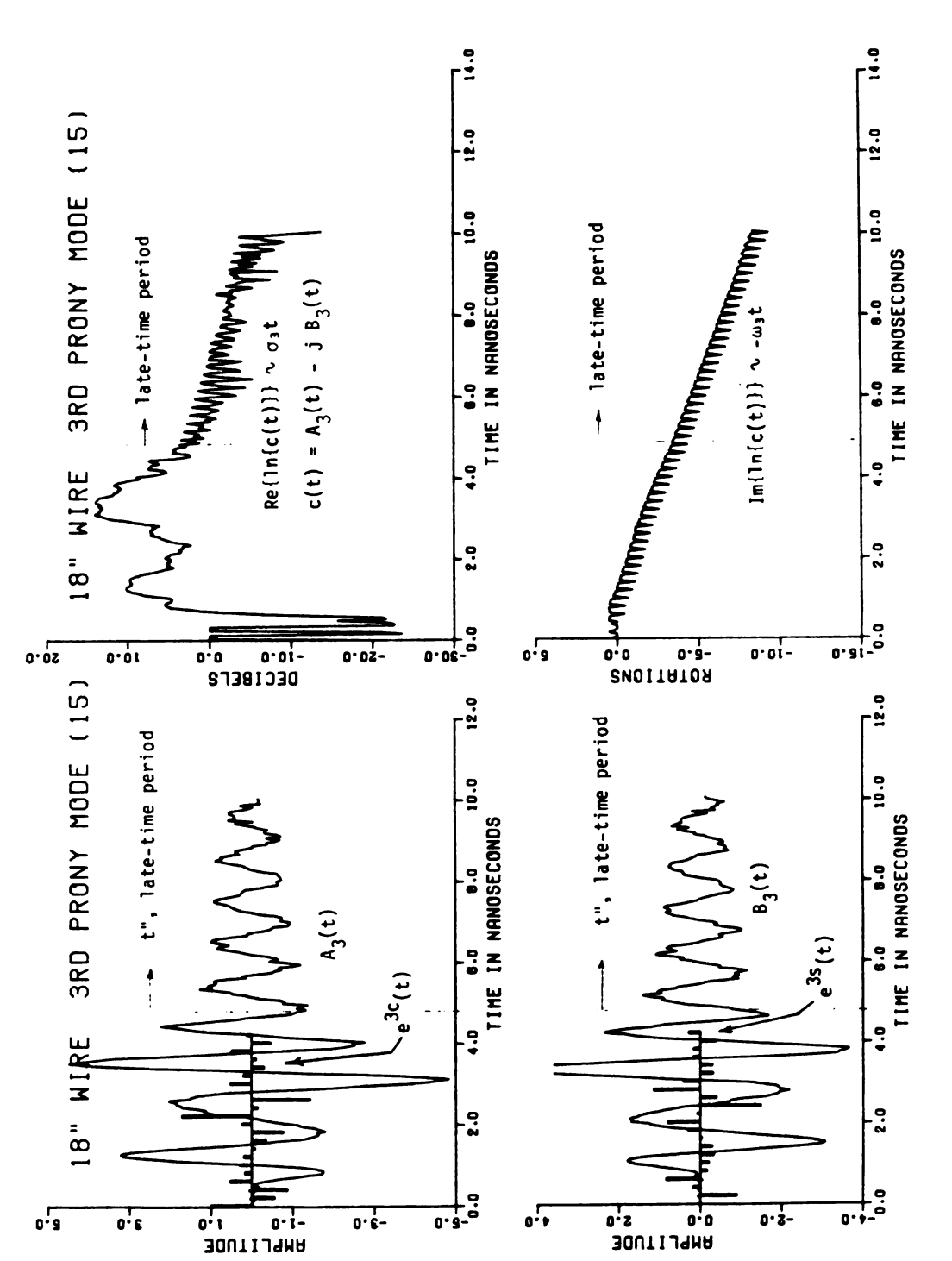
excitation vector for the 3rd mode cosine excitation vector is visible in the upper left plot of this figure, starting a 0 ns and extending to 4.2 ns. The output convolution of this excitation vector with the same skip sampled clutter-reduced radar target antenna terminal response file is shown overlaid. The rectangular A-scope plot for the 3rd mode sine excitation is shown in the lower lift of the figure. The polar mode A-scope plots on the right half of the figure illustrate that the sharp breaks in the rectangular plots between 5 and 9.4 ns were due solely to skip sample point granularity.

Figure 4-8 shows the results of a different synchronization. There exist envelope A-scope variations of several decibels but the rotation rate is virtually constant in the appropriate time interval. None of the data points of this file are in common with the previous Figure 4-7. Hence the thermal and quantitization noise are uncorrelated in the large signal region (starting at 0.5 ns.).

The final illustration in this section of this technique is the convolution of all of the data in the clutter-reduced radar target antenna terminal response file with the 3rd mode excitation vectors. Figure 4-9 shows the result. Note that if Figures 4-7 and 4-8 are overlaid when scales permit, their data are included in Figure 4-9. In the polar mode A-scopes on the right side of Figure 4-9, a ripple with a 0.2 ns period is visible. The origins of this 0.2 ns ripple are well understood for the rotations plot of this particular file. The origin of the m = 0 synchronization is off exactly one unit (the branch cut) from the other synchronizations of the composite response file. There are easy fixes for the composite rotation plot. One is



Convolution of the Third Mode Excitation Vectors of Figure 4-7 with a New Set of Skip Data Points in the Radar Target Response File. Figure 4-8.



Convolution of the Third Mode Excitation Vectors of Figure 4-7 with all of the Data Points in the Radar Target Response File. Figure 4-9.

· ·		

A-scope displays. Only one rotation origin would exist and the resulting rotation plot is extremely linear as can be observed from the limits of the rotation ripple. We do not have as simple a solution for the ripples in the envelope display. The method we shall ultimately adopt is to use very large composite files.

It has been shown in reference 4-9 that these output plots consisting of an elementary natural mode waveform of the radar target all by itself yield readily identifiable aspect-angle invariant parameters of the radar target even in the presence of noise and typical radar hardware distortions.

4.5 Zeros in the Data Matrix and "Class 2 Prony Series"

The topic we shall discuss in this section is related to four other topics we shall discuss in other sections besides this section:

- The "double K-Pulse" technique which is the cornerstone of our radar target discrimination technique may yield similar data types
- 2. The "fast" Prony's method algorithm of the next chapter is similar to the iterative solution procedure of this section
- 3. This is an introduction to a "class 2 Prony series"
- 4. The concept of "root degress of freedom" will draw from this section

We shall now consider what we shall call a "class 2 Prony Series" of N complex exponentials, which is an N term "Prony series"

plus an entire function, W(s), whose time domain, w(t), possesses a limited time duration. This function is nonzero only for a time duration defined by equation (4-21).

$$w_N(t) = \begin{cases} w(t), & 0 \leq t = nT < (N-1)T \\ 0, & \text{otherwise, } n \text{ an integer} \end{cases}$$
 (4-21)

We shall then define the "class 2 Prony series" of N terms by equation (4-22).

$$v(t) = w_N(t) + \sum_{k=1}^{N'} C_k \exp(s_k t), \quad t=nT \ge 0$$
n an integer
$$(4-22)$$

Now for the balance of this section, we shall, for clarity and simplicity, choose a specific entire function, $\hat{W}(s)$, satisfying equation (4-23) in the time domain.

$$w(t) = -\sum_{k=1}^{N'} C_k \exp(s_k t), \quad 0 \leq t = nT < (N-1)T$$
n an integer (4-23)

This means that the first N-1 samples of v(t) will be identically zero. Substituting this particular v(t) into equation (4-14) gives the form of equation (4-24).

$$\begin{bmatrix} v_{N-1} & 0 & \cdots & 0 \\ v_{N} & v_{N-1} & \cdots & 0 \\ \vdots & \vdots & & \vdots \\ v_{2N-2} & v_{2N-3} & \cdots & v_{N-1} \end{bmatrix} \begin{bmatrix} a_{1} \\ a_{2} \\ \vdots \\ a_{N} \end{bmatrix} = - \begin{bmatrix} v_{N} \\ v_{N+1} \\ \vdots \\ v_{2N-1} \end{bmatrix}$$
(4-24)

Note that the prior Prony matrix equation (4-13) is not triangular as may be seen in equation (4-25) after substitution.

$$\begin{bmatrix} v_{N} & v_{N-1} & \dots & 0 \\ v_{N+1} & v_{N} & \dots & 0 \\ \vdots & \vdots & & \vdots \\ v_{2N-2} & v_{2N-3} & \dots & v_{N-1} \\ v_{2N-1} & v_{2N-2} & \dots & v_{N} \end{bmatrix} \begin{bmatrix} 1 \\ a_{1} \\ \vdots \\ a_{N-1} \\ a_{N} \end{bmatrix} = \begin{bmatrix} 0 \\ 0 \\ \vdots \\ 0 \\ 0 \end{bmatrix}$$

$$(4-25)$$

From equation (4-25), it can easily be seen that the "Prony K-Pulse" can easily be obtained iteratively starting with the top row or equation of equation (4-25). For example a_1 is given by equation (4-26).

$$a_1 = -v_N/v_{N-1}$$
 (4-26)

Equation (4-26) is then substituted into equation (4-25) and then the second row of (4-25) is used to solve for the unknown a_2 . For illustration take N' = 1 in equation (4-22), then equation (4-26) will have solved for the single necessary root $z_1 = \exp(s_1T)$. The balance of the a_i will be zero for this special case.

Part 2 of Prony's method is similar. Roots are solved as before. We must be prepared to obtain less than N roots if $a_N=0$, etc. We shall assume here that we have obtained N zeros for Part 3.

Part 3 of Prony's method is significantly different. We have 2N possible discrete time equations to solve for N complex amplitudes as before. For a "Prony series" it makes no difference which of these

N equations we use. So, the first N equations are always used to minimize the computational effort. Equation (4-18) displays the use of the first N equations, but we could have used the last N equations. However, for our particular "class 2 Prony series," it does make a difference which equations we use. Note the right hand side of equation (4-18) is all zeros if we choose the first N equations, but the right hand side is all nonzeros if we choose the last N equations.

Hence there are potentially N sets of amplitude coefficients which we can use to fit sampled data points. One might be tempted to use a least-squares fit to obtain a "best" single fit. We choose not to do this for three reasons:

- 1. We are primarily interested in the t > t" region anyway
- 2. We do not wish to perform an irreversible operation
- We do not mind the early-time varying complex amplitudes which resemble the SEM "class 2" coupling coefficients.

Because of (1), we shall use the last N equations for the "class 1" condition and use the time retarded equation (4-27) to minimize calculations.

$$\begin{bmatrix} 1 & 1 & \cdots & 1 \\ z_1 & z_2 & \cdots & z_N \\ \vdots & \vdots & & \vdots \\ z_1^{N-1} & z_2^{N-1} & \cdots & z_N^{N-1} \end{bmatrix} \begin{bmatrix} c_1 \\ c_2 \\ \vdots \\ c_N \end{bmatrix} = \begin{bmatrix} v_N \\ v_{N+1} \\ \vdots \\ v_{2N-1} \end{bmatrix}$$
(4-27)

where $t_{new} = t - t''$

4.6 The Extended Prony's Method

The extended Prony's method (ref. 4-3) is a least-squares formulation of Prony's method. It is actually a quite different method although the equation formulations look almost identical. Equation (4-28) defines the "Prony K-Pulse" for the extended Prony's method.

$$\begin{bmatrix} v_{N-1} & \cdots & v_0 \\ \vdots & & & & \\ v_{2N-2} & \cdots & v_{N-1} \\ \vdots & & \vdots & & \\ v_{L+2N-2} & \cdots & v_{L+N-1} \end{bmatrix} \begin{bmatrix} a_1 \\ \vdots \\ a_N \end{bmatrix} = - \begin{bmatrix} v_N \\ \vdots \\ v_{L+2N-1} \end{bmatrix}$$
(4-28)

The matrix equation (4-28) contains L simultaneous equations more than the regular Prony's method equation (4-14). Because of these additional equations, we may not be able to obtain an exact solution set or "Prony K-Pulse." A standard least-squares minimization of (4-28) is used which is the reason that the extended Prony's method is an irreversible operation.

Part 2 of the extended Prony's method is identical to the regular Prony's method.

Part 3, the complex amplitudes, of the extended Prony's method can no longer be exactly satisfied for all of the possible values on the right hand side of equation (4-27) or (4-18). Hence, again a least-squares formulation is used again. There is an error associated with both Part 1 and Part 3. There is no known analytical method to simultaneously minimize both of these errors as formulated

here. There are many iterative type techniques to perform this operation if desired.

4.7 Complex Root Degrees of Freedom

In this section we shall introduce the important concept of complex root degrees of freedom which turns out to be an important predictive parameter in forecasting radar target discrimination power. We shall use a synthetic "class 2 Prony series" for illustrating the effect of this parameter. Note that we are going to use early time values of this synthetic waveform which are zero as in the section on Prony's method on triangular data matrix. This particular data file are calculated for a 1 milliradian incidence. So the odd natural frequencies yield natural mode waveforms with large complex amplitudes. There are also 9 even natural mode waveforms with extremely small complex amplitudes. (The reason for 9 and not 10 is that we picked the sample spacing to alias the highest frequency.) The number of independent sample data points constitutes the information content used by Prony's methods. We shall hold this parameter constant throughout this section.

We will analyze the "complex root degrees of freedom" by varying the synchronization or starting time as we use the regular Prony's method and the extended Prony's method. The number of sample data points used is 50. For the regular Prony's method, this means that the equation (4-14) matrix is 25 by 25. For the extended Prony's method we will use the 50 sampled data points in 31 rows and 19 columns, yielding a "Prony K-Pulse" of length 19+1 or 19 roots.

Table 4-1 is summary log of the results for various starting times. Table 4-2 is summary of the results in terms of the complex root degrees of freedom. Here it is visible that increasing the root degrees of freedom enhances our ability to obtain accurate invariant parameters of the radar target, namely its natural frequencies. For the same information content, the extended Prony's method is inferior.

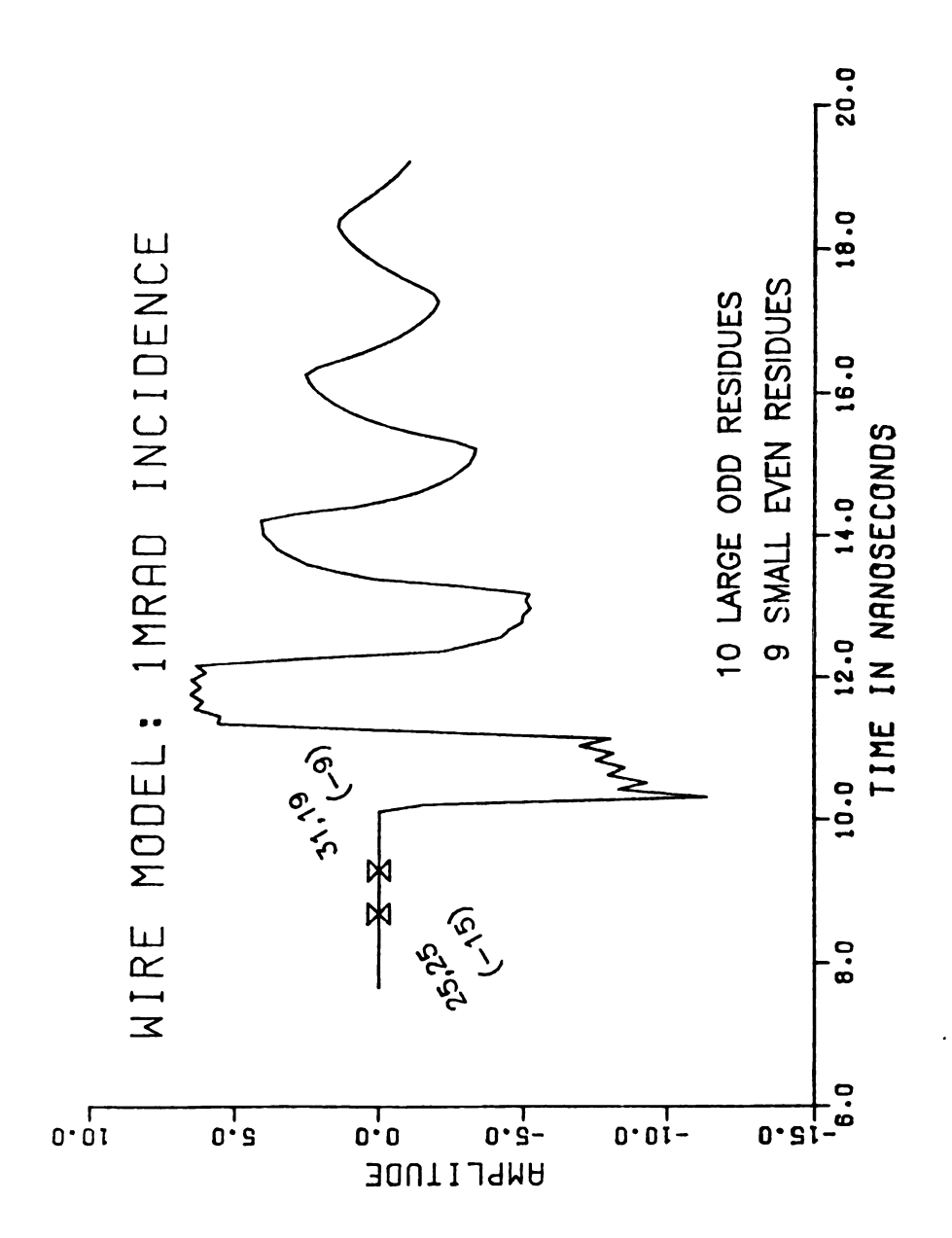


Figure 4-10. Synthetic "Class 2 Prony Series" at 1 Milliradian Incidence.

TABLE 4-1. Prony's Method Tests.

TIME	25x25 Matrix (regular)	x (regular)	31x19 Matr	31x19 Matrix (extended)
Samples before ns start	Correct Odd Roots	Correct Even Roots	Correct Odd Roots	Correct Even Roots
16 8.57	none	none	none	none
15 8.68	all	none	none	none
• • •	•••	•••	•••	•••
10 9.19	all	none	none	none
9 9.29	all	none	all	none
8 9.39	all	none	lla	none
7 9.49	lall	none	all	none
6 9.59	all	all, but 10th	all	none
5 9.70	all	all	all	none
4 9.80	lall	lla	lla	none
3 9.90	1% error	1% error	lla	none
2 10.00	all	all, but 10th	all	none
1 10.10	all	all, but 10th	all	none
0 10.21	וופ	all	all	all
+	*			

Table 4-2. Ldte-Time Model Test of Prony's Methods

lmr Incident from normal of 19 Modes 10 Odd Modes with major amplitudes 9 Even Modes with minor amplitudes All starting at time t_s . Sampling ΔT .	Regular Prony's Method 25 x 25 matrix 25 Root Degrees-of-Freedom (50 sample values used)	Extended Prony's Method 31 x 19 matrix 19 Root Degrees-of-Freedom (50 sample values used)
Earliest correct identification of 9 Minor Modes of model.	time ≥ t _s -6 T all nine simultanously	time > t _S all 9 simultaneously
Earliest correct identification of 10 Odd Modes of Model	time	time > t _S -(19-10) T all 10 simultaneously
Algorithm Error Output	-220 dB to -260 dB No pattern identified	> +0 dB for t< t_s -9.T <-70 dB for t> t_s -9 T <-230dB for t> t_s
Algorithmic Singularity Flag	Occurred occassionally in last loop only.	Did not occur.
K-Pulse error (external to data)	∿10 dB Improvement starting at time t _S -15 T.	Pattern not identified.

CHAPTER 5

THE "FAST" PRONY'S METHOD

5.1 Performance Enhancements for Radar Target Discrimination

Each of the three major parts of Prony's method shown in the block diagram of Figure 5-1 will be altered significantly computationally in order to permit the real time use of discrimination waveforms of up to several thousand sample data points. The suppression of noise, clutter, and radar system distortions are correspondingly enhanced.

In Part 1 of Prony's method the N \times N data matrix is never formed. Only 2N data storage locations are used. The algorithm will be described by means of the original N \times N data matrix, but this is only for illustrative purposes, since we do not perform the N³ multiplications and divisions of a direct matrix solution, but only N² multiplications and divisions.

In Part 2 of Prony's method, we remove the firm requirement to solve for <u>all</u> of the roots. Together with the use of skip data sampling, close estimates of the major target roots can be obtained along with rough estimates of the spacing of nearby roots. A derivative-free accelerated root solver such as the Hooke-Jeeves method can be used to obtain fast solutions even for noise-like data.

In Part 3 of Prony's method we eliminate the second matrix, the transposed Vandermonde matrix, used to solve for the complex

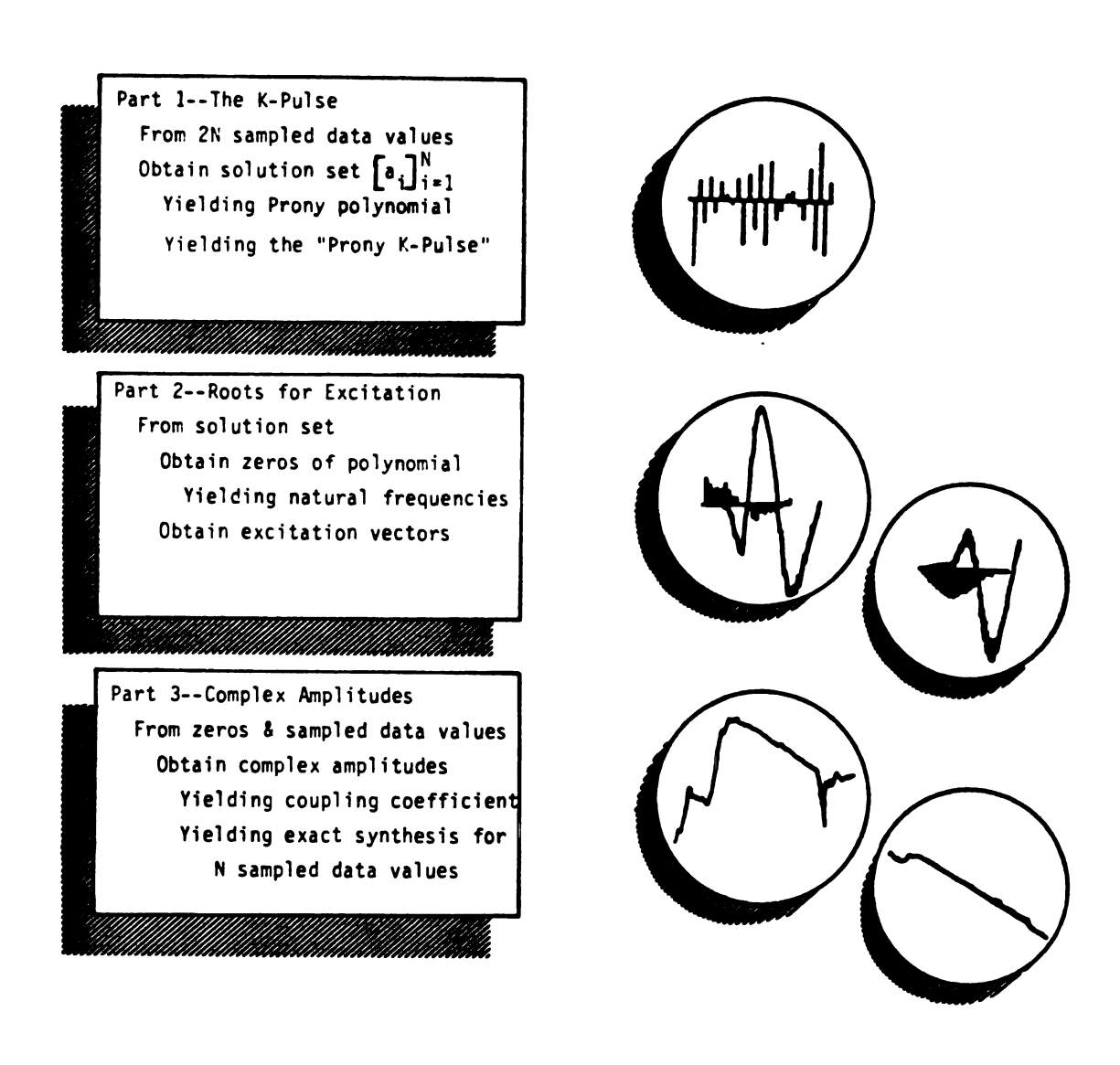


Figure 5-1. Major Parts of Prony's Method Summarized.

amplitudes of the natural mode waveforms. Fortuitously, the fast amplitude solution derived is a ratio of discrimination waveforms which are required for the radar target identification technique derived in the next chapter.

It should be observed in the derivation of the "fast" Prony algorithm, that <u>two</u> solutions sets are necessary in its derivation. Only one is disclosed in the traditional Prony's method. These two different solution sets clarify the operation of the radar target discrimination technique exhibited in the next chapter.

5.2 Part 1--The K-Pulse

In Chapter 4 we noted the Hankel structure of the original Prony formulation of the undetermined coefficients in Figure 4-1 and equation (4-12). In anticipation of this chapter, we performed a trivial reflection of the Hankel form into the more familiar Toeplitz form we observed in equation (4-13). The Toeplitz matrix often results from the discretization of a continuous convolution (ref. 5-9, pp. 50). The most general Toeplitz matrix has identical elements along the diagonals from upper left to lower right. Note that this matrix possesses an odd number of possibly distinct values. It will be more esthetic for us to use 2N+1 sample data values and to obtain two solutions of the undetermined coefficients which when we apply our physical constraint (equation 2-18) becomes our "Prony K-Pulse."

The matrix or data form we must use is never a symmetrical Toeplitz matrix. For the symmetric Toeplitz matrix, the very popular Levison (ref. 5-1) recursion algorithm as refined by Robinson

(ref. 5-2) exists in published form. We will utilize the illuminating matrix description of Robinson in deriving the unsymmetrical Toeplitz recursion. The algorithm which we shall derive with its pair of usable solutions leads to the radar target discrimination technque of the next chapter.

Let us start with Prony's N equations of Figure 4-1 in our notation in equation (5-1).

$$v_{N+1} + a_1 v_N + \dots + a_N v_1 = 0$$

$$v_{N+2} + a_1 v_{N+1} + \dots + a_N v_2 = 0$$

$$\vdots \qquad \vdots \qquad \vdots \qquad \vdots$$

$$v_{2N} + a_1 v_{2N-1} + \dots + a_N v_N = 0$$
(5-1)

In Chapter 4 we performed a standard matrix solution by moving the data values in the first column to the right side. Here our solution will procede by introducing another equation, equation (5-2).

$$v_N + a_1 v_{N-1} + \dots + a_N v_O = \alpha$$
 (5-2)

In equation (5-2) we have now used the 2N+1-th sample data value. Also, a new dependent variable, α , which we shall call the error variable, has been introduced. It may turn out that there is a solution $\{a_i\}_{i=1}^{N}$ to equation (5-1) which permits equation (5-2) to be satisfied with $\alpha=0$. With noisy data this will be highly unusual, but if it happens, we shall claim that we have identified a "Prony series." Note that if we use both equations (5-1) and (5-2) we are using 2N+1 sampled data points, but the last point is superfluous if

we actually have a "Prony series." From now on we shall use equation (5-3) which is a composite of the N+1 equations of equations (5-1) and (5-2).

$$v_{N}$$
 + $a_{1}v_{N-1}$ + ... + $a_{N}v_{0} = \alpha$
 v_{N+1} + $a_{1}v_{N}$ + ... + $a_{N}v_{1} = 0$
 v_{N+2} + $a_{1}v_{N+1}$ + ... + $a_{N}v_{2} = 0$
 \vdots \vdots \vdots \vdots \vdots
 v_{2N} + $a_{1}v_{2N-1}$ + ... + $a_{N}v_{N} = 0$ (5-3)

We shall for the convenience of our "fast" algorithm write the N+1 simultaneous linear equations of equation (5-3) as the matrix equation (5-4).

$$\begin{bmatrix} v_{N} & v_{N-1} & \cdots & v_{0} \\ v_{N+1} & v_{N} & \cdots & v_{1} \\ \vdots & \vdots & & \vdots \\ v_{2N} & v_{2N-1} & \cdots & v_{N} \end{bmatrix} \begin{bmatrix} 1 \\ a_{1} \\ \vdots \\ a_{N} \end{bmatrix} = \begin{bmatrix} \alpha \\ 0 \\ \vdots \\ 0 \end{bmatrix}$$

$$(5-4)$$

Although from equation (5-4) it is partially obscured, we will remember that the $[a_i]_{i=1}^N$ are determined by only the last 2N of our 2N+1 sampled data values. This fact is clearer by the Chapter 4 notation for the now standard matrix notation of Prony's method given by equation (5-5). Equation (5-5) is obtained by deleting the top row of equation (5-4) and moving the left most column of the data matrix to the right hand side.

$$\begin{bmatrix} v_{N} & v_{N-1} & \cdots & v_{1} \\ v_{N+1} & v_{N} & \cdots & v_{2} \\ \vdots & \vdots & & \vdots \\ v_{2N} & v_{2N-1} & \cdots & v_{N} \end{bmatrix} \begin{bmatrix} a_{1} \\ a_{2} \\ \vdots \\ a_{N} \end{bmatrix} = - \begin{bmatrix} v_{N+1} \\ v_{N+2} \\ \vdots \\ v_{2N} \end{bmatrix}$$
(5-5)

Now let us start from the Prony's method of Figure 4-1 once again. This time we shall use the first 2N of the 2N+1 sampled data values. These N simultaneous equations can be written as equation (5-6) instead of equation (5-1).

$$b_{N}v_{N} + b_{N-1}v_{N-1} + \dots + v_{0} = 0$$

$$b_{N}v_{N+1} + b_{N-1}v_{N} + \dots + v_{1} = 0$$

$$\vdots \qquad \vdots \qquad \vdots \qquad \vdots$$

$$b_{N}v_{2N-1} + b_{N-1}v_{2N-2} + \dots + v_{N-1} = 0$$
(5-6)

As we did in equation (5-2) let us introduce another equation with a new dependent error variable, β , given by equation (5-7)

$$b_N v_{2N} + b_{N-1} v_{2N-1} + \dots + v_N = \beta$$
 (5-7)

Again we denote the combined n+1 linear equations by another equation, equation (5-8). For the convenience of the "fast" algorithm, we shall write the N+1 simultaneous linear equations of equation (5-8) as matrix equation (5-9). For completeness and future reference, we will perform the analogous operation by which we obtained equation (5-5). This time we delete the last row of equation (5-9) and move the right most column to the right hand side to obtain equation (5-10).

$$b_{N}v_{N} + b_{N-1}v_{N-1} + \dots + v_{0} = 0$$

$$b_{N}v_{N+1} + b_{N-1}v_{N} + \dots + v_{1} = 0$$

$$\vdots \qquad \vdots \qquad \vdots \qquad \vdots$$

$$b_{N}v_{2N-1} + b_{N-1}v_{2N-2} + \dots + v_{N-1} = 0$$

$$b_{N}v_{2N} + b_{N-1}v_{2N-1} + \dots + v_{N} = \beta$$
(5-8)

$$\begin{bmatrix} v_{N} & v_{N-1} & \cdots & v_{0} \\ v_{N+1} & v_{N} & \cdots & v_{0} \\ \vdots & \vdots & & \vdots \\ v_{2N} & v_{2N-1} & \cdots & v_{N} \end{bmatrix} \begin{bmatrix} b_{N} \\ b_{N-1} \\ \vdots \\ 1 \end{bmatrix} = \begin{bmatrix} 0 \\ 0 \\ \vdots \\ \beta \end{bmatrix}$$
(5-9)

$$\begin{bmatrix} v_{N} & v_{N-1} & \cdots & v_{1} & b_{N} \\ v_{N+1} & v_{N} & \cdots & v_{2} & b_{N-1} \\ \vdots & \vdots & & \vdots & \vdots \\ v_{2N-1} & v_{2N-2} & \cdots & v_{N} & b_{1} \end{bmatrix} = - \begin{bmatrix} v_{0} \\ v_{1} \\ \vdots \\ v_{N-1} \end{bmatrix}$$
(5-10)

Now we wish to reflect on the similiarities and differences of equations (5-5) and (5-10). Note that equation (5-5) did not use one, \mathbf{v}_0 , of the 2N+1 sampled data points and equation (5-10) did not use a different, \mathbf{v}_{2N} , one of the 2N+1 sampled data points. However, the sampled data matrix on the left hand side in each of equations (5-5) and (5-10) is identical. Only the right hand side causes the solutions $[\mathbf{a_i}]_{i=1}^N$ and $[\mathbf{b_i}]_{i=1}^N$ to be different.

In the popular symmetric Toeplitz recursion, the data matrix is symmetric as well as Toeplitz. Hence there are only N+1 distinct values in the 2N+1 sampled data sequence. It can be observed that for this special case from equations (5-5) and (5-10) that the two solutions $[a_i]_{i=1}^N$ and $[b_i]_{i-1}^N$ are, in fact, identical.

With these initial observations out of the way, we shall derive the K-Pulse part of the "fast Prony's method algorithm" by induction or recursively. The induction will start from the middle of the 2N+1 sampled data sequence which is v_N . We shall use increasing larger and larger numbers of the sampled data points such as in equation (5-11) for $m \le N$. We shall by induction be assuming that solutions exist for some m as in equation (5-11).

$$\begin{bmatrix} v_{N} & v_{N-1} & \cdots & v_{N-m} \\ v_{N+1} & v_{N} & \cdots & v_{N-m+1} \\ \vdots & \vdots & & \vdots \\ v_{N+m} & v_{N+m-1} & \cdots & v_{N} \end{bmatrix} \begin{bmatrix} 1 & & & \alpha_{m} \\ a_{1}^{(m)} & & & 0 \\ \vdots & & \vdots & & \vdots \\ a_{m}^{(m)} & & & 0 \end{bmatrix} = \begin{bmatrix} \alpha_{m} & & & \alpha_{m} \\ \vdots & & & \ddots \\ \vdots & & & \vdots \\ a_{m}^{(m)} & & & 0 \end{bmatrix}$$
(5-11)

Simultaneously we use the same data matrix to develop a recursion for our second solution in equation (5-12) which is assumed to exist.

$$\begin{bmatrix} v_{N} & v_{N-1} & \cdots & v_{N-m} \\ v_{N+!} & v_{N} & \cdots & v_{N-m+1} \\ \vdots & \vdots & & \vdots \\ v_{N+m} & v_{N+m-1} & \cdots & v_{N} \end{bmatrix} \begin{bmatrix} b_{m}^{(m)} \\ b_{m-1}^{(m)} \\ \vdots \\ 1 \end{bmatrix} = \begin{bmatrix} 0 \\ 0 \\ \vdots \\ \beta_{m} \end{bmatrix}$$
(5-12)

Note that we must superscript our solution recursions since they may vary substantially from the previous recursion, in general.

The next step in the recursion is to increase the size of the data matrix by one row and one column. This given rise to two new equations (5-13) and (5-14) where $c_{\rm m}$ and $d_{\rm m}$ are new dependent variables resulting.

$$\begin{bmatrix} v_{N} & v_{N-1} & \cdots & v_{N-m} & v_{N-m-1} \\ v_{N+1} & v_{N} & \cdots & v_{N-m+1} & v_{N-m} \\ \vdots & \vdots & & \vdots & & \vdots \\ v_{N+m} & v_{N+m-1} & \cdots & v_{N} & v_{N+1} \\ v_{N+m+1} & v_{N+m} & v_{N+1} & v_{N} \end{bmatrix} \begin{bmatrix} 1 \\ a_{1}^{(m)} \\ \vdots \\ a_{m}^{(m)} \\ 0 \end{bmatrix} = \begin{bmatrix} \alpha_{m} \\ 0 \\ \vdots \\ \alpha_{m} \\ 0 \end{bmatrix}$$
 (5-13)

$$\begin{bmatrix} v_{N} & v_{N-1} & \cdots & v_{N-m} & v_{N-m-1} \\ v_{N+1} & v_{N} & \cdots & v_{N-m+1} & v_{N-m} \\ \vdots & \vdots & & \vdots & & \vdots \\ v_{N+m} & v_{N+m-1} & \cdots & v_{N} & v_{N+1} \\ v_{N+m+1} & v_{N+m} & \cdots & v_{N+1} & v_{N} \end{bmatrix} \begin{bmatrix} 0 \\ b_{m}^{(m)} \\ \vdots \\ b_{1}^{(m)} \\ 1 \end{bmatrix} = \begin{bmatrix} d_{m} \\ 0 \\ \vdots \\ 0 \\ \beta_{m} \end{bmatrix}$$
(5-14)

The matrix equation (5-13) uses a new sampled data point, v_{N+m+1} . This results in the new dependent variable, c_m , on the right hand side. Similarly, equation (5-14) uses a different new sampled data point, v_{N-m-1} . This, in turn, results in the new dependent variable, d_m , on the right hand side of equation (5-14). For measured

data containing "white noise," α_m , β_m , c_m , d_m will typically be non-zero for all m.

Next we shall form a linear combination of equations (5-13) and (5-14) for the purpose of eliminating c_m . We shall multiply equation (5-14) by K_{m+1} and add. In order to keep the notation compact, we form equation (5-15) with the same yet to be determined constant, K_{m+1} .

$$\begin{bmatrix} 1 \\ a_1^{(m+1)} \\ \vdots \\ a_{m+1}^{(m+1)} \end{bmatrix} = \begin{bmatrix} 1 \\ a_1^{(m)} \\ \vdots \\ 0 \end{bmatrix} + K_{m+1} \begin{bmatrix} 0 \\ b_m^{(m)} \\ \vdots \\ \vdots \\ 0 \end{bmatrix}$$
 (5-15)

Using the updated "Prony K-Pulse" of equation (5-15), we may more compactly write the desired linear combination of equations (5-13) and (5-14) as equation (5-16).

$$\begin{bmatrix} v_{N} & v_{N-1} & \cdots & v_{N-m} & v_{N-m-1} \\ v_{N+1} & v_{N} & \cdots & v_{N-m+1} & v_{N-m} \\ \vdots & \vdots & & \vdots & \vdots \\ v_{N+m} & v_{N+m-1} & \cdots & v_{N} & v_{N-1} \\ v_{N+m+1} & v_{N+m} & \cdots & v_{N+1} & v_{N} \end{bmatrix} \begin{bmatrix} 1 \\ a_{1}^{(m+1)} \\ \vdots \\ a_{m+1}^{(m+1)} \\ a_{m+1}^{(m+1)} \end{bmatrix} = \begin{bmatrix} \alpha_{m} + K_{m+1} d_{m} \\ 0 \\ \vdots \\ 0 \\ c_{m} + K_{m+1} d_{m} \end{bmatrix} (5-16)$$

By examination of equation (5-16) we can see that if we K_{m+1} by equation (5-17) and the new α_{m+1} by equation (5-18), we will have advanced the induction or recursion on equation (5-11) by one step.

$$K_{m+1} = -c_m/\beta_m \tag{5-17}$$

$$\alpha_{m+1} = \alpha_m + K_{m+1} d_m \tag{5-13}$$

Note that equation (5-17) is well defined if and only if β_m is not zero. If α_m or β_m is zero, we shall set flag 1 and terminate the K-Pulse part of this algorithm and reset the output length of the K-Pulse at m+1 instead of N+1. Again for noisy measurement data this is unlikely to occur.

Similarly, we shall form a different linear combination of equations (5-13) and (5-14) this time for the purpose of eliminating d_m in equation (5-14). We shall multiply equation (5-13) by L_{m+1} , and add. Again in order to keep the equation compact, we form equation (5-19) with the same yet to be determined constant L_{m+1} .

$$\begin{bmatrix} b_{m+1}^{(m+1)} \\ b_{m+1}^{(m+1)} \\ \vdots \\ b_{1}^{(m+1)} \end{bmatrix} = \begin{bmatrix} 0 \\ b_{m}^{(m)} \\ \vdots \\ b_{1}^{(m)} \end{bmatrix} + L_{m+1} \begin{bmatrix} 1 \\ a_{1}^{(m)} \\ \vdots \\ a_{m}^{(m)} \\ 0 \end{bmatrix}$$

$$(5-19)$$

Using the updated "Prony K-Pulse" of equation (5-19), we may more compactly write the desired linear combination of equations (5-13) and (5-14) as equation (5-20).

$$\begin{bmatrix} v_{N} & v_{N-1} & \cdots & v_{N-m} & v_{N-m-1} \\ v_{N+1} & v_{N} & \cdots & v_{N-m+1} & v_{N-m} \\ \vdots & \vdots & & \vdots & \vdots \\ v_{N+m} & v_{N+m-1} & \cdots & v_{N} & v_{N-1} \\ v_{N+m+1} & v_{N=m} & \cdots & v_{N+1} & v_{N} \end{bmatrix} \begin{bmatrix} b_{m+1}^{(m+1)} \\ b_{m}^{(m+1)} \\ \vdots \\ b_{1}^{(m+1)} \\ 1 \end{bmatrix} = \begin{bmatrix} d_{m} + L_{m+1} \alpha_{m} \\ 0 \\ \vdots \\ 0 \\ \beta_{m} + L_{m+1} \alpha_{m} \\ 0 \end{bmatrix} (5-20)$$

By examination of equation (5-20) we can see that if we may choose L_{m+1} by equation (5-21) and the new β_{m+1} by equation (5-22), we will have advanced the induction or recursion on equation (5-21) by one step on the index m.

$$L_{m+1} = -d_m/\alpha_m \tag{5-21}$$

$$\beta_{m+1} = \beta_m + L_{m+1} c_m$$
 (5-22)

We now possess the (m+1)-th inductive solutions predicated only upon the existence of the m-th solution of equations (5-11) and (5-12) and also $\alpha_{\rm m}\neq 0\neq \beta_{\rm m}$. However, we shall set flag C if $c_{\rm m}=0$ and flag D if $d_{\rm m}=0$. We shall also terminate the K-Pulse part of the algorithm at m for flag C just as we did for flag A. Table 5-1 summarized our conclusions on the significance of these two flag terminations. We may use flag D in the next chapter.

Table 5-1. K-Pulse Termination Flags.

Termination	Flag A (Singular)	Flaġ C	Flag D
$\alpha_{\rm m} = \beta_{\rm m}$	0	≠ 0	≠ 0
(c _m ,d _m)	Not Applicable	(0,d _m)	(c _m ,0)
For nonzero unsymmetric data, Are samples of a "Prony series identified?	Yes	No	No
For nonzero symmetric data are samples of a "double-sided" complex exponential series identified?	Yes	No	No
Is a "class 2 Prony series" a possibility?	Not Applicable	Yes	Yes
<pre>Is a "2nd K-Pulse Convolution" a possibility?</pre>	Not Applicable	Yes	Yes

The induction still requires a starting point for which there exists a solution pair. For m=0, this is easy since equations (5-11) and (5-12) become scalar equations. It is easily seen that if \mathbf{v}_N is nonzero, the solution pair exist. Figure 5-2 is a flow chart diagram for the K-Pulse part of the "fast Prony's method algorithm." For illustrative purposes we shall perform the first two recursions for m=0 and m=1 in detail in Section 5-6.

5.3 Part 2--Roots for Excitation

In the derivation of the regular Prony's method, a Prony polynomial was formed as in equation (5-23).

$$P(z) = z^{N} + a_{1}z^{N-1} + ... + a_{N}$$
 (5-23)

where the solution set $[a_i]_{i=1}^N$ is the final coefficient set obtained in the first part of Prony's method. Since equation (5-23) is of degree N, it possesses N (possibly nondistinct) roots and can be factored as equation (5-24).

$$P(z) = \prod_{i=1}^{N} (z-z_i)$$
 (5-24)

As previously pointed out the same solution set can be used to obtain what we have previously defined as the Prony K-Pulse, given by equation (5-25).

$$[K_n]_{n=0}^N = [a_n]_{n=0}^N$$
 (5-25)

where $a_0 = 1$

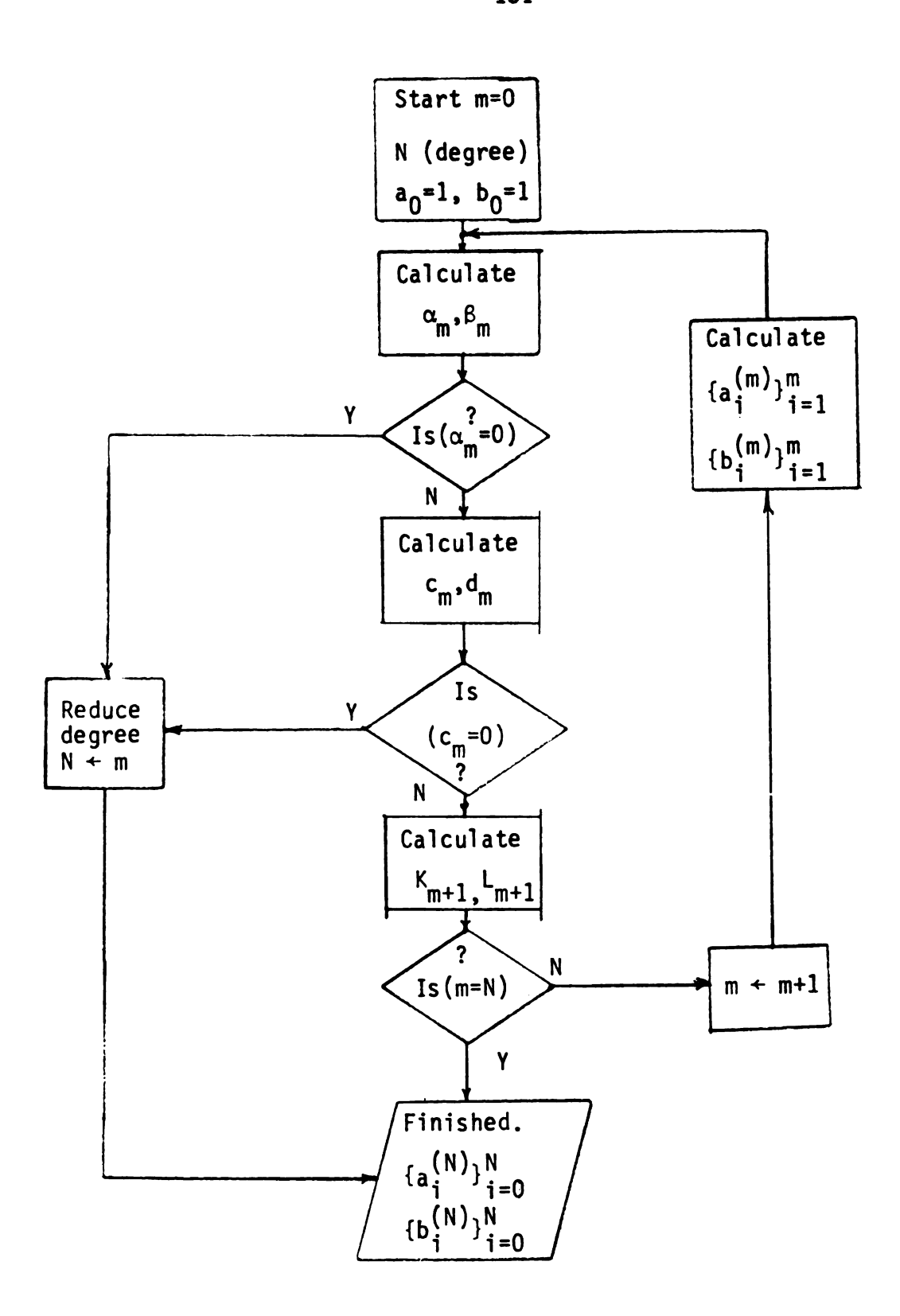


Figure 5-2. Flow Chart for K-Pulse part of "Fast Prony's Method Algorithm".

For the third part of the "Fast" Prony's method, we shall use z-transforms of the Prony K-Pulse sequence which is easily calculated to be equation (5-26).

$$K(z) = \sum_{i=0}^{N} K_i z^{-n}$$
 (5-26)

Note that the z-transform of the Prony K-Pulse contains negative powers of z instead of positive powers of z as in the Prony polynomial. Equation (5-27) gives the relationship between the two.

$$K(z) = z^{-N}P(z) = \prod_{i=1}^{N} (1-z_i/z)$$
 (5-27)

The regular Prony's method requires the determination of all of the roots of the Prony polynomial. This is because the Vandermonde matrix of equation (4-18) requires all N roots. There are many published methods of finding all of these roots. Standard computer library routines such as IMSL appear to perform quite satisfactorily up to N=100 for the Prony algorithms. Numerical conditioning may become a significant problem for very large N. /Rooting algorithms for largest degrees give this warning. For target discrimination we shall require accurate knowledge only of the target natural frequencies which have large amplitudes. This is because they are the invariant parameters of our radar problem.

In Part 3 we alter the method of determining the complex amplitudes so that we relieve the requirement to solve for all of the roots

in Part 2 of this algorithm. This is an order of magnitude reduction in computational requirements. Figure 5-3 illustrates the iterative process by which we avoid solving for all roots in the Prony polynomial of very large degree. We first perform the skip sampled data "fast Prony's method algorith" solving for all roots. We determine which of these natural frequencies has large target return energy. These are the "Targeted Roots" that we shall track and find in the higher degree Prony polynomial for the dense sampled data. By using the properly scaled "target root" and initial step size, we can solve a high degree polynomial by an accelerated method such as the Hooke-Jeeves (pattern search) algorithm. Appendix D contains computer code validatable by reference 5-8.

Since only the natural frequencies are invariant, we must use equation (5-28) in the rooting process, where the subscript m denotes the skip sampled data parameter and n denotes the denser sampled parameter.

$$T_m^{-1} \operatorname{clog}(z_{mi}) = s_i = T_n^{-1} \operatorname{clog}(z_{ni})$$
 (5-28)

Current data sequences tested are less than 256 signal sampled data POints. The limit of this method is well in excess of this number.

With the root Z_{ni} determined, the i-th mode excitation vector, $E^{i}(z)$ is obtained by synthetic division on the K-Pulse, K(z). Since z_{i} has already been determined to be a root, the division is exact.

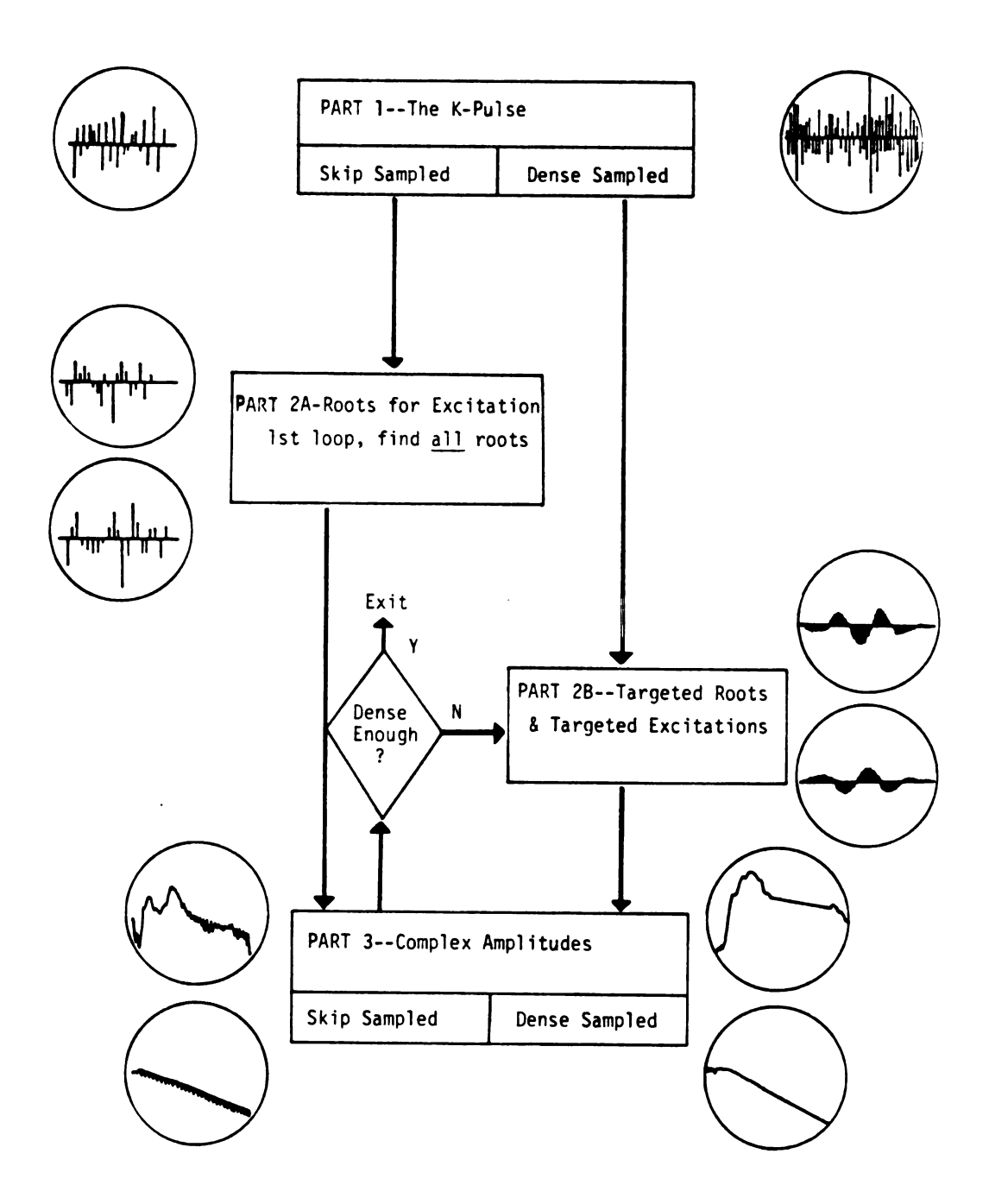


Figure 5-3. "Fast Prony's Method Algorithm" Block Diagram.

5.4 Part 3--Amplitudes and Coupling Coefficients

The third part of Prony's method calculates the complex amplitude or residue of each complex exponential in the Prony series which is written in equation (5-29).

$$[v_n]_{n=0}^{\infty} = \sum_{i=1}^{N} A_i [\exp(s_i T_n)]_{n=0}^{\infty}$$
 (5-29)

Even if equation (5-29) is not true for all time, it can be satisfied exactly for a time sequence of 2N sample data point (contiguous) by allowing exactly N complex modes in equation (5-29).

We can use Part 1 of Prony's method to obtain the Prony
K-Pulse given by equation (28). We can also write it in its equivalent
form of equation (5-30) even if we have not yet solved for all of the
roots or natural frequencies.

$$[k_n]_{n=0}^{N} = [1, -\exp(s_1T)] * ... * [1, -\exp(s_NT)]$$
 (5-30)

Convolving the K-Pulse with the signal sampled data sequence, we obtain equation (5-31)

$$[k_{n}]_{n=0}^{n} * [v_{n}]_{n=0}^{\infty} = [1, -\exp(s_{1}^{T})] * . . .$$

$$*[1, -\exp(s_{N}^{T})] * \sum_{i=1}^{N} A_{i} [\exp(s_{i}^{T}n)]_{n=0}^{\infty}$$
(5-31)

Next recalling our definition of the j-th mode excitation waveform, it can also be written in factored convolutional form as in equation (5-32).

$$[e_n^j]_{n=0}^{N-1} = \prod_{\substack{i \neq j}}^{N} [1]^*[1,-\exp(s_i^T)]$$
 (5-32)

There is one simple identity which we shall use repeatedly. If the convolution of a single complex exponential with the inverse couplet, given by equation (5-33)

$$[\exp(s_i T_n)]_{n=0}^{\infty} * [1, -\exp(s_i T)] = [1, 0, 0...]$$
 (5-33)

Using equations (5-31) and (5-30), equation (5-29) becomes obviously of finite duration and is given by equation (5-34).

$$[k_n]^*[v_n]_{n=0}^{\infty} = \sum_{j=1}^{N} A_j [E_n^j]_{n=0}^{N-1}$$
 (5-34)

Hence the output convolution of a sampled data Prony series with its Prony K-Pulse is of length NT in time and is actually the N different j-th mode excitation waveforms weighted by the complex amplitude of the j-th mode in the original Prony series.

Taking the z-transform of each side of equation (5-34), we obtain equation (5-35).

$$(C(z) = K(z)S(z) = \sum_{i=1}^{N} A_{i} [E_{n}^{i} z^{-n}]_{n=0}^{N-1} = \sum_{i=1}^{N} A_{i} E^{i}(z)$$
 (5-35)

Now the complex amplitude or residue of the j-mode can readily be obtained if the j-th mode excitation waveform and the j-th root are known. But the j-th mode excitation transform is known if the Prony K-Pulse and the j-th root are known. It is given by equation (5-36).

$$E^{j}(z) = K(z)(1-z_{j}/z)^{-1} = \prod_{\substack{i \neq j \\ i \neq j}}^{N} (1-z_{i}/z)$$
 (5-36)

The j-th mode residue or complex amplitude is now easily computed because equation (5-37) hold for each j-th mode excitation transform.

$$E^{j}(z_{k}) = \prod_{i \neq j}^{N} (1-z_{i}/z_{k}) = 0 \quad \text{for } z_{k} \neq z_{j}$$
 (5-37)

But this implies the important equation (5-38).

$$C(z_j) = \sum_{i=1}^{N} A_i E^i(z_j) = A_j E^j(z_j)$$
 (5-38)

Hence the j-th mode complex amplitude is given by the simple formula of equation (5-39).

$$A_{j} = C(z_{j})/E^{j}(z_{j})$$
 (5-39)

Equation (5-39) is an original result. It gives the correct complex amplitude for a "Prony series" without the use of the transposed Vandermonde matrix and without knowing all of the complex roots or natural frequencies. Only the j-th root in addition to the "Prony K-Pulse" is necessary to calculate the complex amplitude, A_j . This formula also provides the link to our "polar mode A-scope" displays which we use whether or not we can positively identify a "Prony series."

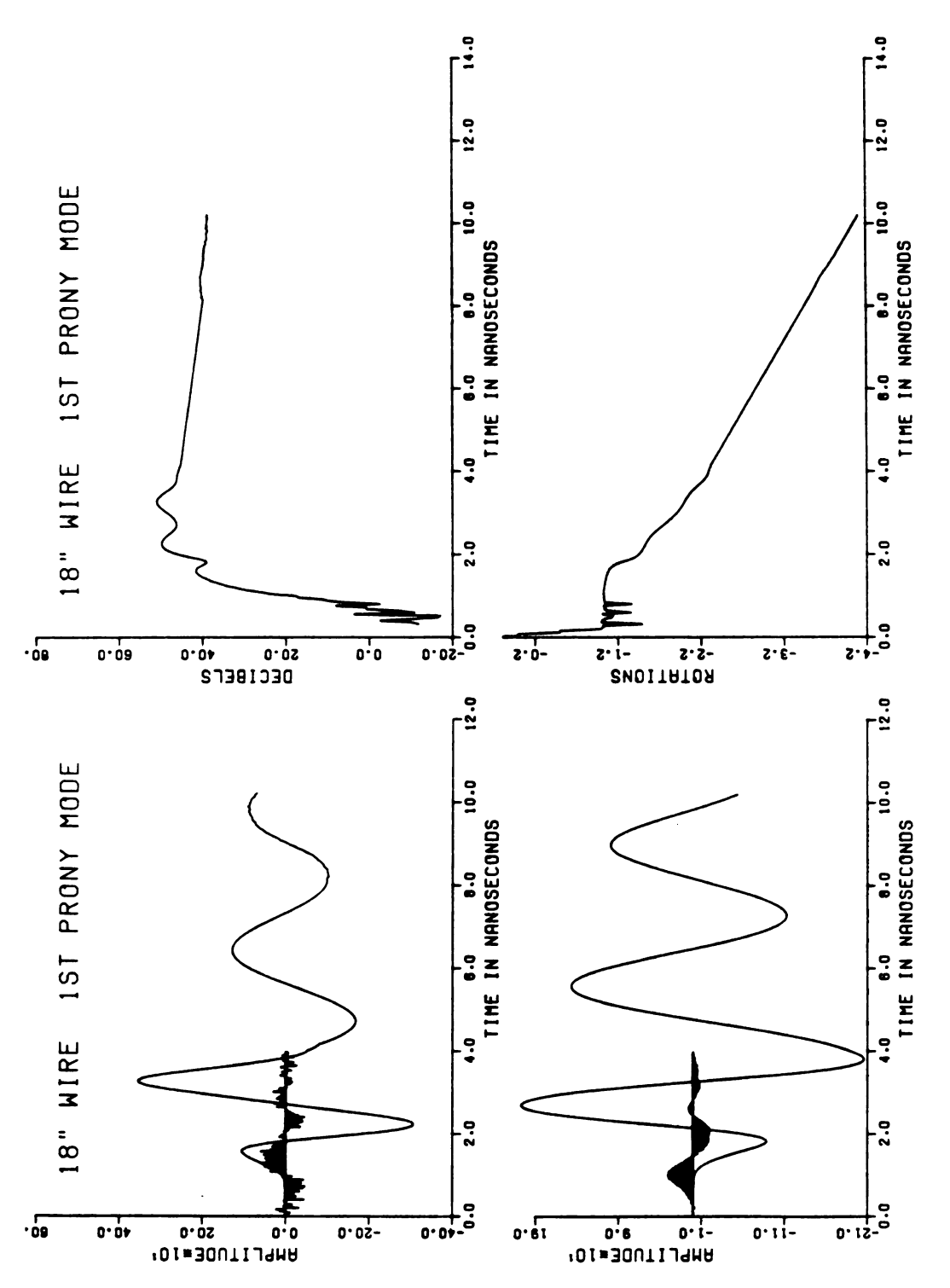
Let us redo the Figures 4-6 and 4-9 without the handicap of standard matrix arithmetic. Figure 5-4 illustrated the 1st mode waveform excitation from 100 value excitation vectors. Similarly Figure 5-5 illustrates the 3rd mode waveform excitation from 100 value excitation vectors. The following are to be observed:

- 1. We avoided two 100 x 100 matrix equations
- 2. No target root splitting occurred
- Excitation vectors give the appearance of being smoother, although this is not observable for the K-Pulse
- 4. A-scope plot is much smoother and without ripples

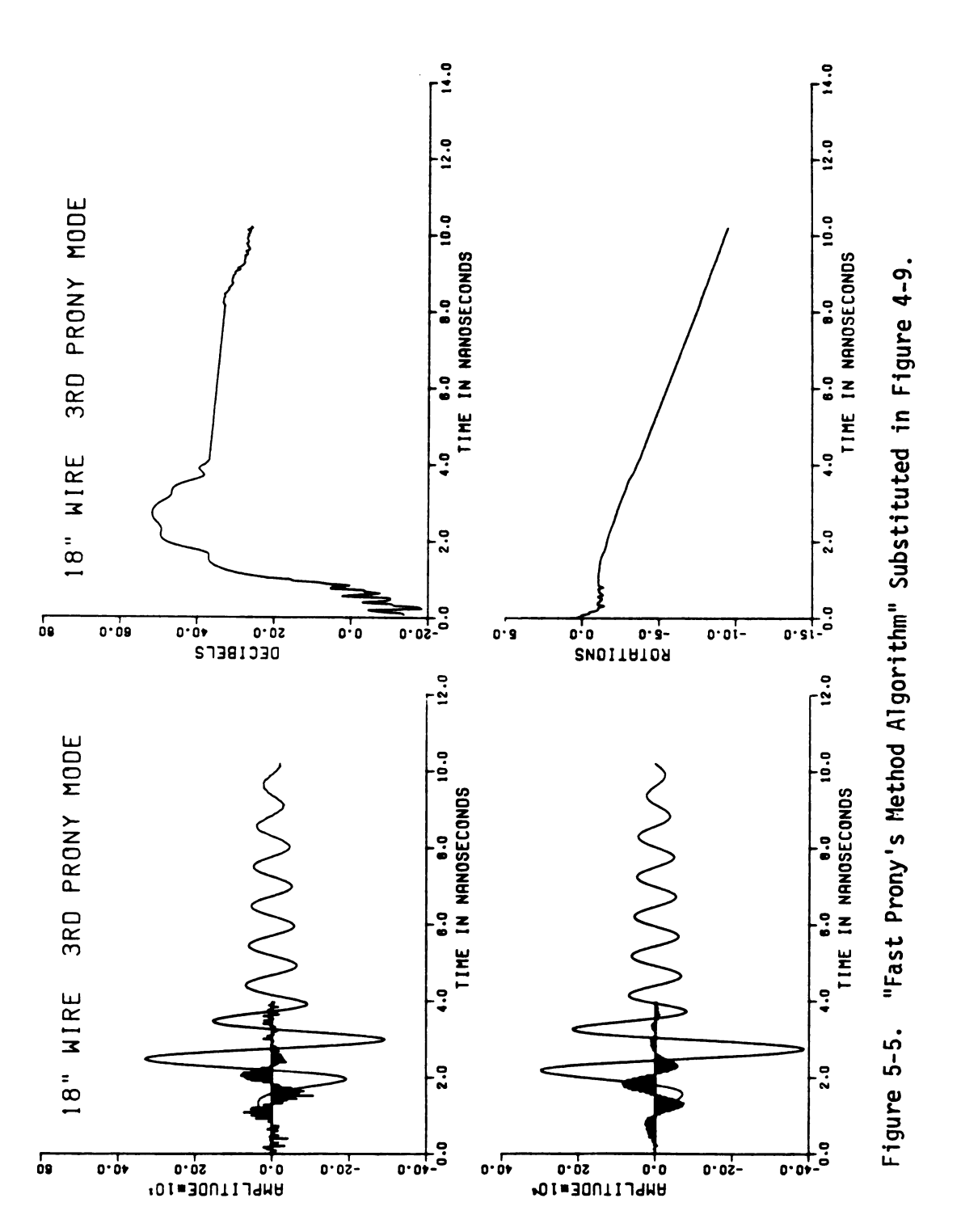
5.5 Computational Comparisons for Part 1

Table 5-2 gives a comparison of the "Fast" Prony's method,
Part 1, with other "fast" algorithms for the computation of the
K-Pulse sequence or Prony polynomial. It should be noted that the
"fast" Prony algorithm consistently has an advantage over these published state-of-the-art algorithms for m as small as 10 or as large
as 1000. For comparison with the common direct matrix algorithms
such as Gaussian elimination is typically M³/3 operations. However,
storage is a more severe problem in direct methods, e.g., the IMSL
routine LEQ2C requires matrices using 2M²+4M storage locations.
This compares with the 4M=1 storage location required by the "fast"
Prony method for the K-Pulse solution.

The surprise depicted in Table 5-3 is a comparison with the Symmetric Toeplitz algorithm as used in the so-called "autocorrelation"



"Fast Prony's Method Algorithm" Substituted in Figure 4-6. Figure 5-4.



141

TABLE 5-2. Computation Comparison for Part 1.

		,	141		
Sum of Operations for M=1000 in units of a million	2.0 +0. 2.0	0.6 —0+ 9.0	170.2 + 0 170.2	335.3 + 4.0 339.3	1.0 +24.6 25.6
Sum of Operations for M=10	242 + 0 242	1091 + 0 1091	540 + 0 540	556 +456 1012	85 +2684 2769
Matrix Load Operations if required	0	0	included	2(M+2)(1-1)	(M+1)(2L-M-2)
K-Pulse Method Algorithm Operations M=degree of polyn. Multiplications plus L=minimum length Divisions	м ² +5м+2	(M+1)L+7M ² +15M-7	м ³ /6+3М ² /2+(M+1)L+M/3	M ³ /3+2M ² +8M/3-4	м ² -зм/2
K-Pulse Method M=degree of polyn. L=minimum length	"Fast" Prony L=2M+1 (2 solutions) (Table 5-2)	Morf Covariance (Ref 5-5,pp 432) L=2M+1 (2 solutions)	Westlake Covar- iance Cholesky (Ref. 5-6) L=2M	Markel & Gray Cholesky Covar. (Ref 5-3,pp 222) L=2M	Markel & Gray Symmetric Toeplitz (Ref 5-3,pp 222) L=12.8M

Table 5-3. Calculations for the "Fast" Prony K-Pulse

Variable on iteration m=1,,M	Multiplications & Divisions
c _m	m
d _m	m
a (m)	m
b (m)	m
α_{m}	1
$\beta_{\rm m} = \alpha_{\rm m}$	0
K _{m+1}	1
L _{m+1}	1
total _m	4m+3
total ₀	2
$\sum_{m=0}^{M} total_{m}$	4(M/2)(M+1)+3M+2 =2M ² +5M+2

method." It might have been suspected that Part 1 of the "fast" Prony method would be twice as slow, require twice as much memory, and twice as many variables to implement and compute for the same physical problem. This is a defective conclusion for three major reasons:

- Raw data are not naturally symmetric (unless noise free). Some processing must have been performed which is typically more computationally intensive (Ref. 5-3) than the symmetric Toeplitz algorithm
- More raw data (>>2N) are required to compute reasonable estimates (Ref. 5-4) of the processed symmetrical sample data points than are required for the "fast" Prony method
- 3. If the raw data are not symmetricized, the "fast" Prony method obtains <u>twice</u> as many solutions, each of which is different and useful in the radar target discrimination problem

5.6 Special Cases for SEM Computations

Numerical zeros play a crucial role in the operation of the "fast Prony's method algorithm." First, if equation (5-40) holds, Part 1 of the algorithm must be terminated, returning the "Prony K-Pulse" of equation (5-41).

$$v(NT) = 0$$
, of the 2N+1 sampled data (5-40)

$$\{k_i\}_{i=0}^{N} = \{1,0,0,\ldots 0\}$$
 (5-41)

This special K-Pulse is just the identity operator and is a necessary form for use in the next chapter. We shall identify equation (5-40) by noting that equation (5-42) occurred in Part 1 of the algorithm.

$$\alpha_0 = 0 \tag{5-43}$$

A much more desirable event to occur is equation (5-53)

$$\alpha_{\mathsf{N}} = 0 \tag{5-43}$$

This event tells us that lower order errors α_0 , α_1 , α_2 , ..., α_{N-1} were all nonzero and that the next iteration is now singular. This means that we have an exact Prony series solution to the 2N+1 sampled data. Note that equation (5-42) is consistent with this interpretation for the $2 \cdot 1 + 1 = 1$ sampled data point.

To illustrate what happens, we take a simple "Prony series" given by equation (5-44).

$$v_n = \begin{cases} Aexp(s_1^{Tn}) = Az_1^n, & n > 0 \\ 0, & \text{otherwise} \end{cases}$$
 (5-44)

This is simple enough; we can perform the computations by hand. We do so on the worksheet of Figure 5-6. Note that α_1 =0. This is our singularity flag A which tells us we have successfully detected a 1 term Prony Series. From the summary of Figure 5-7, we can tell that we have a (forward) Prony K-Pulse given by equation (5-45) with trailing zeros appended if desired.

Function Type is Natural Mode
$$v_{n} = \begin{bmatrix} 0, & n < 0 \\ A_{1} exp(s_{1} Tn) = A_{1} z_{1}^{n}, & otherwise \end{bmatrix}$$
 Upper left corner of Matrix $n = 2$
$$\begin{bmatrix} v_{n} & v_{n-1} \\ v_{n+1} v_{n} \end{bmatrix} \begin{bmatrix} 1 \\ 0 \end{bmatrix} = \begin{bmatrix} \alpha_{0} \\ c_{0} \end{bmatrix} \quad \alpha_{0} = v_{n} = A_{1} z_{1}^{2} \\ c_{0} = v_{n+1} = A_{1} z_{1}^{2} \end{bmatrix}$$

$$\begin{bmatrix} v_{n} & v_{n-1} \\ v_{n+1} v_{n} \end{bmatrix} \begin{bmatrix} 0 \\ 1 \end{bmatrix} = \begin{bmatrix} d_{0} \\ \theta_{0} \end{bmatrix} \quad d_{0} = v_{n-1} = A_{1} z_{1} \\ \theta_{0} = v_{n} = A_{1} z_{1}^{2} \end{bmatrix}$$

$$\begin{bmatrix} \kappa_{1} = -c_{0}/\beta_{0} = -v_{n+1}/v_{n} = -z_{1} \\ c_{1} = -d_{0}/\alpha_{0} = -v_{n-1}/v_{n} = -z_{1}^{-1} \end{bmatrix}$$

$$\begin{bmatrix} 1 \\ a_{1} \end{bmatrix} = \begin{bmatrix} 1 \\ 0 \end{bmatrix} + K_{1} \begin{bmatrix} 0 \\ 1 \end{bmatrix} = \begin{bmatrix} 1 \\ K_{1} \end{bmatrix} = -z_{1}^{-1} \end{bmatrix}$$

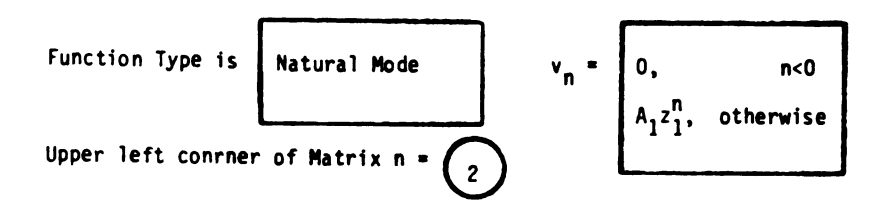
$$\begin{bmatrix} v_{1} & v_{1} & v_{1} & v_{1} \\ v_{1} & v_{1} & v_{1} & v_{1} \\ v_{1} & v_{1} & v_{1} & v_{1} \end{bmatrix} \begin{bmatrix} 1 \\ a_{1} \\ 0 \end{bmatrix} = \begin{bmatrix} \alpha_{1} \\ 1 \end{bmatrix} = -z_{1}^{-1} \end{bmatrix}$$

$$\begin{bmatrix} v_{1} & v_{1} & v_{1} & v_{1} \\ v_{1} & v_{1} & v_{1} & v_{1} \\ v_{1} & v_{1} & v_{1} & v_{1} \end{bmatrix} \begin{bmatrix} 1 \\ a_{1} \\ 0 \end{bmatrix} = \begin{bmatrix} \alpha_{1} \\ 0 \\ c_{1} \end{bmatrix} = A_{1} z_{1}^{2} - z_{1} A_{1} z_{1}^{2} = 0$$

$$\begin{bmatrix} v_{n} & v_{n-1} v_{n-2} \\ v_{n+1} v_{n} & v_{n-1} \\ v_{n+2} v_{n+1} v_{n} \end{bmatrix} \begin{bmatrix} 0 \\ b_{1} \\ 1 \end{bmatrix} = \begin{bmatrix} d_{1} \\ 0 \\ \beta_{1} \end{bmatrix} = A_{1} z_{1}^{2} - z_{1}^{2} A_{1} z_{1}^{2} = 0$$

$$K_{2} = -c_{1}/\beta_{1} = C_{1} + C_{1}/\beta_{1} = C_{1} + C_{1}/\beta_{1} = C_{1}$$

Figure 5-6. Prony K-Pulse Worksheet #1.



1	m	a (m)	b(m)	α _m = β _m	c _m	d _m	K _{m+1}	L _{m+1}
	0	1	1	A ₁ z ₁ ²	A ₁ z ₁ ³	A ₁ z ₁	-z ₁	-z ₁ -1
	1	1 2 1	1 z ₁ -1	0	0	0	0	0
	2							
	3							

Figure 5-7. Prony K-Pulse Worksheet #2.

$$\{k_i\}_{i=0}^{N} = \{1,-z_1\}$$
 (5-45)

So, this singularity flag 1 all by itself tells us we possess an N term Prony series with an exact synthesis for the 2N+1 sampled data values. Note that the ordinary Prony's method performed similarly on 2N data values and handled 2N+1 data values by a differencing operation on the original data. For these cases, the calculation of the amplitude coefficients is flexible: any N of 2N equations can be used in a transposed Vandermonde matrix. We know from section 3.7 there are cases (nonsingular) where this is not true. Hence, the absence of the singularity flag 1 warns us we may not wish to use the standard calculation of the amplitude coefficients given in Chapter 4.

We know that our radar data will not be a perfect "Prony series" even before we test empirical data because our analyses abound with entire functions multiplying and adding to our natural mode waveforms. Hence, we shall show that the "fast Prony's method algorithm" also possesses a second flag which detects some of the "class 2 Prony series" and allows us to successfully compute the time varying amplitude coefficients. We shall change our example by a slight amount to equation (5-46).

$$v_n = \begin{cases} 0, & n \leq 0 \\ Az_1, & n > 0 \end{cases}$$
 (5-46)

Note that we have set the data value in the upper right hand corner of the matrix to zero. We use the worksheet in Figure 5-8 to show that this has a drastic effect on the computation. We no longer

Function Type is Natural Mode late-time not satisfied

Upper left corner of Matrix
$$n = 1$$

$$\begin{bmatrix} v_n & v_{n-1} \\ v_{n+1} v_n \end{bmatrix} \begin{bmatrix} 1 \\ 0 \end{bmatrix} = \begin{bmatrix} \alpha_0 \\ c_0 \end{bmatrix} & \alpha_0 = v_n = A_1 z_1 \\ c_0 = v_{n+1} = A_1 z_1^2 \end{bmatrix}$$

$$\begin{bmatrix} v_n & v_{n-1} \\ v_{n+1} v_n \end{bmatrix} \begin{bmatrix} 0 \\ 1 \end{bmatrix} = \begin{bmatrix} d_0 \\ \theta_0 \end{bmatrix} & d_0 = v_{n-1} = 0 \\ \theta_0 = v_n = A_1 z_1 \end{bmatrix}$$

$$K_1 = c_0 / \theta_0 = -v_{n+1} / v_n = -A_1 z_1^2 / A_1 z_1 = -z_1$$

$$L_1 = -d_0 / \alpha_0 = -v_{n-1} / v_n = 0$$

$$m=1:$$

$$\begin{bmatrix} 1 \\ a_1 \\ 1 \end{bmatrix} = \begin{bmatrix} 1 \\ 0 \\ 1 \end{bmatrix} + K_1 \begin{bmatrix} 0 \\ 1 \end{bmatrix} = \begin{bmatrix} 1 \\ K_1 \end{bmatrix} = -z_1$$

$$\begin{bmatrix} v_n & v_{n-1} v_{n-2} \\ v_{n+1} v_n & v_{n-1} \\ v_{n+2} v_{n+1} v_n \end{bmatrix} \begin{bmatrix} 1 \\ a_1 \\ 0 \end{bmatrix} = \begin{bmatrix} \alpha_1 \\ 1 \\ 0 \end{bmatrix} = \alpha_1 = A_1 z_1^3 - z_1 A_1 z_1^2 = 0$$

$$\begin{bmatrix} v_n & v_{n-1} v_{n-2} \\ v_{n+1} v_n & v_{n-1} \\ v_{n+2} v_{n+1} v_n \end{bmatrix} \begin{bmatrix} 0 \\ b_1 \\ 1 \end{bmatrix} = \begin{bmatrix} d_1 \\ 0 \\ \beta_1 \end{bmatrix} & d_1 = 0$$

$$\begin{bmatrix} v_n & v_{n-1} v_{n-2} \\ v_{n+1} v_n & v_{n-1} \\ v_{n+2} v_{n+1} v_n \end{bmatrix} \begin{bmatrix} 0 \\ b_1 \\ 1 \end{bmatrix} = \begin{bmatrix} d_1 \\ 0 \\ \beta_1 \end{bmatrix} & d_1 = 0$$

$$K_2 = -c_1 / \beta_1 = 0$$

$$L_2 = -d_1 / \alpha_1 = 0$$
Exit on Flag 2.

Figure 5-8. Non-late-time Prony K-Pulse Worksheet #1.

obtain the algorithmic singularity flag 1 since our standard error formula will never go to zero.

We will define the C and D flags to help us identify a "class 2 Prony series" by equations (5-47) and (5-48).

$$c_m = 0 \rightarrow flag C$$
 (5-47)

$$d_{m} = 0 \rightarrow flag D \qquad (5-48)$$

From the summary in Figure 5-9, we may observe that one of the K-Pulses has the correct root. For the flag C condition we are through only with Parts 1 and 2 of the algorithm. Remember that as in equation (4-27) of section 4.7, all of the possible equations for determining the amplitude coefficients do not give the same values. The correct solution, of course, is to use equation (5-37). Further, if equation (5-37) is performed as a convolution as we do for our radar A-scope displays, the time-varying amplitude is obtained.

The previous two examples illustrate the K-Pulse part of the algorithm for a very simple example. We need another level of complexity to observe the effects of amplitudes and possible "ill-conditioning" on the algorithm. Equation (5-49) is a 2-term "Prony series" we shall use.

$$V_{n} = \left\{ \begin{array}{l} 0 & n < 0 \\ A_{1}z_{1}^{n} + A_{2}Z_{2}^{n}, & n \geq 0 \end{array} \right\}$$
 (5-49)

The algorithm calculations on this "Prony series" is carried out in Figure (5-10) through (5-11). In the summary of Figure (5-12) through (5-11). In the summary of Figure (5-12), we note that for m=2, both

Function Type is	Natural Mode late-time not satisfied	v _n =	0, n<1 A ₁ z ₁ , otherwise
Upper left conrne	r of Matrix n = 1		

m	a (m)	b _i (m)	α _m = β _m	c _m	d _m	K m+1	L _{m+1}
0	1	1	A ₁ z ₁	A ₁ z ₁ ²	0	-z ₁	0
1	1 -z ₁	1 0	A ₁ z ₁	0	0	0	0
2							
3							

Figure 5-9. Non-late-time Prony K-Pulse Worksheet #2.

Function Type is Two Natural Modes
$$v_n = \begin{bmatrix} 0, & & & & & \\ A_1z_1^n + A_2z_2^n, & & & \\ & & & & \\ & & & & \\ & & & & \\ & & & & \\ & & & & \\ & & & & \\ & & & & \\ & & & & \\ & & & & \\ & & & & \\ & & & & \\ & & & & \\ & & & \\ & & & & \\ & & & & \\ & & & \\ & & & & \\ & & & & \\ & & & \\ & & & & & \\ & & & & \\ & & & & \\ & & & & & \\ & & & & \\ & & & & \\ & & & & \\ & & & & \\ & & & & \\ & & & &$$

Figure 5-10. Two Mode Prony K-Pulse Worksheet #1.

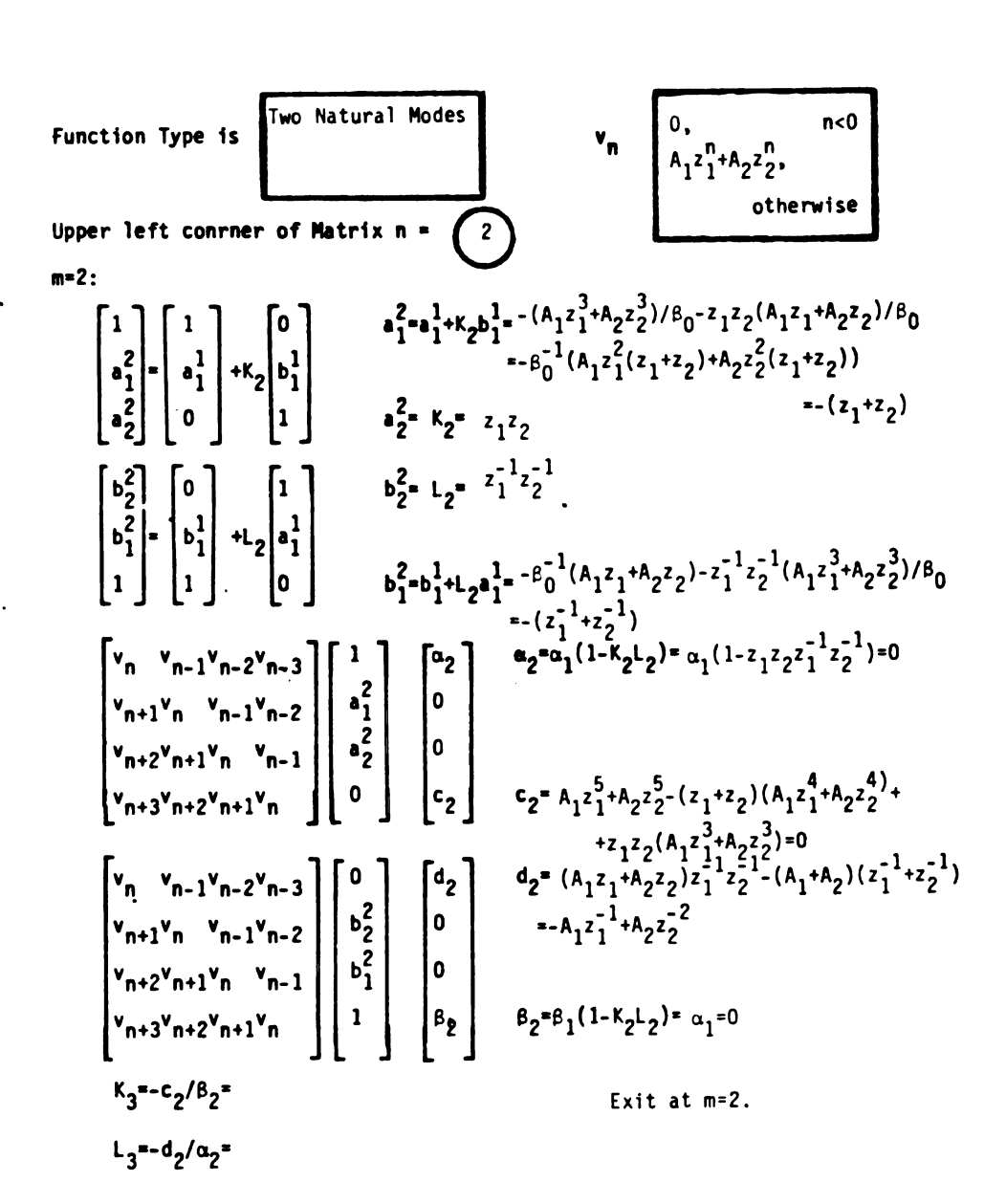
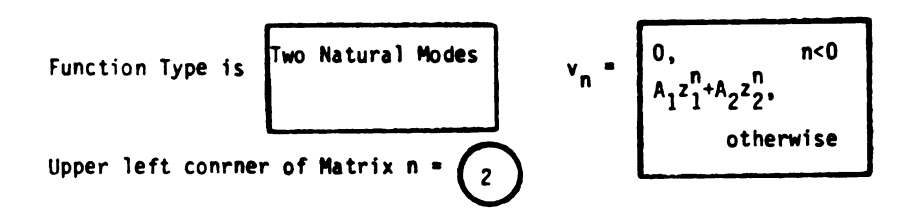


Figure 5-11. Two Mode Prony K-Pulse Worksheet #2.



m	a (m)	b (m)	α _m = β _m	c _m	d _m	K _{m+1}	L _{m+1}
0	1	1	A ₁ z ₁ ² +A ₂ z ₂ ²	A ₁ z ₁ ³ +A ₂ z	A ₁ z ₁ + A ₂ z ₂	$\begin{array}{c} A_1 z_1^3 + A_2 z_2^3 \\ -\beta_0 \end{array}$	A ₁ z ₁ +A ₂ z ₂ -2 ₀
1	1 K ₁	1 (A ₁ z ₁ +A ₂ z ₂) -β ₀	$\frac{\varepsilon_0^{-1}A_1z_1A_2z}{\cdot(z_1^{-z}z_2)^2}$	- ^β 1 ^z 1 ^z 2	$-\frac{\beta_1 z_1^{-1}}{z_2^{-1}}$	² 1 ² 2	z ₁ -1z ₂ -1
2	1 -(z ₁ +z ₂) z ₁ z ₂	1		0	-A ₁ z ₁ ⁻¹ -A ₂ z ₂ ⁻¹		
3							

Figure 5-12. Two Mode Prony K-Pulse Worksheet #3.

K-Pulses has the correct roots with no dependency upon complex amplitudes of the original "Prony Series." Note for the shorter sequencies at m = 1, complex amplitude dependency still exists.

Note carefully, if one amplitude is much larger than the other amplitude, then at m = 1 the shorter sequences approximately contains only one root without amplitude dependency.

Now we shall observe the effect of violating the late-time "Prony series" as we did in section 4.7. Let us alter equation (5-49) by only one sampled data point. The different point is given by equation (5-50).

$$v_{O} = 0 \tag{5-50}$$

We will simply reuse Figures (5-10) through (5-12) and note the differences. First, $a^{(2)}$ sequence is a perfect Prony K-Pulse, but $\alpha_2 \neq 0$. So the algorithm will not be terminated by singularity flag A. Since C_2 and C_3 will be zero, we will terminate at m=2 by means of flag C. Also note that d_2 , L_3 , and $b^{(2)}$ are not the same as before.

Next suppose that equation (5-49) is modified by both equations (5-50) and (5-51)

$$\mathbf{v}_1 = \mathbf{0} \tag{5-51}$$

Recalculating in Figures (5-10) through (5-12) only the steps which differ, we find the short sequence $\mathbf{a}^{(1)}$ is as far as we can go without significant differences. At this step if one of the two amplitudes

were much larger than the other, we would have approximately identified one root without amplitude dependency.

The pattern we are observing is that for a sequence composed of significant energy in only a small number of high amplitude modes, low "complex root degrees of freedom" will yield an approximate short K-Pulse which is amplitude independent of these high amplitude modes. This is compatible with the results of section 3.7 when the identified roots were always identified in batches. All large amplitude modes together and when sufficient "complex root degrees-of-freedom" occurred, the finite remaining small amplitude modes.

CHAPTER 6

RADAR TARGET DISCRIMINATION TECHNIQUE

6.1 Requirements for Automatic Radar Target Discrimination

We have now developed a number of analytical tools for radar target discrimination. The last remaining tool is the radar target discriminant itself. We choose not to embue our radar target processor with any learning ability or artificial intelligence. It must, however, be completely compatible with normal radar defects of clutter, thermal noise, propagation scintillations, receiver distortions, coded transmitter waveforms, etc. We shall adopt the following three processor requirements for the radar target discrimination:

- Criteria must be radar target aspect-angle independent
- 2. Criteria must be radar range independent
- 3. Only reversible operations may be used

 Requirement (1) is obviously desirable since it deletes the necessity of storing extremely complex radar target data files within the discrimination processor. Its implementation may not be obvious.

 Requirement (2) is also desirable and its implementation should be more obvious to a radar designer. Angle tracking radars are required to solve this problem. We choose a monopulse-like technique

for both requirements (2) and (1). By means of a normalizing channel, we shall develop a radar target discriminant from a "mode ratio discrimination detector." Requirement (3) will be achieved by avoiding least-squares techniques in our processor and analyses.

6.2 Discrimination Algorithm for Radar Targets

Figure 6-1 illustrates the discrimination algorithm which we shall test on empirical radar target data. The significant features to be noted are the use of the following original analytical tools:

1

- Dual "polar mode A-scope" displays
- 2. Double "Prony K-Pulse" convolutions
- "Fast Prony's method algorithm"

Data which must be stored in the memory of the radar target discrimination processor are for each radar target in its library:

- "Prony K-Pulse" for the radar target antenna terminal response
- 2. Natural frequencies (or invariant parameters) of the radar target which may have significant energy in the radar return signal

Note that our "Prony K-Pulse" for each specific target is specifically measured (or calibrated) for our specific radar. This K-Pulse file will contain natural mode waveforms of our radar system which may be excited by the radar target.

Table 5-1 gives the functions which the radar target discrimination processor must perform.

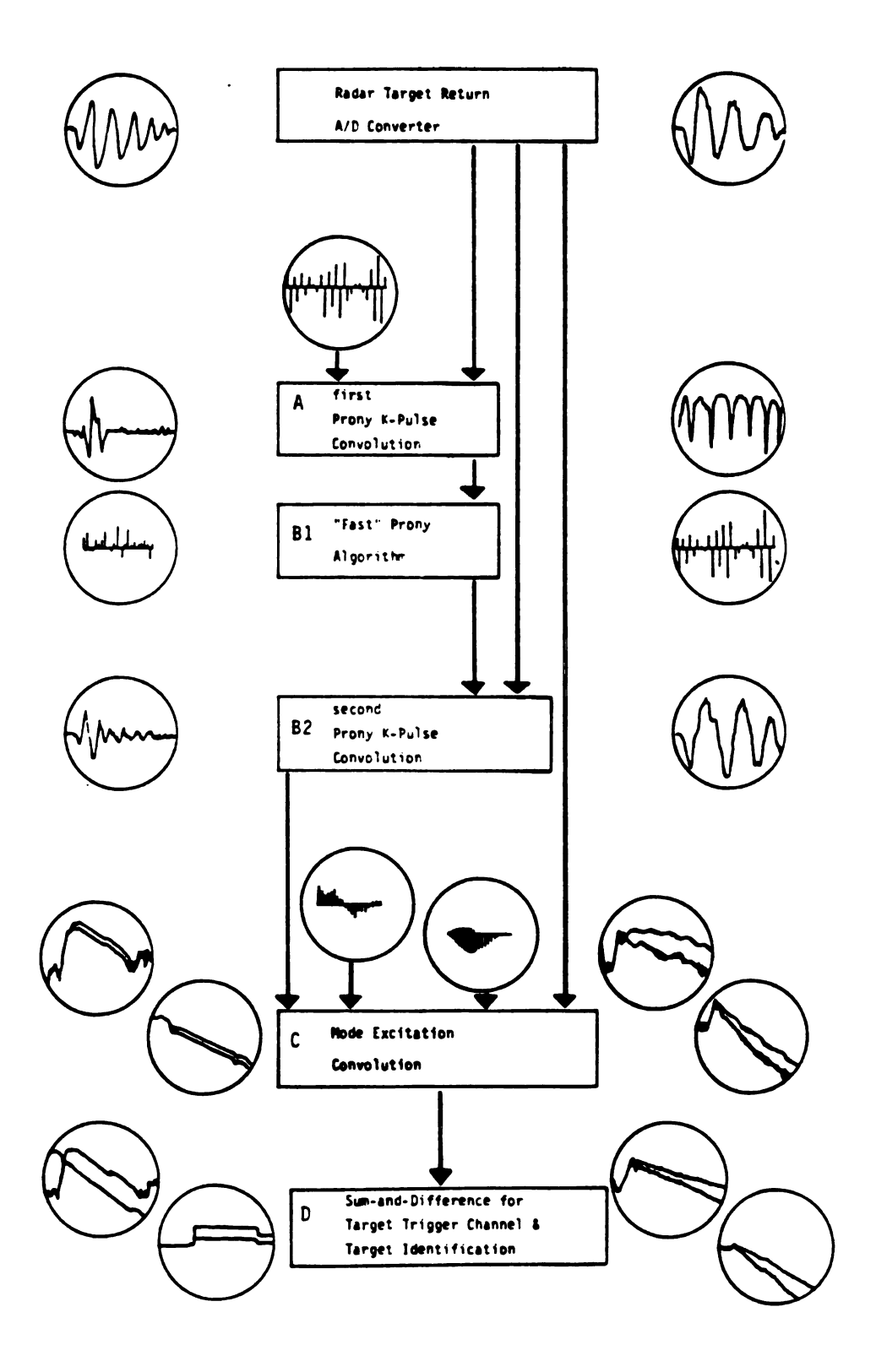


Figure 6-1. Radar Target Discrimination Algorithm Summary.

TABLE 6-1. Radar Target Discriminant

Part Procedure Α Target or 1st Prony K-Pulse convolution is performed using a previously measured K-Pulse on this radar and this target. The output of the convolution should contain not significant natural mode waveforms of the "right target" or the radar system. For the "right target" only return, after the N+1 samples of "early time" response, most remaining energy will simply be thermal noise and nonsuppressed clutter. B-1 "Fast" Prony algorithm is performed to detect any residual natural mode waveforms of significant energy. The primary output of this step is the second "Prony K-Pulse." B-2 The second Prony K-Pulse Convolution is performed on the original clutter-reduced radar target antenna terminal response file. This should kill the unexpected natural mode waveforms of the unknown target and radar system. but not necessarily the natural mode waveforms which are expected and would have been killed by the first "Prony K-Pulse." We shall call this output convolution the "2nd K-Pulsed" file. C We now perform mode excitation convolutions on both the original clutter-reduced radar target antenna terminal response file and the "2nd K-Pulsed" file. The mode excitations are derived from the "Prony K-Pulse" and radar target natural frequency in the manner of the "fast Prony's method algorithm," part 3. The dual "polar mode A-scope" displays are for a human D radar operator discrimination. The machine radar target discriminant uses the sum-and-differences of the dual traces. The difference files must be level even in the presence of thermal noise for a "right" target. The sum file is necessary to detect target energy above a noise threshold.

6.3 Part A--Target Library Prony K-Pulse Convolution

Let us start the analysis without the inclusion of noise. In this case in the frequency domain at the antenna terminal we have equation (6-1) which we have simplified slightly from equation (3-5).

$$\hat{\mathbf{V}}(\mathbf{s}) = \hat{\mathbf{W}}_{\boldsymbol{\theta}}(\P, \mathbf{s}) + \sum_{k=1}^{\infty} \hat{\mathbf{A}}_{k}(\mathbf{s}, \boldsymbol{\theta}, \boldsymbol{\phi})(\mathbf{s} - \mathbf{s}_{k})^{-1}$$
(6-1)

Now W(,s) is the entire function originating in equation (2-15) and the $\hat{A}_k(s,\theta,\phi)$ are the entire functions required by the "class 2" coupling coefficients observed in the retarded scattered E-field. After the sampler, the invertible, but more precise modified z-transform in equation (6-2) is more appropriate.

$$V(z,m) = W_{\theta}(\P,z,m) + z^{-1} \sum_{k=1}^{\infty} A_{k}(z,m,\theta,\phi) z_{k}^{m} (1-z_{k}/z)^{-1}$$
 (6-2)

Stored within the radar target library of our radar target discrimination processor is a specific "Prony K-Pulse" of length N+1 which must contain the radar target invariant parameters for which much of the target energy will be located. Equation (6-3) is the target library K-Pulse.

$$K(z) = \prod_{i=1}^{N} (1-z_i/z)$$
 (6-3)

We first perform a time domain convolution of the clutter-reduced radar target antenna terminal response, v(t,m) from equation (6-2)

with the target library K-Pulse, k(t=nT), of equation (6-3) to obtain the "first K-Pulses convolution," y(t,m), representable as equation (6-4).

$$Y(z,m) = K(z)W_{\theta}(\P,z,m) + z^{-1}\sum_{k=1}^{N}A_{k}(z,m,\theta,\phi)z_{k}^{m}\prod_{i\neq k}(1-z_{i}/z)$$

$$+ z^{-1}\{\prod_{i=1}^{N}(1-z_{i}/z)\}\sum_{k=N+1}^{\infty}A_{k}(z,m,\theta,\phi)z_{k}^{m}(1-z_{k}/z)^{-1}$$

$$= ET_{\theta}(z,m) + NM_{N}(z,m) + LT(z,m)$$
(6-4)

We wish to discuss each of the three terms given by equations (6-5), (6-6), and (6-7) separately.

$$ET_{\theta}(z,m) = K(z)W_{\theta}(\P,z,m)$$
 (6-5)

$$NM_{N}(z,m) = z^{-1} \sum_{k=1}^{N} A_{k}(z,m,\theta,\phi) z_{k}^{m} \prod_{i \neq k} (1-z_{i}/z)$$
 (6-6)

LT(z,m) =
$$z^{-1} \{ \prod_{i=1}^{N} (1-z_i/z) \} \sum_{k=N+1}^{\infty} A_k(z,m,\theta,\phi) z_k^m (1-z_k/z)^{-1}$$
 (6-7)

First of all it should be noted that only LT(z,m) of equation (6-7) has in the time domain, nonzero values in the retarded "late-time" of the processed clutter-reduced radar target antenna terminal response. For the "right target" these are small amplitude natural modes which are not normally excited by this radar transmitted waveform. Or possibly they were not available in sufficient amplitude when the

"Prony K-Pulse" for this "right target" was made. Second the $NM_N(z,m)$ is the residual of the N natural mode waveforms of both the target and radar system which have been killed and in the time domain cease identically after NT retarded time units. Third the contribution due to the entire function, $W_{\theta}($,z,m), alone is known to cease in the retarded "late-time" ("class 1" assumption). However, the composite term, $\mathrm{ET}_{\mathrm{e}}(\mathrm{z},\mathrm{m})$ potentially possesses a time domain convolution response nearly twice as long. Remember this term may (or may not) be required by the Mittag-Laffler theorem and definitely ceases to be necessary if there is any noninfinite representation of equation (6-1) for any reason. Now Prony's method does presume a finite summation of complex exponentials in the time domain or simple pole singularities in the frequency domain (we are for clarity excluding radar targets with repeated natural frequencies). We know from experience that the "Prony K-Pulse" will give us a zero response in the retarded latetime interval NT<t<(2N-)T. So there are two possibilities:

- 1. $\mathbf{w}_{\theta}(\ ,t,m)$ is an error contributor in the determination of the natural frequencies, or
- 2. w_{θ} (,t,m) cancels the effect of the higher indexed natural mode waveforms as indicated by equation (6-8)

$$et_{\theta}(t,m) = lt(t,m) \leq for NT \leq t \leq (2N-1)T$$
 (6-8)

It should be recognized that (6-8) is not likely to be satisfied for all (θ,ϕ) and (θ',ϕ') .

6.4 Part B--"Fast Prony Convolution Algorithm"

Part B of Table 6.1 is described as two parts. The first is identical to the "fast Prony's method algorithm," part 1. In this case we are seeking "Prony K-Pulses" $\{a_i\}_{i=0}^N$ and $\{b_i\}_{i=0}^N$ and $\{b_i\}_{i=0}^N$ on the output of the "Target K-Pulse convolution," y(t,m). If we perform this convolution on the original data file (m-1 and original thermal noise), we will obtain from the 2N+1 sampled data values, a 2N+1 output of N+1 nonzero values followed by N identically zero values. For the $\{a_i\}_{i=0}^N$ "Prony K-Pulse" solution, we obtain matrix equation (6-9).

$$\begin{bmatrix} y_{N} & y_{N+1} & \dots & y_{1} \\ 0 & y_{N} & \dots & y_{2} \\ \vdots & \vdots & & \vdots \\ 0 & 0 & y_{N} & a_{N} \end{bmatrix} \begin{bmatrix} a_{1} \\ a_{2} \\ \vdots \\ a_{N} \end{bmatrix} \begin{bmatrix} y_{N+1}=0 \\ y_{N+2}=0 \\ \vdots \\ y_{2N}=0 \end{bmatrix}$$
(6-9)

The "fast Prony's method algorithm" will return equation (6-10) for this "Prony K-Pulse."

$$\{k^a\} = \{1,0,0,\ldots,0\}$$
 (6-10)

Equation (6-10) should be recognized as the identity operator.

We can, however, do slightly better than equation (6-10) with the "2nd Prony K-Pulse" from equation (6-11). This solution $\{k^b\}$ is similar to the $\{a_i\}$ solution of Figure 5-5. The output of the B Part is given by equation (6-12).

$$\begin{bmatrix} y_{N} & y_{N+1} & \dots & y_{1} \\ 0 & y_{N} & \dots & y_{2} \\ \vdots & \vdots & & \vdots \\ 0 & 0 & y_{N} \end{bmatrix} = \begin{bmatrix} y_{0} \neq 0 \\ y_{1} \neq 0 \\ \vdots & \vdots \\ y_{N-1} \neq 0 \end{bmatrix}$$

$$(6-11)$$

$$u(t,m) = k^{b}(t)*v(t,m)$$
 (6-12)

We shall call u(t,m) the "2nd K-Pulsed convolution." This convolution is on the original clutter reduced radar target antenna terminal response and not y(t,m).

6.5 Part C--Dual "Polar Mode A-Scope" Displays

In Part C of the radar target discrimination algorithm, "polar mode A-Scope" displays are produced for several of the expected large amplitude modes of the radar "right target." This requires the use of the processor target library. The mode excitation waveform is generated from the target library Prony K-Pulse and known radar target natural frequencies. The processed waveforms for both the clutter-reduced radar target antenna response and the "2nd K-Pulsed convolution," u(t,m), are given by equations (6-13) and (6-14), respectively.

$$v^{j}(t,m) = e^{j}(t)*v(t,m)$$
 (6-13)

$$v^{j}(t,m) = e^{j}(t)*u(t,m)$$
 (6-14)

For the human radar operator, these are presented as dual traces on the pair of polar mode A-scopes, the rotation display and the envelope display. Denoting trace 1 as the "2nd K-Pulse convolution" and trace 2 as the original response, we have display equations (6-15) through (6-18).

$$env_1(t) = Real\{clog(u^j(t,m))\}$$
 (6-15)

$$env_2(t) = Real\{clog(v^j(tm,))\}$$
 (6-16)

$$rot_1(t) = Imaginary\{clog(u^{j}(t,m))\}$$
 (6-17)

$$rot_2(t) = Imaginary\{clog(v^{j}(t,m))\}$$
 (6-18)

6.6 Part D--Target Trigger and Identification

Part D of the radar target discrimination algorithm is for the automatic discrimination function. In this case a monopulse-like sum-and-difference operation is performed on the "polar mode A-scope" display files. From this part, we keep them in complex form rather than separate the real and imaginary parts as is required for display. In this process, the sum-and-difference of the dual traces become equations (6-19) and (6-20), respectively.

$$\Sigma^{j}(t,m) = \operatorname{clog}(u^{j}(t,m)) + \operatorname{clog}(v^{j}(t,m))$$
 (6-19)

$$\Delta^{j}(t,m) = \operatorname{clog}(u^{j}(t,m)) - \operatorname{clog}(v^{j}(t,m))$$
 (6-20)

Note that equations (6-19) and (6-20) can be written as equations (6-21) and (6-22) which give better clues as to their use.

$$\Sigma^{j}(t,m) = c\log(u^{j}(t,m)v^{j}(t,m))$$
 (6-21)

$$\Delta^{j}(t,m) = \operatorname{clog}(u^{j}(t,m)/v^{j}(t,m)) \tag{6-22}$$

For our special case of the "right target" equation (6-22) is a complex zone for <u>all</u> time. Even small amounts of thermal noise will not greatly disturb this general flatness. We still need equation (6-21) as a trigger channel for our discrimination processor to tell us when radar target energy is present at the antenna terminals.

Next we need to examine special cases with noise and "wrong target" to fully explore the power of this technique described. The baseline low noise case is summarized in Table 6-2.

Now it should be obvious that thermal noise in the radar system must degrade both our target trigger channel and our target identification channel, $\Delta^{j}(t,m)$. However, since we have performed nonlinear operations, it is not clear what the effect of low level thermal noise might be. We need to return to Part B to evaluate the effect of thermal noise in the radar receiver. Equation (6-9) becomes equation (6-23).

$$\begin{bmatrix} y_{N-1}^{+\varepsilon_{N-1}} & y_{N-2}^{+\varepsilon_{N-2}} & \cdots & y_0^{+\varepsilon_0} \\ \varepsilon_N & y_{N-1}^{+\varepsilon_{N-1}} & \cdots & y_1^{+\varepsilon_1} \\ \vdots & \vdots & & \vdots \\ \varepsilon_{2N-2} & \varepsilon_{2N-3} & y_{N-1}^{+\varepsilon_{N-1}} \end{bmatrix} \begin{bmatrix} \xi_1 \\ \xi_2 \\ \vdots \\ \xi_N \end{bmatrix} = - \begin{bmatrix} \varepsilon_N \\ \varepsilon_{N+1} \\ \vdots \\ \varepsilon_{2N-1} \end{bmatrix}$$
(6-23)

Table 6-2. Mode Ratio Discrimination Detector Performance Summary.

Components of the	Display during "Target Presence"	arget Presence"
Complex Discrimination	"Correct Target"	"Incorrect Target"
Envelope Mean	indicator of	indicator of
Real(Σ ³ /2)	target presence with correct mode damping	target presence with incorrect mode damping
Envelope Difference	flat	definite slope
Real(∆ ^j)	typical positive bias	always negative bias
Rotation Mean	correct mode rotation	incorrect mode
Imaginary $(\Sigma^{\hat{J}}/2)$	rate	rotation rade
Rotation Difference	flat	definite slope
Imaginary(∆ ^j)		

Equation (6-23) cannot be solved by inspection. One would be tempted to speculate that relation (6-24) would hole for small noise levels.

$$|\xi_i| \ll 1$$
, i = 1, 2, . . . , N (6-24)

This does not always seem to hold, but all that is necessary is that $k^p(t-nT)$ act similar to an identity operator on v(t,m). This must be the case unless there are one or more strong complex exponential waveforms within y(t,m). This would be the case for the "wrong target," and complex root degrees of freedom are consumed to kill the complex exponential.

Remember that the error variable, α_m , told us if we successfully found a "class 1" Prony series. Flag C of the Part 1 algorithm told us if we successfully found a "class 2 Prony series." What happens "success" is not complete is not theoretically clear, but empirically it appears that the complex root degrees-of-freedom will suppress some thermal noise in the NT \leq t \leq (2N-1)T retarded time region if not used to kill a complex exponential waveform.

6.7 Empirical Illustration

In this section we shall present the empirical validation of our radar target discrimination algorithm on the radar measurement data received from NSWC. Figure 5-2 shows the two sampled data files we shall use in this section exclusively. The "right target" for which Target Library Prony K-Pulse is obtained is for a 12-inch thin cylinder (L/a = 200) at a 45 degree elevation angle, 12" above the

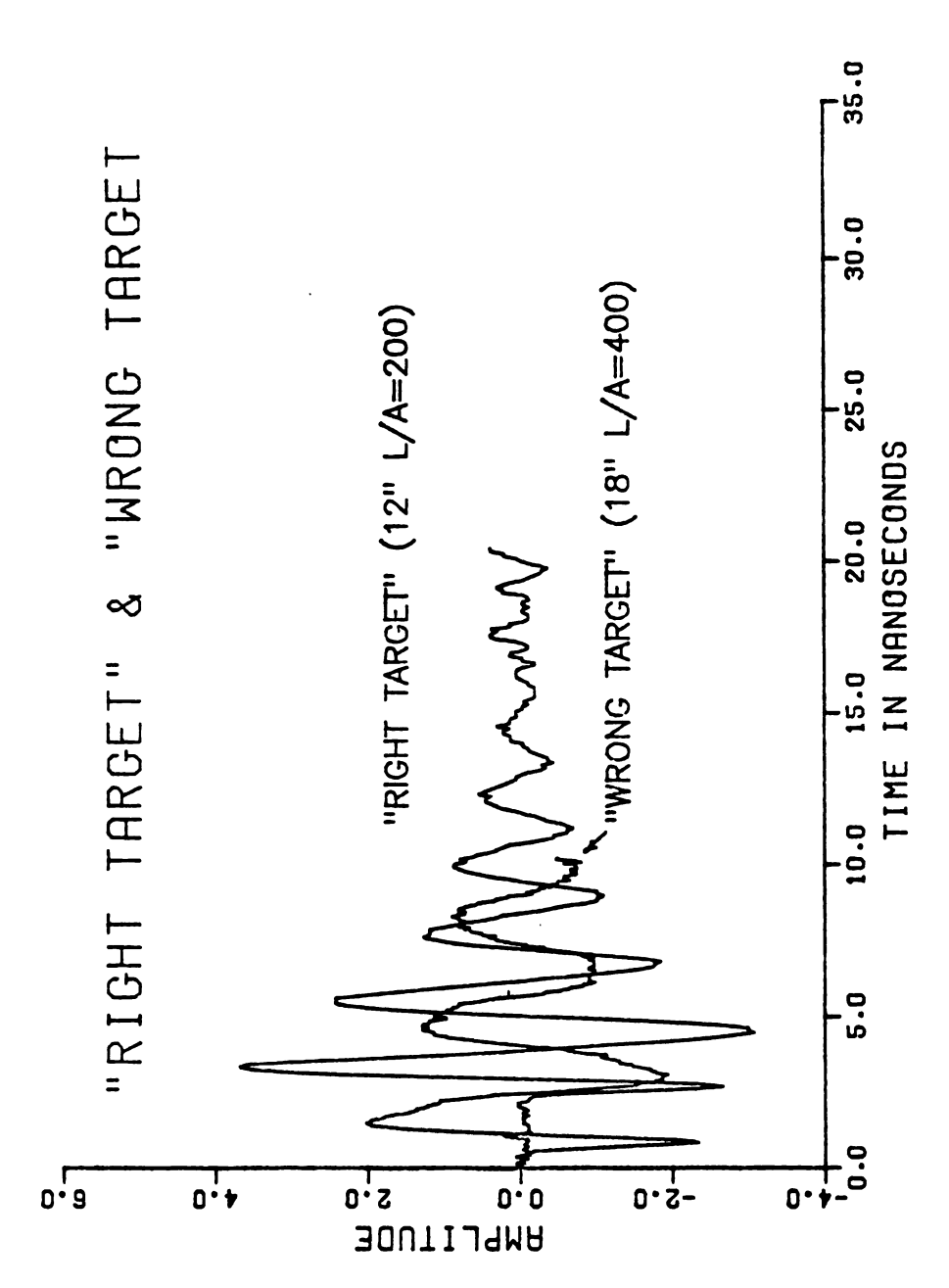


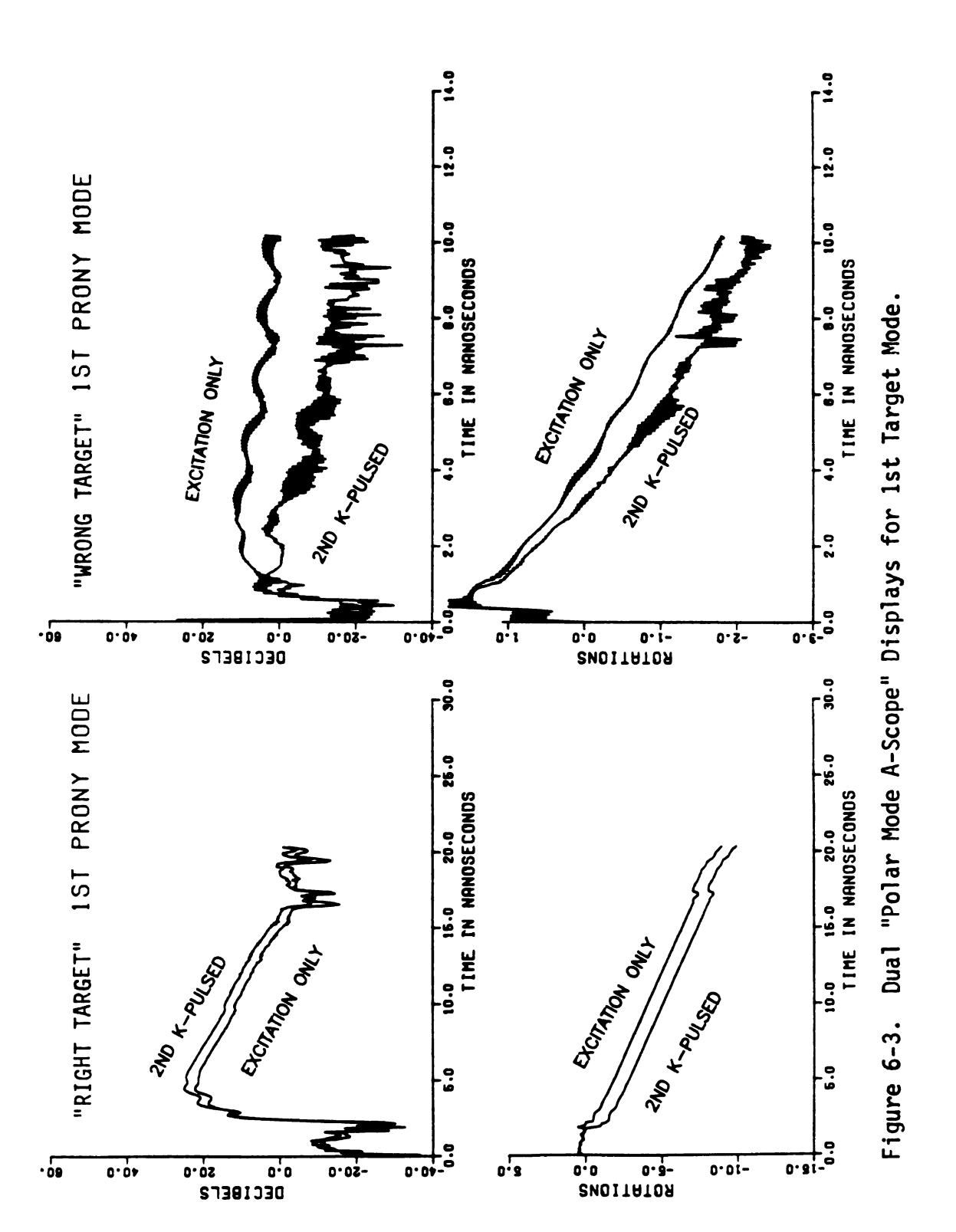
Figure 6-2. "Unknown Target" Sampled Data Files.

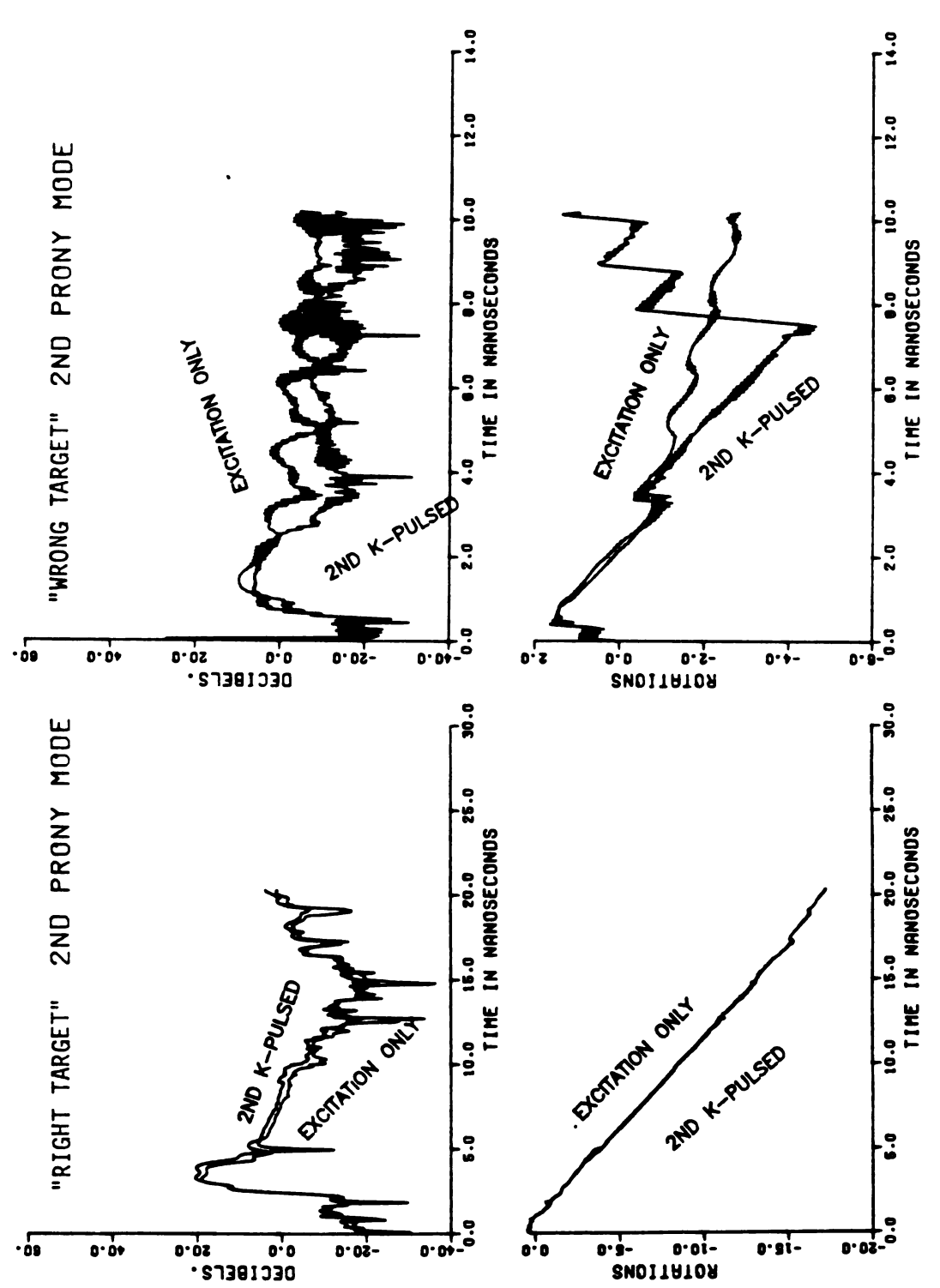
conducting ground plane. The "wrong target" whose target library is not used, is a normal incidence 9" wire (18" imaged with L/a = 400).

Performing the Radar Target Discrimination Algorithm of Figure 6-1 and Table 6-1, we obtained the dual "polar mode A-scope" displays for each target for the first three modes of the "right target." These are displayed in Figures 6-2, 6-3, and 6-4. In each case the "right target" A-scope displays are on the left and the "wrong target" A-scope displays are on the right.

Ideally, a "right target" file with different noise samples should be used in this illustration so that the dual traces of the A-scope displays will not perfectly align. The independent supplier of the data was unable to comply with the request. The next best method was to use a slightly defective 1st (or target) K-Pulse. Note that this part of the technique is performed in the original radar/target calibration and is independent of the real-time target discrimination algorithm. In this case the target K-Pulse was synthesized using the extended (least-squares) Prony's method. This means that there could not be a perfect noise suppression for any part of the data file. This is believed to be the reason that the "2nd K-Pulsed" file in Figure 6-2 shows a 2.6 dB processing gain over the normalizing file in the envelope display.

In both the 1st and 2nd mode displays, the termal noise in the original data does not obscure our discrimination process because we are looking for differences between the dual traces. The differences are alight for the "right target" but quite large for the "wrong target." In the "wrong target" envelope displays there are extended



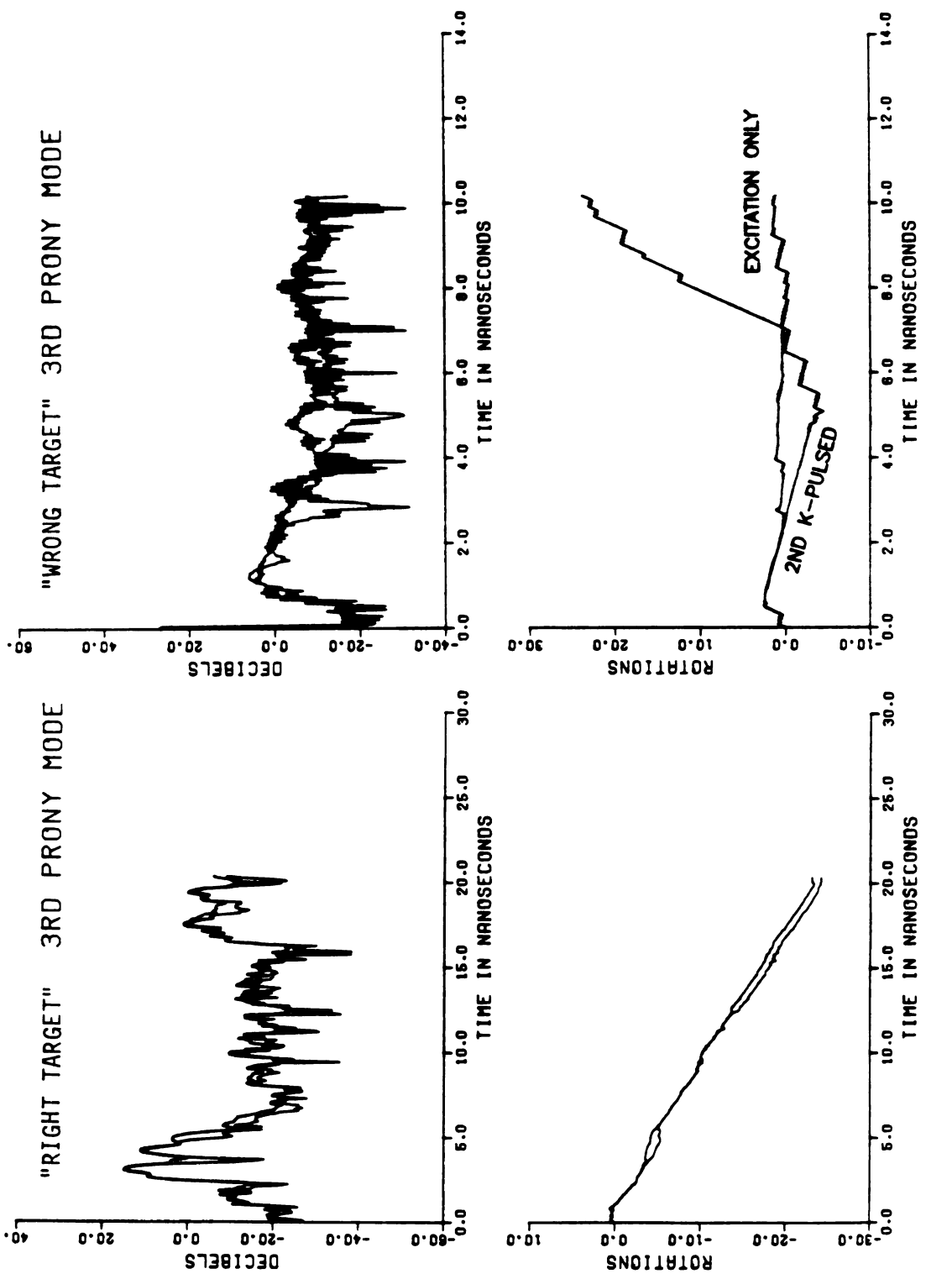


Dual "Polar Mode A-Scope" Displays for 2nd Target Mode. Figure 6-4.

time intervals for which the "2nd K-Pulsed convolution" is 15 dB below the normalizing trace.

In the 3rd mode display of Figure 6-5, the differences are still visible for the "wrong target." For the "right target" it is known that the 3rd mode is at best 11 dB lower in level from the 1st mode. Discrimination in the presence of more noise would likely be difficult for this mode.

This plots illustrate how the radar designer would establish thresholds for Part D of the algorithm for automatic discrimination.



Dual "Polar Mode A-Scope" Displays for 3rd Target Mode. Figure 6-5.

CHAPTER 7

CONCLUSIONS

In Chapters 2 through 5, we developed the analytical tools of the "fast Prony's method algorithm," the "Prony K-Pulse," the "polar mode A-scope," and the "mode discrimination ratio detectors." In the last chapter, using only these basic analytical tools, we developed a radar target discrimination algorithm which worked very well on empirical data from a strong clutter background without Doppler shift exploitation.

Different radar operating modes and environments will require more elaborate radar target discrimination algorithms. To fully exploit these radar target discrimination principles, faster digital logic is advisable. When devices are available which even approach the speed and power of the 100 GHz controllable binary counter of reference 7-1, it is confidently believed that the forecast of the cartoon of Figure 7-1 will become reality.

Original contributions of this dissertation in addition to the primary objective of developing a range and aspect-angle independent radar target discrimination technique potentially compatible with "quiet" radar, are four original analytical tools developed solely for this purpose:

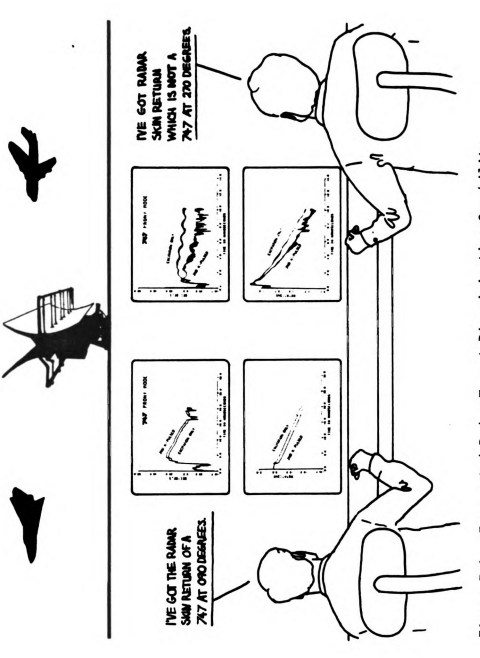


Figure 7-1. Forecasted Radar Target Discrimination Capability.

- "Fast Prony's method algorithm" for real-time invariant parameter calculation of 4-dimensional radar data.
- "Prony K-Pulse" for calculating SEM coupling coefficients from retarded scattered E-field sampled data.
- 3. "Polar mode A-scope" display file processing replacing part of the conventional radar targetindependent matched filter.
- 4. "Mode ratio discrimination detectors" for automatic radar target trigger and identification channels.

APPENDICES

APPENDIX A

LAPLACE TRANSFORMS AND Z-TRANSFORMS FOR PRONY
SERIES

APPENDIX A

LAPLACE TRANSFORMS AND Z-TRANSFORMS FOR PRONY SERIES

A-1 Introduction and Notation

We shall make frequent use of the Laplace transform pairs of electromagnetic quantities which we will consider in this dissertation to have Laplace transforms and inverse transforms for some appropriately defined region of convergence. In addition, for the purpose of the ordinary z-transform only, we must temporarily impose continuity on the time function of the electromagnetic quantity. This is because the integral transforms we shall use, essentially ignore removable points of discontinuity, but these same removable points of discontinuity will drastically effect the ordinary z-transform if they are, in fact, in the sampled data points. This additional requirement of time domain continuity is not required for the modified z-transform unless it is to be compared to the z-transform of a specific discrete sampled data sequence. All electromagnetic quantities shall be presumed to satisfy these requirements and will be denoted in this chapter by the letter v. We will employ the following consistent convention for physical quantities and functions:

- v(t) the time function (in lower case)
- V(s) the Laplace transform (in upper case)
- $\hat{V}(z)$ the z-transform (in upper case)
- V(z,m) the modified z-transform (in upper case)

A-2 Ordinary z-Transform and Laplace Transform

The Laplace transform pairs for time waveform of a continuous causal electromagnetic quantity, v(t), which we shall hereafter assume possesses a Laplace transform given by equation (A-1). The constant a is called the abscissa of absolute convergence of the transform and is determined by the values of s for which the integral converges absolutely. Equation (A-2) is the inversion formula for the inverse Laplace transform.

$$L[v(t)] = \hat{V}(s) = \int_0^\infty v(t) \exp(-st) dt, \quad Re(s) > a \quad (A-1)$$

$$L^{-1}[V(s)] = v(t) = \int_{c-j\infty}^{c+j\infty} \hat{V}(s) \frac{ds}{2\pi j}, c>a, t>0$$
 (A-2)

Figure A-1 is a diagram of a typical continuous transient waveform (v(t) as a function of time. Also indicated in this figure are the discrete sample values v(0T), v(1T), . . . , v(5T). These discrete values are given exactly by equation (A-3)

$$v(nT) - v(t)|_{t-nT}$$
 for $n = 0, 1, ...$ (A-3)

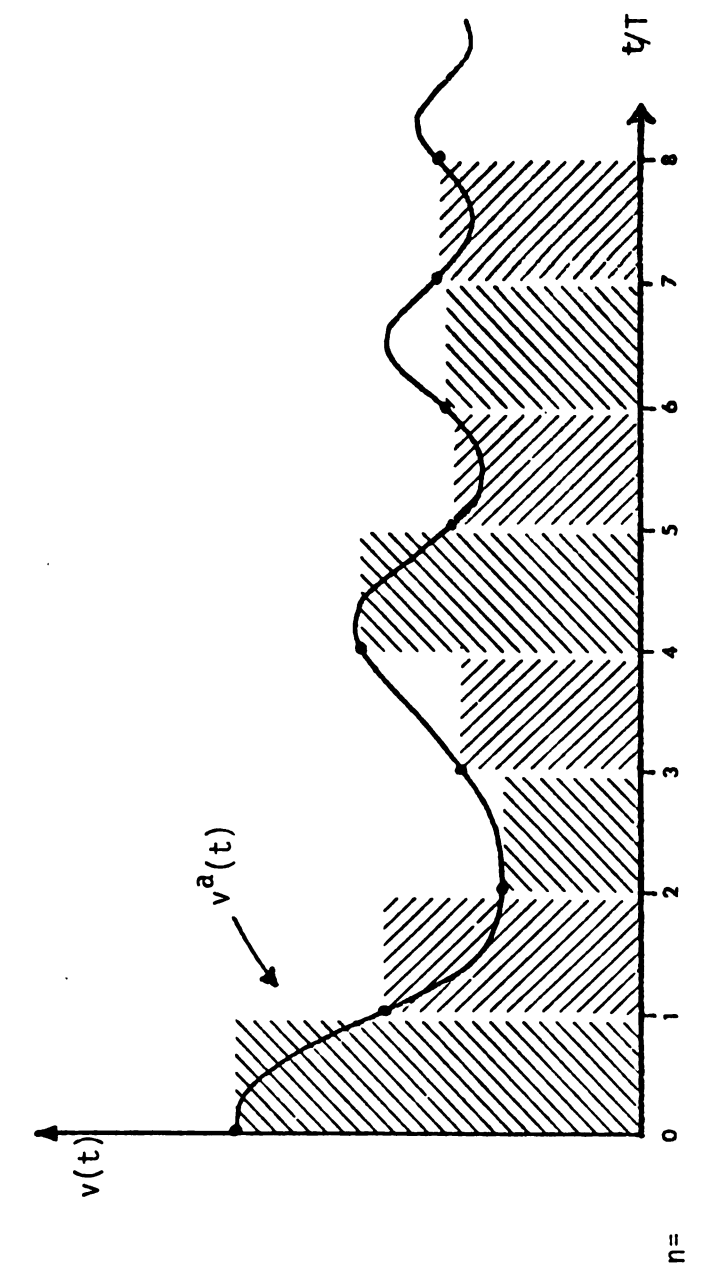


Figure A-1. Approximating Function from Sampled Data.

Next it can be seen that v(t) can be approximated as a function of all time values by a step function of the discrete samples of equation (A-3) by $v^a(t)$ given in equation (A-1).

$$v^{a}(t) = \sum_{n=0}^{\infty} v(nT) p_{T}(t-nT)$$
 (A-4)

 $\rho_{T}(t)$ is a rectangular pulse of area T given by equation (A-5)

$$p_{T}(t) = \begin{cases} 1, & 0 \le t < T \\ 0, & \text{otherwise} \end{cases}$$
 (A-5)

Note that the formula of equation (A-4) is exactly equal to v(t) for the discrete values of time t-nT, $n=0,1,1,\ldots v^a(t)$ may be a good approximation to v(t) for all values of continuous time, but this is not guaranteed. It will depend both on the sample spacing and on the smoothness of v(t) itself.

We now apply the Laplace transform to our step function approximation, $v^a(t)$, and obtain equation (A-6).

$$L[v^{a}(t)] = L\begin{bmatrix} \sum_{n=0}^{\infty} v(nT)p_{T}(t-nT) \end{bmatrix} = \sum_{n=0}^{\infty} v(nT) L[p_{T}(t-nT)]$$
 (A-6)

The Laplace transform of the pulse function $\rho_T(t)$ is given by equation (A-7) and its time shifted version by equation (A-8).

$$L[p_{T}(t)] = L[u_{-1}(t)-u_{-1}(t-T)] = [1-exp(-sT)]/s = \hat{P}_{T}(s)$$
 (A-7)

$$L[p_{T}(t-nT)] = L[p_{T}(t)] \exp((-sTn) = \hat{P}_{T}(s) \exp(-sTn)$$
 (A-8)

This gives equation (A-7) as the Laplace transform of our step function approximation, $v^a(t)$, to v(t).

$$L[v^{a}(t)] = \sum_{n=0}^{\infty} v(nT) \hat{P}_{T}(s) \exp(-sTn) = \hat{P}_{T}(s) \sum_{n=0}^{\infty} v(nT) \exp(-sTn) (A-9)$$

From equation (A-9) it can be seen that the Laplace transform of $v^a(t)$ has two distinct now separated characteristics. $\hat{P}_T(s)$ is related to the shape of the approximating pulse function of equation (A-5). The summation on the right of equation (A-9) is independent of this pulse and dependent on the sampling process.

We shall now rewrite equation (A-9) to emphasize these independent characteristics as in equation (A-10).

$$L[v^{a}(t)] = L[p_{T}(t)] L[v^{d}(t)]$$
 (A-10)

Let us now examine this new function $v^d(t)$ which appears in equation (A-10). It is independent of the pulse shape, $p_T(t)$, used in the synthesis process of approximating v(t). We can obtain a formula for $v^d(t)$ by taking the inverse Laplace transform, equation (A-2) of its transformed value in equation (A-9). This yields equation (A-11).

$$v^{d}(t) = L^{-1}[L[v^{d}(t)]] = L^{-1}[\sum_{n=0}^{\infty} v(nT)exp(-sTn)]$$
$$= \sum_{n=0}^{\infty} v(nT)\delta(t-nT)$$
(A-11)

Note that equation (A-11) is a sum of generalized functions (Dirac delta functions). This is no problem here since from equation (A-10)

it can be seen that there will always be associated with $v^d(t)$ some realizable (but perhaps undesirable) pulse shape, $p_T(t)$, which it is multiplied by in the Laplace domain or convolved in the time domain.

Now we are ready to define the ordinary z-transform of v(t). We will be guaranteed its existence since we are deriving it solely from the Laplace transform, $\hat{V}(s)$, which exists by hypothesis. We define the z-transform of v(t) by equation (A-12), where $v^d(t)$ is given by equation (A-11).

$$V(z) = z[v(t)] = L[v^{d}(t)]|_{s=T^{-1}ln(z)} = \sum_{n=0}^{\infty} v(nT) z^{-n}$$
 (A-12)

for $Re(s=T^{-1}ln(z)) > a$

Rewriting equation (A-12), we obtain an often-used equation (A-13).

$$V(z) = \sum_{n=0}^{\infty} v(nT) z^{-n}, \quad Re(z) > exp(aT)$$
 (A-13)

So we are now capable of computing the z-transform either from the complete sampled data values of v(t) and the region of convergence or from the Laplace transform $L[v^d(t)]$.

Next we wish to obtain an inversion formula for equation (A-12). That is, recover L(v(t)), and therefore v(t), solely from V(z). This inversion cannot be exact for the nonsampled data points of v(t). As a useful intermediary step, we shall first invert equation (A-13). That is, obtain sample data points $[v(nT)]_{n=0}^{\infty}$ from V(z). Note that we can easily obtain the second sampled data value

(n=1) by the use of Cauchy's integral formula on the Laurent series, V(z), as in equation (A-14).

$$v(1T) = \frac{1}{2\pi j} \oint_{|z| = r > exp(aT)} V(z)dz$$
 (A-14)

The circular contour of equation (A-14) is in the region of convergence of V(z) and encloses only one simple pole of V(z) of the sampled data z-transform representation. In general the n-th sampled data point can be obtained by applying the Cauchy integral formula to the function $V(z)z^{n-1}$ as in equation (A-15).

$$v(nT) = \frac{1}{2^r j} \int_{|z| = r > exp(aT)} V(z) z^{n-1} dz$$
(A-15)

Equation (A-15) consitutes an inversion formula for recovery of the time domain sampled data values from the z-transform, V(z). There is another useful form of equation (A-15). By substituting equation (A-16) into (A-15), we obtain equation (A-17).

$$z = \exp(sT) \tag{A-16}$$

$$v(nT) = \frac{1}{2\pi j} \oint_{z=-r}^{z=-r} V(z)z^{n-1}dz$$

$$= \frac{1}{2\pi j} \oint_{z=\exp(sT)=-r}^{z=\exp(sT)=r} V(\exp(st))(\exp(sT))^{n-1}d(\exp(sT))$$

$$= \frac{1}{2\pi j} \int_{sT=cT-j\pi}^{sT=cT+j\pi} V(\exp(sT))\exp(sTn)d(sT)$$
(A-17)

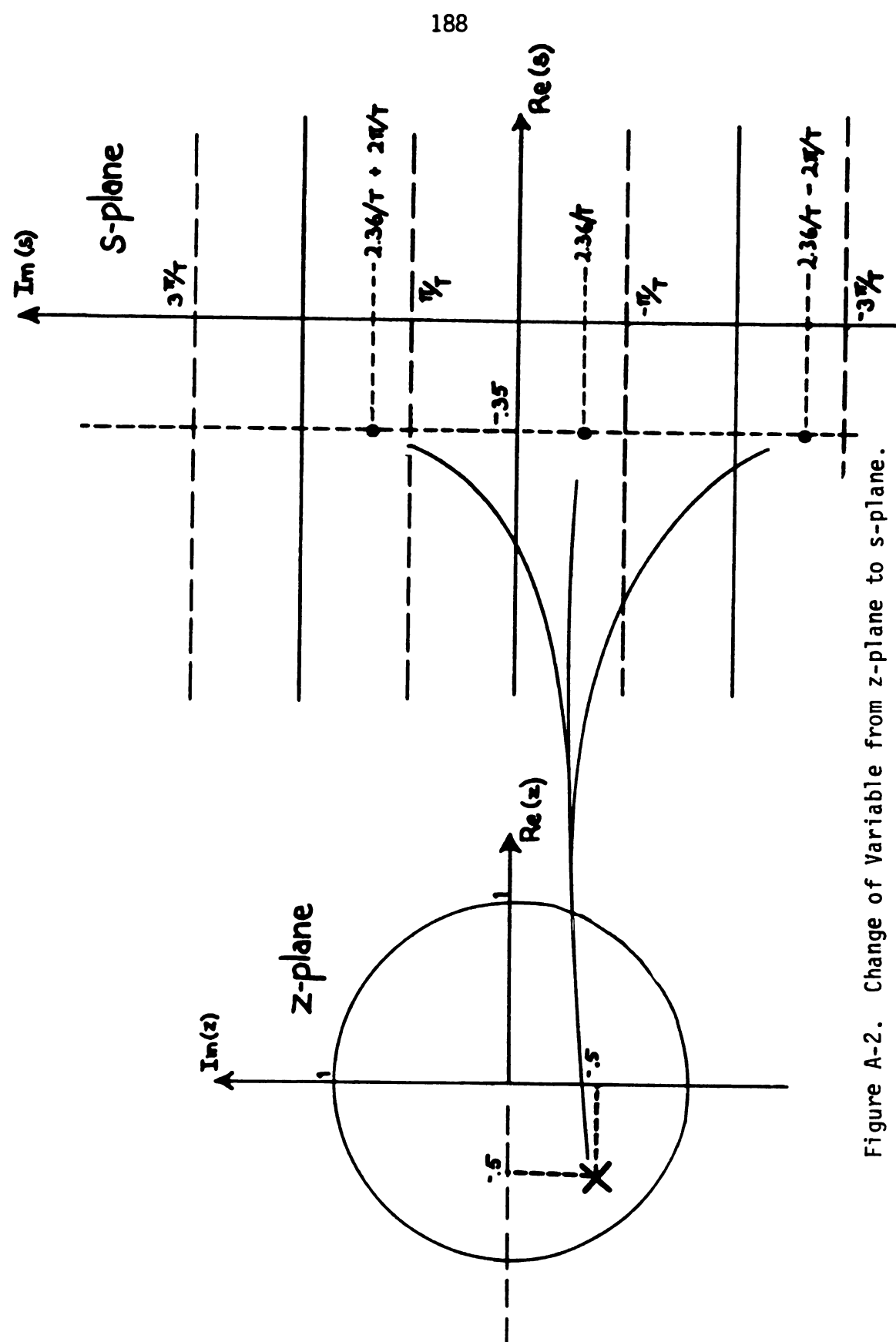
Performing the last substitution in equation (A-17), we obtain equation (A-18).

$$v(nT) = \frac{T}{2\pi j} \int_{c-j\pi/T}^{c+j\pi/T} V[exp(sT)] exp(sTn) ds \qquad (A-18)$$

Equation (A-18) constitutes an inversion formula for recovery of time domain sampled data values from the s-plane. Note that equation (A-18) only requires values of for V(z) for one circle in the z-plane. But one circle in the z-plane is an s-place strip which is of width $2\pi/T$ in the imaginary direction. Furthermore, because the argument of $V(\exp(sT))$ is periodic in s in the imaginary direction, any strip (parallel to the real axis) of width $2\pi/T$ can be used to close the circular contour in the region of convergence in the z-plane. As illustrated in Figure A-1, any of a number of strips in the s-plane can be used to obtain the values in the z-plane necessary to recover any of the original sampled data values $\left[v(nT)\right]_{n=0}^{\infty}$. Now to recover the original v(t) (nonuniquely), we note that equation (A-18) is, in fact, well defined for noninteger values of n. By substituting equation (A-19) into equation (A-18), we obtain a new function $v^{C}(t)$ given by equation (A-20).

$$t = nT (A-19)$$

$$v^{C}(t) = \frac{T}{2\pi j} \int_{C-j\pi/T}^{C+j\pi/T} V[\exp(sT)] \exp(st) ds \qquad (A-20)$$



The function $v^C(t)$ is equal to $v^a(t)$ and v(t) exactly only at the original discrete values of time. Taking the Laplace transform of $v^C(t)$, which was obtained from V(z), we have a Laplace transform $\hat{V}^C(s)$ which satisfies our requirements. Equation (A-21) gives the formula for calculating the Laplace transform of $v^C(t)$.

$$V(s) = \int_{0}^{\infty} v(t) \exp(-st) dt$$

$$= \int_{0}^{\infty} \left\{ \frac{T}{2\pi j} \int_{c-j\pi/T}^{c+j\pi/T} \{V(\exp(qT))\} \exp(qt) dq \} \exp(-st) dt \right\}$$

$$= \frac{T}{2\pi j} \int_{c-j\pi/T}^{c+j\pi/T} \left\{ V(\exp(qT)) \int_{0}^{\infty} \exp(-(s-q)t) dt \} dq \right\}$$

$$= \frac{T}{2\pi j} \int_{c-j\pi/T}^{c+j\pi/T} \frac{V(\exp(qT))}{s-q} dq \qquad (A-21)$$

The notation we shall use for this nonunique inversion is given by equation (A-22).

$$V(s) = \frac{T}{2\pi j} \int_{\mathbf{c}-\mathbf{j}\pi/T}^{\mathbf{c}+\mathbf{j}\pi/T} \frac{V(\mathbf{e} \times \mathbf{p}(\mathbf{q}T))}{s-\mathbf{q}} d\mathbf{q}$$
 (A-22)

A-3 Modified z-transform and the Laplace Transform

Next we will derive a unique correspondence between the Laplace s-plane domain and the z-plane of the modified z-transform. Returning to Figure A-1, let us now assume that not only are the values of v(t) available at the discrete time values t = 0T, lt, 2T, . . ., but for t defined by equation (A-23).

$$t = (n-1+m)T$$
, $n = 0, 1, 2, ... 0 \le m < 1$ (A-23)

Hence v(t) is available for all values of t as in equation (A-24), but may be accessed in the noncontinuous manner of the standard z-transform.

$$v(t) = v(n-1 + m)T$$
 (A-24)

We will again synthesize an approximating step function $v^a(t,m)$ defined by equation (A-25).

$$v^{a}(t,m) = v((n-1_{m})T) p_{T}(t-nt-\sum_{n=0}^{\infty} (v(t-T+mT)\delta(t-nT))$$

$$*p_{T}(t) \qquad (A-25)$$

Carefully note, if m is defined by equation (A-23), then we have the special case of equation (A-26).

$$v^a(t,m) = v(t=nT-T+mT)$$
 for all t (A-26)

Next let us try a different relation m = 1. We now have equation (A-27).

$$v^{a}(t,m=1) = \sum_{n=0}^{\infty} v((n-1+1)T) p_{T}(t-nT) = v^{a}(t)$$
 (A-27)

We now have a more general approximating step function, $v^a(t,m)$, defined by equation (A-25). In this form, we can see the effect of choosing different values of fixed m. Figure A-3 is a picture of what we are doing for m = 1/2. Note that the location of the sampled values has changed and hence the shape of the step function

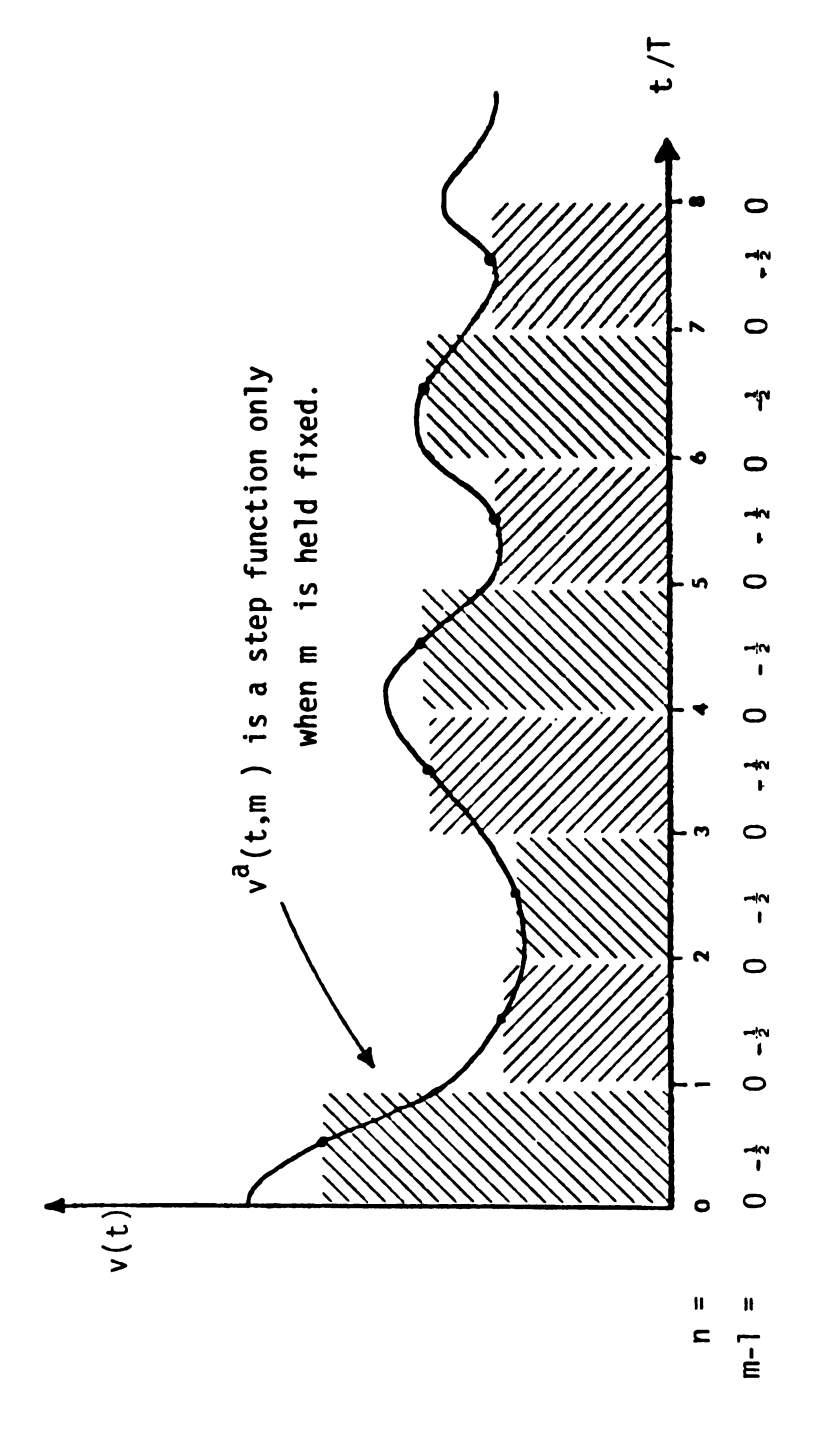


Figure A-3. Approximating Function for Fixed m.

approximation, $v^a(t,m)$. Now the approximation is exact at a different set of waveform values, v(-T/2), v(T/2), . . . , v((n-1/2)T), Next we will take the Laplace transform of $v^a(t,m)$ using equation (A-25) with arbitrary m-dependence to obtain equation (A-28)

$$L[v^{a}(t,m)] = \exp(-sT) \sum_{n=0}^{\infty} L[v(t+mT) \delta(t-nT)] \hat{P}_{T}(s)$$
 (A-28)

Note that the -T in $v(\cdot)$ is a constant time shift which becomes an entire function in the Laplace domain, whereas the mT is still a variable and remains inside the operator. Also, the pulse shape, $P_T(t)$, has been represented as a time domain convolution with the time shifted δ -function so that in the Laplace domain, the $\hat{P}_T(s)$ can be factored out in equation (A-28). What remains within the last operator brackets of equation (A-28) is the product of two time functions. We will now use the convolution theorem of the Laplace transform which is given by equation (A-29). (See Appendix B.)

$$L[f(t)g(t)] = \frac{1}{2\pi j} \int_{c-j\infty}^{c+j\infty} \hat{F}(p) \hat{G}(s-p) dp \qquad (A-29)$$

where $\hat{F}(s) = L[f]$, $\hat{G}(s) = L[g]$, and c is the joint convergence region.

The Laplace transforms for each of the remaining time functions in equation (A-28) are given by equations (A-30) and (A-31).

$$L[v(t+mT)] = \hat{V}(s) \exp(msT)$$
 (A-30)

$$L[\delta(t-nT)] = \exp(-sTn)$$
 (A-31)

Substituting these equations into equation (A-28) and performing the summation of the one-sided power series of equation (A-31) terms, we obtain equation (A-32).

$$L[v^{a}(t,m)] = \exp(-sT)\frac{1}{2\pi j} \int_{c-j\infty}^{c+j\infty} \hat{V}(q)e^{Tqm} \frac{1}{1-\exp(-T(s-q))} dq \cdot \hat{P}_{T}(s) \quad (A-32)$$

As before, we will split $L[v^a(t)]$ into two parts. One of which is solely due to the pulse shape, $P_T(t)$, and the other is independent of the pulse shape. In doing so we define a new function $v^d(t,m)$ given by equation (A-33).

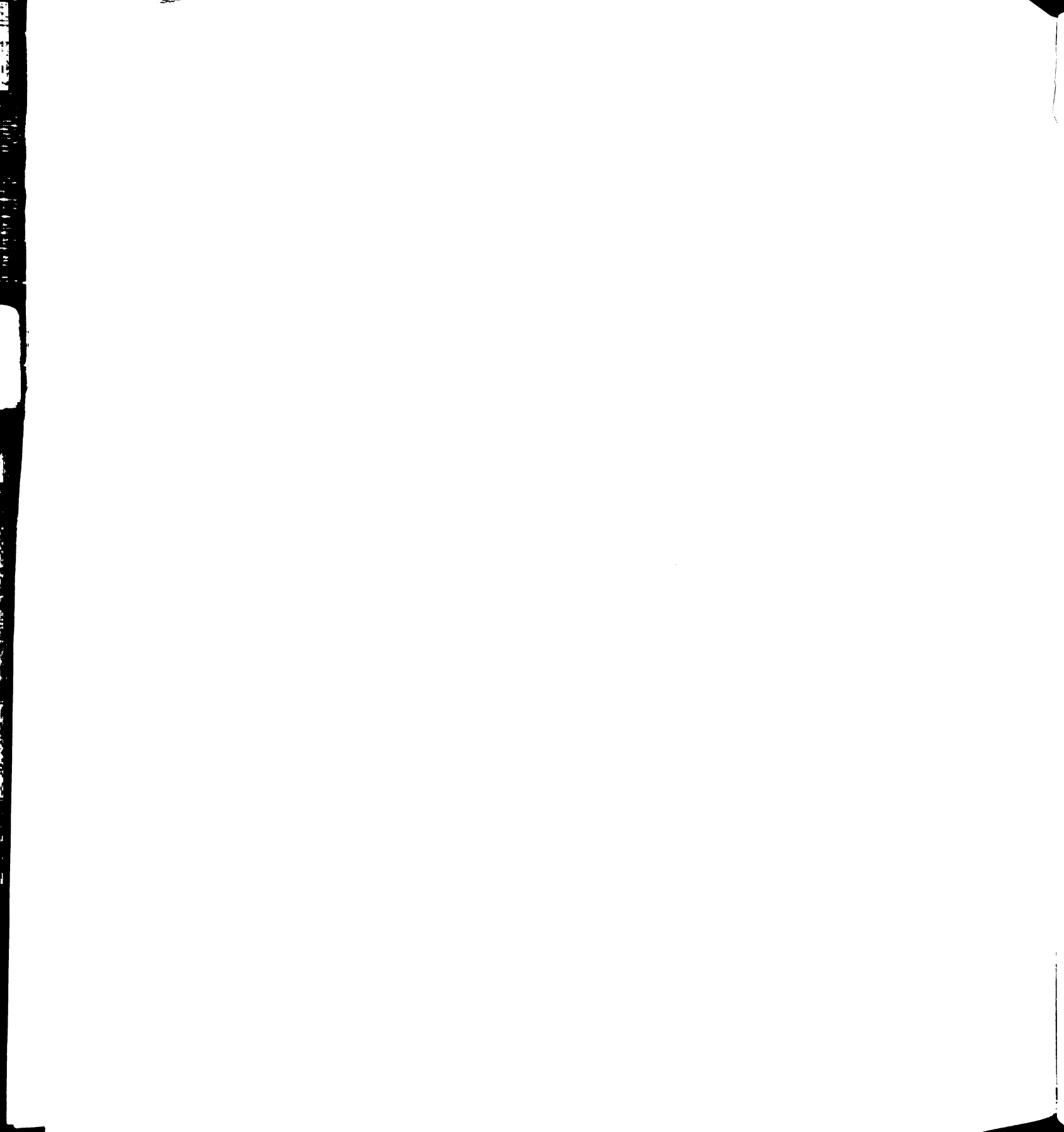
$$L[v^{a}(t,m)] = L[v^{d}(t,m)] L[p_{T}(t)]$$
 (A-33)

Note that if m = 1, then equation (A-33) becomes equation (A-9). The part of equation (A-33) which is independent of the pulse shape we shall define to be the modified z-transform of v(t). The modified z-transform of the original function v(t) will be defined by equation (A-34).

$$V(z,m) = Z_m[L[v(t)]] = L[v^d(t,m)]|_{s=T^{-1}ln(z)}$$
 (A-34)

The formula for computing the modified z-transform from the Laplace transform is given by equation (A-35).

$$Z_{m}[\hat{V}(s)] = \frac{1}{2\pi j} \exp(-sT) \int_{c-j\infty}^{c+j\infty} \hat{V}(q) \exp(Tqm) \frac{1}{1-\exp(-T(s-q))} dq \Big|_{s=T^{-1} \ln(z)}$$
(A-35)



Using the inverse Laplace transform of $L[v^d(t,m)]$, we could obtain $v^d(t,m)$ which when convolved with the pulse function, $p_T(t)$, satisfies equation (A-36).

$$v^{a}(t,m) - v^{d}(t,m) * p_{T}(t)$$
 (A-36)

Note that the synthesizing approximation function, $v^a(t,m)$ is the bridge of two purposes:

- v^a(t,m) is precisely equal to v(t=nT-T+mT) for all values of t, so that the transform relations between the Laplace transforms and the modified z-transforms are unique with extensive tables already in existence
- For a specific value of m, v^a(t,m) gives only discrete values of the original function, v(t), so that the correspondence with the ordinary z-transform can be found

The ordinary z-transform can always be found by equation (A-37) and sometimes by equation (A-38) from the modified z-transform.

$$V(z) = zV(z,m) \Big|_{m=0}$$
 always (A-37)

$$V(z) = V(z,m) \Big|_{m=1}$$
 if $v(t=0)=0$ (A-38)

The next step is to obtain the inverse transformation from Z_m to L, that is, from the modified z-transform to the Laplace transform. This is done by straight forward substitution into equation (1), to obtain equation (A-39).

$$\hat{V}(s) = \int_{0}^{\infty} v(t) \exp(-st) dt = \sum_{n=0}^{\infty} \int_{nT}^{(n+1)T} v(t) \exp(-st) dt$$

$$= \sum_{n=0}^{\infty} \int_{nT}^{(n+1)T} v(nT-T+mT) \exp(-s(n-1+m)T) d(t=nT-T+mT), 0 \le m \le 1$$

$$= \sum_{n=0}^{\infty} \exp(-s(n-1)T) \int_{0}^{1} v(nT-T+mT) \exp(-sTm) T dm$$

$$= T \int_{0}^{1} \exp(+sT(1-m)) \sum_{n=0}^{\infty} v(nT-T+mT) \exp(-sTn) dm$$

$$= T \int_{0}^{1} z^{1-m} \sum_{n=0}^{\infty} v(nT-T+mT) z^{-n} dm \Big|_{z=\exp(sT)}$$

$$= T \int_{0}^{1} z^{1-m} V(z,m) dm \Big|_{z=\exp(sT)}$$
(A-39)

A-4 Transforms of a Prony Series

we shall now use the preceding formalism to obtain the modified z-transform of a Prony series of natural mode waveforms given by equation (A-4).

$$v(t) = \sum_{i=1}^{N} A_i \exp(s_i t)$$
 , $t \ge 0$, $Re(s_i) < 0$ (A-40)

The Laplace transform of equation (A-40) is easily computed from Equation A-1 to be equation (A-41).

$$\hat{V}(s) = \sum_{i=1}^{N} A_{i}(s-s_{i})^{-1}$$
 (A-41)

Substituting equation (A-41) into the formula for the modified z-transform, equation (A-45), yield equation (A-42).

As a verification we will find the unique Laplace transform from this modified z-transform. Substituting equation (A-43) into the inversion formula (A-45), we obtain equation (A-44).

$$\hat{V}(s) = T \int_{0}^{1} z^{1-m} V(z,m) dm \Big|_{z=exp(sT)}$$

$$= T \int_{0}^{1} z^{1-m} z^{-1} \sum_{i=1}^{N} A_{i} \frac{z_{i}^{m}}{1-z_{i}/z} dm = T \sum_{i=1}^{N} \frac{A_{i}}{1-z_{i}/z} \int_{0}^{1} z_{i}^{m} z^{-m} dm$$

$$= T \sum_{i=1}^{N} \frac{A_{i}}{1-z_{i}/z} \int_{0}^{1} exp(m \ln(z_{i}z^{-1})) dm$$

$$= T \sum_{i=1}^{N} \frac{A_{i}}{1-z_{i}/z} \frac{exp(\ln(z_{i}z^{-1})) - 1}{\ln(z_{i}z^{-1})} = T \sum_{i=1}^{N} \frac{A_{i}}{1-z_{i}/z} \frac{z_{i}/z - 1}{\ln(z_{i}) - \ln(z)}$$

$$= T \sum_{i=1}^{N} \frac{-A_{i}}{s_{i}T-sT} = \sum_{i=1}^{N} \frac{A_{i}}{s-s_{i}}$$
(A-44)

This is the correct answer.

We may also obtain the ordinary z-transform of v(t) by substituting equation (A-40) into the formula (A-37) for the ordinary z-transform yielding equation (A-45).

$$V(a) = zV(z,m)\Big|_{m=0} = \sum_{i=1}^{N} A_i (1-z_i/z)^{-1}$$
 (A-45)

This, of course, is an expected result.

$$V(z,m) = \frac{1}{2\pi j} z^{-1} \int_{c-j\infty}^{c+j\infty} \hat{V}(p) \frac{\exp(pTm)}{1-\exp(-(s-p)T)} dp \Big|_{s=T^{-1} \ln(z)} (A-42)$$

If the poles of $\hat{V}(s)$ are distinct, the Cauchy formula is a particular easy method of evaluating equation (A-42). Figure A-4 is a diagram of the finite singularities of the integrand of equation (A-42). By assumptions in equation (A-40) all poles of $\hat{V}(p)$ lie in the left hand plane. The value of c is chosen to pass through an analytical strip of the integrand and in this case leave the poles of the sampling function on the right hand side of the Bromwitch countour set by c. First we will evaluate by using a contour closed on the left as shown in Figure A-4. In this case we will need to evaluate the integrand at the N poles of V(s) which are enclosed by this contour. Using the Cauchy residue formula, we obtain equation (a-43). By closing the contour to the left, the entire function $\exp(mpT)$, remains bounded even at infinity. This was the logic of introducing (1-m)T rather than mT originally.

$$V(z,m) = z^{-1} \sum_{p_{i}} Residue \frac{\hat{V}(p)exp(pTm)}{1-exp(pT)exp(-sT)}$$

$$= z^{-1} \sum_{p_{i}} limit (p-p_{i}) \frac{\hat{V}(p)exp(pTm)}{1-exp(pT)exp(-sT)}$$

$$= z^{-1} \sum_{i=1}^{N} A_{i} \frac{z_{i}^{m}}{1-z_{i}z} - 1 \qquad , 0 < m < 1$$

$$z_{i} = exp(p_{i}T) \qquad (A-43)$$

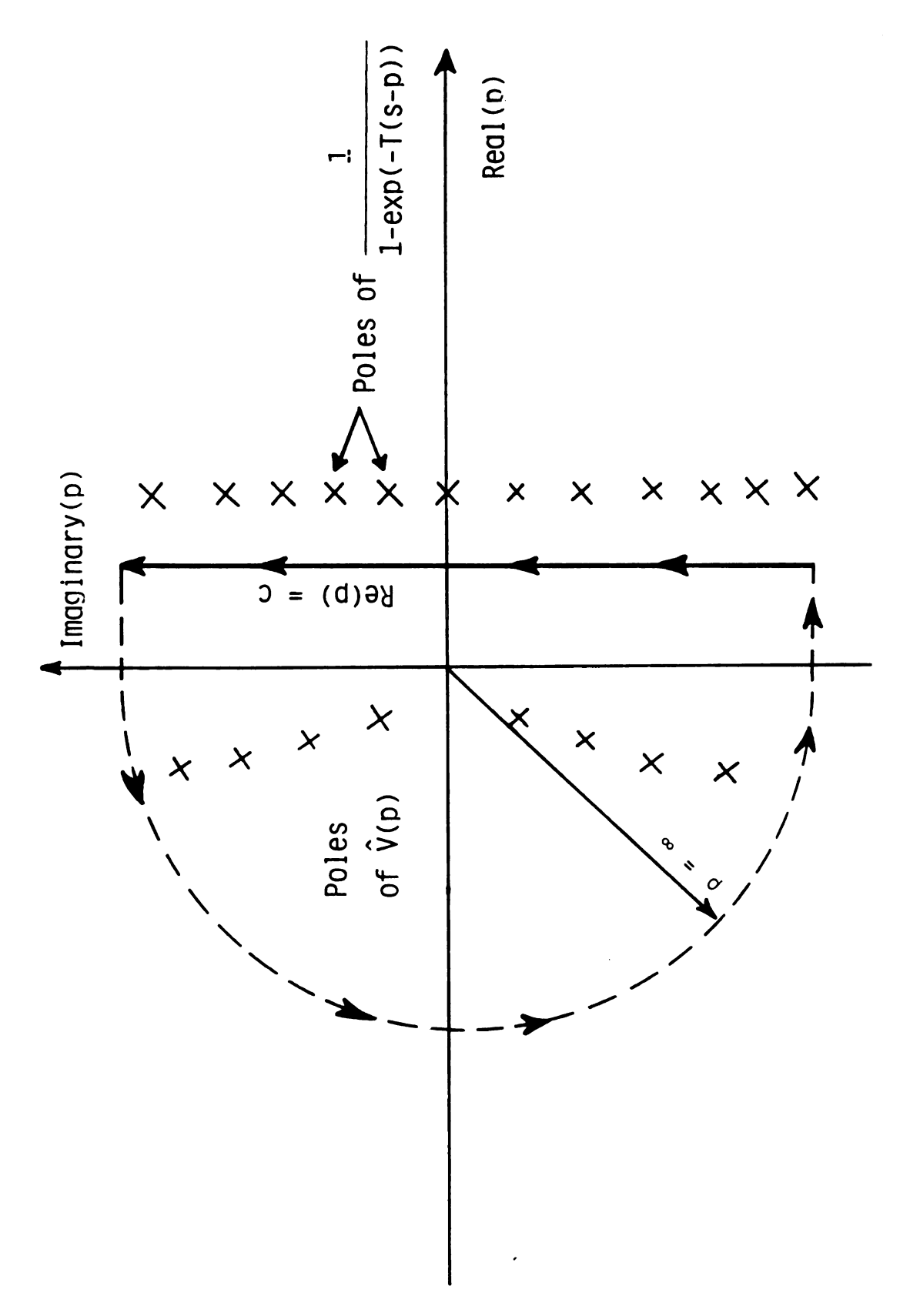


Figure A-4. Contour Integration for V(z,m).

APPENDIX B

LAPLACE TRANSFORM CONVOLUTION THEOREM FOR THE SAMPLER

APPENDIX B

LAPLACE TRANSFORM CONVOLUTION THEOREM FOR THE SAMPLER

Here we wish to derive equation (B-1) with the appropriate region of absolute convergence.

$$L[v(t)g(t)] = \frac{1}{2\pi j} \int_{C-j\infty}^{C+j\infty} \hat{V}(p)\hat{G}(s-p)dp$$
 (B-1)

For our purpose we shall assume v(t) is strictly causal or satisfies equation (B-2) but that g(t) is not necessarily causal. This will give us a derivation adaptable for either the unilateral Laplace transform or the bilateral Laplace transform.

$$v(t) = \begin{cases} v(t), & t > 0 \\ 0, & t \leq 0 \end{cases}$$
 (B-2)

Suppose the Laplace transform pairs of v(t) are given by equations (B-3) and (B-4) where a_1 is the axis of absolute convergence. For this strictly causal function, the region of absolute convergence is the open half plane to the right of the axis of absolute convergence.

$$L[v(t)] = V(s) = \int_{-\infty}^{\infty} v(t) \exp(-st) dt, \quad Re(s) > a_1$$
 (B-3)

$$L^{-1}[\hat{V}(s)] = v(t) = \int_{c_1 - j\infty}^{c_1 + j\infty} \hat{V}(s) \exp(st) \frac{ds}{2\pi j}, c_1 > a_1, t > 0,$$
 (B-4)

Note that we have used the bilateral Laplace transform limits in equation (B-3). However, since v(t) is strictly causal, we could obtain V(s) from the unilateral Laplace transform tables without modification.

Next, the Laplace transform pairs of the double-sided function of time, g(t), are given by equations (B-5) and (B-6), where b_2 and a_2 are the limits of absolute convergence of (B-5).

$$L(g(t)) = \hat{G}(s) = \int_{-\infty}^{\infty} g(t) \exp(-st) dt, \quad a_2 < Re(s) < b_2$$
 (B-5)

$$L^{-1}(\hat{G}(s)) = g(t) = \frac{1}{2\pi j} \int_{c_2 - j^{\infty}}^{c_2 + j^{\infty}} G(s) \exp(st) ds, \ a_2 < c_2 < b_2$$
 (B-6)

Substituting (B-3) into the bilateral Laplace transform formula for the product, v(t)g(t), we obtain equation (B-7).

$$L(v(t)g(t)) = \int_{-\infty}^{\infty} v(t)g(t)exp(-st)dt$$

$$= \int_{-\infty}^{\infty} \left\{ \frac{1}{2\pi j} \int_{c_1 - j\infty}^{c_1 + j\infty} \hat{v}(q)exp(qt) \right\} g(t)exp(-st)dt, c_1 > a_1 \text{ for } v(t)$$

$$= \frac{1}{2\pi j} \int_{c_1 - j\infty}^{c_1 + j\infty} \left\{ \hat{v}(q) \int_{-\infty}^{\infty} g(t)exp(-(s-q)t)dt \right\} dq,$$

$$Re(q) > a_1 \text{ for } \hat{v}(p) \qquad (B-7)$$

So far we clearly have restrictions (B-8) and (B-9) due solely to v(t) and V(q).

$$a_1 < c_1$$
 for absolute convergence of $L(v(t))$ (B-8)

 $Re(q) > a_1$ is the region of absolute convergence of

$$\hat{V}(q)$$
 (B-9)

Continuing, we obtain equation (B-10).

$$L(v(t)g(t)) = \frac{1}{2\pi j} \int_{c_1 - j\infty}^{c_1 + j\infty} \hat{V}(q) \hat{g}(s-q) dq, \quad a_2 < Re(s-q) < b_2$$
 (B-10)

Note that we have picked up another restriction (B-11) due to the region of absolute convergence of G(s-q).

$$a_2 + Re(q) < Re(s) < b_2 + Re(q)$$
 (B-11)

Combining the restrictions (A-9) and (A-11), we obtain equation (B-12).

$$a_1 + a_2 < Pe(q) + a_2 < ReIs)$$
 $b_2 + Re(q)$ (B-12)

Figure A-1 illustrates the region of absolute convergence of equation (B-12) and the remaining constraint (B-8). The final region of absolute convergence in the s-plane can be obtained from the cross-hatched region in the bottom of Figure B-1. In the p-plane the line Re(p) = c must be chosen in this region of absolute convergence (which depends on s). The minimum value of c is given by equation (B-8).

We shall now demonstrate the evaluation of the Laplace transform convolution theorem and its region of absolute convergence on typical electromagnetic quantitites. In these cases both functions are causal with proper choice of time origin. For the strictly causal v(t), we choose for evaluation a two complex mode Prony series as given by equation (B-13).

$$v(t) = \sum_{i=1}^{2} A_i \exp(s_i t), t > 0, Re(s_1) < a_1, Re(s_2) < a_1$$
 (B-13)

We choose for the second function one term of the sampling function used in Appendix A. This single term is given by equation (B-14).

$$g(t) = A_3 \exp(s_3 t), r \ge 0, Re(s_3) < a_2 = 0$$
 (B-14)

The required Laplace transforms are given in equations (B-15) and (B-16).

$$\hat{V}(p) = \sum_{i=1}^{2} A_i (p-s_i)^{-1}, Re(p) > a_1$$
 (B-15)

$$G(s-p) = A_3(s-p-s_3)^{-1}, Re(s-p) > a_2$$
 (B-16)

The desired transform of v(t)g(t) is given by equation (B-17) and its restrictions by equation (B-18).

$$L(v(t)g(t)) = \frac{1}{2\pi j} \int_{\mathbf{c}-j\infty}^{\mathbf{c}+j\infty} \hat{\mathbf{v}}(p) \hat{\mathbf{G}}(s-p) dp$$
 (B-17)

$$a_1 < c, a_1 + a_2 < Re(s)$$
 (B-18)

Note that in (B-18) the region of absolute convergence for s in (B-17) is given by the sum of the axes of absolute convergence for V(s) and G(s). Since only simple poles are involved, the evaluation is a simple Cauchy integral formula which must include a line in the region of absolute convergence as in Figure B-2. Using the closed contour, C_1 , in Figure B-2, equation (B-17) can be evaluated as in equation (B-19).

$$L(v(t)g(t)) = \frac{1}{2\pi j} \int_{C_1} \hat{v}(p)\hat{g}(s-p)dp = \text{Residues } \hat{v}(p)\hat{g}(s-p)$$

$$= \lim_{p \to s_1} t(p-s_1) \left(\frac{A_1}{p-s_1} + \frac{A_2}{p-s_2}\right) \frac{A_3}{s-p-s_3}$$

$$+ \lim_{p \to s_2} t(p-s_2) \left(\frac{A_1}{p-s_2} + \frac{A_2}{p-s_2}\right) \frac{A_3}{s-p-s_3}$$

$$= \frac{A_1A_3}{s-s_1-s_3} + \frac{A_2A_3}{s-s_2-s_3}$$
(B-19)

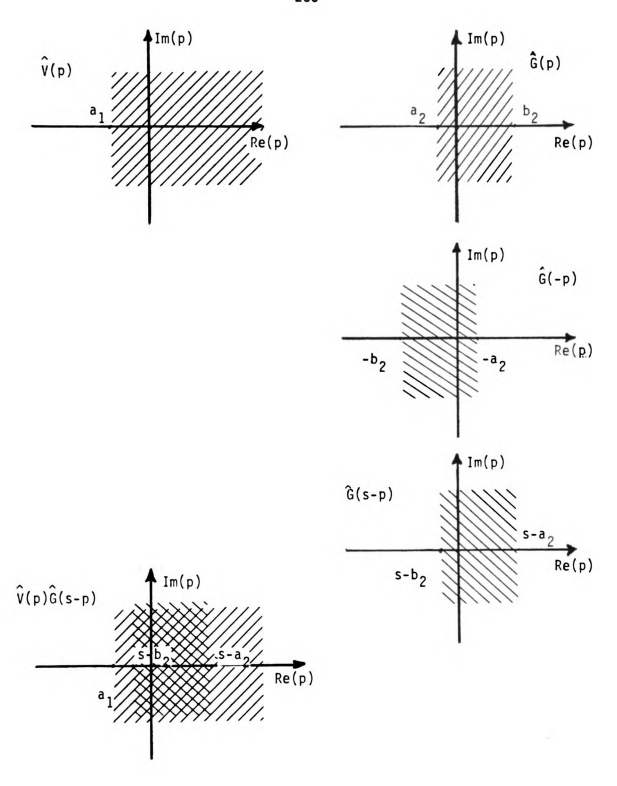


Figure B-1. Region of Absolute Convergence for a Product in Time Domain.

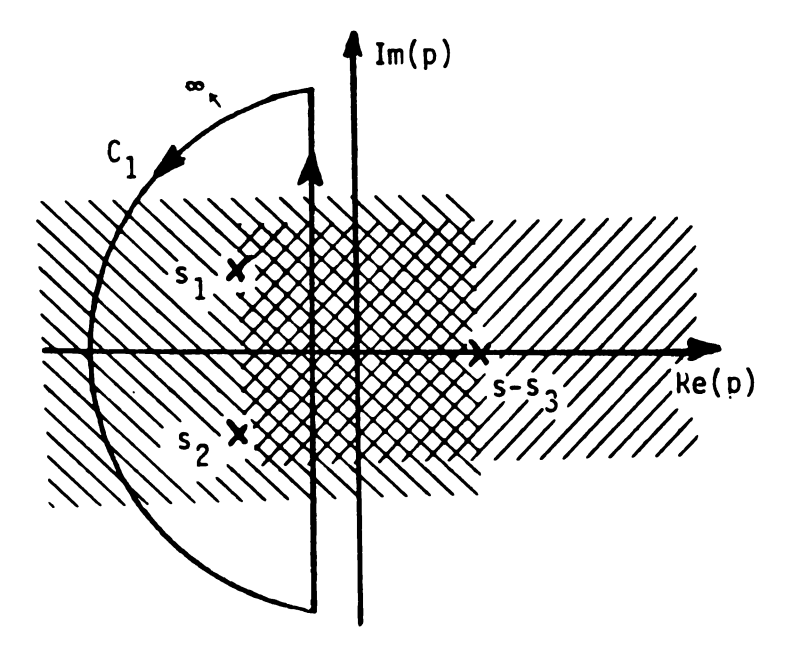


Figure B-2. Counterclockwise Contour Closure.

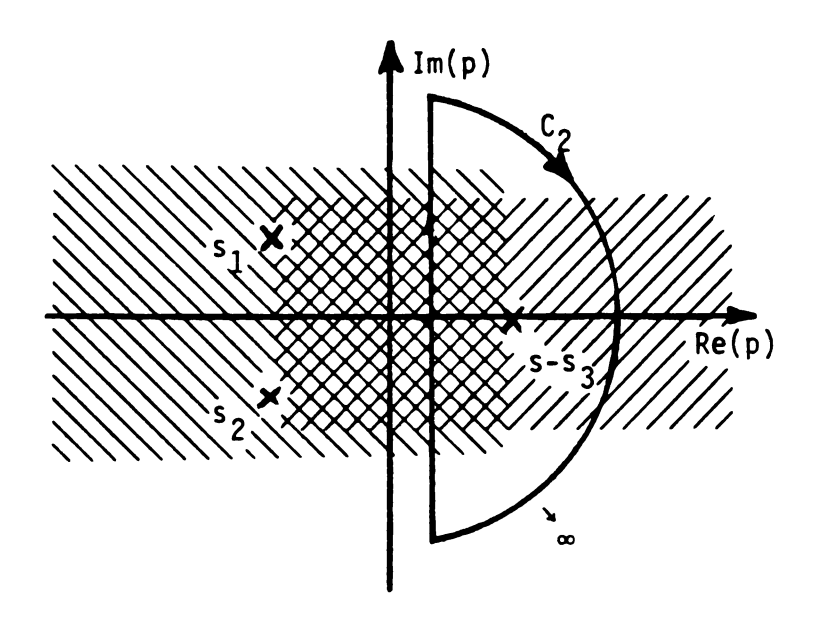


Figure B-3. Clockwise Contour Closure.

Contour C_1 is not the only contour which can be used to evaluate (B-17). Figure B-3, depicts contour C_2 which closes clockwise to the right. This contour which closes on the right hand side at infinity can be used in equation (B-20).

$$L(v(t)g(t)) = \frac{-1}{2\pi j} \oint_{C_2} \hat{V}(p)\hat{G}(s-p)dp = -Residue\hat{V}(p)\hat{G}(s-p)$$

$$= -\lim_{p \to s_3 + s} t(p-s-s_3) \left(\frac{A_1}{p-s_1} + \frac{A_2}{p-s_2}\right) \frac{A_3}{s-p-s_3}$$

$$= -\frac{A_1}{s-s_3-s_1} (-A_3) - \frac{A_2}{s-s_3-s_2} (-A_3)$$

$$= \frac{A_1A_3}{s-s_1-s_2} + \frac{A_2A_3}{s-s_2-s_3}$$
(B-20)

Hence both contours passing through the region of absolute convergence give the same answer.

APPENDIX C

COUPLETS AND THE K-PULSE SINGULARITY THEOREM

APPENDIX C

COUPLETS AND THE K-PULSE SINGULARITY THEOREM

C.1 Definition of Couplets and N-Plets for a Prony Series

Equation (C-1) is the definition of a "Prony series" which our link between a "class 1" SEM time domain solution of a transient electromagnetic boundary value problem and our radar target discrimination technique

$$v(t) = \begin{cases} \sum_{k=1}^{N} C_k \exp(s_k t), & t \ge 0 \\ k = 10, & \text{otherwise} \end{cases}$$
 (C-1)

First using the completely equivalent modified z-transform notation of Appendix A, we obtain equation (C-2).

$$v(t,m) = \begin{cases} \sum_{k=1}^{N} C_k \exp(s_k T n) \exp(s_k T (1-m)), & n \ge 0 \\ 0, & n < 0 \end{cases}$$
 (C-2)

where t = nT - T + mT

n is an integer

$$0 < m \leq 1$$

For sampled data, we shall constantly use a notation given by equation (C-3).

$$z_k = \exp(s_k T) \tag{C-3}$$

Hence equation (C-2) may be given by equation (C-4),

$$v(t,m) = \begin{cases} \sum_{k=1}^{N} c_k z_k^n z_k^{(1-m)}, & n \ge 0 \\ 0 & n < 0 \end{cases}$$
 (C-4)

Note that equation (C-4) is completely equivalent to equation (C-1). Sometimes we are able to successfully ignore the synchronization, m, of the waveform by sitting m = 1. In this case, the simplified notation of equation (C-5) results.

$$y_{n} = \begin{cases} \sum_{k=1}^{N} c_{k} z_{k}^{n}, & n \geq 0 \\ 0 & n < 0 \end{cases}$$
 (C-5)

Convolutions are the fundamental processing technique which we shall use. For a given finite length (or memory) processor a(t), we define the convolution output, c(t,m), as given by equation (C-6).

$$C(t,m) = \int_0^{NT} v(t-t', m) a(t')dt' \qquad (C-6)$$

When synchronization is not important, we obtain equation (C-7).

$$C_{n} = \sum_{i=0}^{N} \bigvee_{n-i} a_{i}$$
 (C-7)

There is a sampled data operator which is of extreme use to use. It is the identity operator with respect to convolution, $\delta_0(t)$ or δ_0 .

We will call it the unit impulse (or unit sample). It is defined by equation (C-8).

$$v_n * \delta_0 = v_n \tag{C-8}$$

We shall also introduce advances or delays by means of this unit impulse operator as given by equations (C-9) and (C-10).

$$v_n * \delta_1 = v_{n+1}$$
 (C-9)

$$v_n * \delta_{-1} = v_{n-1}$$
 (C-10)

The use of these unit impulse functions permits us to represent all values of v_n by a single summation as in equation (C-11).

$$v_{n} = \sum_{k=0}^{\infty} v_{k} \delta_{n-k}$$
 (C-11)

The next important concept we need is the convolutional inverse of v_n , which may or may not exist. We will denote it by v_n^{-1} and it is defined by equation (C-12) if it exists.

$$v_{n}^{-1} * v_{n} = v_{n} * v_{n}^{-1} = \delta_{0}$$
 (C-12)

If v_n is a single term "Prony series" for which we can represent all time values as equation (C-13), then the couplet, c_n , given by equation (C-14) is the convolution inverse.

$$v_n = \sum_{i=0}^{\infty} z_1^i \delta_{n-i}$$
 (C-13)

$$c_n = \delta_0 - z_1 \delta_1$$
 (C-14)

To verify the desired property, we convolve the two functions as in equation (C-15).

$$C_{n} *_{n} = \delta_{0} *_{n} - z_{1} \delta_{1} *_{n}$$

$$= \sum_{i=0}^{\infty} z_{1}^{i} \delta_{n-i} - \sum_{i=0}^{\infty} z_{i}^{i+1} \delta_{n-i+1}$$

$$= \sum_{i=0}^{\infty} z_{i}^{i} \delta_{n-i} - \sum_{i=1}^{\infty} z_{1}^{i} \delta_{n-i} = \delta_{0}$$
(C-15)

Before introducing new complexity, we shall illustrate with two examples. In Figure C-1 top we illustrate a natural frequency and sample spacing which satisfy equation (C-15).

$$\rho = z_1 = s_1 T = 0.75$$
 (C-16)

The couplet which is the convolutional inverse is illustrated immediately below. Similarly in Figure C-2 top we illustrate a natural frequency and sample spacing which satisfy equation (C-17).

$$\rho = z_1 = s_1 T = -0.75 \tag{C-17}$$

The couplet which is the convolutional inverse is illustrated immediately below. Although we cannot conveniently illustrate for a complex root, the same relationships hold.

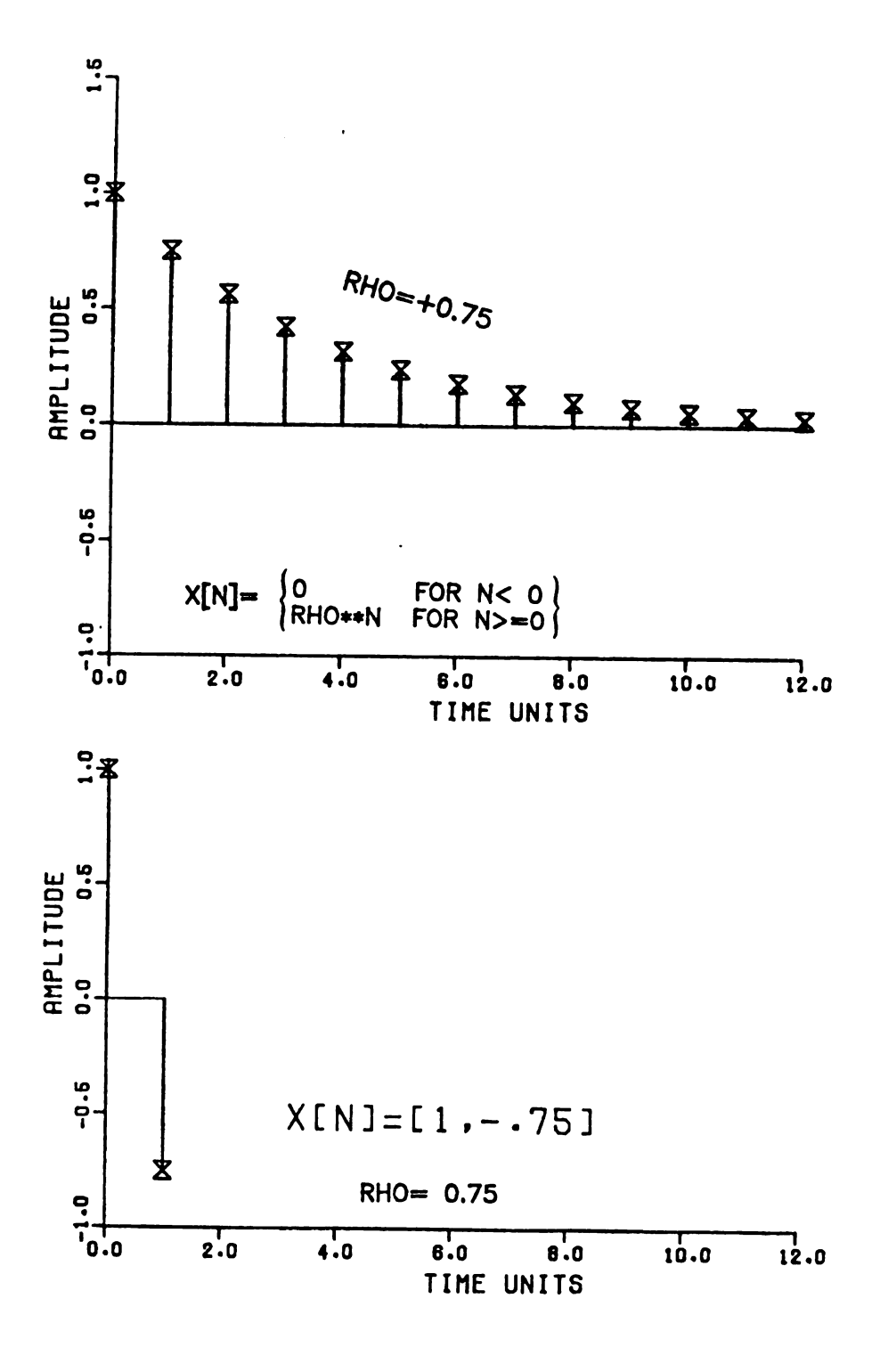


Figure C-1. Single Term "Prony Series," v(t).

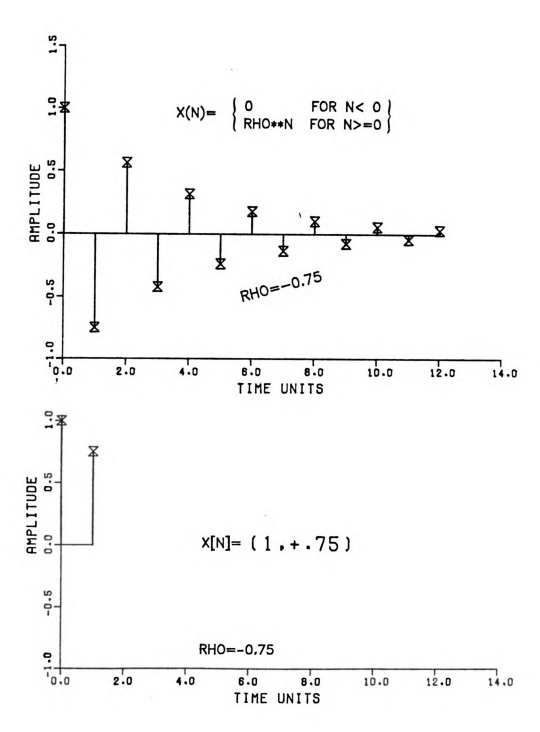


Figure C-2. Single Term "Prony series," w(t).

Next if v_n and w_n are each exponential waveforms and x_n is given by equation (C-18), then

$$x_{n} = v_{n} * w_{n}$$

$$= \sum_{i=0}^{\infty} z_{1}^{i} \delta_{n-i} * \sum_{k=0}^{\infty} z_{2}^{k} \delta_{n-k} \qquad (C-18)$$

The convolutional inverse is given by the triplet y_n defined by equation (C-19)

$$y_{n} = w_{n}^{-1} * v_{n}^{-1} = (\delta_{0} - z_{1}\delta_{1}) * (\delta_{0} - z_{2}\delta_{1})$$

$$= \delta_{0} - (z_{1} + z_{2}) \delta_{1} + z_{1}z_{2}\delta_{2}$$
 (C-19)

Note that observed these exact values in the two-mode Prony K-Pulse Worksheet of Figure 5-12. Hence, one interpretation of a Prony K-Pulse that it is a specific convolutional inverse of a waveform which is the convolution of elementary exponential waveforms.

One must also observe that if we have a waveform which is represented by a couplet such as equation (C-13) its convolutional inverse is given by the infinite term wavefunction given by equation (C-14). There is no finite length convolutional inverse for the couplet.

Now we illustrate a more complex case, the linear combination of two different exponential waveforms as given by equation (C-20).

$$s_n = av_n + bw_n \tag{C-20}$$

This waveform is illustrated in the top of Figure C-3. Not knowing the convolutional inverse of equation (C-19) by inspection, we shall formulate a triplet which resembles our "Prony K-Pulse" which is illustrated in the bottom of Figure C-3. This potential Prony K-Pulse is given by equation (C-21).

$$k_n = w_n^{-1} * v_n^{-1}$$
 (C-21)

We calculate the output of this convolution, c_n , as given by equation (C-22).

$$C_{n} = k_{n} * (av_{n} + bw_{n}) = (w_{n}^{-1} * v_{n}^{-1}) * (av_{n} + bw_{n})$$

$$= av_{n}^{-1} * v_{n}^{-1} * v_{n} + bw_{n}^{-1} * v_{n}^{-1} * w_{n}$$

$$= aw_{n}^{-1} + bv_{n}^{-1} * w_{n}^{-1} * w_{n} = av_{n}^{-1} + bv_{n}^{-1}$$
(C-22)

Note that equation (C-21) is a linear combination of two different couplets. Therefore, in general, c_n cannot be the convolutional identity and s_n cannot have a finite length convolutional inverse because of the arbitrary amplitudes a and b of the exponential waveform.

Generalizing these results to a "Prony series" of N terms, the potential "Prony K-Pulse" is an N-plot. An N-plot is just the N convolutions of the corresponding N couplets. In this case, the output of the potential "Prony K-Pulse" convolved with the "Prony

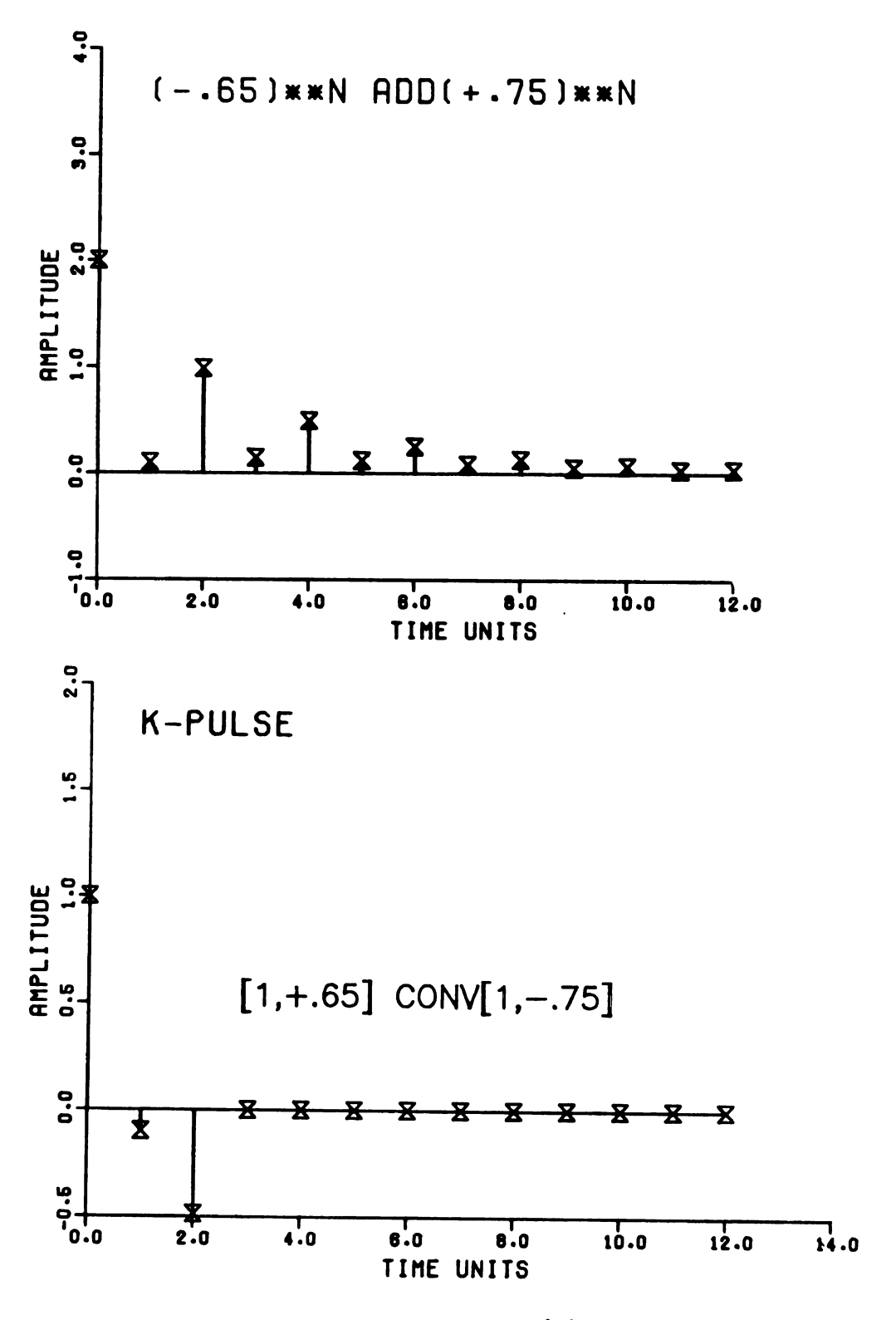


Figure C-3. Two Term "Prony Series," s(t).

series" is itself an (N-1)-plet (N nonzero sampled data values) containing the amplitude dependencies of the exponential waveforms.

Lastly, the "class 2 Prony series" given by equation (C-23)

$$V_n = w_n + \sum_{k=1}^{N} c_k z_k^n$$
 (C-23)

where $_{\rm n}$ is an N-1 length waveform whose transform is an entire function. From Chapter 5, we know that if we possess enough "complex root degrees of freedom," in our "Prony K-Pulse," we can recover both the $z_{\rm k}$'s and $c_{\rm k}$'s.

C-2 K-Pulse Singularity Theorem

In the derivation of the "fast Prony's method" algorithm of Chapter 5, we intentionally detected a flag A or singularity condition. For sampled data waveforms, this sometimes occurs sooner than we might expect from an observation of only the continuous time domain. This optional theorem will give insight into why this happens and also illustrate the use of couplets in analyzing sampled data problems.

First of all, we have observed that for an N term "Prony series" with known 2-way transit time, we can always obtain an N+1 length "Prony K-Pulse" which by the previous section is an N-Plet or repetitive convolution of N couplets. Note that the length of the "Prony K-Pulse" denotes a quantized amount of information content. We shall denote this standard or N+1 values of information content as

the o-th order singularity. When we are able to use only N values of information content, we shall call this the 1-st order singularity times. Similarly the 2-nd order singularity times exists, they will result in an N-1 length "Prony K-Pulse." Still higher order singularity times are similarly defined. We are now ready for the statement of the theorem.

K-Pulse Singularity Theorem:

The first order singular times, T_1 , of the N term real "Prony series" are given by equation (C-24).

$$T_1 = P(2N)HP_m (C-24)$$

where P is a positive integer

 ${\rm HP}_{\rm m}$ is the half-period of any complex natural frequency, ${\rm s}_{\rm m}$.

Proof for P = 1 and any $m \in \{1, 2, \ldots, N\}$:

The sample spacing is T - HP_{m} .

Now the m-th real natural mode is:

$$A_{m} exp(\sigma_{m} Tn) cos(\omega_{m} Tn + \phi_{m}) = (C_{m} \{\rho_{m}^{n}\}_{0}^{\infty} + C_{m}^{*} \{\rho_{m}^{*n}\}_{n}^{\infty})$$

which is the sum of two complex natural modes of the identical period and magnitude of amplitude. Expanding,

$$\{\rho_{n}^{n}\}_{0}^{\infty} = \{\exp(\sigma_{m} T \cdot n) \exp(j\omega_{m} T \cdot n)\}_{0}^{\infty}$$

but

$$\omega_{\rm m}$$
 T = $\omega_{\rm m}$ HP_m = π

So

$$\exp(j\omega_m T^n) = \exp(j\pi n) = (-1)^n$$

$$\{\rho_{m}^{n}\}_{0}^{\infty} = \{\exp(\sigma_{m} T \cdot n)(-1)^{n}\} = \{(-1\rho_{m}1)^{n}\}_{0}^{\infty}$$

Similarly,

$$\{\rho_m^{\star n}\} = \{\exp(\sigma_m T \cdot n)\exp(-j\omega_n T \cdot n)\}$$

But

$$-\omega_{\mathbf{m}} \mathbf{T} = -\omega_{\mathbf{m}} \mathbf{HP}_{\mathbf{n}} = -\pi$$

So

$$\exp(-j\omega_m T \cdot n) = \exp(-j\omega n) = (-1)^n$$

$$\{\rho_{m}^{*n}\}_{0}^{\infty} = \{\exp(\sigma_{m} \cdot T \cdot n)(-1)^{n}\}_{0}^{\infty} = \{(-|\rho_{m}|)^{n}\}_{0}^{\infty}$$

Now the same couplet $(1, + |\rho_m|)$ kills both $\{\rho_m^n\}_0^\infty$ and $\{\rho_m^{\star n}\}_0^\infty$. Hence, if T = HP_m were used in the N term "Prony K-Pulse" with 2N+1 information values, there would be an extra $(1, + |\rho_m|)$ couplet. Only one of the two identical couplets is necessary. The reduced K-Pulse has only 2N information values. Proof for P = 2 and any m:

$$T = 2HP_{m}$$

$$\{\rho_{m}^{n}\}_{0}^{\infty} = \{\exp(\sigma_{m} \cdot 2HP_{m} \cdot n) \cdot \exp(j\omega_{m} \cdot 2HP_{m} \cdot n)\}_{0}^{\infty}$$

But

$$\omega_{\rm m}$$
 • 2HP_m = 2 π

Then

$$\exp(j\omega_{m} \cdot 2HP_{m} \cdot n) = 1$$

$$\{\rho_{\mathbf{m}}^{\mathbf{n}}\}_{\mathbf{0}}^{\infty} = \{\exp(\sigma_{\mathbf{m}} \cdot 2HP_{\mathbf{m}} \cdot \mathbf{n})\}_{\mathbf{0}}^{\infty} = \{|\rho_{\mathbf{m}}|^{\mathbf{n}}\}_{\mathbf{0}}^{\infty}$$

Similarly since – ω • 2HP_m = -2 π

$$\left\{\rho_{m}^{*n}\right\}_{0}^{\infty} = \left\{\left|\rho_{n}\right|^{n}\right\}^{\infty}$$

Hence, the couplet (1, - $|\rho_{\mbox{\scriptsize m}}|$) kills two complex natural modes:

$$\{\rho_m^n\}_0^\infty$$
 and $\{\rho_m^{\star m}\}_0^\infty$

One of the two identical couplets can be deleted, yielding a reduced N-term "Prony K-Pulse" of only 2N information values instead of 2N+1 for arbitrary T.

Proof for P odd and any m (of N):

$$T_1 = P \cdot HP_m$$

$$\exp(j\omega_{m} \cdot P \cdot HP_{m} \cdot n) = (-1)^{n}$$

$$\{\rho_{m}^{n}\}_{0}^{\infty} = \{(-|\rho_{m}|)^{n}\}_{0}^{\infty}$$

$$\left\{\rho_{m}^{\star n}\right\}_{0}^{\infty} = \left\{\left(-\left|\rho_{m}\right|\right)^{n}\right\}_{0}^{\infty}$$
 same result as P = 1.

where $|\rho_{m}| = \exp(\sigma_{m} \cdot P \cdot HP_{m})$

Proof for P even and any m (of N):

$$\exp(j\omega_m \cdot \rho \cdot HP_m \cdot n) = (+1)^n$$

$$\left\{\rho_{m}^{n}\right\}_{0}^{\infty} = \left\{\left|\rho_{m}\right|^{n}\right\}_{0}^{\infty}$$

$$\{\rho \star_{m}^{n}\}_{0}^{\infty} = \{|\rho_{m}|^{n}\}_{0}^{\infty}$$
 same result as $P = 2$.

where $|\rho_N| = \exp(\sigma_m \cdot P \cdot HP_m)$

Converse Proof: Suppose T \neq P \cdot HP_m for any M ϵ (1, . . . , N)

then $\{\rho_m^n\}_0^\infty \neq \{\rho_m^{*n}\}_0^\infty$ for all m, since $\omega_m \neq 0$ for all m. Hence the same couplet $(1, -\rho)$ does not kill both $\{\rho_m^n\}_0^\infty$ and $\{\rho_m^{*n}\}_0^\infty$.

Suppose, however, that T is such that one of the 2N couplets, (1,a) of the N-Mode K-Pulse kills both $\{\rho_m^n\}_0^\infty$ and $\{\rho_k^n\}_0^\infty$, $\ell \in \{1,\ldots,N\}$. But if this is true, then (1,a*) which is also a member of the N-Mode K-Pulse kills both $\{\rho_m^{*n}\}_0^\infty$ and $\{\rho_k^{*n}\}_0^\infty$. But this means that this T defines a 2nd (or higher) order singularity which was deleted by hypothesis. Hence we have shown that if T \neq P \cdot HP $_m$ for some m \in (1, ..., N), then either T $_1$ = P \cdot 2N \cdot T is not a singular time or T $_1$ is singular of order greater than 1.

APPENDIX D

COMPUTER CODE FOR "FAST PRONY'S METHOD ALGORITHM"

PARTS AND OTHER PROGRAMS

```
2
1
  END

LEVEL 1: DICTION, SEARCH, START, CONVOLU, PLOTS, DIFCLAS

SUBROUTINE DICTION

IMPLICIT COMPLEX(C)

CHARACTER LFN*7, PFN*14

PARAMETER (NP=101, NTOT=NP+256)

DIMENSION CX (NTOŤ), T(NTOŤ), S(NTOŤ), CFA(NP), CSA(NP), RFA(NP)

CALL PF('ATTACH', 'DIFSKEW', 'DIFSKEW')

CALL PF('ATTACH', 'WIRE18', 'EIGHTEEN6')

CALL PF('ATTACH', 'SKEW', 'N308217N')

OPEN(99, ACCESS='DIRECT', RECL=1)

CPEN(100, ACCESS='DIRECT', RECL=1)

CLOSE(116)

PRINT*, 'ENTER EXCITATION PFN='

READ(*, '(A14)')PFN

WRITE(*, '(5H PFN=, A14)')PFN

LFN=PFN

WRITE(*, '(5H LFN=, A7)')LPN

CALL PF('ATTACH', LFN, PFN)

OPEN(116, FILE=LFN)

CALL EXCITES(116, DELT, CFA, T, 1, NP, NP, MLENGTH)

RETURN
   ENTRY PLOTS
PRINT*, OUTPUT EXCITATION TAPE#=? '
READ*, NOUT
IF (NOUT.EQ.0) CALL EXIT
CALL BARPLOT(1, NOUT, CSA, NOEXCIT, T, MLENGTH)
                    ŘETURN
***************
```

ENTRY DIFCLAS

```
3
  31
                                                       PRINT*, 'COMPUTED ISKIP= ',ISKIP
RETURN

ENTRY CONVOLU

CALL SIGNAL(109,1,1,5,Ms,T,DeLN,Length)
CALL REVERSE(CSA,MLENGTH)
NSKIP=MS/ISKIP
PRINT*, 'COMPUTED NSKIP=',NSKIP
CALL BARPLOT(ISKIP,15,CSA,MLENGTH,T,NSKIP)
DO 2 II=7,16
REWIND II
IANS=0
IF(ISKIP,NE.1)THEN
PRINT*, 'ENTER 0 FOR NO DEMULTIPLEX ?'
READ*,IANS
END IF
NSKIP=(MS+ISKIP-ISTART)/ISKIP
MAXLENG=MLENGTH+NSKIP-1
CALL DCONVOL(CX,CSA,MLENGTH,ISKIP,S,ISTART,NSKIP)
CALL WROUT(ISKIP,CX,MLENGTH,T,ISTART,NSKIP,9)
IF(IANS.EO.0)THEN
CALL WROUT(ISKIP,CX,MLENGTH,T,ISTART,NSKIP,13)
END IF
CONTINUE
IF(IANS.NE.0)THEN
KR=9
CALL WROUT(ISKIP,S,MS,T,KR)
CALL DMUX(KR,ISKIP,S,MS,T,KR)
CALL D
2
                 LEVEL 2A: EXCITES, EXCITE, REVERSE, BARPLOT, DECONVOL, SIGNAL ROTATE WROUT, CLINE
                                                              SUBROUTINE DCONVOL(CX,CFA,M,ISKIP,S,ISTART,NMAX)
IMPLICIT COMPLEX(C)
DIMENSION CX(NMAX+M-1),CFA(M),RFA(M),S(ISKIP,NMAX),T(ISKIP,NMAX)
PRINT*, ISTART=',ISTART,' NMAX=',NMAX
DO 1 17=1,NMAX+M-1
CX(IT)=0,
IMIN=MIN(IT,M)
JMIN=MAX(IT-NMAX+1,1)
```

```
DO 11 J=JMIN, IMIN

CX(IT)=CX(IT)+CFA(J)*S(ISTART, IT-J+1)

CONTINUE

RETURN
11
                                 ENTRY EXCITES(LW,DELT,CFA,T,ISKIP,NMAX,M,MLENGTH)

REWIND LW

READ(LW,*,END=23,ERR=24)TFIRST,CFA(1)

READ(LW,*,END=23,ERR=24)TT,CFA(2)

PRINT*,1,TFIRST,NS'

DELT=TT-TFIRST

REWIND LW

READ(LW,*)TEARLY,CC

DO 31 IPAGE=1 M

DO 3 K=2.513

WRITE(100,REC=IPAGE)K-1

TLARGE=TEARLY+DELT*1.1

READ(LW,*,END=23,ERR=24)TT,CC

IF((TT.LT,TEARLY),OR.(TT.GT.TLARGE))THEN

READ(LW,*,END=23,ERR=24)TT,CC

IF((TT.LT,TEARLY),OR.(TT.GT.TLARGE))THEN

READ(100,REC=IPAGE)MLENGTH

GO TO 311

END IF

TEARLY=TT

CONTINUE
С
                                   TEARLY=TT
CONTINUE
CONTINUE
IF (IPAGE/4.NE.(IPAGE+1)/4)THEN
PRINT*,IPAGE+1,TEARLY, NS'
END IF
PRINT*,IPAGE+1,K,TT,CC
CONTINUE
CONTINUE
RETURN
311
31
23
                                 ENTRY EXCITE(LW,DELT,CFA,T,ISKIP,NMAX,M,MLENGTH)
REWIND 117
READ(100,REC=IPAGE)MLENGTH
PRINT*,'DELT= ',DELT
PRINT*,'CYCLE=',IPAGE,' HAS LENGTH=',MLENGTH
PRINT*,'WHAT CYCLE # DO YOU WANT?'
READ*,NCYCLE
REWIND LW
DO 7 IPAGE=1,NCYCLE
READ(100,REC=IPAGE)MLENGTH
DO 71 K=1,MLENGTH
READ(LW,*,END=73,ERR=24)T(ISKIP,K),CFA(K)
IF(IPAGE,EO,NCYCLE)THEN
CFA(K)=CONJG(CFA(K))
IF(K,EQ,1).OR.(K,EQ,2))THEN
TI=T(ISKIP,K)
PRINT 10,IPAGE,K,T(ISKIP,K),K,CFA(K)
END IF
WRITE(117,*)T(ISKIP,K),',',CFA(K)
                                                    PRINT 10,1PAGE,K,T(ISKIP,K),K,CEA(K)

END IF

END IF

CONTINUE

K=MLENGTH

TF=T(ISKIP,K)

PRINT 10,1PAGE,K,T(ISKIP,K),K,CFA(K)

ITINUE
71
        TF=T(ISKIP,K)
PRINT 10,IPAGE,K,T(ISKIP,K),K,CFA(K)
CONTINUE
RETURN
FORMAT('T(',I2'',I3')='F5.2''NS,CFA(',I3')=',2F5.1)
PRINT*,'THERE ARE ONLY'',I-1,'CYCLES ON THIS PILE'
PRINT*,'ERROR ON READING FILE=',LW
READ(100,REC=IPAGE)MLENGTH
PRINT*,'LENGTH OF ',IPAGE,' CYCLE ON FILE=',MLENGTH
CALL EXIT
RETURN
*******
ENTRY TRIPLET(CZI,T,ISKIP,NMAX,LW)
IF(CZI,EO,O,)RETURN
CCZI=CONJG(CZI)
WRITE(LW,*)T(ISKIP,1),'',CMPLX(1,0.)
WRITE(LW,*)T(ISKIP,2),'',CZI+CCZI
PRINT*,'CZ(I)='CZI
PRINT*,'CZ(I)='CZI
PRINT*,'CZ(I)='CZI
PRINT*,'T(',ISKIP,',1)=',T(ISKIP,1)
RETURN
******
ENTRY SIGNAL(LS,ISKIP,IS,S,NMAX,T,DELN,LENGTH)
7
                                   ENTRY SIGNAL(LS, ISKIP, IS, S, NMAX, T, DELN, LENGTH)
IF (IS. EO. 1) REWIND LS
DO 2 K=1, NMAX
```

```
2
27
            ENTRY WROUT(ISKIP,CX,M,T,KK,NMAX,LT)
DO 4 K=1,NMAX
IF((T(KK,K).EQ.TF).AND.(LT.EQ.9))THEN
CXTF=CX(K)
PRINT*,'TF,CX=',TF,CXTF
END IF
WRITE(LT,*)T(KK,K),',',REAL(CX(K))
WRITE(LT+1,*)T(KK,K),',',AIMAG(CX(K))
CONTINUE
RETURN
ENTRY POTATE(CY M NMAY)
C *
            51
5
C **
             ENTRY RPULSE(CFA,M,RFA)
DO 81 I=1,M
RFA(I)=RÉAL(CFA(I))
RETURN
81
             ENTRY BARPLOT(ISKIP, LU, CFA, M, T, NMAX)

DO 61 I=0, 1
    REWIND LU+I

CONTINUE
D=T(1,2)-T(1,1)
DTAU=D*, 2
PRINT*, 'SAMPLE SPACING=',D,' NS'
WRITE(99, REC=1)D

DO 6 K=1, M
61
```

```
A=REAL(CFA(K))
B=AIMAG(CFA(K))
TT=T(1,1)+D*FLOAT(K-1)
CALL RECPLOT(TT,DTAU,A,LU)
CALL RECPLOT(TT,DTAU,B,LU+1)
 RETURN
END
    1
    CONTINUE
REWIND LW
DO 11 I=1 MS
WRITE(LW,*)T(I),',',S(I)
RETURN
END
11
   C ****
4
   7
8
   1
```

```
SUBROUTINE MINSN (NR, X, XMIN, INDEX)
IMPLICIT COMPLEX (C)
DIMENSION X (NR), CFA (NR)
INDEX = 1
DO 1 I = 1, NR
CONTINUE
XMIN = X (INDEX)
RETURN
ENTRY POLYN (CFA NR CV)
1
        8
        ENTRY SWITCH(CG,CH)
CC=CG
CG=CH
CH=CC
RETURN
SUBROUTINE RECPLOT(TAU,DTAU,A,MU)
WRITE(MU,*)TAU,',',A
WRITE(MU,*)TAU+DTAU,',',A
WRITE(MU,*)TAU+DTAU,',',A
WRITE(MU,*)TAU+DTAU,',',0.
RETURN
END
        2
```

```
FAST PRONY'S METHOD ALGORITHM K-PULSE & ANALYSES * *

* FILE PURPOSE * * * * * FILE PURPOSE * * *

* FILE PURPOSE * * * * * * * * * * * * *

80 SYNTHETIC FREQ. 109 INPUT WAVEFORM
110 PRINT 111 K-PULSE
114 C-PULSE 113 SPECTRA NORMALIZED
114 C-PULSE 115 MODEL
116 SYNTHETIC C-PULSE 117 TRIPLETS

PROGRAM FPRONYD(INPUT, OUTPUT)
DO 7 I=0,8
REWIND 109+I
CONTINUE
WRITE(110,'(///)')
CALL FRAME
CALL LOOPSET
CALL POLYNOM
STOP
END

EL 1: FRAME, LOOPSET, FRAMES, POLYNOM.
7
      LEVEL 1: FRAME, LOOPSET, FRAMES, POLYNOM.
     SUBROUTINE DICTION
IMPLICIT COMPLEX(C)
IMPLICIT DOUBLE PRECISION(W)
IMPLICIT CHARACTER*7(O)
PARAMETER(N=256,NCOLS=51,NP=100,NPP=NP+1,LR=109,LW=LR+1)
PARAMETER(OPRONY=' PRONY')
DIMENSION CX(N),CF(NP),CAM(NP),CFA(NPP),CZ(NP)
DIMENSION WB(NP+1),CS(NP)
DIMENSION WB(NP+1),CS(NP)
DIMENSION WAVEIN(N),CFASIG(NP+1),CZNUM(NP)
DIMENSION WFA(NPP),WFASIG(NP),RFA(NPP),RFASIG(NPP)
EQUIVALENCE(CF(1),CFA(2))
                       ENTRY FRAME

CALL PF('ATTACH','LOA200','WIRE10ROOTSLOA200')

CALL PF('ATTACH','LOA400','WIRE10ROOTSLOA400')

REWIND 12

CALL TARGET(NM, LR, LW)

CALL TIME(NR, TTIME, CX, ISKIP, LR)

PRINT*,'#ROWS+#COLUMNS=',NR,'+',NR,' RE-ENTER #ROWS '

READ*,NC
NC=MAX(NC,NR)

CONTINUE

NC=NDOINTS-(NC+ND)*ISKID-(ISKID-1)
                       33
                      ENTRY LOOPSET

ISTART=0

IP(NFINAL.LT.MFINAL)THEN

PRINT* 'IST FRAME START @ 0.0 NS, ENTER START TIME= '
READ*, STARTIN

ISTART=STARTIN/TTIME*ISKIP

PRINT* ISTART

IF(ISTART.NE.0)THEN

PRINT* 'INCREMENT=',INCROW,'ENTER NEW INCREMENT= '
READ*, INCROW

END IF

END IF
                        END IF
ISTART=MIN(ISTART,NFINAL)
PRINT*,ISTART,NFINAL,INCROW
OANS='FAST'
WRITE(LW,'(1x,2A7)')OANS,OPRONY
RETURN
```

	, the con-	1
		:
		i
-		1
		1
		1
		- 1
₹		
b		
E		
\$		
4		

```
11
                                                                                                                                                                                                                                                                                                                                                                                                                                                   .GE.IS+INCROW)GO TO 1
110
                                                                                                                                              ENTRY INNAME(CX.NR.NC.WAVEIN.W.WA.IP.ISKIP.NDOF)
NN.NP-NC
NDOF-NE
DOWN THE STATE OF THE STATE OF
13
14
```

```
| SED-IP-15K1P*(J-1)-1
| WITTE(*, (51x,F5.2)))T(ISEQ),WGRC(J),WSQ(J),WA(
| WITTE(T, T), WALP
| NT | LPHA: WALP
| WITTE(T, T), WALP
                                                                                                            ENTRY SOLN(WA, RFA, CFA, NR)
DO 141 I=1, NR+1
RFA(I)=SNGL(WA(I))
CFA(I)=CMPLX(WA(I))
RETURN
                                                                                                            21
                                                                                                                                                                                                                                  E READ(LR,*,END=22)T(I),CX(I)
                                                                                                                                                     END TE

NITHUE

NITHUE

THE TIST TO THE PECONTIES

PROPER TO THE PECONTIES

PROPER TO THE PECONTIES

PROPER TO THE PECONTIES

NITHUE TO THE PECONTIES TO THE PECONTIES TO THE PECONTIES

NITHUE TO THE PECONTIES T
322
23
                                                                                                                 READ*, NDOF
RETURN
IFLAG=1
PRINT* 'FILE COMPLEX'
GO TO 21
20
                                                                                                            ENTRY TARGET (NH. LB. +LP.)

PRINT : SELECT TARGET ENTER 5,19,6,120,45,90,DEFAULT)

PRINT : SELECT TARGET ENTER 5,19,6,120,45,181

CLOSE (80)

If (18,0)

PRINT (18,0)
                                                                                                                                                                                                                                                                                                     18) THEN CH', WIRELS', EIGHTEEN6')
WIRELS ON DIFMIRE: DIFMIRES', OIFWIRELS', OIFWIRELS', OIFWIRELS')
$ (A77) LE'N DIFMIRES', OIFWIRELS', O
                                                                                                                                                     ADCTIME-18.6/1/wrst.A//)LPN

DEPNIS LEGISTRONG BRR-99)

ADCTIME-18-10-A400 BRR-99)

ADCTIME-18-10-A400 BRR-99)

ADCTIME-19-10-A400 BRR-99)

ADCTIME-19-10-A400 BRR-99)

ADCTIME-19-10-A400 BRR-19-10-A400 BRR-19-10-A400
```

```
ACCTIME=1.2
OPEN(LR,FILE='DPULSE' ERR=99)
WRITE(LW,*)' DIFFERENCED PULSE'

ELSE

ACCTIME=1
OPEN(80,FILE='LOA200', ERR=99)
WRITE(LW,*)' SYNTHETIC' 12" WIRE'
IF(II.EQ.0) THEN
CALL PF'.ATTACH', S000', S000')
CALL PF'.ATTACH', S000', S001', S000')
PRINT* S000 OR S001: ', S001')
PRINT* S000 OR S001: ', S001')
PRINT* S000 OR S001: ', S001')
WRITE(LW,*)' INCIDENCE AT 0 DEGREES'
READ(LR,FILE=LFN,ERR=99)
WRITE(LW,*)' INCIDENCE AT 90 DEGREES'
OPEN(LR,FILE=S990',ERR=99)

ELSE IF(II.EQ.45) THEN
CALL PF'.ATTACH' S999', S999')
WRITE(LW,*)' INCIDENCE AT 90 DEGREES'
OPEN(LR,FILE='S990',ERR=99)

ELSE IF(II.EQ.45) THEN
CALL PF'.ATTACH' S707', S707')
WRITE(LW,*)' INCIDENCE AT 45 DEGREES'
OPEN(LR,FILE='S707',ERR=99)

ELSE ALL PF'.ATTACH' S502', S502')
OPEN(LR,FILE='S502',ERR=99)

ELSE ALL PF'.ATTACH' S502', S502')
OPEN(LR,FILE='S502',ERR=99)

END IF
INOUIRE(80, EXIST=EXISTS,NUMBER=NUM,NAMED=NMD,NAME=OFN)
IF(EXISTS)' THEN
WRITE(LW,*)' INCIDENCE AT 30 DEGREES WITH GHOST'
END IF
INOUIRE(80, EXIST=EXISTS,NUMBER=NUM,NAMED=NMD,NAME=OFN)
IF(EXISTS)' THEN
WRITE(*, (IX,A7,17H OPENED AS NUMBER,I2)') OFN,NUM
ELSE
PRINT* 'UNIT=80 IS UNOPENED AS NUMBER,I2)') OFN,NUM
ELSE
TRY INSTANCE LENGTH=',TKPULSE,' NS'
RETURN
PRINT* 'UNIT=80 IS UNOPENED YET'
OPEN(80,FILE='LOA200',ERR=99)

END IF
CALL EXIT
                                     99
```

```
50
60
C
              71
72
               ENTRY WROUT(CFA,NR,LU)
DO 41 I=1,NR+1
WRITE(LU,*)T(IP+ISKIP*(I-1)+1),',',CFA(I)
CONTINUE
RETURN
41
              6
               ENTRY WMODES(CS,NR,IP,ISKIP,MCOUNT,CZ,LM)
DO 64 I=2,NR+1
CFA(I)=0.
CFA(I)=1.
NCOUNT=0
64
              CFA(1)=1.
NCOUNT=0
MCOUNT=0
MCOUNT=0
DO 63 I=1,NR
CGHZ=CS(I)*DT/TTIME
SIGMA=REAL(CS(I))
IF(SIGMA.LT.0,)THEN
AICS=AIMAG(CS(I))
CALL POLYN(CFA,NR+1,CZ(I))
NCOUNT=NCOUNT+1
IF(AICS.GT.0,01)THEN
EWAVE=1./(1.-EXP(REAL(CGHZ)*0.04*2.))
SPECTRU=10.*ALOG10(REAL(CD)**2*EWAVE)
WRITE(LM*3,*)AIMAG(CS(I))''.SPECTRU
WRITE(12,70)T(IP+1),AICS,SPÉCTRU
MCOUNT=MCOUNT+1
CS(MCOUNT)=CS(I)
CAM(MCOUNT)=CAM(I)
END IF
END IF
CONTINUE
DO 65 I=0,NCOUNT
WRITE(LM*4,*)T(IP+ISKIP*I+1),',',CFA(NCOUNT+1-I)
CONTINUE
FORMAT(3F8.3)
65
70
C *
               ENTRY NATFREQ (NMODES, NM, CS, CZ, NR, NC, CFA, LW)
```

```
PI=ACOS(-1.)

LF=80

REWIND LF
DO 84 1 = 1,40

READ(LF,*,END=842)CS(I)

NMODES=1-1

PRINT*,NMODES=',NMODES

REWIND LF
DO 84 J=2,NR+1

CFA(1)=0.

CFA(1)=1

C
841
842
84
8
811
81
861
86
                                                                   311
 31
                                                                          ENTRY AMPADE(CFASIG,CZ,NR,CAM)
DO 32 J=1,NR
CRHO=1.
CNUM=0.
CDENOM=1.
DO 321 I=1,NR
CNUM=CNUM+CFASIG(I)*CRHO
IF(J.NE.I)CDENOM=CDENOM*(CZ(J)-CZ(I))
CRHO=CRHO*CZ(J)
```

```
321
32
 LEVEL 3: SWITCH, POLYN, REVERSE, MINSN.

SUBROUTINE SWITCH(CG,CH)

IMPLICIT COMPLEX(C)

DIMENSION CF(NR),X(NR)

CC=CG

CG=CH

CH=CC

RETURN
С
  8
С
      ENTRY REVERSE(CF,NR)
DO 9 J=1 NR/2
CC=CF(J)
CF(J)=CF(NR-J+1)
CF(NR-J+1)=CC
CONTINUE
PRINT*, 'POLYNOMIAL REVERSED'
RETURN
9
 1
C
2
```

```
B(J)=RCBACK*A(0)
IF(ERRORF.EQ.0.)THEN
PRINT* 'PRONY SERIES IDENTIFIED DOF=',J
WRITE(110,*)'PRONY SERIES IDENTIFIED DOF=',J
RETURN
END IF
IF((RCFORW.EQ.0.).AND.(RCBACK.EQ.0.))THEN
PRINT* 'CLASS 2 PRONY SERIES, DOF=',J
WRITE(110,*)'CLASS 2 PRONY SERIES, DOF=',J
RETURN
END IF
RETURN
CONTINUE
RETURN
END IF

3 CONTINUE
RETURN
END SERIES
CONTINUE
RETURN
END SERIES
SOON
```

```
PROGRAM JEEVES(INPUT, OUTPUT)
IMPLICIT COMPLEX(C)
EXTERNAL F
REWIND 8
WRITE(8,'(//)')
WRITE(8,*)' BAZARAA & SHETTY ** CORRECTION TO PAGE 280'
WRITE(8,*)' METHOD OF HOOKE AND JEEVES WITH DISCRETE STEPS'
CD1=CMPLX(1..0')
CD2=CMPLX(0..1')
CX=CMPLX(0..1')
CX=CMPLX(0..1')
CX=CMPLX(2..1')
CALL HOOKEJ(F.CX,CD1,CD2)
WRITE(8,*)'NOTE ROUND-OFF ERROR IN BOOK AT ITERATION K=6,J=2'
STOP
END
SUBROUTINE HOOKEJ(F.CX.CD1.CD2)
                                 SUBROUTINE HOOKEJ(F,CX,CD1,CD2)
IMPLICIT COMPLEX(C)
LOGICAL LFLAG,SFLAG
CHARACTER*3 AS,AF,AV
F(C) = (REAL(C) - 2.) **4+(REAL(C) - 2.*AIMAG(C))**2
DATA AS,AF/'(S)','(F)'
DELTA=0.2
EPSILON=0.1
ALPHA=1.
CY=CX
Y1=F(CY)
J=1
С
DON:0.1

CY=CX
Y1=F(CY)
J=1
K=1
X1=Y1
WRITE(8,40)
WRITE(8,10)
******************
DO 1 KK=1,200
IF(JEO,2)THEN
CD=CD2*DELTA
ELSE
CD=CD1*DELTA
END IF
CO=CD1*DELTA
CYP=CY+CD
YP=F(CYP)
IF(Y2-LT.Y1)THEN
LY2-LAG=.TRUE.
CY2-CYP
ELSE
LFLAG=.FALSE.
CYN=CY-CD
YN=F(CYN)
Y2=YN
IF(Y2-LT.Y1)
SFLAC
FT
         Y2=YN
IF (Y2.LT.Y1) THEN
SFLAG=.TRUE.
CY2=CY-CD
ELSE
CY2=CY
Y2=Y1
SFLAG=.FALSE.
END IF
END IF
CONTINUE
                             CONTINUE

IF (J.LT.2) THEN

IF (LFLAG) THEN

WRITE (8,20) K, DELTA, CX, J, CY, CD1, CYP

WRITE (8,30) X1, Y1, Y2, AS

ELSE

WRITE (8,30) X1, Y1, YP, AF, YN, AV

END IF

J=2

Y1=2

Y1=2

CY=CY2

GO TO 1

ELSE

IF (LFLAG) THEN

WRITE (8,50) J, CY, CD2, CY2

WRITE (8,60) Y1, YP, AS

ELSE

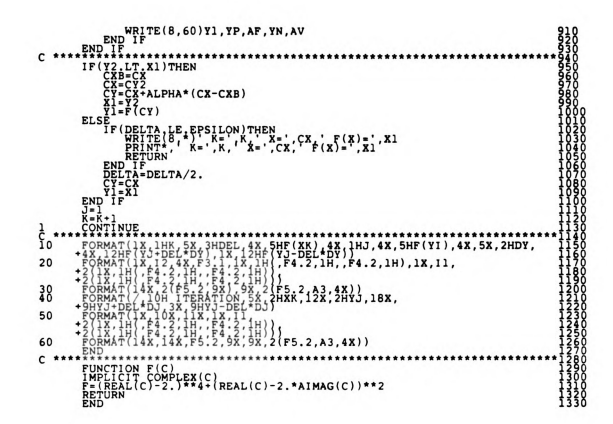
ELSE

ELSE

ELSE

ELSE

ELSE
                                                 ELSE
AV=AF
IF(SFLAG)AV=AS
WRITE(8,50)J,CY,CD2,CYP,CYN
```



REFERENCES

REFERENCES

Chapter 2

- 2-1 R. S. Elliott, <u>Antenna Theory and Design</u>. Englewood Cliffs: Prentice-Hall, 1981, pp. 11-26.
- 2-2 C. E. Baum, "The singularity expansion method," in <u>Transient Electromagentics</u>. Ed., L. B. Felsen. New York: Springer-Verlag, 1976, pp. 129-179.
- C. E. Baum, "Emerging technology for transient and broad-band analysis and synthesis of antennas and scatterers'," Proc. IEEE, Vol. 64, No. 11, November 1976, pp. 1598-1616.
- Kun-Mu Chen, "Radar waveform synthesis method--A new radar detection scheme," IEEE Trans. Antennas & Propagation, Vol. AP-29, No. 4, July 1981, pp. 553-566.
- 2-5 L. L. Webb, B. Drachman, K. M. Chen, D. P. Cyquist, C-I Chuang, Bruce Hollmann, "Convolution of synthesized radar signals for single or zero-mode excitation with experimental radar returns," 1983 National Radio Science Meeting, University of Colorado, 5-7 January 1983, CR2-6.
- 2-6 J. G. Proakis, <u>Digital Communications</u>. New York: McGraw-Hill, 1983, pp. 72.
- 2-7 D. C. Schleher, ed., <u>MIT Radar</u>. Dedham, Mass.: Artech House, 1978.
- 2-8 R. O'Dennell, C. Muehe, M. Labitt, & L. Carthledge, "Advanced signal processing for airport surveillance radars," <u>EASCON-74</u>, 1974, pp. 71-71F, also reprinted in <u>MIT Radar</u> above.
- 2-9 A. S. B. Holland, <u>Introduction to the Theory of Entire Functions</u>. New York: Academic Press, 1973, pp. 102.

<u>Chapter 3</u>

- 3-1 D. R.Rhodes, <u>Synthesis of Planar Antenna Sources</u>. Oxford: Clarendon Press, 1974, pp. 10, 43-46.
- E. M. Kennaugh, "The K-Pulse concept," <u>IEEE Transactions on Antennas & Propagation</u>, Vol. AP-29, No. 2, March 1981, pp. 327-331.

- Lance Webb, Byron Drachman, K. M. Chen, K. P. Nyquist, C-I Chang, Bruce Hollmann, "Convolution of synthesized radar signals for single- or zero-mode excitation with experimental radar returns," <u>USNC/URS National Radio Science Meeting</u>, 6 January 1983, B4-1.
- Lance Webb, K. M. Chen, D. P. Nyquist, Bruce Hollmann, "Extraction of single-mode backscatters by convolving synthesized radar signals with a radar return," 1982 International IEEE/APS Symposium, University of Houston, APS-8-3, May 26, 1983.
- R. E. Crochiere & L. R. Rabiner, <u>Multirate Digital Signal Processing</u>. Englewood Cliffs, N.J.: Prentice-Hall, 1983, pp. 30.
- J. M. Tribolet, <u>Seismic Application of Homorphic Signal</u> Processing. Englewood Cliffs, N.J.: Prentice-Hall, 1979.
- 3-7 William K. Pratt, <u>Digital Image Processing</u>. New York: John Wiley & Sons, 1978, pp. 410-415.
- Wayne T. Ford & James H. Hearne, "Least-squares inverse filtering," <u>Geophysics</u>, Vol. 31, No. 5, pp. 907-926 (also reprinted in G. M. Webster, <u>Deconvolution</u>. Tulse: Society of Exploration Geophysicists, 1978).
- 3-9 K. M. Chen & D. Westmoreland, "Radar waverform synthesis for exciting single-mode backscatters from a sphere and application for target discrimination," <u>Radio Science</u>, Vol. 17, No. 3, pp. 574-588.

Chapter 4

- R. Prony, "Essai experimental et analytiques sur les lois de la dilatabilité des fluides élastiques et sur celles de la Force expansive de la vapeur de l'eau et de la vapeur de l'alkool, á différentes températures," <u>Journal de l'Ecole</u> Polytechnique (Paris), Vol. 1, Cahier 2, Floreal et Prairial, An. III (1795), pp. 24-76.
- 4-2 M. K. Kay, & L. M. Marple, Jr., "Spectrum analysis--A modern perspective," <u>Proceedings IEE</u>, Vol. 69, No. 11, November, 1981, pp. 1380-1419.
- John Makhoul, "Linear prediction: A tutorial review," Proc. IEEE, Vol. 63, No. 4, April 1975, pp. 561-580.
- 4-4 E. M. Kennough, "The K-Pulse concept," <u>IEEE Trans A&P</u>, Vol. AP-29, No. 2, pp. 327-331.

- Martin Morf, et al., "Efficient solution of covariance equations for linear prediction," <u>IEEE Trans. on acoustics, speech & signal processing</u>, Vol. ASSP-25, No. 5, October 1977, pp. 429-433.
- F-C, Chang, & H. Mott, "On the Matrix Related to the Partial Fraction Expansion of a Proper Rational Function," <u>Proc. IEEE</u>, August 1974, pp. 1162-1163.
- 4-7 L. Weiss, & R. N. McDonough, "Prony's method, z-transforms, and Pade approximation," <u>SIAM Review</u>, Vol. 5, No. 2, April 1963, pp. 145-149.
- Francis Brophy & A. C. Salazar, "Consideration of the Pade approximant technique in the synthesis of recursive digital filters," <u>IEEE Trans. on Audio & Electroacoustics</u>, Vol-21, No. 5, December 1973, pp. 500-505.
- 4-9 L. Webb, K-M. Chen, D. P. Nyquist, B. Hollmann, "Extraction of single-mode backscatters by convolving synthesized radar signals with a radar return," IEEE/APS Symposium at University of Houston, APS-8-3, May 26, 1983.
- Norman Levinson, <u>Journal of Mathematics and Physics</u>, Vol. XXVI, No. 2, July 1947, pp. 110-119.
- E. A. Robinson & M. T. Silva, <u>Deconvolution of Geophysical Time Series in the Exploration for Oil & Natural Gas</u>,"
 Elsevier, 1979, pp. 195-198.
- J. D. Market & A. H. Gray, Jr., <u>Linear Prediction of Speech</u>. New York: Springer-Verlag, 1976.
- I. C. Gohberg & I. A. Fel'dman, Convolutional equations and projection methods for their solution," American Mathematical Society, Providence, R.I., 1974.
- 5-5 Martin Morf, B. Dickinson, T. Kailath, & A. Vieira, "Efficient solution of covariance equations for linear prediction," IEEE Transactions on Acoustics, Speech, and Signal Processing, Vol. ASSP-25, No. 5, October 1977, pp. 429-433.
- J. R. Westlake, <u>A Handbook of Numerical Matrix Inversion and Solution of Linear Equations</u>. New York: Wiley, 1968.
- R. Hooke, & T. A. Jeeves, "Direct search solution of numerical and statistical problems," <u>Journal of Association Computer Machinery</u>, 8, pp. 212-229, 1961.
- Hokhtar S. Bazaraa & C. M. Shetty, Nonlinear Programming. New York: John Wiley & Sons, 1979.

Chapter 7

7-1 C. A. Hamilton & F. L. Lloyd, "100 GHz binary counter based on DC SQUID's," <u>IEEE Elec. Dev. Letts</u>, Vol. EDL-3, No. 11, pp. 335-338.

Appendix A

- A-1 A. Nehorai, G. Su, M. Morf, "Estimation of Time Differences of Arrival by Pole Decomposition," <u>IEEE Trans. on Acoust.</u>, <u>Speech, Signal Processing</u>, Vol. ASSP-31, No. 6, pp. 1478-1491, December 1983.
- A-2 R. H. Barker, "The pulse transfer function and its application to sampling servo systems," Proceedings IEE (London), Vol. 99, Part IV, 1952, pp. 202-317.
- A-3 J. R. Ragazzina, G. F. Franklin, <u>Sampled-Data Control Systems</u>. Englewood Cliffs, N.J.: Prentice-Hall, 1983.
- A-4 A. V. Oppenheim, A. S. Willsky, <u>Signals and Systems</u>. Englewood Cliffs, N.J.: Prentice-Hall, 1983.
- A-5 E. I. Jury, <u>Sampled Data Control Systems</u>. New York: John Wiley & Sons, 1958.
- A-6 E. I. Jury, "A note on the steady-state response of linear time-invariant systems," <u>I.R.E. Proceedings (Correspondence)</u>, Vol. 48, No. 5, pp. 942-4.
- A-7 A. V. Oppenehim, R. W. Schafer, <u>Digital Signal Processing</u>. Englewood Cliffs, N.J.: Prentice-Hall, 1975.
- A-8 A. R. Bergen, & J. R. Ragazzini, "Sampled-Data Processing Techniques for Feedback Control Systems," <u>Trans. AIEE</u>, Vol. 73, 1954.
- A-9 E. I. Jury, "Snythesis and critical study of sampled-data control systems," <u>Trans. AIEE</u>, Part II, Paper 56-208, July 1956.

Appendix B

B-1 Bracewell, <u>Fourier Integral and its Applications</u>. New York: McGraw-Hill, 2nd edition, 1982, pp. 224.